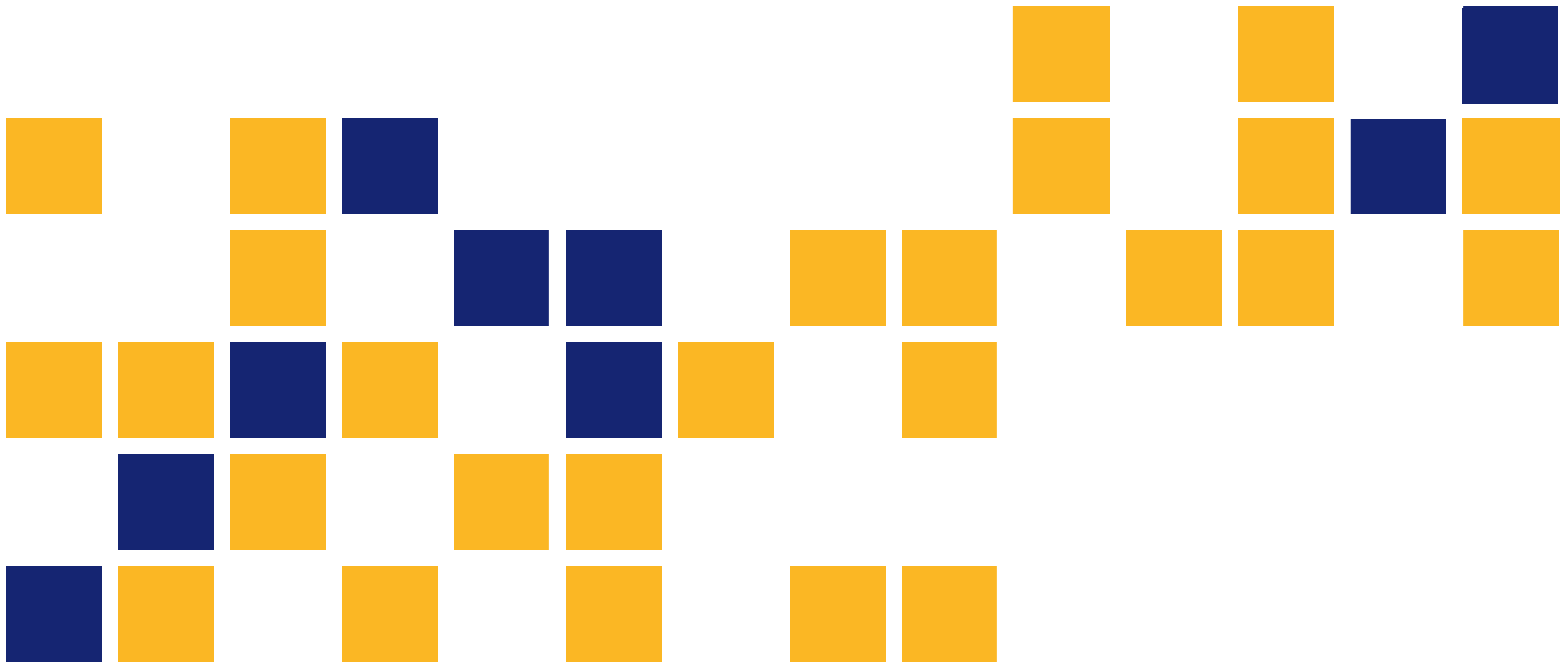


Performance and Capacity Assessment of Reinforced Concrete Bridge Piers Considering the Current Load and Resistance Factor Design Provisions and Plastic Hinge Length in Kansas

Asad Esmaily, Ph.D., P.E.
Fatemeh Shirmohammadi
Kansas State University Transportation Center



A cooperative transportation research program between
Kansas Department of Transportation,
Kansas State University Transportation Center, and
The University of Kansas

1 Report No. K-TRAN: KSU-11-5	2 Government Accession No.	3 Recipient Catalog No.	
4 Title and Subtitle Performance and Capacity Assessment of Reinforced Concrete Bridge Piers Considering the Current Load and Resistance Factor Design Provisions and Plastic Hinge Length in Kansas		5 Report Date May 2014	
		6 Performing Organization Code	
7 Author(s) Asad Esmaeily, Ph.D., P.E.; Fatemeh Shirmohammadi		8 Performing Organization Report No.	
9 Performing Organization Name and Address Department of Civil Engineering Kansas State University Transportation Center 2118 Fiedler Hall Manhattan, Kansas 66506		10 Work Unit No. (TR AIS)	
		11 Contract or Grant No. C1883	
12 Sponsoring Agency Name and Address Kansas Department of Transportation Bureau of Research 2300 SW Van Buren Topeka, Kansas 66611-1195		13 Type of Report and Period Covered Final Report December 2010–December 2013	
		14 Sponsoring Agency Code RE-0548-01	
15 Supplementary Notes For more information, write to address in block 9.			
16 Abstract <p>Kansas Department of Transportation (KDOT) has implemented the new AASHTO-LRFD provisions in the state specific LRFD design procedure (KDOT LRFD). Most of the existing bridges constructed before the new provisions, have been designed based on the old provisions. In this study, these changes have been assessed based on the latest pertinent research, and two representative bridges, representing state bridges designed and constructed based on the new and old code versions have been studied and their performance were analyzed considering their real performance and new code revisions.</p> <p>In general, the two representative bridges provided by KDOT for this study, can safely address the demanded loads considering their actual strength and bridge structural-redundancy and load redistribution process. So, there is no immediate concern in terms of serviceability or collapse of these bridges under demanded loads, including the extreme vehicular impact load. However, the calculated shear strength of most of the columns designed and constructed based on the old codes may not be enough considering the new vehicular impact load required by the new code revisions.</p> <p>While no immediate action seems to be necessary in terms of serviceability and safety of these bridges, engineering judgment and a realistic case-based performance assessment is needed to decide if enhancement of the shear strength and the amount of lateral reinforcement within the plastic hinge length is necessary. Proper methods to retrofit these types of columns as detailed in Chapter 4 can be used, once a decision is made for a case to implement the aforesaid enhancement. The case-based appropriate retrofitting method can be specified for each case considering the column geometry, service load, reinforcement details and material properties.</p>			
17 Key Words Bridge, LRFD, Structures		18 Distribution Statement No restrictions. This document is available to the public through the National Technical Information Service www.ntis.gov .	
19 Security Classification (of this report) Unclassified	20 Security Classification (of this page) Unclassified	21 No. of pages 207	22 Price

This page intentionally left blank.

**Performance and Capacity Assessment of Reinforced Concrete Bridge
Piers Considering the Current Load and Resistance Factor Design
Provisions and Plastic Hinge Length in Kansas**

Final Report

Prepared by

Asad Esmaily, Ph.D., P.E.
Fatemeh Shirmohammadi

Kansas State University Transportation Center

A Report on Research Sponsored by

THE KANSAS DEPARTMENT OF TRANSPORTATION
TOPEKA, KANSAS

and

KANSAS STATE UNIVERSITY TRANSPORTATION CENTER
MANHATTAN, KANSAS

May 2014

© Copyright 2014, **Kansas Department of Transportation**

PREFACE

The Kansas Department of Transportation's (KDOT) Kansas Transportation Research and New-Developments (K-TRAN) Research Program funded this research project. It is an ongoing, cooperative and comprehensive research program addressing transportation needs of the state of Kansas utilizing academic and research resources from KDOT, Kansas State University and the University of Kansas. Transportation professionals in KDOT and the universities jointly develop the projects included in the research program.

NOTICE

The authors and the state of Kansas do not endorse products or manufacturers. Trade and manufacturers names appear herein solely because they are considered essential to the object of this report.

This information is available in alternative accessible formats. To obtain an alternative format, contact the Office of Public Affairs, Kansas Department of Transportation, 700 SW Harrison, Topeka, Kansas 66603-3754 or phone (785) 296-3585 (Voice) (TDD).

DISCLAIMER

The contents of this report reflect the views of the authors who are responsible for the facts and accuracy of the data presented herein. The contents do not necessarily reflect the views or the policies of the state of Kansas. This report does not constitute a standard, specification or regulation.

Abstract

The Kansas Department of Transportation (KDOT) has implemented the new AASHTO-LRFD provisions in the state specific load and resistance factor design (LRFD) design procedure (KDOT-LRFD). Most of the existing bridges constructed before the new provisions, have been designed based on the old provisions. In this study, these changes have been assessed based on the latest pertinent research, and two representative bridges, representing state bridges designed and constructed based on the new and old code versions have been studied and their performance were analyzed considering their real performance and new code revisions.

In general, the two representative bridges provided by the KDOT for this study, can safely address the demanded loads considering their actual strength and bridge structural-redundancy and load redistribution process. So, there is no immediate concern in terms of serviceability or collapse of these bridges under demanded loads, including the extreme vehicular impact load. However, the calculated shear strength of most of the columns designed and constructed based on the old codes may not be enough considering the new vehicular impact load required by the new code revisions.

While no immediate action seems to be necessary in terms of serviceability and safety of these bridges, engineering judgment and a realistic case-based performance assessment is needed to decide if enhancement of the shear strength and the amount of lateral reinforcement within the plastic hinge length is necessary. Proper methods to retrofit these types of columns as detailed in Chapter 4 can be used, once a decision is made for a case to implement the aforesaid enhancement. The case-based appropriate retrofitting method can be specified for each case considering the column geometry, service load, reinforcement details and material properties.

Acknowledgements

The authors wish to acknowledge the financial support of the Kansas Department of Transportation (KDOT) for this research project numbered as K-TRAN: KSU-11-5.

The help and assistance by the project monitor Mr. Jeffrey Ruby, including and not limited to careful selection of representative bridges appropriate for this study, providing technical information, reviewing the project technical reports, and administrative assistance where needed, is warmly acknowledged and appreciated.

Table of Contents

Abstract	v
Acknowledgements	vi
Table of Contents	vii
List of Tables	xi
List of Figures	xiii
Chapter 1: Introduction	1
1.1 Overview	1
1.2 Background	2
1.3 Basic Goals	3
1.4 Outline	3
Chapter 2: Literature Review	5
2.1 Material Models	5
2.2 Monotonic Models	5
2.2.1 Steel	5
2.2.1.1 Ramberg and Osgood's Model	8
2.2.1.2 Giuffre and Pinto's Model	9
2.2.1.3 Menegotto and Pinto's Model	9
2.2.1.4 Park and Paulay's Model	11
2.2.1.5 Mander et Al.'s Model	12
2.2.1.6 Balan et Al.'s Model	12
2.2.1.7 Esmaeily's Model	15
2.2.2 Concrete	16
2.2.2.1 Richart's Model	17
2.2.2.2 Sheilkh and Uzumeri's Model	18
2.2.2.3 Mander et Al.'s Model	20
2.2.2.4 Fafitis and Shah's Model	22
2.2.2.5 Sakino and Sun's Model	24
2.2.2.6 Saatcioglu and Razavi's Model	26
2.2.2.7 KSU-RC Model Based on Mander's Model	28

2.3 Hysteretic (Cyclic) Response	30
2.3.1 Steel.....	31
2.3.1.1 Simple Bi-Linear Hysteretic Model.....	31
2.3.1.2 Ramberg-Osgood Model.....	32
2.3.1.3 Michio Tri-Linear Model.....	33
2.3.1.4 Gomes and Appleton’s Model	33
2.3.1.5 Balan et Al.’s Model.....	34
2.3.1.6 Esmaeily Steel Hysteretic Model Developed and Used in KSU-RC.....	39
2.3.2 Concrete	41
2.3.2.1 Park et Al.’s Model.....	42
2.3.2.2 Kuramoto et Al.’s Model	42
2.3.2.3 Mander et Al.’s Model.....	44
2.3.2.4 Model Developed and Used in KSU-RC	45
2.3.2.5 KSU-RC Cover Concrete.....	48
2.4 Definition of Plastic Hinge Length.....	49
2.5 Plastic Hinge’s Models and Studies.....	51
2.5.1 Baker’s Model.....	51
2.5.2 Baker and Amarakone’s Model	52
2.5.2 Mattock’s Model.....	52
2.5.3 Sawyer’s Model	52
2.5.4 Corley’s Model	53
2.5.5 Mattock’s Model.....	53
2.5.6 Park et Al.’s Model.....	53
2.5.7 Priestley and Park’s Model	54
2.5.8 Sakai and Sheikh’s Investigations	54
2.5.9 Paulay and Priestley’s Model.....	54
2.5.10 Riva and Cohn’s Model	55
2.5.11 Mendis’s Studies.....	56
2.5.12 Correal et Al.’s Studies	56
2.5.13 Berry et Al.’s Model	57
2.5.14 Bae and Bayrak’s Model.....	57

2.5.15 Mortezaei and Ronagh's Model.....	58
2.5.16 Esmaeily's Model One.....	58
2.5.17 Esmaeily's Model Two	63
Chapter 3: AASHTO and KDOT	69
3.1 AASHTO LRFD Bridge Design Specification	69
3.1.1 Load and Load Factors.....	69
3.1.2 Vehicular Collision Force (<i>CT</i>)	70
3.1.3 Vessel Collision (<i>CV</i>).....	73
3.1.4 Earthquake Effects (<i>EQ</i>).....	76
3.1.5 Concrete Bridge Reinforcement	80
3.2 KDOT-LRFD Design Manual	83
3.2.1 Loads and Load Factors.....	83
3.2.2 Vehicular Collision Force (<i>CT</i>)	83
3.2.3 Earthquake Effects (<i>EQ</i>).....	87
3.2.4 Concrete Bridge Reinforcement	88
3.3 Evaluation of Two Representative Existing Reinforced Concrete Bridge Piers under New Code Requirement.....	89
3.4 Assessment of Concrete Bridge Piers under Earthquake Loads	90
3.4.1 Response Spectrum.....	90
3.4.2 Equivalent Static Seismic Loading.....	93
3.4.2.1 Equivalent Static Seismic Loading for Bridge No. 1.....	96
3.4.2.2 Equivalent Static Seismic Loading for Bridge No. 2.....	105
3.4.3 Vehicle Collision Force for Columns of the Two Existing Bridges.....	113
3.4.3.1 Demand Forces Due to Vehicular Collision Force in Bridge No. 1	116
3.4.3.2 Demand Forces Due to Vehicular Collision Force in Bridge No. 2	118
3.4.4 Investigation of the Flexural Capacity of the Existing Columns.....	120
3.4.5 Investigation of the Shear Capacity of the Existing Columns.....	125
3.4.5.1 Assessment of Shear Capacity Based on AASHTO-LRFD (2010).....	126
3.4.5.2 Assessment of the Shear Capacity Based on the ACI-318	127
3.4.6 Investigation of the Plastic Hinge Length for the Existing Columns	134
3.4.7 Investigation of the Displacement Capacity of the Existing Columns	139

Chapter 4: Retrofitting-----	144
4.1 Retrofitting-----	144
4.2 Retrofitting by Fiber Reinforced Polymer (FRP) -----	145
4.2.1 FRP-Confined versus Steel-Confined Concrete Behavior.....	146
4.2.2 Carbon Fiber Jacketing	147
4.2.3 Aramid and Glass Fiber Jacketing	150
4.3 Retrofitting Using Steel Jackets -----	153
4.3.1 Steel Jacket Configuration	153
4.3.2 Advantages of Steel Jackets.....	157
4.4 Retrofitting by Precast Concrete Segment Jacket and Cable-Strand Jacket-----	158
Chapter 5: Conclusion and Recommendations-----	159
5.1 Conclusion -----	159
5.1.1 Flexural Capacity	160
5.1.2 Shear Capacity	160
5.1.3 Plastic Hinge Region.....	161
5.2 Recommendations -----	162
References-----	163
Appendix A: KSU-RC Program-----	169
Appendix B: Representative Bridges-----	180

List of Tables

TABLE 3.1 Load Combinations and Load Factors	70
TABLE 3.2 Site Class Definition	77
TABLE 3.3 Seismic Coefficient of Three Cities in Kansas.....	90
TABLE 3.4 Site Factors for Three Cities in Kansas State.....	91
TABLE 3.5 Acceleration Coefficient for Three Cities in Kansas State.....	93
TABLE 3.6 Demand Forces for Column No. 1 in Bridge No. 1	104
TABLE 3.7 Demand Forces for Column No. 2 in Bridge No. 1	104
TABLE 3.8 Demand Forces for Column No. 3 in Bridge No. 1	105
TABLE 3.9 Demand Forces for Column No. 1 in Bridge No. 2	113
TABLE 3.10 Demand Forces for Column No. 2 in Bridge No. 2	113
TABLE 3.11 Demand Forces in Extreme Event II for Column No. 1 in Bridge No. 1.....	114
TABLE 3.12 Demand Forces in Extreme Event II for Column No. 2 in Bridge No. 1.....	114
TABLE 3.13 Demand Forces in Extreme Event II for Column No. 3 in Bridge No. 1.....	115
TABLE 3.14 Demand Forces in Extreme Event II for Column No. 1 in Bridge No. 2.....	115
TABLE 3.15 Demand Forces in Extreme Event II for Column No. 2 in Bridge No. 2.....	116
TABLE 3.16 The Internal Forces in Bent No. 1 in Bridge No. 1	117
TABLE 3.17 The Internal Forces in Bent No. 2 in Bridge No. 1	118
TABLE 3.18 The Internal Forces in Bent No. 3 in Bridge No. 1	118
TABLE 3.19 The Internal Forces in Bent No. 1 in Bridge No. 2	120
TABLE 3.20 The Flexural Capacity of Column No. 1 in Bridge No. 1 Subjected to Different Axial Forces	121
TABLE 3.21 The Flexural Capacity of Column No. 2 in Bridge No. 1 Subjected to Different Axial Forces	122
TABLE 3.22 The Capacity Flexural of Column No. 3 in Bridge No. 1 Subjected to Different Axial Forces	123
TABLE 3.23 The Flexural Capacity of Column No. 1 in Bridge No. 2 Subjected to Different Axial Forces	124
TABLE 3.24 The Flexural Capacity of Column No. 2 in Bridge No. 2 Subjected to Different Axial Forces	125

TABLE 3.25 The Shear Capacity of Column No. 1 in Bridge No. 1.....	129
TABLE 3.26 The Shear Capacity of Column No. 2 in Bridge No. 1.....	130
TABLE 3.27 The Shear Capacity of Column No. 3 in Bridge No. 1.....	131
TABLE 3.28 The Shear Capacity of Column No. 1 in Bridge No. 2.....	132
TABLE 3.29 The Shear Capacity of Column No. 2 in Bridge No. 2.....	133
TABLE 3.30 The Plastic Hinge Lengths for Column No. 1 in Bridge No. 1	134
TABLE 3.31 The Plastic Hinge Lengths for Column No. 2 in Bridge No. 1	135
TABLE 3.32 The Plastic Hinge Lengths for Column No. 3 in Bridge No. 1	136
TABLE 3.33 The Plastic Hinge Lengths for Column No. 1 in Bridge No. 2	137
TABLE 3.34 The Plastic Hinge Lengths for Column No. 2 in Bridge No. 2	138
TABLE 3.35 The Displacement Capacity of Column No. 1 in Bridge No. 1.....	139
TABLE 3.36 The Displacement Capacity of Column No. 2 in Bridge No. 1.....	140
TABLE 3.37 The Displacement Capacity of Column No. 3 in Bridge No. 1.....	141
TABLE 3.38 The Displacement Capacity of Column No. 1 in Bridge No. 2.....	142
TABLE 3.39 The Displacement Capacity of Column No. 2 in Bridge No. 2.....	143

List of Figures

FIGURE 2.1 Typical Stress-Strain Curves for Cast Iron and Mild Steel.....	6
FIGURE 2.2 Typical Monotonic Curve for Mild Reinforcing Steel in Tension	7
FIGURE 2.3 Menegotto-Pinto Model.....	10
FIGURE 2.4 The Proposed Stress-Strain Curve by Mander et al. (1984) and Park and Paulay (1975)....	11
FIGURE 2.5 Stress-Strain Curve Defined by Equation 2.19	14
FIGURE 2.6 Monotonic Stress-Strain Curve for Reinforcing Steel (Balan et al. 1998)	15
FIGURE 2.7 KSU-RC Model for Monotonic Stress-Strain Curve of Steel.....	16
FIGURE 2.8 Samples of Some Proposed Stress-Strain Models for Confined Concrete	17
FIGURE 2.9 Sheikh and Uzumeri’s Model	20
FIGURE 2.10 Mander et Al.’s Model.....	22
FIGURE 2.11 Confined and Cover Concrete Envelope Curves As Used in KSU-RC for Analysis	30
FIGURE 2.12 Simple Bi-Linear Hysteretic Model for Steel	31
FIGURE 2.13 Hysteretic Response of Steel, Based on Ramberg-Osgood Equations	32
FIGURE 2.14 Michio Tri-Linear Hysteretic Curve for Reinforcing Steel	33
FIGURE 2.15 Load Reversal from Yield Plateau.....	37
FIGURE 2.16 Load Reversal from Strain-Hardening Region	38
FIGURE 2.17 Load Reversal from Reversal Curve.....	39
FIGURE 2.18 Esmaeily Steel Hysteretic Curve As Modeled in KSU-RC	41
FIGURE 2.19 Hysteretic Behavior of Concrete As Modeled by Park et Al.....	42
FIGURE 2.20 Kuramoto et Al.’s Model for Hysteretic Behavior of Concrete.....	43
FIGURE 2.21 Stress-Strain Curve for Unloading Branch and Determination of Plastic Strain As Proposed by Mander et Al.	43
FIGURE 2.22 Assumed Deterioration in Tensile Strength of Concrete Due to Prior Compression Loading in the Model Proposed by Mander et Al.	44
FIGURE 2.23 Stress-Strain Curve for Reloading Branch in the Model Proposed by Mander et Al.	45
FIGURE 2.24 KSU-RC Confined Concrete Hysteretic Model, Ascending Path	47
FIGURE 2.25 KSU-RC Confined Concrete Hysteretic Model, Descending Path.....	48
FIGURE 2.26 Confined Concrete Hysteretic Behavior Curve, a Sample Based on the Data from KSU-RC	48

FIGURE 2.27 Definition of Plastic Hinge Length.....	50
FIGURE 2.28 Esmaily's Plastic Hinge, Method One.....	60
FIGURE 2.29 Flowchart Summarizing the First Method for Plastic Hinge.....	63
FIGURE 2.30 Distribution of Curvature along the Column Height As Assumed in Esmaily's Second Method.....	65
FIGURE 2.31 Flowchart Summarizing the Second Method for Plastic Hinge.....	68
FIGURE 3.1 Impact Force versus Approach Speed Relationship for Ford Truck.....	71
FIGURE 3.2 Impact Force versus Approach Speed Relationship for Chevy Truck.....	72
FIGURE 3.3 Ship Impact Concentrated Force on Pier.....	75
FIGURE 3.4 Ship Impact Line Load on Pier.....	75
FIGURE 3.5 Barge Impact Force on Pier.....	76
FIGURE 3.6 Peak Ground Acceleration.....	77
FIGURE 3.7 Column Location and Clear Zone.....	84
FIGURE 3.8 Column Location and Clear Zone.....	84
FIGURE 3.9 Column and 42" (TL5) Barrier Location.....	85
FIGURE 3.10 Column and 54" (TL5) Barrier Location.....	85
FIGURE 3.11 Distance of Pier from Tracks Is More than 50'.....	86
FIGURE 3.12 Distance of Pier from Tracks Is More than 25' and Less than 50'.....	86
FIGURE 3.13 Distance of Pier from Tracks in Less than 25'.....	87
FIGURE 3.14 Fort Riley Military Influence for Seismic Detailing.....	88
FIGURE 3.15 Seismic Column Detailing.....	89
FIGURE 3.16 The Five-Percent-Damped-Design Response Spectrum for Manhattan.....	91
FIGURE 3.17 The Five-Percent-Damped-Design Response Spectrum for Topeka.....	92
FIGURE 3.18 The Five-Percent-Damped-Design Response Spectrum for Kansas City.....	92
FIGURE 3.19 Bridge Deck Subjected to Assumed Transverse Loading.....	94
FIGURE 3.20 Bridge Deck Subjected to Assumed Longitudinal Loading.....	94
FIGURE 3.21 The Stiffness of Column Subjected to a Horizontal Unit Displacement.....	97
FIGURE 3.22 The Slab Section for Bridge No. 1.....	98
FIGURE 3.23 The Section of Girder.....	98

FIGURE 3.24 Bridge Deck Subjected to Assumed Transverse Loading.....	99
FIGURE 3.25 The Bridge Subjected to the Transverse Uniform Loads	103
FIGURE 3.26 The Slab Section for Bridge No. 2.....	106
FIGURE 3.27 Bridge Deck Subjected to Assumed Transverse Loading.....	107
FIGURE 3.28 The Bridge Subjected to the Transverse Uniform Loads	112
FIGURE 3.29 A Bent in Bridge No. 1 with Vehicular Collision Force Acting on the First Column.....	117
FIGURE 3.30 A Bent in Bridge No. 1 with Vehicular Collision Force Acting on the Second Column ..	117
FIGURE 3.31 A Bent in Bridge No. 2 with Vehicular Collision Force Acting in the First Column.....	119
FIGURE 3.32 A Bent in Bridge No. 2 with Vehicular Collision Force Acting in the Second Column ...	119
FIGURE 3.33 Illustration of Terms <i>bv</i> and <i>dv</i>	127
FIGURE 3.34 The Plastic Hinge Lengths for Column No. 1 in Bridge No. 1.....	134
FIGURE 3.35 The Plastic Hinge Lengths for Column No. 2 in Bridge No. 1.....	135
FIGURE 3.36 The Plastic Hinge Lengths for Column No. 3 in Bridge No. 1.....	136
FIGURE 3.37 The Plastic Hinge Lengths for Column No. 1 in Bridge No. 2.....	137
FIGURE 3.38 The Plastic Hinge Lengths for Column No. 2 in Bridge No. 2.....	138
FIGURE 4.1 Classification of Stress-Strain Curve of FRP-Confined Concrete. (a) Increasing Type; (b) Decreasing Type with $f_{cu}' > f_{co}'$; (c) Decreasing Type with $f_{cu}' < f_{co}'$	145
FIGURE 4.2 Modeling of Behavior of Concrete Confined with Steel, CFRP, and GFRP: (a) Axial Stress versus Axial Strain, (b) Lateral Strain versus Axial Strain.....	147
FIGURE 4.3 Wrapping of Carbon Fiber Sheet: (a) Pasting Glue, (b) Wrapping the First Layer and (c) Bonding on the First Layer	148
FIGURE 4.4 Effect of Carbon Fiber Sheet Jacketing for Circular Column.....	149
FIGURE 4.5 Carbon Fiber Sheet Jacketing of Hollow Reinforced Concrete Column, Sakawa-Gawa Bridge, Tomei Expressway.....	149
FIGURE 4.6 Retrofitting by Aramid Fiber; (a) Braided Tape and Unidirectional Tape, (b) Sheet.....	150
FIGURE 4.7 Aramid Fibers Reinforced Plastic Jacketing.....	151
FIGURE 4.8 Effect of Retrofitting by Different Types of Aramid Fiber	151
FIGURE 4.9 Rectangular Column with Glass Fiber-Epoxy Rectangular Jacket. (a) Failure by Jacket Fracture; (b) Lateral Force-Displacement Response.....	152
FIGURE 4.10 Glass Fiber Jacketing.....	153

FIGURE 4.11 Lateral Force-Displacement Response of Columns Retrofitted with Steel Jackets for Enhanced Ductility..... 154

FIGURE 4.12 Elliptical and Circular Steel Jacket over Rectangular Column..... 155

FIGURE 4.13 Retrofit for Rectangular Column 155

FIGURE 4.14 Hysteretic Response of Rectangular Flexural Columns 156

FIGURE 4.15 (a) Engagement Joint, (b) Effective Use of Engagement Joint for Retrofit at High Location 157

Chapter 1: Introduction

1.1 Overview

State Departments of Transportation (DOTs) are expected to use the latest American Association of State and Highway Transportation Officials (AASHTO) Load and Resistance Factor Design (LRFD) bridge design code. There are many considerable differences between the AASHTO Standard Specifications and AASHTO-LRFD Code, including the reliability-based limit-state approach, new live load and dynamic pre-stressed concrete design; and shear design for concrete.

With the completion of a National Cooperative Highway Research Program (NCHRP) project known as NCHRP Project 12-49 “Comprehensive Specification for the Seismic Design of Bridges,” NCHRP Report 472, with the same name was issued, and new seismic design specifications were proposed. The new seismic design specification was considered by the (AASHTO) as a replacement for its existing aged seismic design provisions.

Accordingly, the seismic provisions in the 2007 edition of the AASHTO LRFD Specifications were updated. In the updated version, the return period of the design earthquake was changed from 500-years to 1000-years, and the specifications were updated considering the recent developments in the seismic design of bridges.

The changes in return period for characterizing the seismic hazard necessitated changing the 1988 United States Geological Survey (USGS) maps in the current specifications to new maps developed at the request of the AASHTO T-3 Committee by USGS. These maps provide not only the required initial data for assessment of the seismic loads, such as the peak ground acceleration (PGA) coefficient for the Conterminous United States with the percent probability of exceeding in 75 years ($[100/75]*75=1071$ or approximately 1000 years return period) but also values of the spectral acceleration at 2.0 second (S_2) and 1.0 second (S_1) allowing an improved spectral shape to be used for defining the seismic response coefficient. Consequential changes include new zone boundaries, new soil factors, new minimum design forces and displacements, introduction of $p - \Delta$ requirements, and a revised factor for flexural resistance.

The increase in the return period of the design earthquake from 500 to 1000 years, has affected seismic design provisions even in Zone 1. As example, the new zone boundaries are

higher, and consequently, the minimum support lengths for bridges in Zone 1 and 2 are increased. Similarly, the horizontal design connection force in the restrained direction in Zone 1 has increased.

Most of the state of Kansas is in Zone 1 (classified based on the ground acceleration with a ground acceleration of 0.075 g) except for a small area on the north east that falls into Zone 2A (with 0.15g). Based on the AASHTO-LRFD provisions (4.7.4.1) bridges in Seismic Zone 1 need not to be analyzed for seismic loads, regardless of their importance and geometry. However, the minimum requirements, as specified in Article 4.7.4.4 and 3.10.9 shall apply.

1.2 Background

As of 2012, the KDOT LRFD Bridge Design Manual has been based on the new AASHTO provision and the latest changes implemented in the AASHTO provisions. Considering seismic loads, as detailed in Part 3 of the new LRFD Design Manual, as well as other special loads such as braking force, vehicular collision (a static force of 400 *kip* 4 *ft* above the ground, updated to a static force of 600 *kip* 5 *ft* above the ground in 2012), are among the new load requirements addressing the AASHTO-LRFD provisions. Since the KDOT LRFD Bridge Design Manual is periodically updated to be consistent with the current AASHTO LRFD provisions, a review of the new provisions on Seismic Loading and Vehicular Collision forces was deemed beneficial.

Section 3.5.1 (Concrete Structure) of the KDOT LRFD Bridge Design Manual details the column and bridge pier design provisions based on the AASHTO-LRFD Bridge Design Specifications, and addresses the very recent changes implemented in the AASHTO provisions following the approval of the LRFD Seismic Ballot by the AASHTO Bridge Committee.

States throughout the United States, have adopted the new AASHTO provisions and recent changes by customizing them as per their special needs, considering factors such as seismicity, soil condition, etc. Some states have studied their new requirements and details, through some research programs by state universities, to make sure that they meet the intent of the AASHTO design code.

1.3 Basic Goals

The basic goals of this study were to investigate the new KDOT requirements in terms of the column design procedure and detailing and its consistency with AASHTO provisions; verification of the KDOT assumptions for the plastic hinge regions for columns and bridge piers by analyzing the performance of a typical bridge pier using the KDOT guidelines and the 2010 Fifth Edition AASHTO LRFD Bridge Design Specifications; assessment of the load capacity of the existing columns and bridge piers in the light of the new specifications and using the new load demand as in the new provisions; and recommendations for columns and bridge piers that do not meet the new requirements.

To address the analytical needs of the aforesaid goals, the windows-based computer application developed by the author was used and upgraded where required (Esmaily and Peterman 2007). This application, currently called KSU-RC (Esmaily 2013) can be used for an accurate and realistic assessment of the performance and capacity of bridge piers with various geometry, reinforcement, and under any load/displacement condition. The program has been benchmarked against experimental data (Esmaily and Xiao 2004) from a number of reinforced concrete bridge columns tested under a wide range of loading patterns, including non-proportional axial load and cyclic lateral displacement.

1.4 Outline

The results of this study are presented in this report in the following order:

In Chapter 1, the introductory material is provided and Chapter 2 includes a comprehensive literature review, discussing different material models for reinforcing steel, plain and confined concrete. The models cover the monotonic stress-strain relationship of steel, plain concrete, and confined concrete; as well as the cyclic rules applicable to the hysteresis performance of each material. These models and rules are the critical components of the analytical procedure to assess the real performance of a reinforced concrete section (monotonic and/or cyclic moment-curvature or force-deflection response of a structural column under various load patterns). Additionally, various assumptions on the curvature distribution along reinforced concrete columns, namely, different plastic hinge models, are reviewed and presented.

In Chapter 3, the new requirement of KDOT in terms of designing columns and its consistency with the AASHTO provisions are discussed. To explore the effect of new requirements on the analysis and design of bridge columns, columns from two existing bridges, designed based on previous edition of AASHTO and KDOT are assessed. The resulting force components due to seismic excitation and vehicular collision are determined and the efficiency of existing columns based on the new requirements is investigated. Furthermore, for the aforesaid existing bridge columns, plastic hinge length is calculated using the most proper and realistic analytical models, proposed by various researchers. The plastic hinge length, calculated based on these analytical models, is then compared against the length proposed by the new AASHTO and KDOT specifications.

Chapter 4 explores various methods to enhance the flexural capacity, the shear capacity and also the ductility of the existing columns to meet the new requirements of AASHTO (2010) and KDOT codes.

The main conclusions and recommendations of this study; and possible future research on this topic are provided in Chapter 5.

Chapter 2: Literature Review

This chapter provides a comprehensive review of the material models for monotonic and cyclic stress-strain relationship of steel, plain concrete and confined concrete; cyclic rules; and different assumptions on the curvature distribution over the height of columns including the latest plastic hinge models.

2.1 Material Models

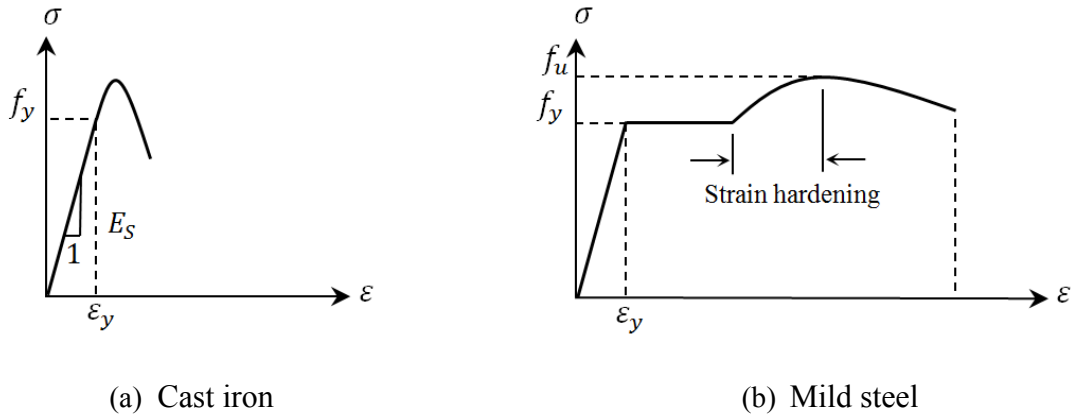
Different models have been proposed for stress-strain relation of material used in reinforced concrete members. The monotonic response of material's model serves as the envelop curve for the hysteric behavior model (Esmaily and Xiao 2002). In this section, the monotonic models, proposed by different researchers for steel, plain concrete and confined concrete will be introduced followed by the hysteretic models and rules for hysteresis behavior or steel, plain concrete and confined concrete.

2.2 Monotonic Models

Experimentally, the monotonic stress-strain curves for steel and concrete can be obtained by monotonic-loading of the steel bars in tension and concrete specimens in compression. Various researchers have used the experimental data as the backbone of the analytical models proposed to simulate the stress-strain relationship of these material. As mentioned earlier, these monotonic curves serve as the envelop curve for the hysteretic models when implementing cyclic rules in the analysis.

2.2.1 Steel

In term of ductility, steel is categorized in two major different groups, cast iron which has the brittle behavior and mild steel which has the ductile behavior. Figure 2.1 shows the typical stress-strain curves for cast iron and mild steel (Esmaily and Xiao 2002).

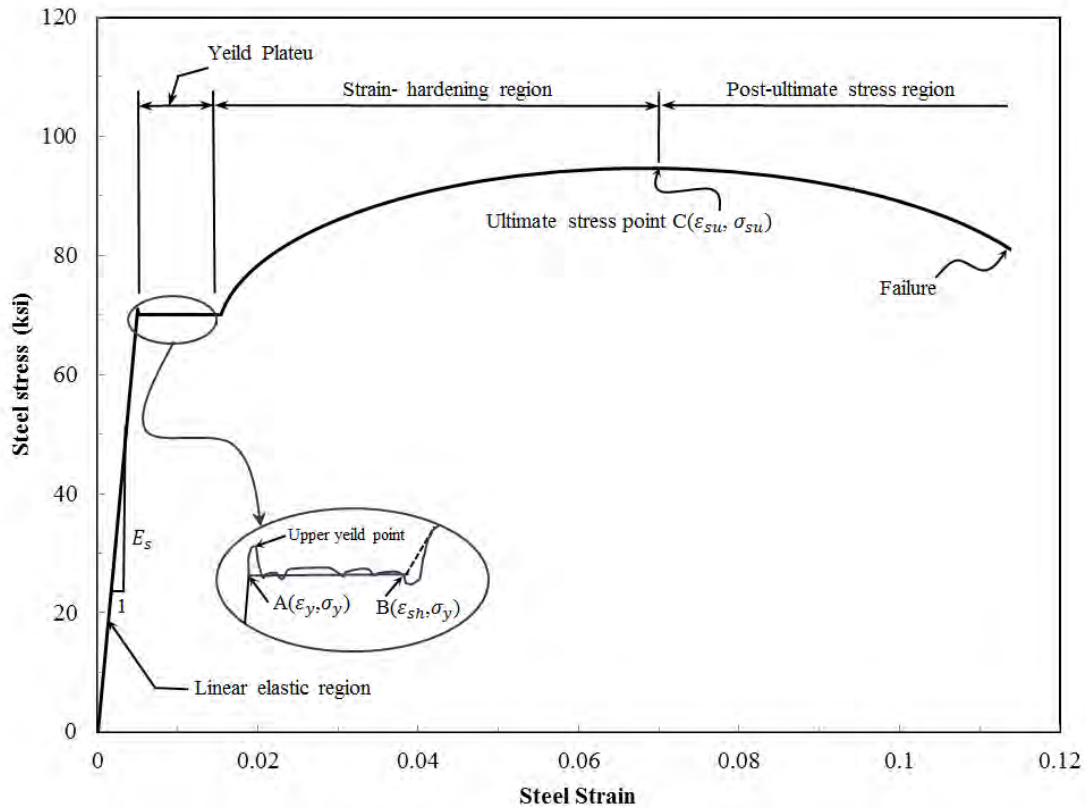


(Source: Esmaily and Xiao 2002)

FIGURE 2.1
Typical Stress-Strain Curves for Cast Iron and Mild Steel

Because the reinforcing steel used in reinforced concrete structures and members is generally from the mild type, all the models discussed in this report are in this category. The curve in Figure 2.2 displays a linear elastic region up to the yield stress, the curve then is defined by a horizontal plateau where the stress is approximately equal to the yield stress. As the strain continues to increase through the yield plateau region, it reaches a point which marks the beginning of the strain hardening region. Stress will increase through the strain hardening region until it reaches its ultimate strength, after that, it will degrade in strength until failure.

Different models are proposed to simulate the monotonic stress-strain response of steel with this behavior up to a certain level of accuracy for. In the following sections, some of these models are briefly discussed.



(Source: Balan et al. 1998)

FIGURE 2.2
Typical Monotonic Curve for Mild Reinforcing Steel in Tension

The first models used to describe the stress-strain behavior of steel were the idealized elastic-perfectly plastic model and the multi-linear models. In these models, several straight lines approximate the stress-strain curve. The slope of the first segment is equal to the modulus of elasticity of the steel, and the slope of the following segment are defined to be either a portion of the initial slope or zero, depending on the real observed stress-strain curve for which the approximation is applied. In most cases, two lines approximate the curve, the first segment having the modulus of elasticity of steel as the slope, while the second has either a smaller slope, or a slope equal to zero.

2.2.1.1 Ramberg and Osgood's Model

Ramberg and Osgood (1943) developed a nonlinear expression to define the stress-strain curve of metals using three parameters; namely, Young's modulus and two secant yield strengths. The stress-strain relationship, proposed by Ramberg and Osgood is as follows:

$$\varepsilon = \sigma + \frac{1 - m_1}{m_1} \sigma^n \quad \text{Equation 2.1}$$

where

$$\varepsilon = \frac{eE}{s_1} \quad \text{Equation 2.2}$$

$$\sigma = \frac{s}{s_1} \quad \text{Equation 2.3}$$

In above equations, s , e , and E are strain, stress, and Young's modulus, respectively. s_1 is the secant yield strength, equal to the ordinate of the intersection with the stress-strain curve of a line through the origin having a slope equal to $m_1 E$ and m_1 is the chosen constant between zero and one ($0 < m_1 < 1$) that based on experimental data, Ramberg and Osgood decided to use the value of 0.7 for m_1 . The shape parameter n is conveniently derived by using a second secant yield strength $s_2 = m_2 eE$, as follows (Ramberg and Osgood 1943):

$$n = 1 + \frac{\log\left(\frac{m_2(1 - m_1)}{m_1(1 - m_2)}\right)}{\log\frac{s_1}{s_2}} \quad \text{Equation 2.4}$$

The value of second secant yield strength was chosen as $m_2 = 0.85$; therefore, the shape parameters can be obtained by substituting values of m_1 and m_2 in Equation 2.4 as follows:

$$n = 1 + \frac{0.3853}{\log\frac{s_1}{s_2}} \quad \text{Equation 2.5}$$

2.2.1.2 Giuffre and Pinto's Model

Giuffre and Pinto (1970) proposed a stress-strain relationship for the elastic-perfectly plastic, without hardening, for monotonic behavior of steel:

$$\sigma_s^* = \frac{\varepsilon_s^*}{(1 + |\varepsilon_s^*|^R)^{1/R}} \quad \text{Equation 2.6}$$

In their model stress and strain are normalized according to Mading's hypothesis (Giuffre and Pinto 1970):

For first loading curve

$$\varepsilon_s^* = \frac{\varepsilon_s}{\varepsilon_{sy}} \quad \sigma_s^* = \frac{\sigma_s}{\sigma_{sy}} \quad \text{Equation 2.7}$$

After first reversal

$$\varepsilon_s^* = \frac{\varepsilon_s - \varepsilon_r}{2\varepsilon_{sy}} \quad \sigma_s^* = \frac{\sigma_s - \sigma_r}{2\sigma_{sy}} \quad \text{Equation 2.8}$$

where $(\varepsilon_{sy}, \sigma_{sy})$ is the yielding point and Equation 2.6 represents a curve with tangent line slope at the origin $E_{s0} = \sigma_{sy}/\varepsilon_{sy}$ and with horizontal asymptote line $(\varepsilon_s^* \rightarrow \infty) \sigma_s = \sigma_{sy}$. The parameter R governs the curvature around the intersection point between the two lines.

2.2.1.3 Menegotto and Pinto's Model

Menegotto and Pinto (1973) modified the Giuffre-Pinto model (Giuffre and Pinto 1970) to account for strain hardening also. The general Menegotto-Pinto law is written as follows:

$$\sigma_s = E_\infty \varepsilon_s + \frac{(E_{s0} - E_\infty) \varepsilon_s}{[1 + (\varepsilon_s/\varepsilon_0)^R]^{1/R}} \quad \text{Equation 2.9}$$

This equation represents a curve with tangent at the origin:

$$\sigma_s = E_{s0} \varepsilon_s$$

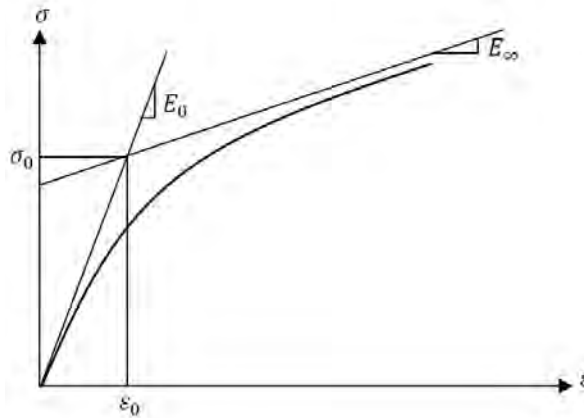
Equation 2.10

and with a straight line asymptote for $\varepsilon_s \rightarrow \infty$

$$\sigma_s = E_{\infty} \varepsilon_s + (E_{s0} - E_{\infty}) \varepsilon_0$$

Equation 2.11

where, E_{s0} is the initial tangent modulus of the stress-strain curve, E_{∞} , R , $\varepsilon_0 = \sigma_0/E_{s0}$, σ_s , and ε_s are secondary tangent modulus, independent parameter which defines the curvature, strain at the intersection point between the tangent at the origin and the asymptote, stress and strain, respectively.



(Source: Menegotto and Pinto 1973)

FIGURE 2.3
Menegotto-Pinto Model

The Mengotto-Pinto model had some advantages over the Ramberg-Osgood model (Ramberg and Osgood 1943) in that it used more variables to define the curves geometry, which could be manipulated independently and identified on experimental diagrams. Also, the model was defined in stress as a function of strain being adaptable for use in stiffness method analysis. The deficiencies with both the Ramberg-Osgood and Menegotto-Pinto equations were that they did not accurately model the yield plateau or strain hardening region.

2.2.1.4 Park and Paulay's Model

Park and Paulay (1975) modeled the actual stress-strain curve of steel, in general shape. The proposed stress-strain curve for steel by them is shown in Figure 2.4. The governing equations for this model are as follows:

- region AB

$$f_s = \varepsilon_s E_s \quad \text{Equation 2.12}$$

- region BC

$$f_s = f_y \quad \text{Equation 2.13}$$

- region CD

$$f_s = f_y \left[\frac{m(\varepsilon_s - \varepsilon_{sh}) + 2}{60(\varepsilon_s - \varepsilon_{sh}) + 2} + \frac{(\varepsilon_s - \varepsilon_{sh})(60 - m)}{2(30r + 1)^2} \right] \quad \text{Equation 2.14}$$

where

$$m = \frac{(f_{su}/f_y)(30r + 1)^2 - 60r - 1}{15r^2} \quad \text{Equation 2.15}$$

and

$$r = \varepsilon_{su} - \varepsilon_{sh} \quad \text{Equation 2.16}$$

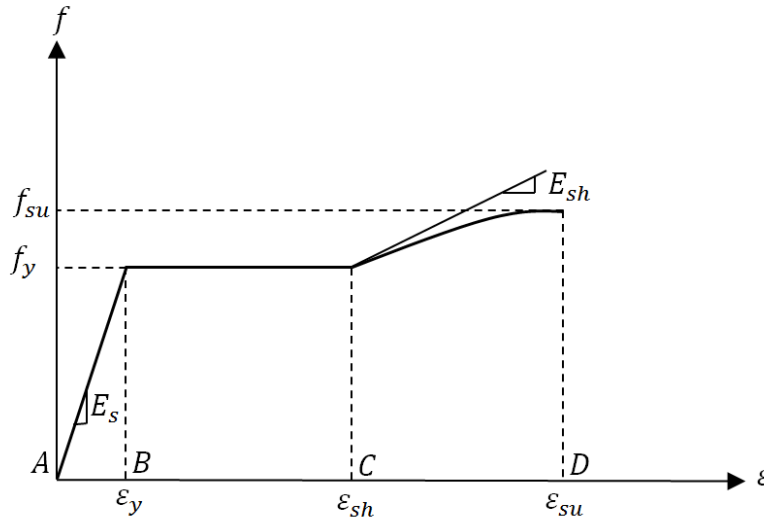


FIGURE 2.4
The Proposed Stress-Strain Curve by Mander et al. (1984)
and Park and Paulay (1975)

2.2.1.5 Mander et Al.'s Model

In some models, in order to have a better agreement with the actual behavior of mild steel, the strain hardening of steel may be approximated by a curve. One of these models is the model, proposed by Mander et al. (1984). Using proper parameters, the steel's stress-strain relationship, can be modeled accurately by Mander et al.'s model. The governing equations for Mander et al.'s model are as follows:

$$f_s = \begin{cases} E_{s0}\varepsilon_s & \varepsilon_s < \varepsilon_{sy} \\ f_{sy} & \varepsilon_{sy} < \varepsilon_s < \varepsilon_{sh} \\ f_{su} + (f_{sy} - f_{su})\left(\frac{\varepsilon_{su} - \varepsilon_s}{\varepsilon_{su} - \varepsilon_{sh}}\right)^p & \varepsilon_{sh} < \varepsilon_s < \varepsilon_{su} \end{cases} \quad \text{Equation 2.17}$$

where, ε_s is the steel strain; ε_{sh} , ε_{su} , f_s , f_{su} , f_{sy} and E_{s0} are the steel strain at the commencement of strain hardening, the steel strain at f_{su} , the steel stress, the ultimate tensile strength of the steel (Mander et al. 1984), the yield strength of the steel and the initial modulus of steel, respectively. The exponential p in above equations is defined as follow:

$$p = E_{sh} \left(\frac{\varepsilon_{su} - \varepsilon_{sh}}{f_{su} - f_{sy}} \right) \quad \text{Equation 2.18}$$

where, E_{sh} is the strain hardening modulus of steel (tangent at the commencement of the strain hardening branch).

2.2.1.6 Balan et Al.'s Model

Balan et al.'s model (1998) is based on the assumption that in natural coordinate the monotonic curve in compression is equal and opposite to the tension curve. Their proposed monotonic stress-strain relationship for reinforcing steel in tension in the engineering coordinate system is formulated as follow:

$$f_s = f_y \frac{(1 - \rho)}{2} \left[1 + \frac{(1 + \rho) \varepsilon_s}{(1 - \rho) \varepsilon_y} - \sqrt{\left(\frac{\varepsilon_s}{\varepsilon_y} - 1 \right)^2 + \delta} \right] \quad \text{Equation 2.19}$$

where, $\rho = E_h/E_s$ =hardening ratio, E_s , E_h , f_y , ε_y , f_s , and ε_s are the initial elastic modulus, the slope of the asymptote in the strain hardening region, the yield stress, the yield strain, steel stress and steel strain in engineering coordinate system, respectively. Equation 2.19 describes a family of parallel hyperbolas with two asymptotes. These parallel curves depend on the parameter δ , defined by:

$$\delta = \frac{\delta_0}{1 - \rho} \quad \text{Equation 2.20}$$

where, δ_0 can be interpreted as the area of the triangle bounded by two asymptotes and the tangent to the hyperbola at its vertex point. Equation 2.19 can be extended to generate the idealized tension and compression monotonic curves. In a single equation the following expression defined the linear region, the yield plateau and the strain-hardening region:

$$f_s = f_y' \frac{(1 - \rho')}{2} \left[1 + \frac{(1 + \rho') \varepsilon_s - \varepsilon_0}{(1 - \rho') \varepsilon_y'} - \sqrt{\left(\frac{\varepsilon_s - \varepsilon_0}{\varepsilon_y} - 1 \right)^2 + \delta'} \right] \quad \text{Equation 2.21}$$

where,

$$f_y' = \begin{cases} f_y & \text{for } \varepsilon_s \leq \varepsilon_{sh} \\ E_s \varepsilon_y' & \text{for } \varepsilon_s > \varepsilon_{sh} \end{cases} \quad \text{Equation 2.22}$$

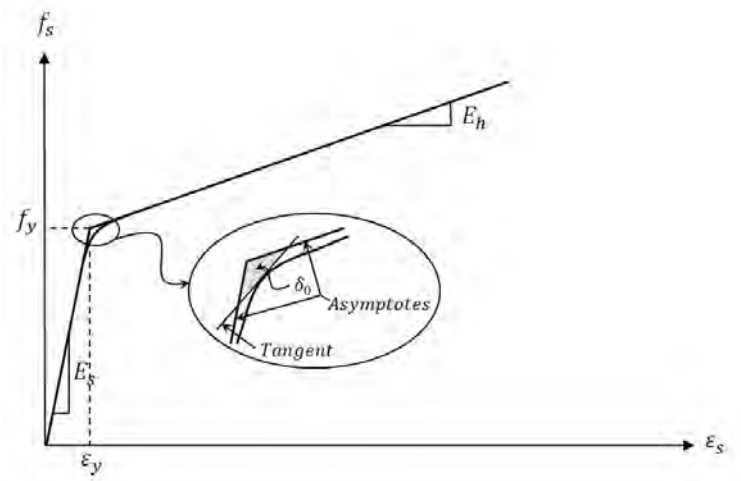
$$\rho' = \begin{cases} 0 & \text{for } \varepsilon_s \leq \varepsilon_{sh} \\ \frac{E_h}{E_s} & \text{for } \varepsilon_s > \varepsilon_{sh} \end{cases} \quad \text{Equation 2.23}$$

$$\delta' = \begin{cases} \delta_0 & \text{for } \varepsilon_s \leq \varepsilon_{sh} \\ \left(\frac{\varepsilon_{sh}}{\varepsilon_y} - 1 \right)^2 \delta_0 & \text{for } \varepsilon_s > \varepsilon_{sh} \end{cases} \quad \text{Equation 2.24}$$

$$\varepsilon_0 = \begin{cases} 0 & \text{for } \varepsilon_s \leq \varepsilon_{sh} \\ \left(\varepsilon_{sh} - \frac{f_y}{E_s}\right)^2 \delta_0 & \text{for } \varepsilon_s > \varepsilon_{sh} \end{cases} \quad \text{Equation 2.25}$$

$$\varepsilon'_y = \frac{1}{E_s(1 - \rho')} [(f_{su} - f_y) - (\varepsilon_{su} - \varepsilon_{sh})E_s\rho'] \quad \text{Equation 2.26}$$

where, ε_{sh} , f_{su} and ε_{su} are the strain at the onset of strain hardening, the ultimate stress and the ultimate strain, respectively. All the parameters, used in Equations 2.21 to 2.26 are shown in Figure 2.5.



(Source: Balan et al. 1998)

FIGURE 2.5
Stress-Strain Curve Defined by Equation 2.19

At first, the tension curve is defined in the engineering coordinate system, and is converted to the natural coordinate system using following equations:

$$\bar{\varepsilon} = \ln(1 + \varepsilon) \quad \text{Equation 2.27}$$

$$\bar{\sigma} = \sigma(1 + \varepsilon) \quad \text{Equation 2.28}$$

Where, $\bar{\varepsilon}$ and $\bar{\sigma}$ are the strain and stress in natural coordinate system.

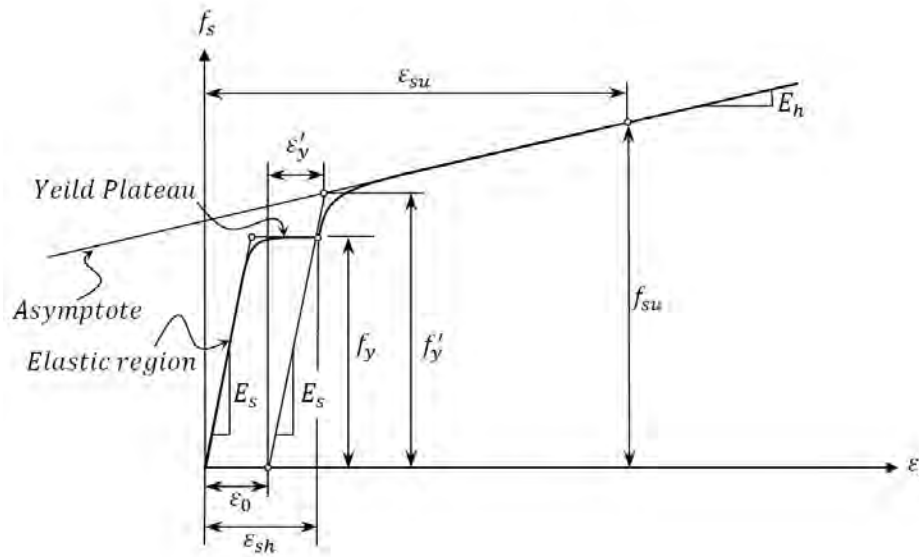
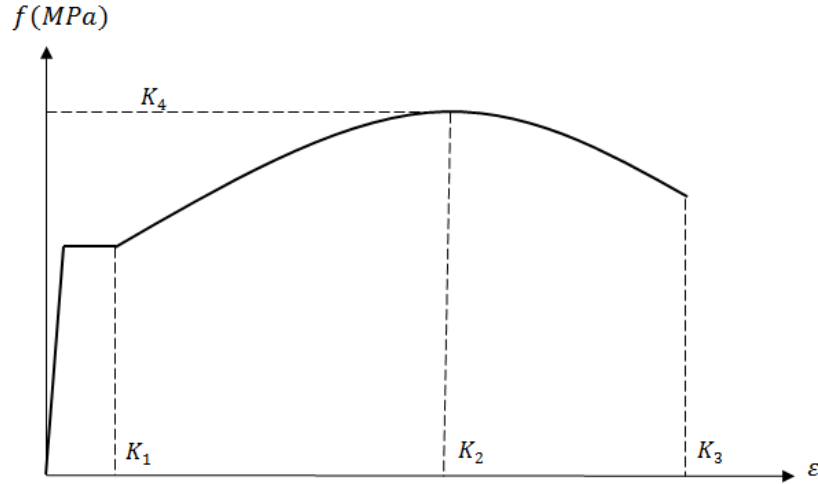


FIGURE 2.6
Monotonic Stress-Strain Curve for Reinforcing Steel (Balan 1998)

2.2.1.7 Esmaeily's Model

Esmaeily (Esmaeily and Xiao 2002) derived the following monotonic stress-strain curve shown in Figure 2.7 to model the response of steel in their computer program for reinforced concrete. The four parameters, used in this model, are defined by:

1. K_1 is the ratio of the strain at the start of the strain hardening to yield strain.
2. K_2 is the ratio of the strain at the ultimate stress to the yield strain.
3. K_3 is the ratio of the ultimate strain to the yield strain.
4. K_4 is the ratio of the ultimate stress to the yield stress.



(Source: Esmacily and Xiao 2002)

FIGURE 2.7
KSU-RC Model for Monotonic Stress-Strain Curve of Steel

The mathematical formulation of the model is as follows:

- For $0 < \varepsilon < \varepsilon_y \rightarrow \sigma = E_s \varepsilon$ where ε is the strain, ε_y is the yield strain of steel, σ is the stress and E_s is the modulus of elasticity of steel.
- For $\varepsilon_y < \varepsilon < K_1 \varepsilon_y \rightarrow \sigma = E_s \varepsilon_y$
- For $K_1 \varepsilon_y < \varepsilon < K_3 \varepsilon_y \rightarrow \sigma = \frac{E_s(1-K_4)[\varepsilon^2 + 2K_2(K_4-1)E_s|\varepsilon| + E_s\varepsilon_y(K_1^2K_4 - 2K_1K_2K_4 + K_2^2)]\varepsilon}{\varepsilon_y|\varepsilon|(K_1^2 - 2K_1K_2 + K_2^2)}$
- For $\varepsilon > K_3 \varepsilon_y \rightarrow \sigma = 0$

2.2.2 Concrete

A reinforced concrete section is usually composed of two parts, confined concrete and plain concrete. Many different models, some shown in Figure 2.8, have been suggested to simulate the monotonic behavior of confined and unconfined concrete. These models play an important role in compatibility of the data with the experimental test results. The following is a review of some of the existing models.

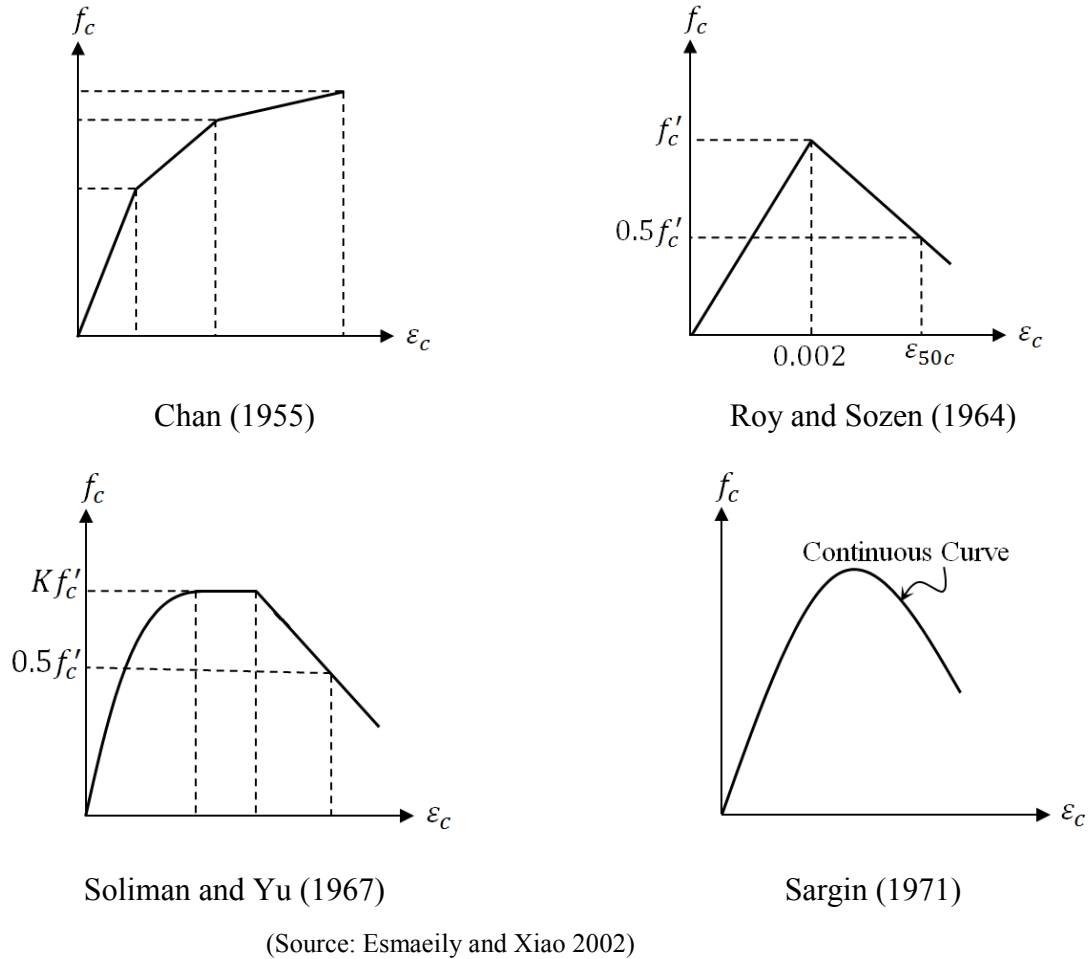


FIGURE 2.8
Samples of Some Proposed Stress-Strain Models for Confined Concrete

2.2.2.1 Richart's Model

One of the first works on the effect of transverse reinforcement on concrete compression behavior was conducted by Richart et al. (1928). In their tests, $100\text{mm} \times 200\text{mm}$ concrete cylinder specimens were subjected to different types of transverse pressure. By means of test results, he found out that strength and corresponding strain of the concrete were increasing proportional to the increase in transverse pressure. According to their test results, the compression strength of the concrete was expressed as follow:

$$f'_{cc} = f'_{co} + k \cdot f_r \quad \text{Equation 2.29}$$

where, f'_{cc} is the compression strength of the concrete with transverse pressure, f'_{co} , f_r , k and are the strength without pressure, the transvers pressure and the experimental coefficient, proposed as being 4.1 by Richart et al. (1928), respectively. The peak strain ϵ_{cc} , at the compression strength of confined concrete was expressed as:

$$\epsilon_{cc} = \epsilon_{co} \left[1 + 5 \left(\frac{f'_{cc}}{f'_{co}} - 1 \right) \right] \quad \text{Equation 2.30}$$

where, ϵ_{co} is the peak strain at the strength of plain concrete cylinders. This equation represent the simplest form of the Mohr-Coulomb two-parameter criterion, defining the shear stress as the function of the normal stress (Chen and Saleeb 1982).

2.2.2.2 Sheilkh and Uzumeri's Model

Sheikh and Uzumeri's model (1982) is one of the earliest models, developed for prediction of stress-strain relationship of confined concrete in tied columns. They conducted 24 tests and proposed their model according to those tests. Their model consists of three main sections. The first section represents a parabolic curve with its center coordinate (f_{cc}, ϵ_{s1}) , the second one is a horizontal line up to the strain ϵ_{s2} , and the third one represents an inclined line with a slop Z , continuing up to the point where the stress becomes $0.3f_{cc}$, after which it again continues horizontally. The complete mathematical expression of Sheikh and Uzumeri's model is expressed as follows:

$$f_{cc} = K_s f'_{co} \quad \text{Equation 2.31}$$

$$\epsilon_{s1} = 0.55 K_s f'_{co} \times 10^{-6} \quad \text{Equation 2.32}$$

$$\epsilon_{s2} = \epsilon_{co} \left[1 + \frac{0.81}{C} \left(1 - 5.0 \left(\frac{S}{B} \right)^2 \right) \frac{\rho_s f'_s}{\sqrt{f'_{co}}} \right] \quad \text{Equation 2.33}$$

where, f_{cc} is the strength of the confined concrete, ϵ_{s1} , ϵ_{s2} , and f'_{co} are the minimum strain corresponding to the maximum stress of the confined concrete, maximum strain corresponding to

the maximum stress of the confined concrete, and cylinder strength in *psi*. Here all stress are in *psi*, C is in inches. ϵ_{co} is the strain corresponding to the maximum stress in plain concrete specimen. The parameter K_s which is called strength gain factor was determined from regression analysis based on test of confined concrete columns:

$$K_s = 1.0 + \left[\frac{2.73B^2}{P_{occ}} \left(1 - \frac{nC^2}{5.5B^2}\right) \left(1 - \frac{s}{2B}\right)^2 \right] \sqrt{\rho_s f'_s} \quad \text{Equation 2.34}$$

where, f'_s is the stress in the lateral reinforcement in *ksi* and P_{occ} is in *kips*. The slope Z for the third section of the stress-strain curve is expressed as:

$$Z = \frac{0.5}{\frac{3}{4} \rho_s \sqrt{\frac{B}{s}}} \quad \text{Equation 2.35}$$

where, s is the spacing of the transvers reinforcement; C , n , and ρ_s are center to center distance between longitudinal bars, the number of curvature between the longitudinal bars and the volumetric ratio of transvers reinforcement, respectively. P_{occ} is described by the following equation:

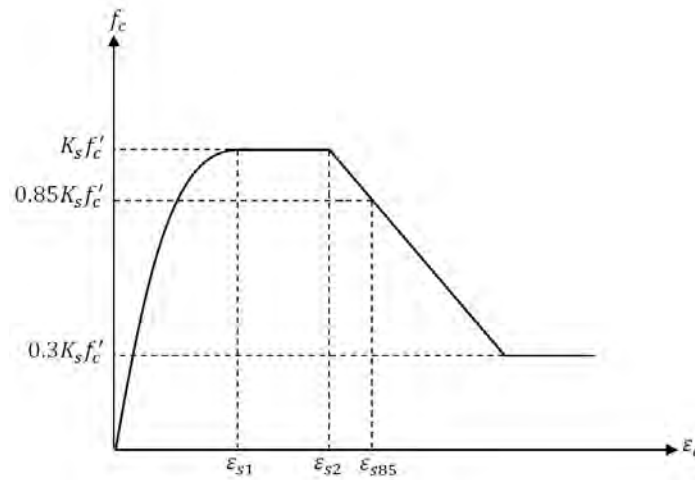
$$P_{occ} = f'_{co} (A_{co} - A_s) \quad \text{Equation 2.36}$$

$$\text{Equation 2.37}$$

where

$$A_{co} = B \times H$$

In above equations, A_s is the total sectional area of the longitudinal steel bars; A_{co} is the area of the confined concrete core, B and H center to center distance of perimeter hoop of the rectangular concrete core.



(Source: Sheikh and Uzumeri 1982)

FIGURE 2.9
Sheikh and Uzumeri's Model

Sheikh and Uzumeri (1982) mentioned that the maximum error in the predicted K_s value on the unsafe side is less than 4%, and the maximum conservative error is about 7%. They also proposed ε_{s85} , confined strain corresponding to 85% of the maximum concrete stress on the unloading of the stress-strain curve, as follow:

$$\varepsilon_{s85} = 0.225\rho_s \sqrt{\frac{B}{S}} + \varepsilon_{s2} \quad \text{Equation 2.38}$$

It is assumed as the ultimate strain of confined concrete.

2.2.2.3 Mander et Al.'s Model

Mander et al. (1988) developed a general model for concrete which is confined by various type of transverse reinforcement. Their model has been widely used in analyzing columns with both circular and rectangular cross section (Xiao 1996). The transverse reinforcement can be circular or spiral, rectangular hoops with or without cross ties. Furthermore, load application can be either static or dynamic, applied monotonically or by load cycles. Mander et al. conducted tests on full-scale confined reinforced concrete columns, with

concrete strength of 30 MPa and steel yield strength of 300 MPa. The mathematical expression of Mander's et al. model is expressed as follows:

$$f_c = \frac{f'_{cc} x r}{r - 1 + x^r} \quad \text{Equation 2.39}$$

where, x is the strain to the stress at peak point, f'_{cc} and r are the peak stress for confined concrete and the ratio of concrete's initial modulus of elasticity to the different of initial and secant modulus of elasticity.

$$x = \frac{\varepsilon_c}{\varepsilon_{cc}} \quad \text{Equation 2.40}$$

$$\varepsilon_{cc} = \left[R \left(\frac{f'_{cc}}{f'_{co}} - 1 \right) + 1 \right] \varepsilon_{co} \quad \text{Equation 2.41}$$

$$r = \frac{E_c}{E_c - E_{sec}} \quad \text{Equation 2.42}$$

$$E_c = 5000 \sqrt{f'_{co}} \quad (\text{MPa}) \quad \text{Equation 2.43}$$

$$E_{sec} = \frac{f'_{cc}}{\varepsilon_{cc}} \quad \text{Equation 2.44}$$

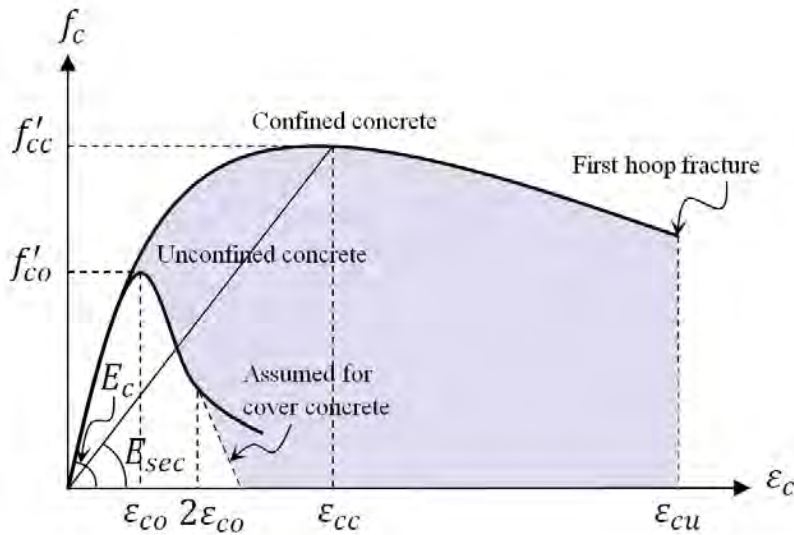
where, f'_{co} is the concrete strength, ε_c , R , and f'_{cc} are the strain corresponding to the cylinder strength, an empirical value determined experimentally that based on Mander et al. research, it varies from 3 for high strength concrete to 6 for normal strength concrete and the peak longitudinal compressive stress for confined concrete which is expressed as follow:

$$f'_{cc} = f'_{co} \left(2.254 \sqrt{1 + \frac{7.84 f'_l}{f'_{co}} - \frac{2 f'_l}{f'_{co}} - 1.254} \right) \quad \text{Equation 2.45}$$

where, f'_l is the effective lateral confining stress, defined as:

$$f'_l = \frac{1}{2} K_e \rho_s f_{yh} \quad \text{Equation 2.46}$$

In equation 2.46, K_e is the confinement effectiveness coefficient and it takes into account the efficiency of different types of transverse reinforcement. Based on different types of transverse reinforcement, Mander et al. proposed different equations for this parameter.



(Source: Mander et al. 1988)

FIGURE 2.10
Mander's Model

2.2.2.4 Fafitis and Shah's Model

Fafitis and Shah's model (1985) is based on their experimental test results. Their model initially developed for circular columns. For columns with square section, they proposed that these types of columns can be treated as circular columns with core diameters equal to the side of square core. The confinement index to estimate the effective confining pressure was defined as:

$$f_r = \frac{A_{sh} f_{yh}}{d_c s} \quad \text{Equation 2.47}$$

where, A_{sh} is the total section area of the transverse reinforcement in vertical cross section within spacing s , d_c and f_{yh} are the equivalent diameters for a square column section, assuming

it equals to the side of the confined square concrete core and yield strength of confinement steel, respectively.

The complete stress-strain curve includes two branches, ascending branch and descending branch. Both branches meet at the peak point with a zero slop that avoids any discontinuity. The complete mathematical expressions describing Fafitis and Shah's model are:

$$f_c = f'_c \left[1 - \left(1 - \frac{\varepsilon_c}{\varepsilon_{cc}} \right)^A \right] \quad \text{for } 0 < \varepsilon_c \leq \varepsilon_{cc} \quad \text{Equation 2.48}$$

$$f_c = f'_{cc} \cdot \exp[-k(\varepsilon_c - \varepsilon_{cc})^{1.15}] \quad \text{for } \varepsilon_c > \varepsilon_{cc}$$

where, f'_{cc} is the confined concrete strength and ε_{cc} is the strain at confined concrete which are calculated based on the unconfined concrete cylinder strength f'_c and the confinement index f_r .
And:

$$A = E_c \frac{\varepsilon_{cc}}{f'_{cc}} \quad \text{Equation 2.49}$$

$$k = 24.65 f'_c \cdot \exp\left(-0.01 \frac{f_r}{\lambda_1}\right) \quad \text{Equation 2.50}$$

$$E_c = 33 \omega^{1.15} \sqrt{f'_c} \text{ (psi)} \quad \text{Equation 2.51}$$

$$\lambda_1 = 1 - 25 \left(\frac{f_r}{f'_c} \right) (1 - \exp(-3.24 f'_c)^9) \quad \text{Equation 2.52}$$

The factor λ_1 depends on the concrete strength and degree of the confinement. This model can be easily used for unconfined concrete by taking $f_r = 0$. The value of the parameter k is equal to zero corresponds to perfectly brittle behavior, while an infinity large k corresponds to perfectly plastic behavior of confined concrete.

2.2.2.5 Sakino and Sun's Model

Sakino and Sun (1993) proposed a model for confined concrete stress-strain relationship, based on the tests, he conducted on circular and rectangular columns under axial loading. The main stress-strain equation is as:

$$\sigma_c = \sigma_{cB} \frac{AX + (D - 1)X^2}{1 + (A - 2)X + DX^2} \quad \text{Equation 2.53}$$

where, σ_{cB} is the confined concrete strength and is determined as:

$$\sigma_{cB} = \sigma_p + \kappa \rho_h \sigma_{yh} \quad \text{Equation 2.54}$$

where, σ_{yh} is the steel strength, σ_p stands for plain concrete stress and is determined as follow:

$$\sigma_p = \mu \sigma_B \quad \text{Equation 2.55}$$

In Equation 2.55, σ_B and μ are the strength of a standard concrete cylinder, and a coefficient which is 0.8 for circular columns and 1.0 for square columns, respectively. κ is a coefficient which is different for circular and square columns. For square columns it is determined as:

$$\kappa = k_s \left(\frac{d''}{C} \right) \left(1 - \frac{s}{2D_c} \right) \quad \text{Equation 2.56}$$

where, $k_s = 11.5$, D_c and C are the center to center dimension of a steel hoop and transverse distance between any two anchored longitudinal bars, respectively. The following are the three parameters used in Equation 2.57:

$$X = \frac{\varepsilon_c}{\varepsilon_{co}} \quad \text{Equation 2.57}$$

$$A = \frac{E_c \varepsilon_{co}}{\sigma_{cB}} \quad \text{Equation 2.58}$$

$$K = \frac{\sigma_{cB}}{\sigma_p} \quad \text{Equation 2.59}$$

In the equations above, ε_{co} is the strain corresponding to peak stress of confined concrete member and it's determined as:

$$\varepsilon_{co} = \varepsilon_o \begin{cases} 1 + 4.7(K - 1) & K \leq 1.5 \\ 3.35 + 20(K - 1.5) & K \geq 1.5 \end{cases} \quad \text{Equation 2.60}$$

where, ε_o is the cylinder strain at peak stress and it's expressed as:

$$\varepsilon_o = 0.5243(\sigma_{cB})^{\frac{1}{4}} \times 10^{-3} \quad \text{Equation 2.61}$$

and, E_c is the Young modulus which is calculated as follow:

$$E_c = 4k \left(\frac{\sigma_{cB}}{1000} \right)^{\frac{1}{3}} \times 10^5 \times \left(\frac{\gamma}{2.4} \right)^2 \quad \text{Equation 2.62}$$

k is the empirical coefficient, depending on the raw material type in concrete mix and it is expressed as:

$$k = \begin{cases} 1.0 \\ 1.2 \\ 0.9 \end{cases} \quad \text{Equation 2.63}$$

The variable D in the main stress-strain equation is determined as:

$$D = \alpha + \beta \sigma_B + \gamma \sqrt{\frac{(K - 1) \sigma_B}{23}} \quad \text{Equation 2.64}$$

where, $\alpha = 1.5$; $\beta = -1.68 \times 10^{-3}$; and $\gamma = 0.75$ for steel tube and $\gamma = 0.50$ for square hoops.

2.2.2.6 Saatcioglu and Razavi's Model

The model proposed by Saatcioglu and Razvi (1992) for confined concrete consists of two parts: a parabolic ascending branch and a linear descending branch. Lateral reinforcement in the form of equivalent lateral pressure in both circular and rectangular columns was used to develop the model characteristics for strength and ductility of the confined concrete. They used different types of lateral reinforcement such as spiral, rectangular hoops, and cross-ties and compared their model with different types of column tests, including circular, square and rectangular columns. In this report we just represent a part of their model for square columns. Confined concrete strength is calculated as:

$$f'_{cc} = f'_{co} + k_1 f_1 \quad \text{Equation 2.65}$$

where, f'_{cc} and f'_{co} are confined and unconfined strength of concrete in a member, respectively. Coefficient k_1 depends on uniform lateral confining pressure f_1 . Based on the test results, a relationship between these two parameters have been established as:

$$k_1 = 6.7(f_1)^{-0.17} \quad \text{Equation 2.66}$$

Unconfined concrete strength f'_{co} is the plain concrete strength in a member under concentric loading. It might be different with the standard cylinder strength. Obtaining the lateral confining pressure from circular column tests which is different with square and rectangular columns, the effective lateral pressure f_{le} has been proposed by:

$$f_{le} = k_2 f_1 \quad \text{Equation 2.67}$$

and

$$f_l = \frac{\sum A_s f_{yt} \sin \alpha}{s b_c} \quad \text{Equation 2.68}$$

where, k_2 and α are the 1.0 for circular columns and square columns with closely spaced lateral and laterally supported longitudinal reinforcement and the angle between transverse reinforcement and b_c which is equal to 90° if they are perpendicular. In general k_2 is expressed as follow:

$$k_2 = 0.26 \sqrt{\left(\frac{b_c}{s}\right) \left(\frac{b_c}{s_l}\right) \left(\frac{1}{f_l}\right)} \quad \text{Equation 2.69}$$

where, f_l is in MPa. The strain corresponding to the peak stress of confined concrete f'_{cc} is denoted as ε_1 and is calculated like previous researchers (Balmer 1949, Mander et al. 1988):

$$\varepsilon_1 = \varepsilon_{01}(1 + 5K) \quad \text{Equation 2.70}$$

and

$$K = \frac{k_1 f_{le}}{f'_{co}} \quad \text{Equation 2.71}$$

where, ε_{01} is the strain corresponding to peak stress of confined concrete which should be determined under the same rate of loading used for the confined concrete. In the absence of experimental data, the value 0.002 may be used. This includes the first part of this model, the ascending branch which is expressed as follow, based on all above mentioned:

$$f_c = f'_{cc} \left[2 \left(\frac{\varepsilon_c}{\varepsilon_1} \right) - \left(\frac{\varepsilon_c}{\varepsilon_1} \right)^2 \right]^{\frac{1}{1+2K}} \leq f'_{cc} \quad \text{Equation 2.72}$$

The second part of this model, descending branch of the curve is linear and connects the point (f'_{cc}, ε_1) and $(0.85f'_{cc}, \varepsilon_{85})$ on the plain of the stress-strain curve. The following is the value of strain corresponding to 85% of confined concrete strength:

$$\varepsilon_{85} = 260\rho\varepsilon_1 + \varepsilon_{085} \quad \text{Equation 2.73}$$

where, ρ is the volumetric ratio of transvers reinforcement and is expressed as:

$$\rho = \frac{\sum A_s}{s(b_{cx} + b_{cy})} \quad \text{Equation 2.74}$$

and ε_{085} is the strain corresponding to 85% strength level beyond the peak stress of unconfined concrete and it should be determined by experimental results. In absence of test results, the value 0.0038 might be used.

2.2.2.7 KSU-RC Model Based on Mander's Model

The monotonic stress-strain model for confined and plain concrete, employed in KSU-RC for analysis of the seismic behavior of bridge piers under different loading condition, is as model, proposed by Mander et al. (1988) (see Figure 2.10). The ultimate strain for cover and confined concrete is determined based on the energy based principle proposed by Mander. Based on this method, by equating the ultimate strain energy capacity of the confining reinforcement per unit volume of concrete core (U_{sh}) to the difference in area between the confined (U_{cc}) and unconfined (U_{co}) concrete stress-strain curves, plus additional energy required to maintain yield in the longitudinal steel in compression (U_{sc}), the longitudinal concrete compressive strain corresponding to hoop fracture can be calculated. Therefore:

$$U_{sh} = U_{cc} + U_{sc} - U_{co} \quad \text{Equation 2.75}$$

Substituting corresponding values in above equation gives:

$$\rho_s A_{cc} \int_0^{\varepsilon_{sf}} f_s d\varepsilon_s = A_{cc} \int_0^{\varepsilon_{cu}} f_c d\varepsilon_c + \rho_{cc} A_{cc} \int_0^{\varepsilon_{cu}} f_{sl} d\varepsilon_c - A_{cc} \int_0^{\varepsilon_{sp}} f_c d\varepsilon_c \quad \text{Equation 2.76}$$

where, ρ_s , A_{cc} , f_s , ε_s , ε_{sf} , f_c , ε_c , ε_{cu} , ρ_{cc} , f_{sl} , and ε_{sp} are ratio of volume of transverse reinforcement to volume of concrete core; area of the concrete core; stress in transverse reinforcement, strain in transverse reinforcement, fracture strain of transverse reinforcement, longitudinal compressive stress, longitudinal compressive strain, ultimate longitudinal concrete compressive strain, ratio of volume of longitudinal reinforcement to volume of concrete core; stress in longitudinal reinforcement, and spalling strain of unconfined concrete.

In the first term of the left hand side of Equation 2.77, the expression

$$\int_0^{\varepsilon_{sf}} f_s d\varepsilon_s = U_{sh} \quad \text{Equation 2.77}$$

is the total area under stress-strain curve for the transverse reinforcement up to fracture strain ε_{sf} . Mander et al. have concluded from several test results that the above value is independent of bar size or yield strength and can be taken within 10% accuracy as:

$$U_{sh} = 110 \text{ MJ/m}^3 \quad \text{Equation 2.78}$$

The area under the stress-strain curve for unconfined concrete may be approximated as:

$$\int_0^{\varepsilon_{sp}} f_c d\varepsilon_c = 0.017 \sqrt{f'_{co}} \text{ MJ/m}^3 \quad \text{Equation 2.79}$$

where, f'_{co} is the quasi static compressive strength of concrete in MPa. Thus Equation 2.66 simplifies to:

$$110\rho_s = \int_0^{\varepsilon_{cu}} f_c d\varepsilon_c + \rho_{cc} \int_0^{\varepsilon_{cu}} f_{sl} d\varepsilon_c - 0.017\sqrt{f'_{co}} MJ/m^3 \quad \text{Equation 2.80}$$

Knowing the preliminary data, unlimited confined concrete strain at the first rupture of transverse steel can numerically be evaluated. This model has been implemented in KSU-RC to evaluate the ultimate confined concrete strain.

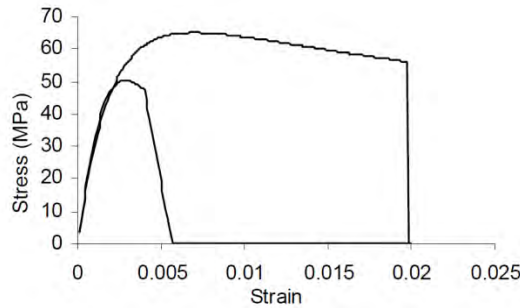


FIGURE 2.11
Confined and Cover Concrete
Envelope Curves As Used in KSU-
RC for Analysis

2.3 Hysteretic (Cyclic) Response

Because hysteretic behavior of steel and concrete have remarkable effect on the hysteretic behavior of reinforced concrete member, simulating the hysteretic behavior of steel and concrete are crucial in detailed study. General observations show that the hysteretic response curve includes three components for any material of a structural member. The following are these three components:

- Envelope curves which are the backbone of the general hysteretic response. The envelope curves can be fixed or re-located. By shifting and scaling the envelope curves, one can simulate the degradation of material, the phenomenon that has been observed during almost all the experiments. Degradation also can be simulated by shifting the returning point. On the other hand, the return point to an envelope curve should be different with the point that the last reversal occurred from.

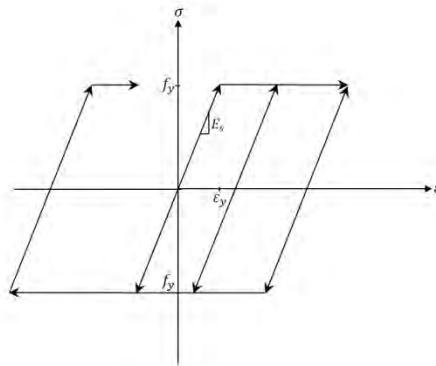
- Connection curve which are the connections between envelop curves. Usually more than one equation should be used to simulate these kinds of curves; since there are several inflection points in these curves to represent pinching, and other softening and hardening phenomena within material or structural element.
- Transition curves which are employed when a reversal from a connecting curve takes place to make the transition to the connecting curve that goes in the opposite direction.

There are many different hysteretic models to simulate the hysteretic behavior of steel and concrete. The following are some hysteretic models, proposed for steel and concrete.

2.3.1 Steel

2.3.1.1 Simple Bi-Linear Hysteretic Model

A simple hysteretic model, shown in Figure 2.12, is a bi-linear stress-strain relationship of steel. The results, obtained by using this model in analysis, are not good as the results from a more realistic model. This model doesn't consider any degradation in stiffness or strength and the stiffness hardening is also ignored as for the bi-linear monotonic stress-strain curve.



(Source: Esmaily and Xiao 2002)

FIGURE 2.12
Simple Bi-Linear Hysteretic
Model for Steel

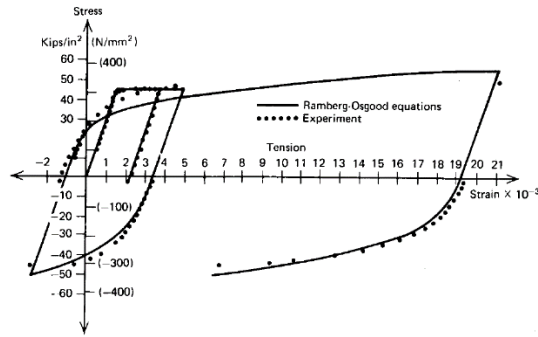


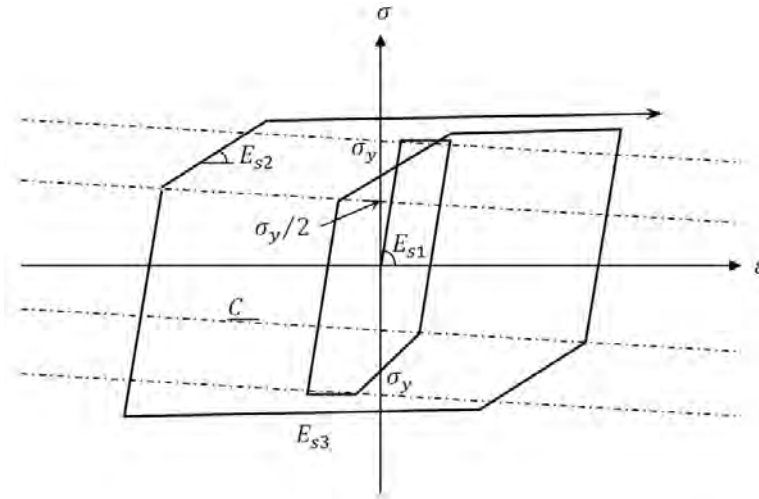
FIGURE 2.13
Hysteretic Response of Steel, Based
on Ramberg-Osgood Equations

2.3.1.2 Ramberg-Osgood Model

Using the Ramberg-Osgood model (1943), hysteretic behavior of reinforcing steel can be calculated. This model, in comparison to experimental data on a sample with the same specifications in terms of yield, ultimate strength, and modulus of elasticity, is shown in Figure 2.13. The Ramberg-Osgood model equation is as follows:

$$\varepsilon_s - \varepsilon_{si} = \frac{f_s}{E_s} \left(1 + \left| \frac{f_s}{f_{ch}} \right|^{r-1} \right) \quad \text{Equation 2.81}$$

where r and f_{ch} are the parameters dependent on the loading run number and stress dependent on the yield strength and the plastic in the steel produced in the previous loading run which have been chosen empirically; ε_s , ε_{si} , f_s , and E_s are steel strain, steel strain at zero stress at beginning of loading run, steel stress and modulus of elasticity of steel.



(Source: Michio 1982)

FIGURE 2.14
Michio Tri-Linear Hysteretic Curve for Reinforcing Steel

2.3.1.3 Michio Tri-Linear Model

Michio tri-linear model is shown in Figure 2.14. As shown in Figure 2.14, yield strength in both tension and compression sides are assumed to be equal. The second and third level stiffness can be tuned to get closed to a desired response. Kuramoto et al. (Kuramoto 1995) in their research on influence of axial deformation on ductility of high-strength reinforced concrete columns under varying tri-axial forces, have taken the post yield stiffness E_{s3} , and reduced stiffness because of Baushinger effect E_{s2} as 1/200 and 1/10 of the elastic stiffness, respectively. The model, used to simulate the hysteretic behavior of reinforcing steel in KSU-RC, is similar to this model; although, its flexibility is more than this model.

2.3.1.4 Gomes and Appleton's Model

Gomes and Appleton (1997) modified the Menegotto-Pinto cyclic stress-strain relationship to take into account the effect of inelastic buckling of the longitudinal reinforced bars. For the first loading a bi-linear diagram with hardening was adopted that expressed as follows:

$$\sigma_s = \begin{cases} \varepsilon_s E_s & \text{if } |\varepsilon_s| < \varepsilon_{s0} \\ \sigma_{s0} + (\varepsilon_s - \varepsilon_{s0}) E_{s1} & \text{if } \varepsilon_s > \varepsilon_{s0} \\ -\sigma_{s0} - (\varepsilon_s - \varepsilon_{s0}) E_{s1} & \text{if } \varepsilon_s < -\varepsilon_{s0} \end{cases} \quad \text{Equation 2.82}$$

where, ε_s , σ_s , ε_{s0} , σ_{s0} , E_s and E_{s1} are steel strain, steel stress, yield strain, yield stress, tangent modulus of elasticity at origin and tangent modulus of elasticity of hardening branch, respectively.

2.3.1.5 Balan et Al.'s Model

Balan et al. (1998) proposed a macroscopic hysteretic model of the short-term cyclic behavior of ordinary and high-strength reinforcing steel. The monotonic model, expressed before in Equation 2.19 is used as backbone for the general hysteretic material model for reinforcing steel which its origin is shifted to point in order to describe cyclic response. Taking into account the shift transformation, Equation 2.19 becomes:

$$f_s = f_y' \frac{(1 - \rho')}{2} \left[1 + \frac{(1 + \rho')}{(1 - \rho')} \frac{\varepsilon_s - \varepsilon_0'}{\varepsilon_y'} - \sqrt{\left(\frac{\varepsilon_s - \varepsilon_0'}{\varepsilon_y'} - 1 \right)^2 + \delta'} \right] \quad \text{Equation 2.83}$$

where,

$$f_y' = \begin{cases} f_y & \text{for } \varepsilon_s - \varepsilon_0 \leq \varepsilon_{sh} \\ E_s \varepsilon_y' & \text{for } \varepsilon_s - \varepsilon_0 > \varepsilon_{sh} \end{cases} \quad \text{Equation 2.84}$$

$$\rho' = \begin{cases} 0 & \text{for } \varepsilon_s - \varepsilon_0 \leq \varepsilon_{sh} \\ \frac{E_h}{E_s} & \text{for } \varepsilon_s - \varepsilon_0 > \varepsilon_{sh} \end{cases} \quad \text{Equation 2.85}$$

$$\delta' = \begin{cases} \delta_0 & \text{for } \varepsilon_s - \varepsilon_0 \leq \varepsilon_{sh} \\ \left(\frac{\varepsilon_{sh}}{\varepsilon_y} - 1 \right)^2 \delta_0 & \text{for } \varepsilon_s - \varepsilon_0 > \varepsilon_{sh} \end{cases} \quad \text{Equation 2.86}$$

$$\varepsilon_0' = \begin{cases} \varepsilon_0 & \text{for } \varepsilon_s - \varepsilon_0 \leq \varepsilon_{sh} \\ \varepsilon_0 + \left(\varepsilon_{sh} - \frac{f_y}{E_s} \right) & \text{for } \varepsilon_s - \varepsilon_0 > \varepsilon_{sh} \end{cases} \quad \text{Equation 2.87}$$

$$\varepsilon_y' = \frac{1}{E_s(1 - \rho')} [(f_{su} - f_y) - (\varepsilon_{su} - \varepsilon_{sh})E_s\rho'] \quad \text{Equation 2.88}$$

Differentiation of Equation 2.89 with respect to the strain, yields the tangent modulus E_t on the envelope branches in the engineering coordinate:

$$E_t = \frac{E_s}{2}(1 - \rho) \left[\frac{(1 + \rho)}{(1 - \rho)} - \frac{\left(\frac{\varepsilon_s - \varepsilon_0}{\varepsilon'_y} - 1\right)}{\sqrt{\left(\frac{\varepsilon_s - \varepsilon_0}{\varepsilon'_y} - 1\right)^2 + \delta'}} \right] \quad \text{Equation 2.89}$$

Reversal Branches

When a load reversal takes place, the stress-strain behavior of steel is described by a reversal branch which is approximated by a hyperbola in this model. In engineering coordinate, this reversal branch is obtained by rewriting Equation 2.83 as follows:

$$f_s = {}^k f_y \frac{(1 - \rho')}{2} \left[1 + \frac{(1 + \rho) \varepsilon_s - {}^k \varepsilon_r}{(1 - \rho) {}^k \varepsilon_y} - \sqrt{\left(\frac{\varepsilon_s - {}^k \varepsilon_r}{{}^k \varepsilon_y} - 1\right)^2 + {}^k \delta} \right], \quad (k = 0, 1, \dots, n)$$

Equation 2.90

Where superscript k indicate the unloading-reloading cycles. ε_r , $\rho = E_h / {}^k E_u$, ${}^k E_u$, ${}^k f_y$, and, ${}^k \varepsilon_y$ are reversal strain, instantaneous hardening, unloading modulus, instantaneous yield stress and strain, respectively. All parameters that have superscript k are updated after each load reversal. The instantaneous yield stress is defined as follow:

$${}^k f_y = {}^k E_u {}^k \varepsilon_y, \quad (k = 0, 1, \dots, n) \quad \text{Equation 2.91}$$

where

$${}^k \varepsilon_y = \varepsilon_y \frac{\rho}{(1 - \rho)} {}^k \varepsilon_0, \quad (k = 0, 1, \dots, n) \quad \text{Equation 2.92}$$

and

$${}^k \varepsilon_0 = {}^k \varepsilon_r - \frac{{}^k f_r}{{}^k E_u}, \quad (k = 0, 1, \dots, n) \quad \text{Equation 2.93}$$

In Equations 2.91 to 2.93, ${}^k\varepsilon_0$, ε_y , ${}^k f_r$, and ${}^k\varepsilon_r$ are the strain at the intersection of the instantaneous unloading asymptote with the strain axis after the k-reversal, initial engineering yield strain, stress and strain, respectively. The yield stress ${}^k f_y$ and the yield strain ${}^k\varepsilon_y$ are the coordinate of the point that unloading and strain hardening asymptotes intersect.

In these equations, called degradation parameters, is the parameter that shapes the transition between two asymptotes and allows for a good representation on Bauschinger effect. Degradation parameter defined as follow which is applicable to both normal and high strength steel bars:

$${}^k\delta = \frac{\delta_0}{1-\rho} \left[1 + {}^k a \left(\frac{{}^k\varepsilon_p}{{}^k\varepsilon_y} \right)^2 \right], \quad (k = 0, 1, \dots, n) \quad \text{Equation 2.94}$$

where ${}^k\varepsilon_p$ is the plastic strain amplitude, δ_0 is the initial value of δ that is defined as follow:

$$\delta_0 = \begin{cases} 0.005 & \text{for ordinary steel (grades 40 and 60)} \\ 0.01 & \text{for high - strength steel (higher grade)} \end{cases} \quad \text{Equation 2.95}$$

and ${}^k a$ is the amplitude parameter that is the difference between complete and incomplete reversals and defined as follow:

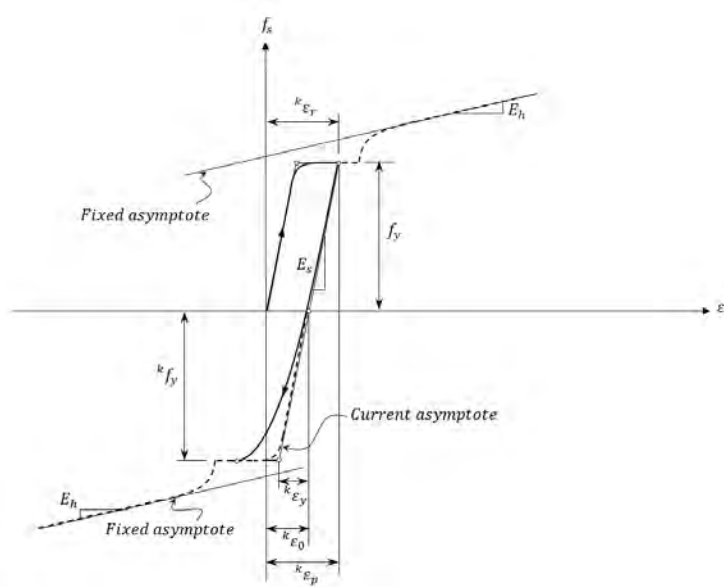
$${}^k a = \begin{cases} 6 & \text{for } \frac{{}^k f_r - {}^{k-1} f_r}{f_y} \geq 2 \\ 3 & \text{for } \frac{{}^k f_r - {}^{k-1} f_r}{f_y} < 2 \end{cases} \quad \text{Equation 2.96}$$

The tangent modulus is obtained upon differentiation of Equation 2.90 with respect to the steel strain:

$${}^k E_t = \frac{{}^k E_u}{2} (1 - \rho) \left[\frac{(1 + \rho)}{(1 - \rho)} - \frac{\left(\frac{\varepsilon_s - k\varepsilon_r}{k\varepsilon_y} - 1 \right)}{\sqrt{\left(\frac{\varepsilon_s - k\varepsilon_r}{k\varepsilon_y} - 1 \right)^2 + k\delta}} \right] \quad \text{Equation 2.97}$$

Although, in all practical purposes the unloading modulus can be assumed equal to the initial stiffness, Balan et al. (1998) used the expression which is proposed by Dodd and Restrepo-Posada for unloading modulus that is defined as follows:

$${}^k E_u = E_s \left[0.83 + \frac{0.001}{0.006 + ({}^k \varepsilon_p - \varepsilon_y)} \right] \quad \text{Equation 2.98}$$



(Source: Balan et al. 1998)

FIGURE 2.15
Load Reversal from Yield Plateau

In this model, three types of reversals are defined that are described briefly as follows:

1. Reversal from yield plateau

As shown in Figure 2.15, in this case the reversal curve is described by a softened envelope shifted in the opposite direction.

2. Reversal from strain hardening region

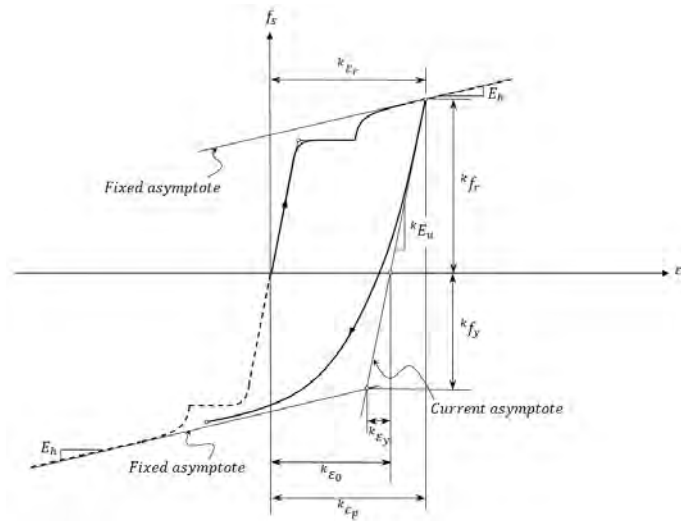
As shown in Figure 2.16 when the reversal takes place from the strain-hardening region of the envelope curve, the reversal is described by a softened hyperbola curve, defined in Equation 2.90.

3. Reversal from reversal curves

If the following condition is not satisfied, the reversal assumed to be incomplete.

$${}^k f_r - {}^{k-1} f_r \geq 2f_y \quad \text{Equation 2.99}$$

Both complete and incomplete reversals follow the same rules as the reversal from the strain-hardening region of the envelope. As mentioned the only difference between these two, is in amplification parameter.



(Source: Balan et al. 1998)

FIGURE 2.16
Load Reversal from Strain-Hardening Region

As shown in Figure 2.17, the reversal curve from a reversal has two asymptotes, an initial one with slope ${}^k E_u$, defined by Equation 2.98 and the strain-hardening asymptote with constant slope E_h .

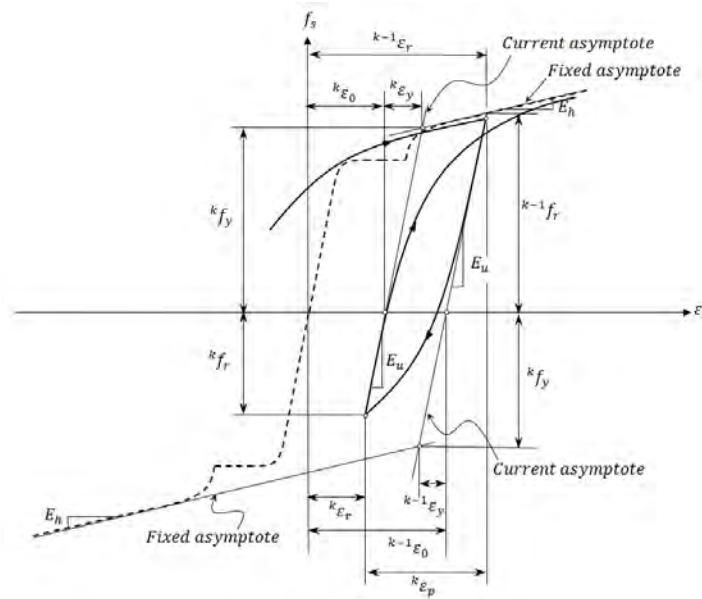


FIGURE 2.17
Load Reversal from Reversal Curve

2.3.1.6 Esmaily Steel Hysteretic Model Developed and Used in KSU-RC

The model, developed and used in KSU-RC mode, is very similar to Michio tri-linear model and has three major parts as is common for any hysteretic model. At first, the stress and strain follow the monotonic stress-strain curve for steel which is explained in the previous section. At the strain reversal point the modulus of elasticity assumed to be equal to the initial modulus of elasticity of steel. After the stress sign changes from positive to negative or vice versa, the same elasticity is assumed up to a stress where its absolute value is a portion of the yield strength of the steel. This value can be set with parameter P_1 and the value stress is $P_1 f_y$, where f_y is the yield strength of steel. At this point, the stiffness changes to a fraction of the initial stiffness simulating the Bauchinger effect. The value of the secondary stiffness can be tuned by changing parameter P_2 or P_3 . In this model, for the first and third quarter of the coordinate plane, the secondary stiffness would be $P_2 E_s$; while, for the second and fourth quarter of the coordinate plan it would be $P_3 E_s$. These changes in stiffness are for better simulating the strain hardening effect. At the end, the stress-strain curve follows a linear path on the same stress side, connecting the point at ultimate strain (ϵ_u or $-\epsilon_u$) and strength (f_y) to the point with a stress $P_4 f_y$ on the opposite strain side and at the ultimate strain ($-\epsilon_u$ or ϵ_u). Due to assuming a

symmetrical stress-strain curve for steel, the behavior of the model is symmetric with respect to the origin and the direction of movement is as shown in Figure 2.18.

The model can be expressed mathematically, by defining the stress and strain situation for the states where the previous stress and strain state (ε_p and σ_p) is one of the point 1, 2, or 3 as follows:

- For point 1, provided no strain reversal has occurred previously for strains more than the yield strain in positive or negative direction (tension or compression), the movement follows the monotonic stress-strain curve of steel.

- For point 2:
If $\varepsilon > \varepsilon_p - \frac{\sigma_p + P_1 f_y}{E_s}$

$$\sigma = \sigma_p + E_s(\varepsilon - \varepsilon_p) \leq f^{+line}(\varepsilon) \quad \text{Equation 2.100}$$

- For point 2:
If $\varepsilon \leq \varepsilon_p - \frac{\sigma_p + P_1 f_y}{E_s}$

$$\sigma = P_1 f_y + (P_3 E_s(\varepsilon - \varepsilon_p + \frac{\sigma_p + P_1 f_y}{E_s})) \leq f^{-line}(\varepsilon) \quad \text{Equation 2.101}$$

Where:

$$f^{+line} = \left(\frac{f_u - P_4 f_y}{2\varepsilon_u} \right) \varepsilon + \frac{f_u + P_4 f_y}{2} \quad \text{Equation 2.102}$$

$$f^{-line} = \left(\frac{f_u - P_4 f_y}{2\varepsilon_u} \right) \varepsilon - \frac{f_u + P_4 f_y}{2} \quad \text{Equation 2.103}$$

In the above equations, f_u is the ultimate strength of steel, f_y is the yield stress of steel, ε_u is the rupture strain of steel, and P_1 , P_2 , P_3 , and P_4 , are parameters as already defined. In the KSU-RC, the values for these parameters are 0.333, 0.17, 0.1, and, 0.9, respectively.

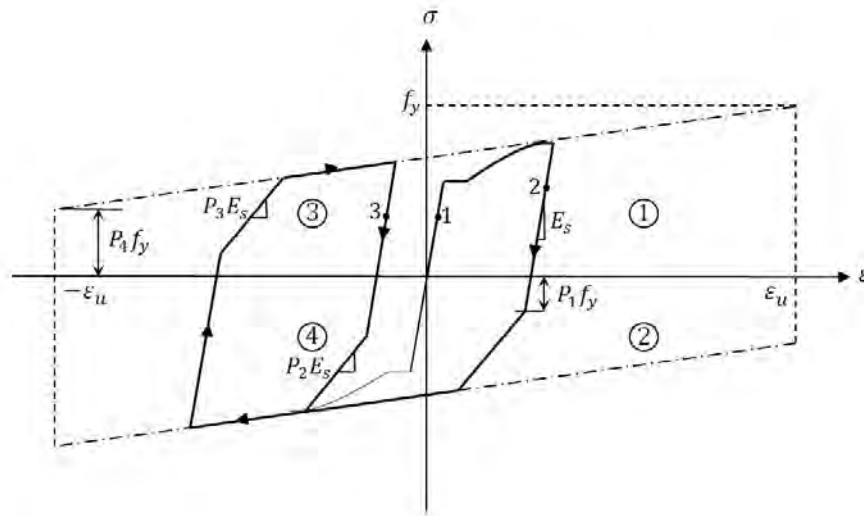
- For point 3:

The behavior for point 3 is same as behavior explained for point 2, with the only one expectation:

$$\text{If } \varepsilon \leq \varepsilon_p - \frac{\sigma_p + P_1 f_y}{E_s}$$

$$\sigma = P_1 f_y + (P_2 E_s (\varepsilon - \varepsilon_p + \frac{\sigma_p + P_1 f_y}{E_s})) \leq f\text{-line}(\varepsilon)$$

Equation 2.104



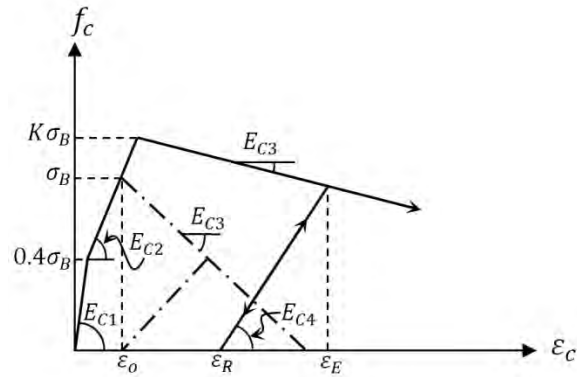
(Source: Esmaily and Peterman 2007)

FIGURE 2.18
Esmaily Steel Hysteretic Curve As Modeled in KSU-RC

Note that the behavior is symmetric with respect to the origin. In other words, moving in the other direction for point 2 (increase strain) is identical with a decrease in strain for point 3 and vice versa.

2.3.2 Concrete

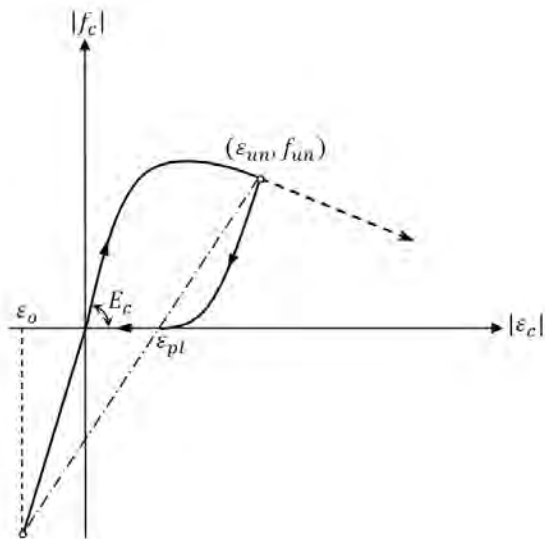
The number of models, developed for simulating hysteretic behavior of reinforced concrete is more than models, proposed for steel. Most of these models are based on empirical parameters and in some cases some theoretical explanation. The following are some of these models, explained briefly. The method used in KSU-RC is also explained.



(Source: Kuramoto et al. 1995)

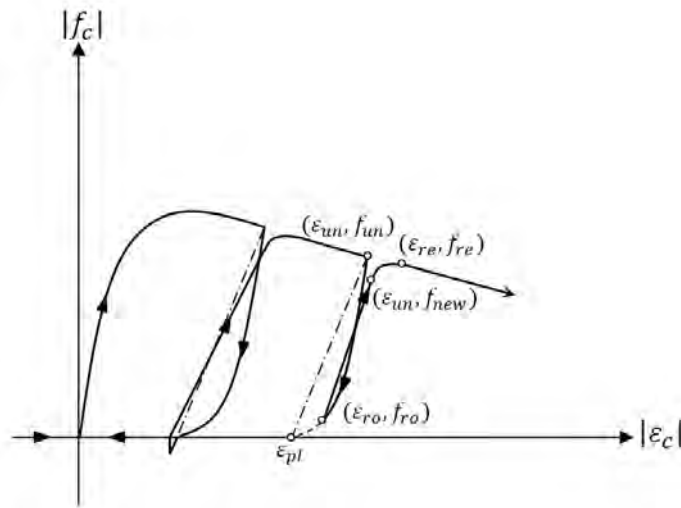
FIGURE 2.20
Kuramoto et Al.'s Model for Hysteretic Behavior of Concrete

In Figure 2.20, σ_B , K , and E_{C1} are the cover concrete strength, the confinement coefficient and the initial stiffness of cover concrete which is taken to be the same for confined concrete, respectively. All other parameters are self-evident and their values can be tuned based on the needs, as has been done by Kuramoto et al. (1995).



(Source: Mander et al. 1988)

FIGURE 2.21
Stress-Strain Curve for Unloading Branch and Determination of Plastic Strain As Proposed by Mander et Al.



(Source: Mander et al. 1988)

FIGURE 2.23
Stress-Strain Curve for Reloading Branch in the
Model Proposed by Mander et Al.

The procedure, proposed by Mander et al. (1988) to define hysteretic curve, is relatively complicated. Unloading branch and determination of plastic strain are shown in Figure 2.23. In Figure 2.23 ϵ_{un} , f_{un} and ϵ_{pl} are unloading strain, unloading stress, and the plastic strain, respectively. Deterioration in tensile strength of concrete because of prior compression loading in the model is shown in Figure 2.22. In this figure, ϵ_t , f'_t and f'_{cc} are the tensile strain, initial tensile strength and the compressive strength of concrete, respectively.

2.3.2.4 Model Developed and Used in KSU-RC

The envelope for the model, developed in KSU-RC, for the hysteretic behavior of concrete is the monotonic stress-strain curve as shown in Figure 2.11, which is based on Mander's model. The response of this model is closed to the response of Mander's model but with less computational effort. At the strain reversal the curve follows a parabolic path that is concave upward. The initial slope of the reversal curve is taken to equal to the initial stiffness of confined concrete. As the strain is decreased, the slope gradually is reduced and will be close to zero when the stress approaches zero. The stress remains zero for strain less than this value. At

the second reversal of strain, the stress remains zero up to a strain where the stress had vanished in the first reversal, and then it grows with a slope equal to initial stiffness of confined concrete, in the beginning. The slope decreases as the strain and corresponding stress increase. The stress increases up to the envelope curve and then follows that curve. Furthermore, for ascending and descending path of the hysteretic curve, we may apply two different initial stiffnesses that in turn may be different from the confined concrete initial stiffness. In the analysis regarding the experimental results, and implemented by KSU-RC, these values have been chosen to be identical. The model developed and used in KSU-RC mathematically is as follows:

- For ascending and descending within the elastic range of confined concrete response (defined here within a strain of 0.015 for confined concrete) the path follows the monotonic stress-strain curve as described before.
- For ascending from a point with a strain of ε_p and a stress of σ_p as shown in , the stress is valued as:

$$\sigma = -\frac{E_{c1}^2}{4f_{cc}} \left(\varepsilon - \varepsilon_p + \frac{2f_{cc}}{E_{c1}} - \frac{2\sqrt{f_{cc}(f_{cc} - \sigma_p)}}{E_{c1}} \right)^2 + E_{c1} \left(\varepsilon - \varepsilon_p + \frac{2f_{cc}}{E_{c1}} - \frac{2\sqrt{f_{cc}(f_{cc} - \sigma_p)}}{E_{c1}} \right)$$

Equation 2.105

Where, $0 \leq \sigma \leq f^{con}(\varepsilon)$, E_{c1} , f_{cc} , ε and $f^{con}(\varepsilon)$ are the slope when stress is zero, the confined concrete strength, the new strain, the monotonic stress of confined concrete at the new strain, respectively.

- For descending from a point with a strain of ε_p and a stress of σ_p as shown in Figure 2.24, the stress is evaluated as follows:

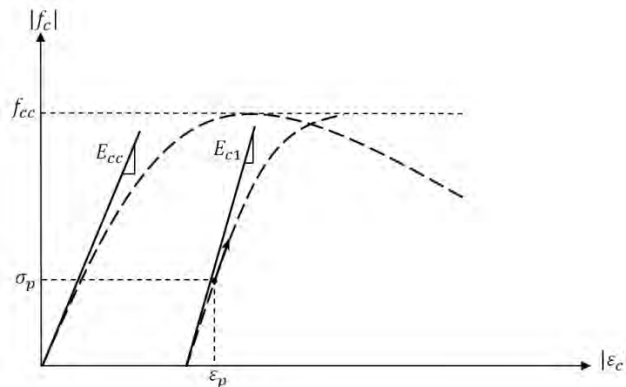
$$\text{For } \varepsilon > \varepsilon_p - \frac{2\sqrt{f_{cc}\sigma_p}}{E_{c2}}$$

$$\sigma = -\frac{E_{c1}^2}{4f_{cc}} \left(\varepsilon - \varepsilon_p + \frac{2f_{cc}}{E_{c1}} - \frac{2\sqrt{f_{cc}(f_{cc} - \sigma_p)}}{E_{c1}} \right)^2 \leq f^{con}(\varepsilon) \quad \text{Equation 2.106}$$

$$\text{For } \varepsilon \leq \varepsilon_p - \frac{2\sqrt{f_{cc}\sigma_p}}{E_{c2}}$$

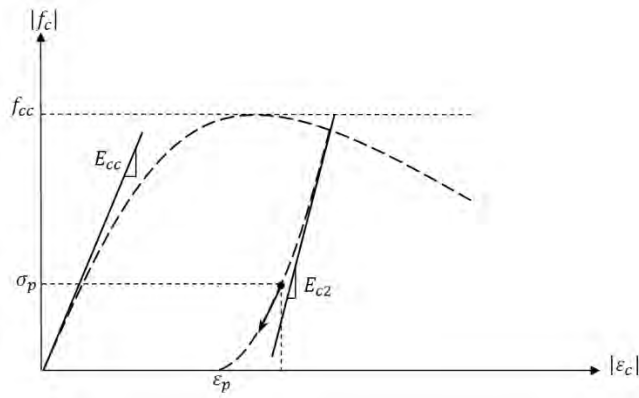
$$\sigma = 0 \quad \text{Equation 2.107}$$

In this model, E_{c1} and E_{c2} can be provided as is proper by the user. In KSU-RC values have been chosen to be the same as initial stiffness of confined concrete. Also, tensile stress of concrete has been ignored, but it is not difficult to consider it in the model. Considering the tensile strength of concrete with the deterioration caused by the previous compressive loading, and replacing the ascending curve with a line, makes the model vary close to what has been proposed by Mander et al. for the hysteretic behavior of concrete. Another model similar to this model, but with a linear path for descending and ascending branches was developed for the very preliminary testing of the code. Since this preliminary simple hysteretic model is not used in KSU-RC, it will not be discussed in this report.



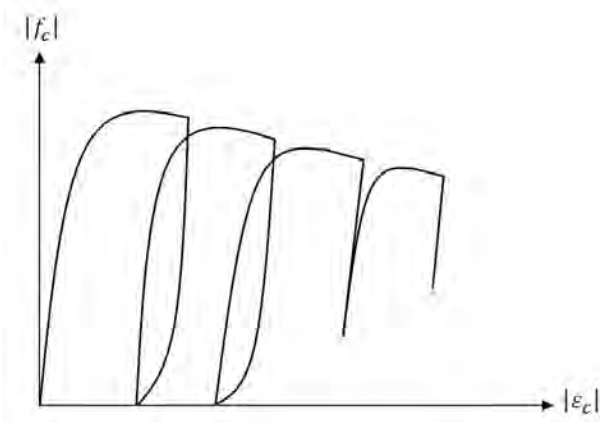
(Source: Esmaily and Xiao 2002)

FIGURE 2.24
KSU-RC Confined Concrete Hysteretic Model,
Ascending Path



(Source: Esmaily and Xiao 2002)

FIGURE 2.25
KSU-RC Confined Concrete Hysteretic Model,
Descending Path



(Source: Esmaily and Xiao 2002)

FIGURE 2.26
Confined Concrete Hysteretic Behavior
Curve, a Sample Based on the Data from
KSU-RC

2.3.2.5 KSU-RC Cover Concrete

The hysteretic model for cover concrete is in general similar to the model used for confined concrete. The difference is the envelope curve and the initial stiffness and ultimate strength. The envelope for the cover concrete is also based on the model proposed by Mander et al. (1988) In this model, if the confinement coefficient is taken to be zero, the resulting curve can be used to simulate the envelope for cover concrete stress-strain curve, with the exception that

the ending tail of the curve at strains beyond 0.004 is replaced by a straight line (Esmaeily and Xiao 2002).

2.4 Definition of Plastic Hinge Length

Analysis of force-deflection response of a reinforced concrete column beyond its linear range of performance, and especially beyond its peak lateral strength, requires a reasonable assumption on the curvature distribution along the column. While evaluation of the lateral displacement of a column when subjected to a lateral force less than its peak lateral strength is possible by commonly used analytical methods, such as fiber-model, a proper assumption on the curvature distribution along the column when the deflection has passed the peak strength is necessary. Various plastic hinge models have been proposed by researchers to address this need. Displacement capacity of a reinforcement concrete column is a function of plastic hinge length, curvature capacity of the critical section, and column height. In literature, the certain length of flexural member that experiences severe deformation and damage due to large inelastic curvature is called plastic hinge length (Figure 2.27). A plastic hinge is a type of energy dampening device, allowing plastic rotation of a rigid column connection. The dampening is done by having a portion of the column reach the plastic, nonlinear range. Plastic hinges protect connecting members from major damage during a seismic event by absorbing most of the seismic energy, thereby allowing the other members to operate in the elastic range. As Bae and Bayrak said:

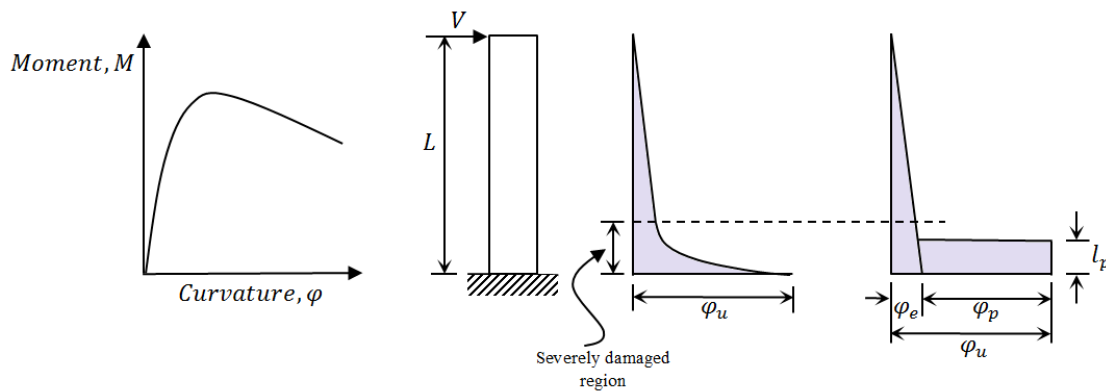
“A plastic hinge can be thought of as a fuse in an electrical circuit; when too much seismic energy (current) reaches the plastic hinge (fuse) region of the column, it yields (melts) to protect the rest of the building (circuit). The length of plastic hinge depends on many factors that are as follows (Bae 2008):

1. Level of axial load;
2. Moment gradient;
3. Level of shear stress in the plastic hinge region;
4. Mechanical properties of longitudinal and transvers reinforcement;
5. Concrete strength and
6. Level of confinement and its effectiveness in the potential hinge region.”

In the 1950s and 1960s, researchers studied the plastic hinge length to estimate the flexural deformation capacity of reinforcement concrete beams and tip deflection of

reinforcement concrete columns. The tip deflection of column is an important factor in designing structures because building codes limit the maximum allowable inter-story drift.

To calculate the tip deflection, one must know the curvature and overall length of the member. In the case of a column that is entirely in the elastic region, the curvature can be easily obtained for the entire column using mechanics of materials. However, in seismic events, columns are not in the elastic range for their entire length, so the curvature can't be as easily determined. This is because the curvature at the column's base is dependent on how much it is pushed once it is in the plastic region. To simplify, as shown in Figure 2.27, Park and Paulay (1975) assumed that the curvature is constant in plastic hinge region.



(Source: Park and Paulay 1975)

FIGURE 2.27
Definition of Plastic Hinge Length

In Figure 2.27 the actual curvature distribution along the reinforced concrete member is idealized into elastic and inelastic regions. With this approximation, knowing plastic hinge length and using second moment area theorem, the tip displacement of a column can be obtained by integrating curvature along the length of the column. This equation takes into account both the plastic and elastic regions of the column.

$$\Delta_{tip} = \Delta_y + \Delta_p = \frac{\varphi_y L^2}{3} + (\varphi_u - \varphi_y) l_p (L - 0.5 l_p)$$

Equation 2.108

Where Δ_p and Δ_y are the plastic and elastic deflection. L , l_p , φ_y and φ_u are the length of the column, the plastic hinge length, curvature at first yield of tension steel and the ultimate curvature, respectively.

By further simplification, Park and Paulay (1975) obtained the relationship between curvature and displacement ductility. The following two equations, suggested by Park and Paulay, can include the effect of bar slip and shear displacement also.

$$\mu_{\Delta} = 1 + 3(\mu_{\varphi} - 1) \frac{l_p}{L} (1 - 0.5 \frac{l_p}{L}) \quad \text{Equation 2.109}$$

2.5 Plastic Hinge's Models and Studies

A large number of past experimental and theoretical studies have tried to suggest a reliable formula for evaluating the plastic hinge length in columns with different material properties, cross section, longitudinal and lateral reinforcement. Some of these models are summarized as follows:

2.5.1 Baker's Model

In 1956, Baker conducted 94 beam/column tests to investigate the moment-curvature relationship of beams and columns. The main test variable included concrete strength, yield strength or amount of tension reinforcement, amount of compression reinforcement, single or double concentrated loads and axial load. Baker proposed the following equation to calculate the plastic hinge length (Baker 1956).

$$l_p = k_1 k_2 k_3 \left(\frac{z}{d}\right)^{0.25} d \quad \text{Equation 2.110}$$

Where, z is the distance between the critical section and the point of contra-flexure and d is the effective depth of a beam. In Baker's plastic hinge equation, k_1 accounts for the steel strength and it's 0.7 for mild steel or 0.9 for cold-worked steel, $k_2 = 1 + (0.5 P_u/P_0)$ which P_u is the axial compressive force and P_0 is the load capacity for an axially loaded column, and k_3 accounts for

the concrete compressive strength and it's 0.6 when $f'_c = 5100 \text{ psi}$ or 0.9 when $f'_c = 1700 \text{ psi}$. Baker reported that l_p ranged from $0.4d$ to $2.4d$ for the particular value of z/d .

2.5.2 Baker and Amarakone's Model

After further research, Baker and Amarakone (1964) simplified Baker's plastic hinge length equation, eliminating the axial load factor, k_2 .

$$l_p = 0.8k_1k_3\left(\frac{z}{d}\right)c \quad \text{Equation 2.111}$$

Where c is the natural axis depth at ultimate moment.

2.5.2 Mattock's Model

Mattock (1964) investigated the effect of various parameters on the behavior of reinforcement concrete beams by conducting 37 simply supported beam tests. The parameters, studied by Mattock were concrete strength ($f'_c = 4000 \text{ to } 6000 \text{ psi}$), effective depth of beam ($d = 10 \text{ to } 20 \text{ in.}$), moment gradient ($\frac{z}{d} = 2.7 \text{ to } 11$), amount ($\rho = 1 \text{ to } 3\%$) and yield strength of tension reinforcement ($f_y = 47 \text{ to } 60 \text{ ksi}$). Based on the test results, Mattock suggested the following equation to calculate the plastic hinge length (l_p):

$$l_p = \frac{d}{2} \left[1 + (1.14 \times \sqrt{\frac{z}{d}} - 1) \left\{ 1 - \left(\frac{q - q'}{q_b} \right) \sqrt{\frac{d}{16.2}} \right\} \right] \quad \text{Equation 2.112}$$

2.5.3 Sawyer's Model

Sawyer (1964) suggested the following equation for calculating the plastic hinge length:

$$l_p = 0.25d + 0.075z \quad \text{Equation 2.113}$$

The plastic hinge which is obtained by Equation 2.113 is the plastic hinge length on the one side of critical section. Where the bending moment is reduced to M_y , it's assumed that the zone of yielding extend a distance $d/4$ beyond the section.

2.5.4 Corley's Model

After that, Corley (1996) expand Mattock's (1964) work by conducting 40 simple supported concrete beams subjected to single point loads. Effects of confinement and size were studied by Corley. Based on the scatter in the measured values of the plastic hinge lengths, he ignored the effect of term $(\frac{q-q'}{q_b})$ in Equation 2.112. He reported that the plastic hinge length primarily is a function of the geometry of a concrete beam. In addition, he showed that the size of a beam doesn't have a significant effect on the rotational capacity. Corley suggested the simple following equation for calculating the plastic hinge length (l_p):

$$l_p = \frac{d}{2} + 0.2 \frac{z}{\sqrt{d}} \quad \text{Equation 2.114}$$

2.5.5 Mattock's Model

Later in 1967, Mattock simplified his own equation (Equation 2.112) to the following equation (Mattock 1967):

$$l_p = \frac{d}{2} + 0.5z \quad \text{Equation 2.115}$$

In his opinion, although there was considerable scatter, the trend in the measured l_p could be represented by above equation reasonably.

2.5.6 Park et Al.'s Model

In 1982, Park et al. conducted four full scale concrete columns with square cross section of $22 \times 22 \text{ in}^2$ and $L/h = 2$. The axial loads applied to the column specimens ranges from $0.2f'_c A_g$ to $0.6f'_c A_g$. Based on their test results the level of axial load doesn't have any effect on

the plastic hinge length and the average value of l_p is $0.42h$, where h is the overall depth of the column. They suggested using a simple $0.4h$ for concrete columns (Park 1982).

2.5.7 Priestley and Park's Model

Using similar approach of Park's model, Priestley and Park (1987) suggested the following equation for the calculation of the plastic hinge length in reinforced concrete columns:

$$l_p = 0.08L + 6d_b \quad \text{Equation 2.116}$$

The current equation has two terms. The first term was considered for column bending, and the second one was considered for bar slip as the elongation of longitudinal bars beyond the theoretical base.

2.5.8 Sakai and Sheikh's Investigations

In 1989, Sakai and Sheikh (1989), based on their review of the literature, reported that the plastic hinge length was affected by the amount of transverse reinforcement, axial load level, and aspect ratio (L/h or L/D). They expressed that l_p increased when aspect ratio increased and bilinear curves that illustrated the relationship between l_p and the aspect ratio were reported by them.

2.5.9 Paulay and Priestley's Model

In 1992, Paulay and Priestley (1992) revised their equation by following expression for different grades of flexural reinforcement:

$$\begin{aligned} l_p &= 0.08L + 0.15d_b f_y & (f_y \text{ in ksi}) \\ l_p &= 0.08L + 0.022d_b f_y & (f_y \text{ in MPa}) \end{aligned} \quad \text{Equation 2.117}$$

Paulay and Priestley expressed that the above equation resulted in $l_p = 0.5h$ for typical columns.

Sheikh and Khoury (1993), Sheikh et al. (1994), and Bayrak and Sheikh (1998) also conducted column tests. The plastic hinge, measured in their tests, was equal to $0.1h$ where h is the dimension of the column section in the direction of lateral load. It should be noted that their column tests were conducted under high axial loads.

2.5.10 Riva and Cohn's Model

Riva and Cohn (1990) conducted a nonlinear analysis of 56 simple supported beams and 32 cantilever reinforced and pre-stressed beams and proposed an equation for the plastic hinge length. They also performed a parametric study on the moment-curvature relationship of these beams.

The effect of load distribution, percentage of tension steel, shape of the section, support condition and pre-stressing were studied. Based on their research, the l_p/z ratio is not significantly affected by the variation of the z/h ratio but rather is influenced mostly by the bending moment distribution and the steel percentage. The following expressions were proposed for l_p/z for three different loading phases:

- From cracking to yielding limit state:

$$\frac{l_p}{z} = \left(A - \frac{B}{800\omega} \right) \left(\frac{\varphi_p}{\varphi_{py}} \right)^{\left(\frac{c}{80\omega} \right)} \left(\frac{b'}{b_\omega} \right)^{-\left(\frac{D}{640\omega^2} \right)} f(\gamma) \quad \text{Equation 2.118}$$

- From yielding to reinforcement strain hardening:

$$\frac{l_p}{z} = (l_p^z)^y \left(\frac{\varphi_p}{\varphi_{py}} \right)^{-(0.9-0.8\gamma)} \quad \text{Equation 2.119}$$

- Ultimate limit state (only if > 7.0)

$$\frac{l_p}{z} = \left(\frac{E}{100} + \frac{F}{1000} \frac{\varphi_p}{\varphi_{py}} \right) \left(\frac{b}{b_w} \right)^G$$

Equation 2.120

Where l_p in Equation 2.119 is the value of l_p/z from Equation 2.118 when $\frac{\varphi_p}{\varphi_{py}} = 1$, b is the width of the compression flange and b_w is the web width. The constants A, B, C, D, E, F, G and $f(\gamma)$ depend on the bending moment distribution considered and can be found elsewhere (Riva and Cohn 1990).

2.5.11 Mendis's Studies

Mendis (2001) conducted 13 simple supported concrete beam tests subjected to single point loads. Based on a four column test with low axial level, he reported that the plastic hinge length is not sensitive to the axial load level. In addition, he expressed that l_p increased as the aspect ratio or the longitudinal reinforcement ratio increased, but decreased as the amount of lateral reinforcement increased. At the end, he concluded that the American Concrete Institute (ACI) formula is reliable for estimating l_p for high strength concrete beams and columns with low axial loads (Mendis 2001).

2.5.12 Correal et Al.'s Studies

In 2007, Correal et al. conducted six large-scale spiral column model tests on a shaker table at the University of Nevada, Reno. They studied the effect of shear level, spiral distance and cross-ties on the plastic hinge length. Their results showed that the plastic hinge length increased by 10% to 20% as the distance of the spiral sets increased from 1.0R to 1.5R, depending on the level of shear, where R is the radius of the spiral columns (Correal et al. 2007).

2.5.13 Berry et Al.'s Model

Berry et al. (2008) suggested the following equation for calculating the plastic hinge length:

$$l_p = 0.05L + \frac{0.1f_y d_b}{\sqrt{f'_c}} \quad (MPa) \quad \text{Equation 2.121}$$
$$l_p = 0.05L + \frac{0.008f_y d_b}{\sqrt{f'_c}} \quad (psi)$$

Equation 2.121 considers the strength of concrete and the properties and amount of longitudinal steel; however they don't predict the plastic hinge length accurately, especially when P/P_0 is more than 0.2 (Berry et al. 2008).

2.5.14 Bae and Bayrak's Model

In 2008, Bae and Bayrak (2008) designed and tested four full-scale concrete columns under moderate to high axial load levels and reversed cyclic displacement excursions. Using their test results, they developed a procedure for estimating the plastic hinge length. This procedure is called the Concrete Compression Strain Method (CCSM). Using the CCSM, they investigated the effect of axial load level and the amount of longitudinal reinforcement on the l_p . They reported that the axial load level and the amount of longitudinal reinforcement are the main parameters for estimating the plastic hinge length. Based on these observations, a linear relationship between these parameters was assumed in developing a new expression of l_p for simplicity. Least square analyses were used to identify a coefficient for each parameter.

$$\frac{l_p}{h} = \left[0.3 \left(\frac{P}{P_0} \right) + 3 \left(\frac{A_s}{A_g} - 0.1 \right) \right] \left(\frac{L}{h} \right) + 0.25 \geq 0.25 \quad \text{Equation 2.122}$$

Where h is the overall depth of column, P is the applied axial load, P_0 is the nominal axial load capacity, A_s , A_g and L are the area of tension reinforcement, the gross area of concrete section and the distance from critical section to point of contra-flexure (Bae and Bayrak 2008).

2.5.15 Mortezaei and Ronagh's Model

In 2011, Mortezaei and Ronagh (2011) expressed that the formation of a plastic hinge in reinforced concrete column in region that experience inelastic action depends on the characteristics of the earthquakes as well as the column details. In their study, 1316 inelastic time-history analyses were performed to predict the nonlinear behavior of reinforced concrete columns under both far-fault and near-fault ground motion by finite element method. The effect of axial load, height-over-depth ratio, and amount of longitudinal reinforcement, as well as different characteristics of earthquakes were evaluated. Based on their results, two expressions were proposed for estimating plastic hinge length of reinforced concrete columns under both far-fault and near-fault earthquakes. These equations are as follows:

$$\frac{l_p}{h} = \left[0.4 \left(\frac{P}{P_0} \right) + 3 \left(\frac{A_s}{A_g} \right) - 0.1 \right] \left(\frac{H}{h} \right) + 0.6 \geq 0.6 \quad \text{For far-fault earthquakes}$$

Equation 2.123

$$\frac{l_p}{h} = \left[0.4 \left(\frac{P}{P_0} \right) + 3 \left(\frac{A_s}{A_g} \right) - 0.1 \right] \left(\frac{H}{h} \right) + 0.45 \geq 0.45 \quad \text{For near-fault earthquakes}$$

Equation 2.124

Where, h , P , P_0 , A_s , A_g , and H are the overall depth of column, the applied axial load, the nominal axial load capacity, the area of tension reinforcement, the gross area of concrete section, the distance from critical section to the point of contra-flexure, respectively.

2.5.16 Esmaeily's Model One

This method assumes that the curvature between the point of first yield and the critical section is linearly distributed (Esmaeily and Xiao 2005). The first yield point is either due to the first yield of the longitudinal bar on the section or to the first yield of the concrete. The yield of the concrete is defined to be at a strain of 0.002 and when the furthestmost fiber of the section undergoes this strain while the steel strain on the opposite side is still less than the yield strain, it

is assumed that the section has experienced its yield, which is due to concrete. The distance between the section where the first yield occurs to the critical section is treated as the length on which the transition occurs and will be referred to as l_p . As the lateral force grows for the first time, and while the moment at the critical section is less than the yield moment for the existing axial load, all the length is in a linear elastic state and there is no l_p . The evaluation of the displacement for any situation is straightforward, in this case, a reversal of the loading. As the moment at the critical section reaches the yield moment, this value starts to increase and reaches its maximum when the critical section experiences the maximum moment. l_p is evaluated as:

$$l_p = l \left(1 - \frac{M_y}{M_u}\right) \quad \text{Equation 2.125}$$

where l is the total length, M_y is the yield moment for the existing axial load, and M_u is the moment at the critical section. Let this maximum value be $l_{p\text{-max}}$. Note that in this method it is assumed that when a section experiences a plastic deformation, it cannot be treated as elastic in a different situation, such as reversal of loading as explained earlier. So, the l_p is always either growing or constant with its maximum achieved value so far. When the curvature is less than the curvature corresponding to the maximum moment (for the existing force at the step) and no reversal has occurred, the curvature at the top of the plastic hinge is equal to the actual analytical value corresponding to the moment situation. Analytically, it is equal to the yield curvature, Φ_y , and its corresponding moment is M_y , which is also equal to:

$$M_y = M_{l_p} = \frac{(l - l_p)}{l} M_u \quad \text{Equation 2.126}$$

$$M_y = M_{(l-l_p)} = \frac{(l - l_p)}{l} M_u \quad \text{Equation 2.127}$$

When the curvature on the critical section exceeds the curvature corresponding to the maximum moment or when a reversal of loading happens, the curvature at the top of this l_p drops linearly with the part above it that has been within the elastic-linear range so far. Suppose that the

moment at this instance is M_u and the yield curvature and moment corresponding to the existing situation is M_y and Φ_y , respectively. Then the curvature at the top of l_p is equal to:

$$\Phi_{l_p} = \Phi_y \left(\frac{M_{l_p}}{M_y} \right) \quad \text{Equation 2.128}$$

where Φ_{l_p} is the curvature at the top of the plastic hinge, Φ_y is the first yield curvature, M_{l_p} is the moment at the top of the plastic hinge and is calculated as:

$$M_{l_p} = \frac{(l - l_p)}{l} M_u \quad \text{Equation 2.129}$$

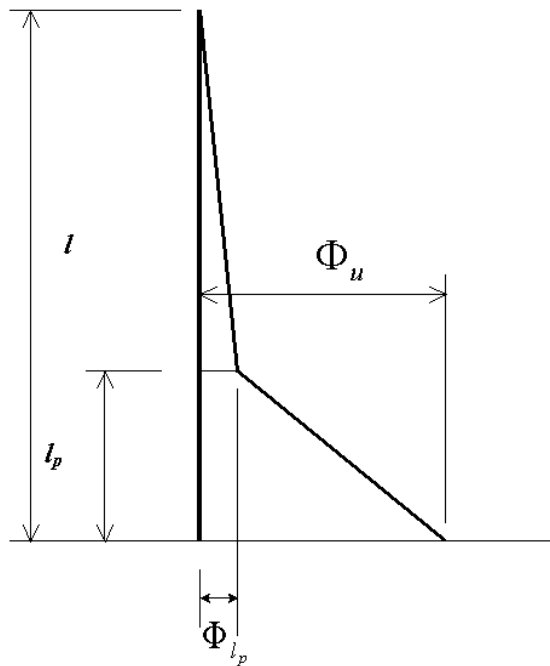


FIGURE 2.28
Esmaily's Plastic Hinge, Method One

therefore:

$$\Phi_{l_p} = \Phi_y \left(\frac{M_u}{M_y} \right) \cdot \frac{(l - l_p)}{l} \quad \text{Equation 2.130}$$

Then the displacement Δ will be:

$$\Delta = \Delta_e + \Delta_p \quad \text{Equation 2.131}$$

where Δ_p is the plastic flexural deflection and is calculated as:

$$\Delta_p = \int_0^{l_p} \left[\Phi_{l_p} + \frac{(\Phi_u - \Phi_{l_p})}{l_p} x \right] (l - l_p + x) . dx \quad \text{Equation 2.132}$$

or

$$\Delta_p = \Phi_{l_p} . l_p . \left(l - \frac{l_p}{2} \right) + \frac{1}{2} . (\Phi_u - \Phi_{l_p}) . l_p . \left(l - \frac{l_p}{3} \right) \quad \text{Equation 2.133}$$

and Δ_e is the elastic deflection which is evaluated as:

$$\Delta_e = \int_0^{l-l_p} \frac{\Phi_{l_p}}{(l-l_p)} . x . dx \quad \text{Equation 2.134}$$

or

$$\Delta_e = \frac{1}{3} \Phi_{l_p} . (l - l_p)^2 \quad \text{Equation 1.135}$$

The algorithm for the method can be summarized as follows:

Initially l_p is equal to zero. For a given displacement Δ and axial load P , calculate Δ_y as:

$$\Delta_y = \frac{1}{3} \Phi_y \cdot l^2 \quad \text{Equation 2.136}$$

where Φ_y is the yield curvature for the given axial load and l is the total length. If $|\Delta| \leq \Delta_y$, then:

$$\Phi_u = \frac{3\Delta}{l^2} \quad \text{Equation 2.137}$$

where Φ_u is the curvature at the critical section. Use Φ_u to evaluate M_u (moment at the critical section), and then the lateral force would be:

$$F = \frac{M_u}{l} \quad \text{Equation 2.138}$$

during a reversal of loading and while $|\Delta| \leq \Delta_y$ for the case, the problem is linear and the aforesaid process is applied. If $|\Delta| > \Delta_y$ then by trial and error find the proper $\Phi_u > \Phi_y$ for which $l_p = l \cdot (1 - \frac{M_y}{M_u})$ and the curvature at the top of l_p is Φ_y , as can also be calculated using Equation 2.130 so that proper Δ is achieved. Then the corresponding lateral force is simply evaluated as above. During the process keep the record of the maximum and minimum achieved values for lateral force, and displacement, and the maximum achieved value for l_p . When the value of lateral force falls below the maximum lateral load evaluated so far, or when there is a reversal of loading, l_p (as is the maximum evaluated value so far) is used and the same trial and error process is applied to find the proper Φ_u , where the curvature at the top of l_p is calculated using Equation 2.130.

A simplified general flowchart for the method is as in Figure 2.29. Intermediate algorithms, namely trial and error on the plastic hinge length, or evaluation of the moment curvature are not shown.

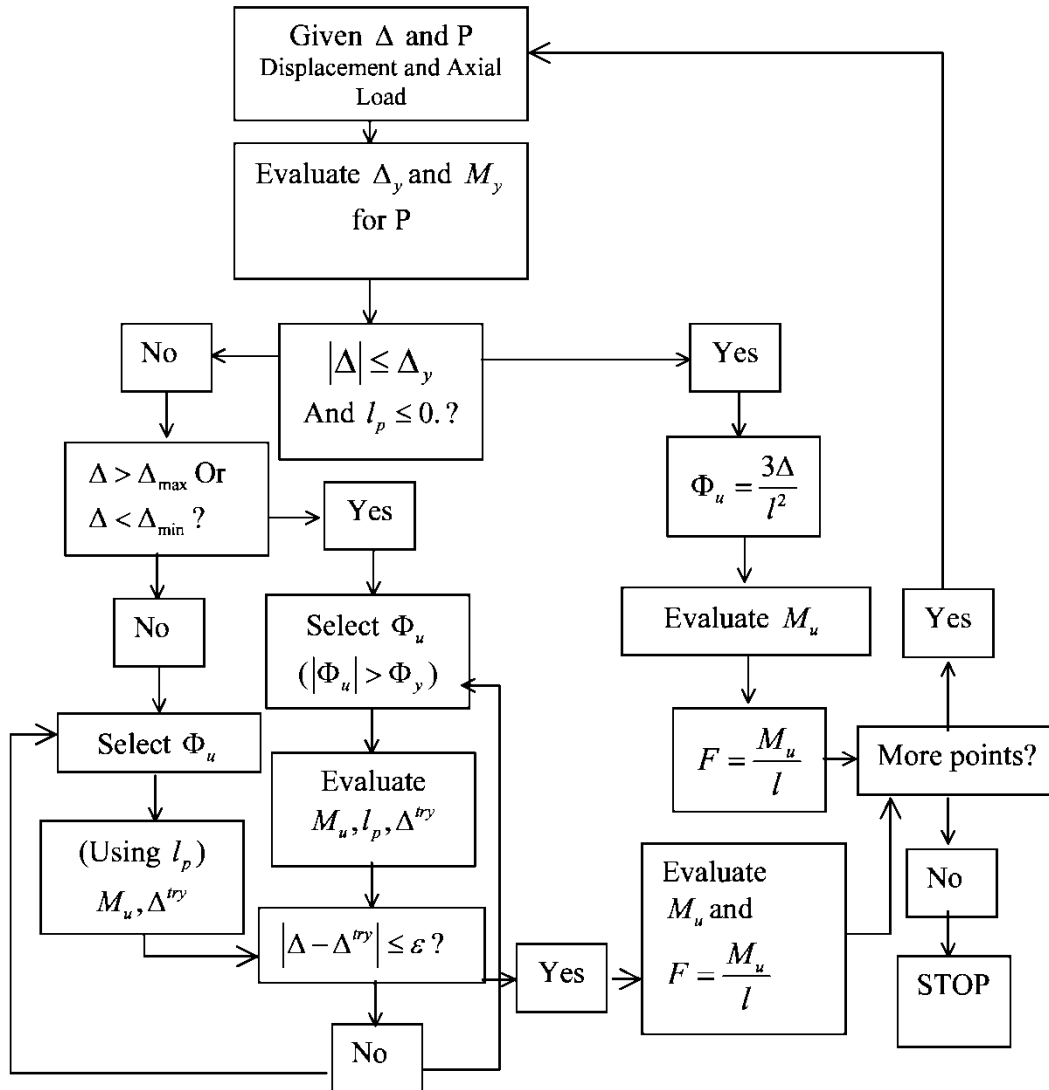


FIGURE 2.29
Flowchart Summarizing the First Method for Plastic Hinge

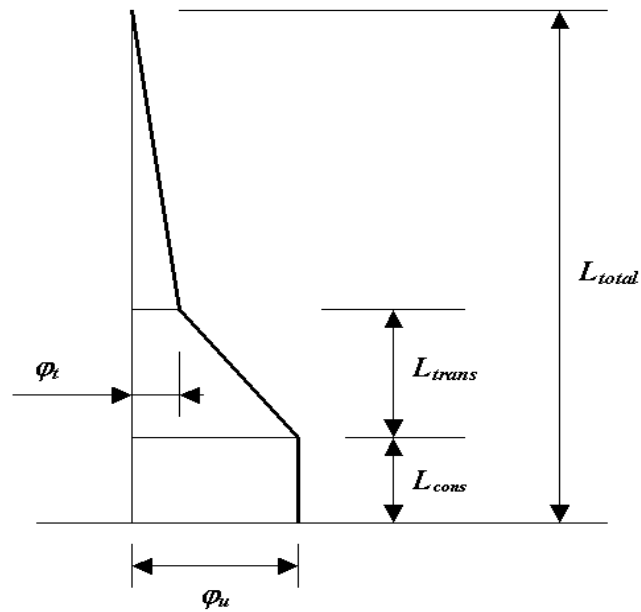
2.5.17 Esmaily's Model Two

As shown by Park et al. (1982), a constant plastic hinge length works relatively well for a member under a constant axial load and a monotonic lateral displacement compared to

experimental results. They have defined this constant length as $l_p = 0.08L + 0.15d_b f_y$ (or $l_p = 0.08L + 0.022d_b f_y$ in SI).

Sheikh et al. (1994) also claimed that assuming a plastic hinge length equal to the section depth is a good assumption and yields results comparable to test results. The concept of a fixed plastic hinge length, specifically the Park and Priestley method, was applied by the authors to the cases of pushover analysis under a fixed axial load, and the predictions were satisfactory. The only deficiency of the method in pushover cases under a constant axial load is that the variation of the plastic hinge length, which is evident in the experimental results, is ignored.

On the other hand, for a case with a variable axial load and a cyclic lateral displacement or load, these methods are not applicable. The method presented here combines the idea of a constant plastic hinge length and the idea presented in the first method to account for the variation of the plastic hinge length due to both the lateral force and axial load. The total length of the member is divided into three different areas. A constant length (D , can be considered as $0.08l + 0.15f_y d$ or the section depth) close to the critical section, a transition length taken as $0.15f_y d_b$ (or $0.022f_y d_b$ [SI]) and the rest of the member length that always stays within the elastic range. The curvature on the part close to the critical section is assumed to be uniform. The curvature on the transition part changes linearly from the curvature on the previous part to a curvature which depends on the level of the first yield curvature for the existing axial load and the level of the lateral force at the moment, as will be discussed. As previously explained, Figure 2.30 shows the assumed distribution of curvature along the column height. At any level of axial load and displacement, depending on the previous conditions for the base curvature, the new curvature at the critical section is found by trial and error so that the desired displacement is achieved. The process needs a trial and error phase because the curvature φ_t (curvature at the top of L_{trans}) is dependent on the level of the base moment and the yield curvature for the existing axial load. The process is summarized as follows:



(Source: Esmaily 2010)

FIGURE 2.30
Distribution of Curvature along the Column
Height As Assumed in Esmaily's Second
Method

1. Take $l_{cons} = D$, where D is the section depth. For columns with a height to depth ratio of more than 12.5 use $l_{cons} = 0.08l$.
2. For a given axial load and lateral displacement, evaluate the first yield curvature Φ_y and moment M_y . The process is to evaluate the curvature and moment corresponding to the first yield of the longitudinal steel, and also corresponding to a strain of 0.002 for the concrete under the existing axial load. Then, the yield moment and curvature for this level of axial load is the one having the smaller moment.
3. Knowing the previous base curvature and lateral displacement (zero for the first point) and the new target lateral displacement, estimate a new base curvature and evaluate the corresponding moment. Note that the moment is evaluated using the moment-curvature analysis module, where the hysteretic behavior of the section is considered through implementing the hysteretic response of the material on the

fiber-modeled section. So, the moment is dependent on the previous history of the curvature experienced by the section.

4. For the base moment, knowing the yield moment and curvature and assuming that the height above the top of the transition length is linearly elastic, evaluate the curvature at the top of transition length Φ_t . The value is evaluated as:

$$\Phi_t = \Phi_y \left(\frac{M_u}{M_y} \right) \cdot \frac{(l - l_{cons} - l_{trans})}{l} \quad \text{Equation 2.134}$$

where Φ_y is the yield curvature and M_y is the yield moment for the current axial load level, M_u is the base moment, l is the column height, l_{cons} is the length of the segment close to the base, l_{trans} is the transition length, and Φ_t is the curvature at the top of the transition length.

5. Evaluate the lateral displacement. The lateral displacement consists of two elastic and inelastic parts. The inelastic part is evaluated as:

$$\begin{aligned} \Delta_p = & \Phi_t \cdot l_{trans} \cdot \left(l - l_{cons} - \frac{l_{trans}}{2} \right) + \frac{1}{2} \cdot (\Phi_u - \Phi_t) \cdot l_{trans} \cdot \left(l - l_{cons} - \frac{l_{trans}}{3} \right) \\ & + \Phi_u \cdot l_{cons} \cdot \left(l - \frac{l_{cons}}{2} \right) \end{aligned} \quad \text{Equation 2.135}$$

and the elastic part is:

$$\Delta_e = \frac{1}{3} \Phi_t (l - l_{cons} - l_{trans})^2 \quad \text{Equation 2.136}$$

and the total deflection is:

$$\Delta = \Delta_e + \Delta_p \quad \text{Equation 2.137}$$

6. Compare the displacement with the desired value and repeat the process from number 2, until the lateral displacement is achieved with the desired accuracy. Then the corresponding lateral force is evaluated as:

$$F = \frac{M_u}{l - \frac{l_{cons}}{2}} \quad \text{Equation 2.138}$$

It should be noted that the pull-out action of the bars or, more precisely, the rotation imposed by the foundation is not explicitly considered in the two aforesaid methods. A third method addresses this effect explicitly by defining a penetration length, as in the Park et al. (1982) method ($0.022f_y d$ [SI] or $0.15f_y d$ [English System]). In this case the length denoted L_{cons} should be revised and the curvature linearly distributed over the penetration length, starting from Φ_u at the column-footing interface to zero at the end of this length. This method is summarized in a flowchart in Figure 2.31.

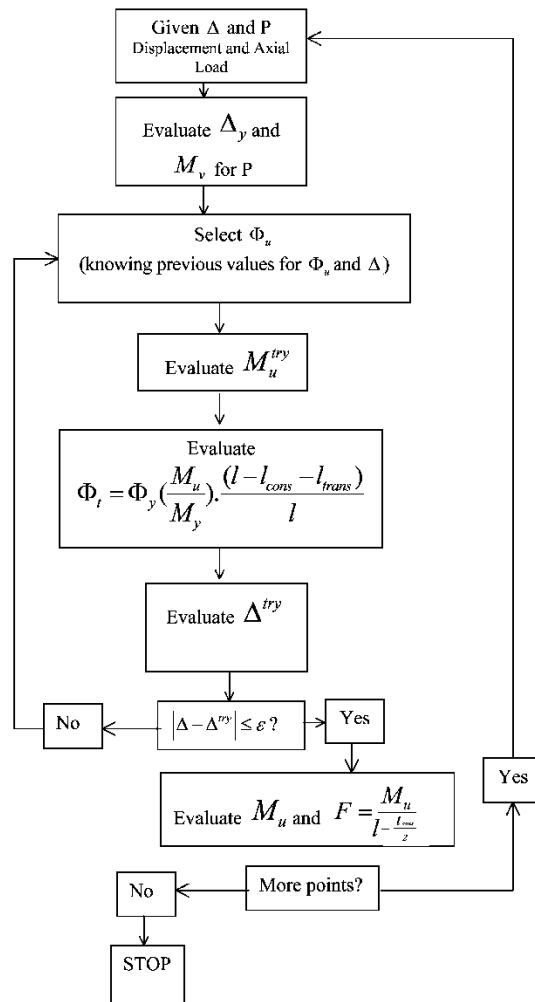


FIGURE 2.31
Flowchart Summarizing the Second
Method for Plastic Hinge

Chapter 3: AASHTO and KDOT

3.1 AASHTO LRFD Bridge Design Specification

The current version of American Association of State Highway and Transportation Officials (AASHTO) (at the time of this study was the Fifth Edition with 2010 interim revisions, even if the following changes in 2012 have been considered in the analytical assessments in this program. This version has been changed in some cases. The following are some changes done in the new 2010 edition of AASHTO-LRFD (2010) in terms of bridge pier design:

- Loads and load factors
- Earthquake load (new seismic requirements)
- Plastic hinge length

The updated provisions in the new version have been studied as follows:

3.1.1 Load and Load Factors

AASHTO-LRFD Bridge Design Specifications provides thirteen load combinations that should be used in concrete bridges design. Two of these combinations are related to extreme event limit states. Extreme Event I load combination includes water load and stream pressure (*WA*), friction load (*FR*) and primarily earthquake load (*EQ*). Meanwhile, Extreme Event II load combination considers water load and stream pressure (*WA*), friction load (*FR*), ice load (*IC*), vehicular collision force (*CT*), and vessel collision force (*CV*). Events are specified to be applied separately, since the joint probability of these events is extremely low. Both Extreme Event combinations include other dead and live loads as can be seen in Table 3.1. This table summarizes all load combinations and load factors. In AASHTO-LRFD (2007) Fourth Edition, there was only one load combination for Fatigue; while in AASHTO-LRFD (2010) there are two load combinations related to Fatigue (Fatigue I and Fatigue I II). The Fatigue load combination in AASHTO-LRFD (2007) is named as Fatigue I II in AASHTO-LRFD (2010).

**TABLE 3.1
Load Combinations and Load Factors**

Load Combination Limit State	DC DD DW EH EV ES EL PS CR SH	LL IM CE BR PL LS	WA	WS	WL	FR	TU	TG	SE	Use One of These at a Time			
										EQ	IC	CT	CV
Strength I (unless noted)	γ_p	1.75	1.00	–	–	1.00	0.50/1.20	γ_{RG}	γ_{SE}	–	–	–	–
Strength II	γ_p	1.35	1.00	–	–	1.00	0.50/1.20	γ_{RG}	γ_{SE}	–	–	–	–
Strength III	γ_p	–	1.00	1.40	–	1.00	0.50/1.20	γ_{RG}	γ_{SE}	–	–	–	–
Strength IV	γ_p	–	1.00	–	–	1.00	0.50/1.20	–	–	–	–	–	–
Strength V	γ_p	1.35	1.00	0.40	1.0	1.00	0.50/1.20	γ_{RG}	γ_{SE}	–	–	–	–
Extreme Event I	γ_p	γ_{EQ}	1.00	–	–	1.00	–	–	–	1.00	–	–	–
Extreme Event II	γ_p	0.5	1.00	–	–	1.00	–	–	–	–	1.00	1.00	1.00
Service I	1.00	1.00	1.00	0.30	1.0	1.00	1.00/1.20	γ_{RG}	γ_{SE}	–	–	–	–
Service II	1.00	1.30	1.00	–	–	1.00	1.00/1.20	–	–	–	–	–	–
Service III	1.00	0.80	1.00	–	–	1.00	1.00/1.20	γ_{RG}	γ_{SE}	–	–	–	–
Service IV	1.00	–	1.00	0.70	–	1.00	1.00/1.20	–	1.0	–	–	–	–
Fatigue I_LL, IM & CE only		1.50	–	–	–	–	–	–	–	–	–	–	–
Fatigue II_LL, IM & CE only		0.75	–	–	–	–	–	–	–	–	–	–	–

(Source: AASHTO-LRFD 2010 Table 3.4.1-1)

3.1.2 Vehicular Collision Force (CT)

Article 3.6.5 in AASHTO-LRFD (2010) specifies vehicular collision force load as the following:

“Useless the Owner determined that site conditions indicate otherwise, abutments and piers located within distance of 30.0 ft to the edge of the roadway, or within a distance of 50.0 ft to the centerline of a railway track shall be investigated for collision.”

“Where the design choice is to provide structural resistance, the pier or abutment shall be designed for an equivalent static force of 400 kip, which is assumed to act in any direction in a horizontal plane, at a distance of 4.0 ft above ground.”

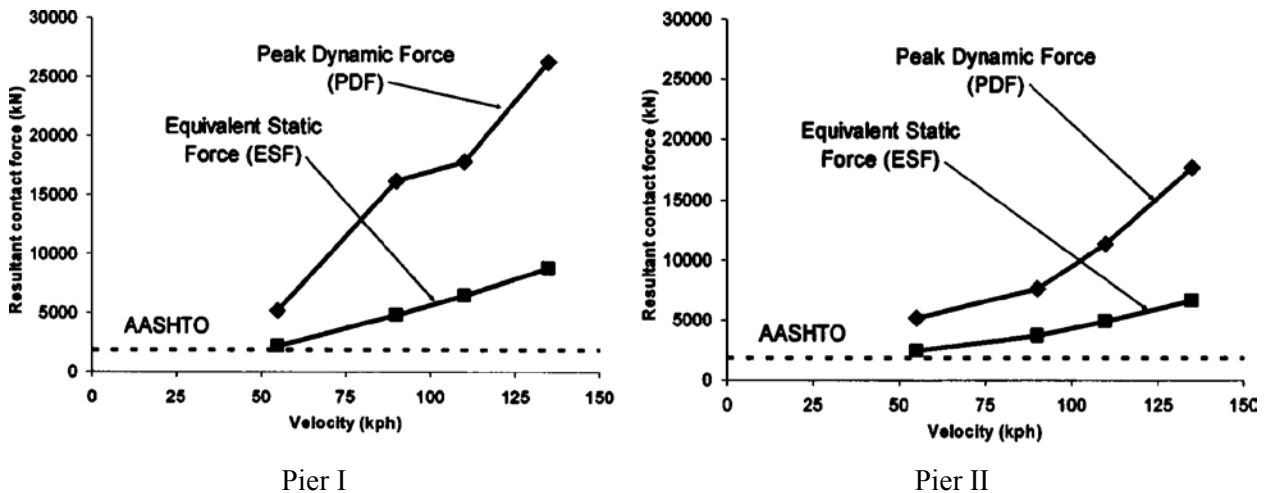
Note that this requirement was modified to 600 kips to be applied at a height of 5 ft above the ground at angles from zero to fifteen degrees. This update requirement has been considered in this study in addition to the 2010 version.

Commentary C3.6.5.1 says:

“The equivalent static force of 400 kip is based on the information from full-scale crash tests of barriers for redirecting 80.0 kip tractor trailers and from analysis of other truck collisions.”

This provision need not be considered if structures are protected by:

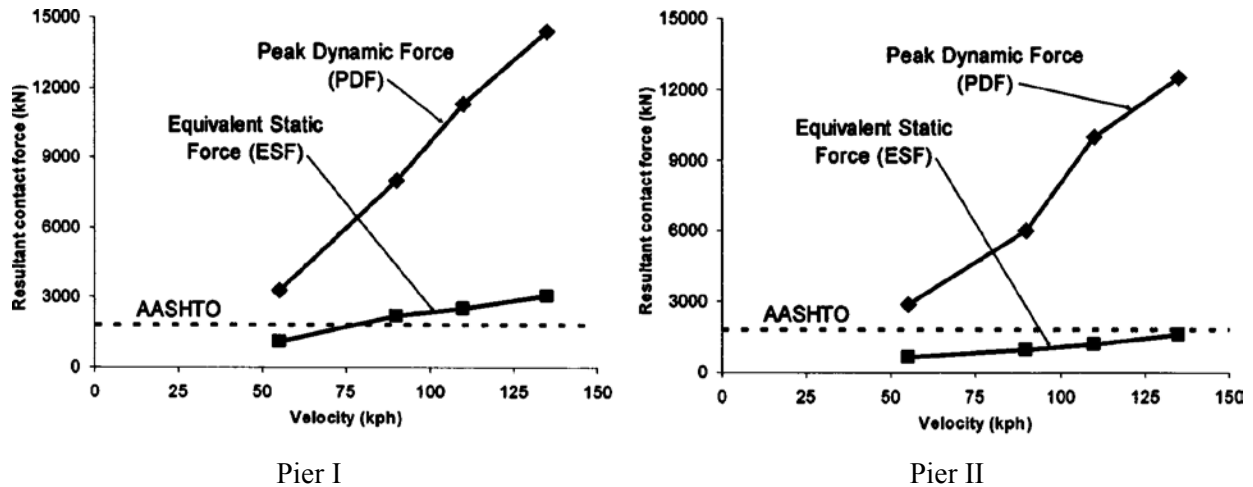
- An embankment;
- A structurally independent, crashworthy ground-mounted 54.0 inch high barrier, located within 10.0 ft from the component being protected; or
- A 42.0 inch high barrier located at more than 10.0 ft from the component being protected.



(Source: El-Tawill et al. 2005)

FIGURE 3.1
Impact Force versus Approach Speed Relationship for Ford Truck

However, recent research shows that AASHTO-LRFD (2010) provisions for vehicular collision force could not be conservative. El-Tawil et al. (2005) analyzed different vehicle/pier collisions using finite element method, and the equivalent static forces obtained from this analysis are significantly higher than AASHTO-LRFD (2010) 400 kip force.



(Source: El-Tawil et al. 2005)

FIGURE 3.2
Impact Force versus Approach Speed Relationship for Chevy Truck

It seems that there is no difference between AASHTO-LRFD (2010) and AASHTO-LRFD (2007) about the vehicular collision force.

In the 2012 edition of AASHTO-LRFD (2012), the vehicular collision force and the distance from the ground that this load should be applied are changed. Based on AASHTO-LRFD (2012):

“Unless the owner determines that site conditions indicate otherwise, abutment and piers located within a distance of 30.0 ft or the edge of roadway shall be investigated for collision. Collision shall be addressed by either providing structural resistance or by redirecting or absorbing the collision load. The provision of Article 2.3.2.2.1 shall apply as appropriate.”

“Where the design choice is to provide structural resistance, the pier or abutment shall be designed for an equivalent static force of 600 kip, which is assumed to act in a direction of zero to 15 degrees with the edge of the pavement in a horizontal plane, at a distance of 5.0 ft above ground.”

Commentary 3.6.5.1 says:

The equivalent static force of 600 kip is based on the information from full-scale crash tests of rigid columns impacted by 80.0-kip tractor trailer at 50 mph.

Same as AASHTO-LRFD (2010) this provision need not to be considered for the cases, as mentioned in AASHTO-LRFD (2010).

3.1.3 Vessel Collision (CV)

Based on AASHTO-LRFD (2010), all bridge components in a navigable waterway crossing, located in depth not less than 2.0 ft shall be designed for vessel impact. Article 3.14.1 in AASHTO-LRFD (2010) states: “The minimum design impact load for substructure design shall be determined using an empty hopper barge drifting at a velocity equal to the yearly mean current for the waterway location. The design barge shall be a single 35.0 ft × 195 ft barge, with an empty displacement of 200 ton, unless approved otherwise by the owner.”

“Where bridge span deep draft waterways and are not sufficiently high to preclude contact with the vessel, the minimum superstructure design impact may be taken to be the mast collision impact load specified in Article 3.14.10.3.

In navigable waterway where vessel collision is anticipated, structure shall be:

- Designed to resist vessel collision forces, and/or
- Adequately protected by fenders, dolphins, berms, islands, or other sacrifice-able devices.
- Waterway geometry,
- Size, type, loading condition, and frequency of vessels using the waterway
- Available water depth,
- Vessel speed and direction, and
- The structural response of the bridge to collision.”

As mentioned in commentary C3.14.8, determining the impact load on a bridge structure due to a ship collision, is complex and depends on following factors:

- Structural type and shape of the ship’s bow,
- Degree of water ballast carried in the forepeak of the bow,

- Size and velocity of the ship,
- Geometry of the collision, and
- Geometry and strength characteristics of the pier.”

According to research conducted by Woision (1979) in West Germany, Article 3.14.8 in AASHTO-LRFD (2010) presents the following equation for head-on ship collision impact force:

$$P_S = 8.15V\sqrt{DWT}$$

Equation 3.1

Where, P_S is the equivalent static vessel impact force (kip), DWT is the deadweight tonnage of vessel (tonne) and V is the vessel impact velocity (ft/s).

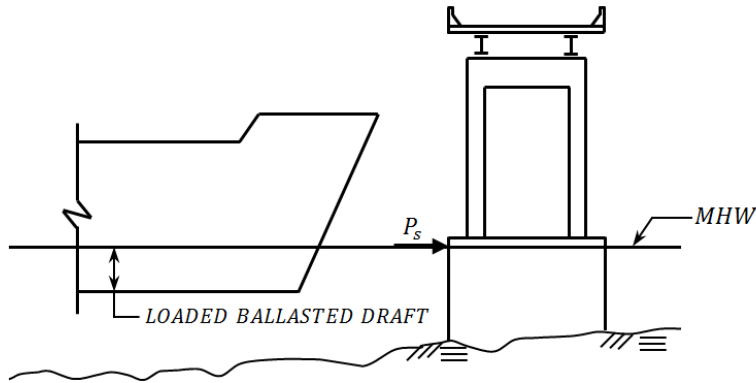
Article 3.14.14.1 in AASHTO-LRFD (2010) says:

“For substructure design, equivalent static force, parallel and normal to the centerline of the navigable channel, shall be applied separately as follows:

- 100 percent of the design impact force in a direction parallel to the alignment of the centerline of the navigable channel, or
- 50 percent of the design impact force in the direction normal to the direction of the centerline of the channel.

The impact force in both design cases, specified herein, shall be applied to a substructure in accordance with the following criteria:

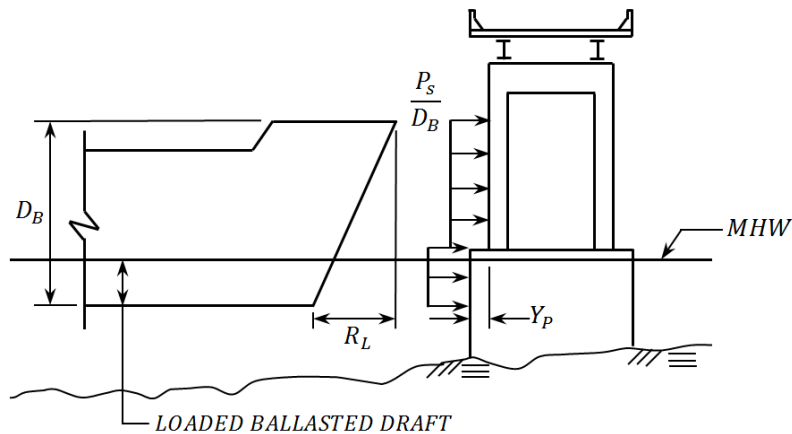
- For overall stability, the design impact force is applied as a concentrated force on the substructure at the mean high water level of the waterway, as shown in Figure 3.3, and



(Source: AASHTO 2010, Figure 3.14.14.1-1)

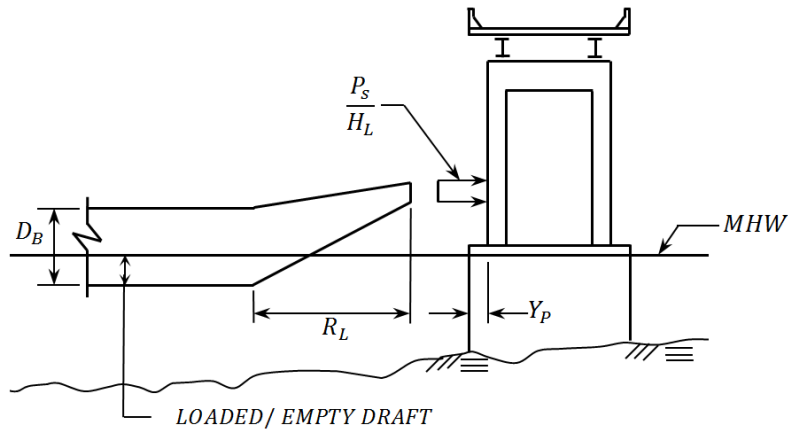
FIGURE 3.3
Ship Impact Concentrated Force on Pier

- For local collision forces, the design impact force is applied as a vertical line load equally distributed along the ship's bow depth, as shown in Figure 3.4. The ship's bow is considered to be raked forward in determining the potential contact area of the impact force on the substructure. For barge impact, the local collision force is taken as a vertical line load equally distributed on the depth of the head block, as shown in Figure 3.5.”



(Source: AASHTO 2010, Figure 3.14.14.1-2)

FIGURE 3.4
Ship Impact Line Load on Pier



(Source: AASHTO 2010, Figure 3.14.14.1-3)

FIGURE 3.5
Barge Impact Force on Pier

3.1.4 Earthquake Effects (EQ)

Calculation of design forces is sequential process that includes several steps as described by AASHTO Section 3.10:

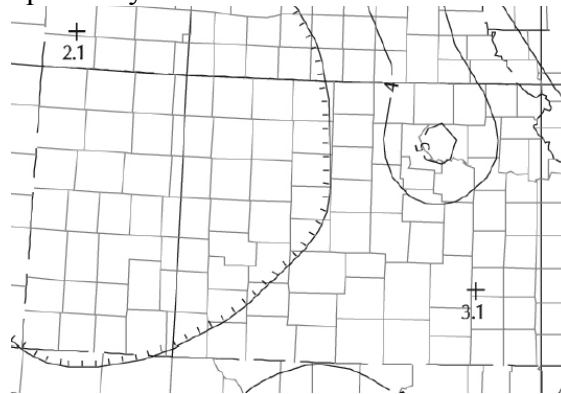
1. **Site class specification:** Every site shall be classified as A through F according to site class definition in Table 3.2 (AASHTO Table 3.10.3.1-1). This classification divides classes according to the soil properties. For example, site class A includes soils as a hard rock with measured shear wave velocity greater than 5,000 ft/s; on the other hand, class F includes soils with specific site evaluation requirements, such as high plasticity clays.

**TABLE 3.2
Site Class Definition**

Site Class	Soil Type and Profile
A	Hard Rock with measured shear wave velocity, $\bar{v}_s > 5,000 \text{ ft/s}$
B	Rock with $2,500 \text{ ft/sec} < \bar{v}_s < 5,000 \text{ ft/s}$
C	Very dense soil and soil rock with $1,200 \text{ ft/sec} < \bar{v}_s < 2,500 \text{ ft/s}$, Or with either $\bar{N} > 50 \text{ blows/ft}$, or $\bar{s}_u > 2.0 \text{ ksf}$
D	Stiff profile with $600 \text{ ft/sec} < \bar{v}_s < 1,200 \text{ ft/sec}$, or with either $15 < \bar{N} < 50 \text{ blows/ft}$ or $1.0 < \bar{s}_u < 2.0 \text{ ksf}$
E	Soil profile with $\bar{v}_s < 600 \text{ ft/s}$ or with either $\bar{N} < 15 \text{ blows/ft}$ or $\bar{s}_u < 1.0 \text{ ksf}$, or any profile with more than 10 ft of soft clay defined as soil with $PI > 20$, $w > 40$ percent and $\bar{s}_u < 0.5 \text{ ksf}$
F	Soil requiring site-specific evaluations, such as: <ul style="list-style-type: none"> • Peats

(Source: AASHTO 2010 Table 3.10.3.1-1)

where in Table 3.2, \bar{v}_s , \bar{N} , \bar{s}_u , PI and w are average shear wave velocity for the upper 100 ft of the soil profile, average Standard Penetration Test (SPT) blow count (blows/ft) (ASTM D1586) for the upper 100 ft of the soil profile, average undrained shear strength in ksf (ASTM D2166 or ASTM D2850) for the upper 100 ft of the soil, plasticity index (ASTM D4318), and moisture content (ASTM D2216), respectively.



(Source: KDOT LRFD 2010)

**FIGURE 3.6
Peak Ground Acceleration**

2. **Coefficients PGA , S_s , and S_1 :** Peak Ground Acceleration coefficient (PGA), and short- and long-period spectral acceleration coefficients, S_s and S_1 respectively, are necessary to calculate design forces. These coefficients can be found on maps in AASHTO-LRFD (2010), including section 3.10.2.1.
3. **Site Factors:** Site factors F_{pga} , F_a , and F_y for the zero-period, short period range, and long-period range, respectively shall be obtained from AASHTO-LRFD tables in Section 3.10.3.2. These factors rely on Site Class, and coefficients PGA , S_s , and S_1 .
4. **Elastic Seismic Response Coefficient:** This coefficient shall be obtained for different periods according AASHTO-LRFD, Section 3.10.4.2. This coefficient determines the magnitude of the total lateral force acting on the construction due to earthquake activity.
5. **Seismic Performance Zones:** AASHTO-LRFD requires each bridge to be assigned into one of the four seismic zones in terms of the coefficient S_{D1} . This coefficient shall be calculated using equation $S_{D1} = F_y \times S_1$. For each Seismic Zone, AASHTO-LRFD provides specific design provisions. Kansas is mostly in Seismic Zone 1 and only the small part, in northwest of Kansas state, is in Seismic Zone 2.

AASHTO-LRFD (2010) has been changed significantly compared to the previous version (AASHTO-LRFD 2007) in terms of seismic provisions. Article 3.10.9.2 in AASHTO-LRFD (2010) expresses:

“For bridge in Zone 1 where the acceleration coefficient, A_s , as specified in Eq. 3.10.4.2-2, is less than 0.05 (This value is equal to 0.025 in AASHTO-LRFD (2007)), the horizontal design connection force in the restrained direction shall not be less than 0.15 (This value is equal to 0.1 in AASHTO-LRFD (2007)) times the vertical reaction due to the tributary permanent load and the tributary live loads assumed to exist during an earthquake.

For all other sites in Zone 1, the horizontal design connection force in the restrained direction shall not be less than 0.25 (This value is equal to 0.2 in AASHTO-LRFD (2007)) times the vertical reaction due to the tributary permanent load and the tributary live loads assumed to exist during an earthquake.”

In addition, Article 5.10.11.2 in AASHTO-LRFD (2010) also specifies provisions for seismic design of Seismic Zone 1 as follows:

“For bridges in Seismic Zone 1 where the response acceleration coefficient, S_{D1} , specified in Article 3.10.4.2, is less than 0.10, no consideration of seismic zone forces shall be required for the design of the structural components, except that the design of the connection of the superstructures to the substructure shall be specified in Article 3.10.9.2.

For bridges in Seismic Zone 1 where the response acceleration coefficient, S_{D1} , is greater than or equal to 0.10 but less than or equal to 0.15, no consideration of seismic forces shall be required for the design of structural components, except that:

- The design of the connection of the superstructure to the substructure shall be as specified in Article 3.10.9.2.
- The transverse reinforcement requirement at the top and bottom of a column shall be as specified in Article 5.10.4.1d and 5.10.11.4.1c.”

These requirements for Zone 1 are a departure from those in the previous edition of these Specifications. These changes are necessary because the return period of the design event has been increased from 500 to 1000 years, and the Zone boundaries (Table 3.10.6-1) have been increased accordingly. The high end of the new Zone 1 ($0.10 < S_{D1} < 0.15$) overlaps with the low end of the previous Zone 2. Since performance expectations have not change with increasing return period, the minimum requirements for bridge in the high end of Zone 1 should therefore be the same as those for the previous Zone 2. Requirements for the reminder Zone 1 ($S_{D1} < 0.10$) are unchanged.

In previous version, AASHTO-LRFD (2007), only considerations specified in Article 3.10.9.2 shall be required for design of the connection of superstructure to the substructure in Seismic Zone 1 (Article 5.10.11.2 in AASHTO-LRFD (2007)).

Since a small area in northeast Kansas falls into Zone 2, the provisions for Seismic Zone 2 are required to be explained herein. For bridge in Seismic Zone 2, Article 3.10.9.3 in AASHTO-LRFD (2010) says:

“Structures in Seismic Zone 2 shall be analyzed according to the minimum requirement specified in Article 4.7.4.1 and 4.7.4.3.

Except for foundations, seismic design force for all components, including pile bents and retaining walls and retaining walls, shall be determined by dividing the elastic seismic forces, obtained from Article 3.10.8, by the appropriate response modification factor, R , specified in Table 3.10.7.1-1.”

In addition, Article 5.10.11.3 in AASHTO-LRFD (2010) specifies provisions for seismic design of Seismic Zone 2 as follows:

“The requirement of Article 5.10.11.4 shall be taken to apply to bridges in Seismic Zone 2 except that the area of longitudinal reinforcement shall not be less than 0.01 or more than 0.06 times the gross section area, A_g .

Bridges in Seismic Zone 2 have a reasonable probability of being subjected to seismic forces that will cause yielding of the columns. Thus, it is deemed necessary that columns have some ductility capacity, although it is recognized that the ductility demand will not be as great as for columns of bridges in Seismic Zone 3 and 4. Nevertheless, all of the requirement for Zone 3 and 4 shall apply to bridges in Zone 2, with exception of the upper limit on reinforcing steel. This is a departure from the requirement in the previous edition of these Specifications in which selected requirement in Zone 3 and 4 were required for Zone 2. Satisfying all of the requirements, with one exception, is deemed necessary because the upper boundary for Zone 2 in the current edition is significantly higher than in the previous edition due to the increase in the return period for the design earthquake from 500 to 1000 yr.”

3.1.5 Concrete Bridge Reinforcement

Section 5 of AASHTO-LRFD (2010) is comprehensive part of the code that provides all specific provisions for design of concrete bridges. In terms of our topic, several articles are essential. First of all, Article 5.10.11.4.1e determines length of possible plastic hinge zones that can occur in the concrete columns and spacing for transverse reinforcement. It says:

“Transverse reinforcement for confinement shall be:

- Provided at the top and bottom of the column over a length not less than the greatest of the maximum cross-sectional column dimensions, one-sixth of the clear height of the column, or 18.0 inches;
- Extended into the top and bottom connections as specified in Article 5.10.11.4.3;
- Provided at the top of piles in pile bents over the same length as specified for columns;
- Provided within piles in pile bents over a length extending from 3.0 times the maximum cross-sectional dimension below the calculated point of moment fixity to a distance not less than the maximum cross-sectional dimension or 18.0 in. above the mud line; and
- Spaced not to exceed one-quarter of the minimum member dimension or 4.0 in. center-to-center.”

It should be noted that there is not any difference between the plastic hinge lengths, specified in AASHTO-LRFD (2010) and the one, specified in the previous version (AASHTO-LRFD 2007).

After defining possible plastic hinge zones, the transverse reinforcement requirements can be specified. Articles 5.7.4.6, 5.10.6, and 5.10.11.4.1d provide information for circular columns. Specifically, the volumetric ratio of lateral reinforcement should be at least the minimum of the following two values:

$$\rho_s \geq 0.45 \left(\frac{A_g}{A_c} - 1 \right) \frac{f'_c}{f_{yh}} \quad \text{Equation 3.2}$$

or

$$\rho_s \geq 0.12 \frac{f'_c}{f_y} \quad \text{Equation 3.3}$$

where, A_g , A_c , f'_c , and f_y are the gross area of the section, area of core measured to the outside diameter of the spiral, strength of concrete, and the yield strength of spiral reinforcement, respectively.

Article 5. 10.11.4.1d also defines requirements for rectangular column. The total gross sectional area of rectangular hoop reinforcement should be at least the minimum of the following two values:

$$A_{sh} \geq 0.30sh_c \frac{f'_c}{f_y} \left(\frac{A_g}{A_c} - 1 \right) \quad \text{Equation 3.4}$$

or

$$A_{sh} \geq 0.12sh_c \frac{f'_c}{f_y} \quad \text{Equation 3.5}$$

where, s , A_c , A_g , A_{sh} , f_y , and h_c are vertical spacing of hoops (not exceeding 4.0 inches), area of the column core (in²), gross area of column (in²), total cross-sectional area of tie reinforcement, including supplementary cross-ties having a vertical spacing of s and crossing a section having a core dimension of h_c (in²), yield strength of tie or spiral reinforcement (ksi), and core dimension of tied column in the direction under consideration (inches). In comparison, the expressions for both circular and rectangular column are very similar.

For longitudinal reinforcement, AASHTO-LRFD (2010) specifies these limits in *Article 5.7.4.2*. The minimum longitudinal reinforcement shall be as follows:

$$\frac{A_s f_y}{A_g f'_c} + \frac{A_{ps} f_{pu}}{A_g f_y} \geq 0.135 \quad \text{Equation 3.6}$$

The maximum longitudinal reinforcement shall be as follows:

$$\frac{A_s}{A_g} + \frac{A_{ps} f_{pu}}{A_g f_y} \leq 0.08 \quad \text{Equation 3.7}$$

and:

$$\frac{A_{ps} f_{pe}}{A_g f'_c} \leq 0.30 \quad \text{Equation 3.8}$$

where, A_s , A_g , A_{ps} , f_{pu} , f_y , f'_c , and f_{pe} are area of non-pre-stressed tension steel (in²), gross area of section (in²), area of prestressing steel (in²), specified tensile strength of pre-stressing steel

(ksi), specified yield strength of reinforcing bars (ksi), specified compressive strength of concrete (ksi), and effective prestress (ksi), respectively.

3.2 KDOT-LRFD Design Manual

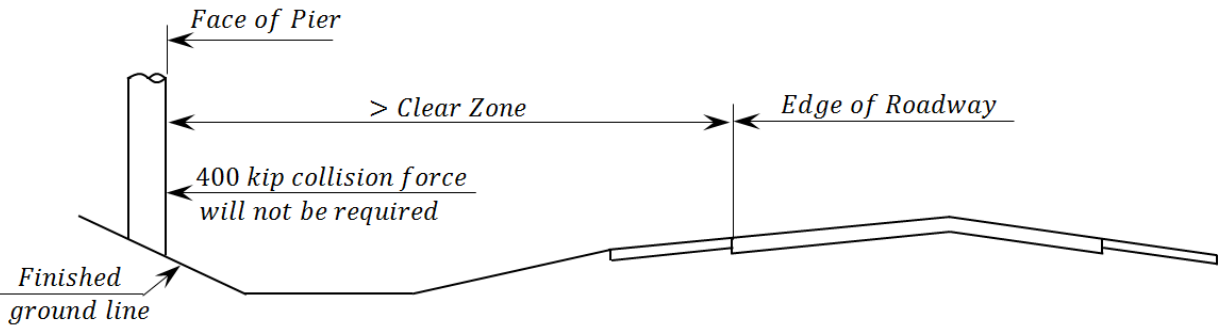
KDOT-LRFD Design Manual is a codebook provided by the Kansas Department of Transportation. This code shall be used in bridge design in Kansas. The KDOT-LRFD Design Manual uses AASHTO-LRFD and is primarily aimed to address particular conditions that are specific to the state of Kansas. The following are the changes, done in terms of designing bridge piers:

3.2.1 Loads and Load Factors

Eleven of the thirteen load combinations from AASHTO-LRFD (2010) are included in KDOT-LRFD (2011) Design Manual. Service IV and Fatigue I II load combinations specified in AASHTO-LRFD (2010) codebook are not required. Service IV and Fatigue I II combinations are not important to our subject since they are related to the pre-stressed concrete beams in tension, and finite load-induced fatigue life, respectively.

3.2.2 Vehicular Collision Force (CT)

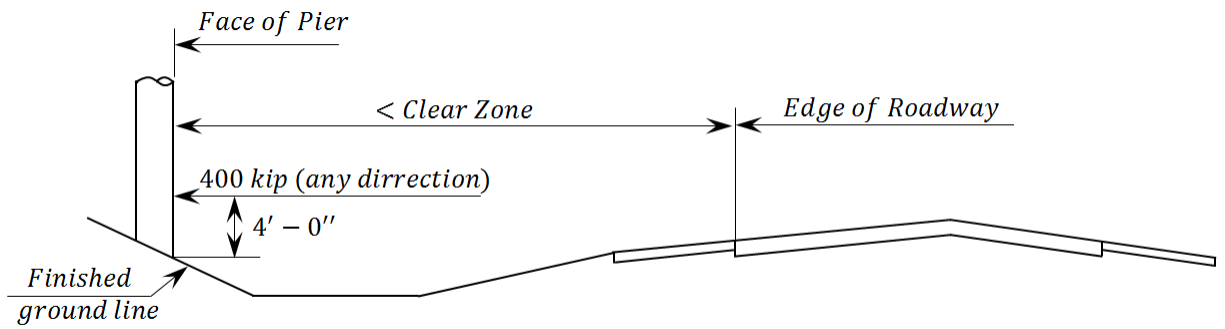
KDOT-LRFD (2011) has its own policy related to *Article 3.6.5* that provides provision for vehicular collision force. KDOT-LRFD (2011) also requires a pier to be designed for a 400 kip force acting in any direction. However, design does not have to count for this if the face of the pier to be located outside of the clear zone. Even if the clear zone is less than 30 ft, the collision force is not required as shown in Figure 3.7. Clear zone is an unobstructed, traversable roadside area that allows a driver to stop safely, or regain control of a vehicle that has left the roadway as seen in the figure below. The width of this zone varies from 10 ft on low speed, low volume roadways to 46 ft on high speed roadways. Detailed specification can be found in the AASHTO Roadside Design Guide.



(Source: KDOT-LRFD 2011)

FIGURE 3.7
Column Location and Clear Zone

If it is required that the face of the pier be located inside the Clear Zone, as shown in Figure 3.8, the design of the pier must include the 400 kip collision force.

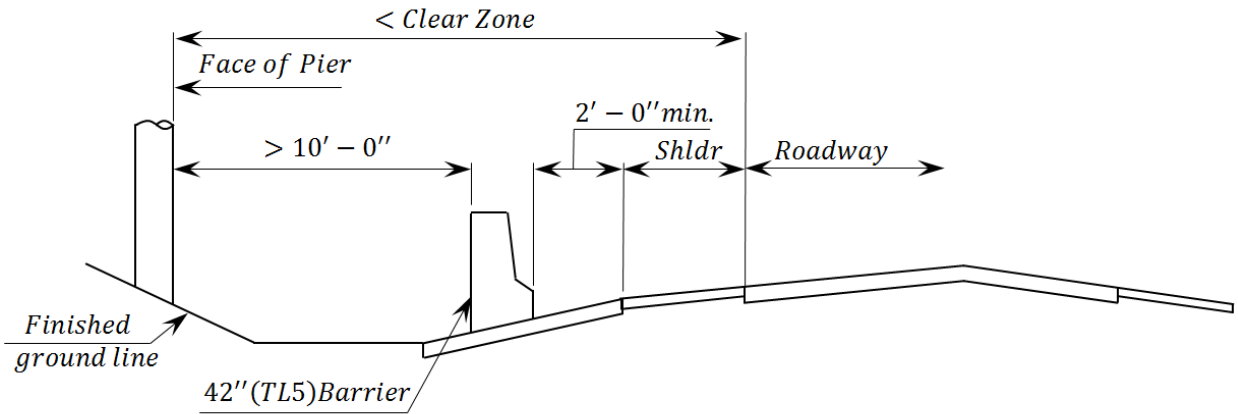


(Source: KDOT-LRFD 2011)

FIGURE 3.8
Column Location and Clear Zone

The 400 kip force can be also avoided in design if the following is true:

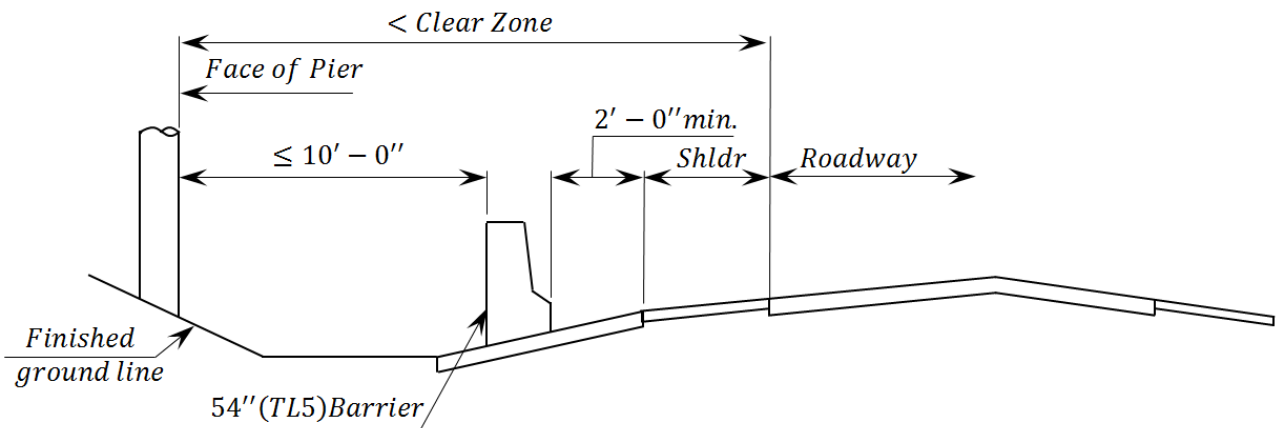
- If the barrier is located greater than 10' to 0" from the face of the pier, use a 42" (TL5) Barrier Rail as shown in Figure 3.9.



(Source: KDOT-LRFD 2011)

FIGURE 3.9
Column and 42" (TL5) Barrier Location

- If the barrier is located 10' to 0" or less from the face of the pier, use 54" high (TL5) Barrier Rail as shown in Figure 3.10.



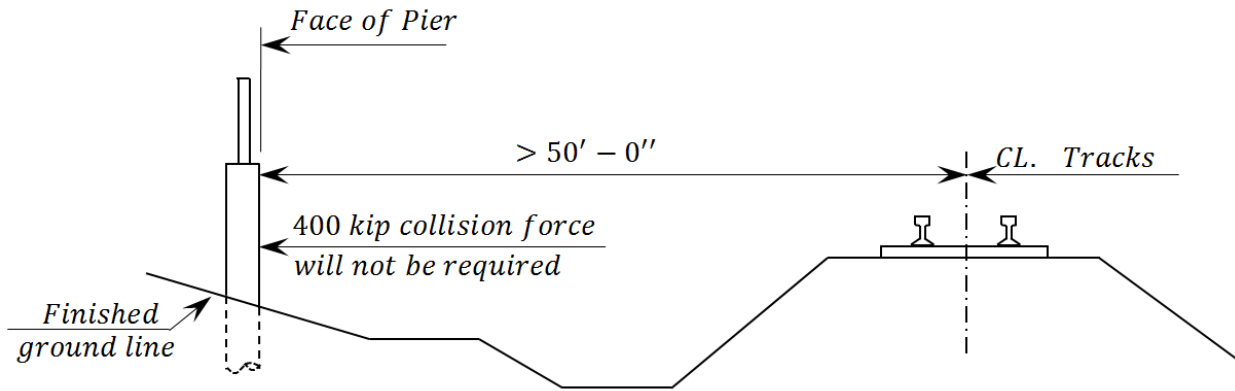
(Source: KDOT-LRFD 2011)

FIGURE 3.10
Column and 54" (TL5) Barrier Location

As seen, all the KDOT-LRFD requirements in terms of vehicular collision force, are consistent with AASHTO-LRFD (2010).

For a bridge over a railroad, KDOT says: the interpretation of Article 3.6.5 shall be follows (in order of preference):

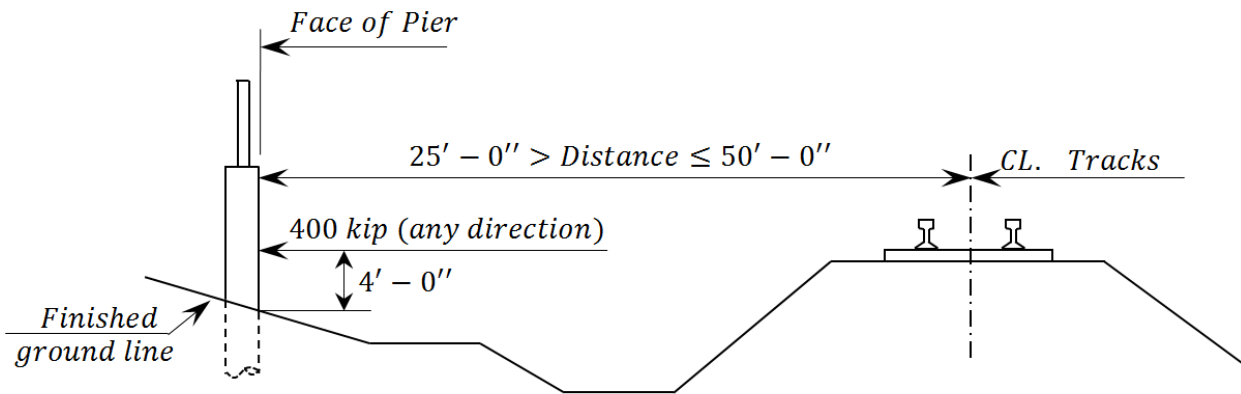
1. If the face of a pier is located greater than 50' from the centerline of the tracks, the collision force on the pier will not be required



(Source: KDOT-LRFD 2011)

FIGURE 3.11
Distance of Pier from Tracks Is More than 50'

2. If the face of a pier is located less than 50' and greater than 25' from the centerline of the tracks, the design of the pier must include the 400 kip collision force.

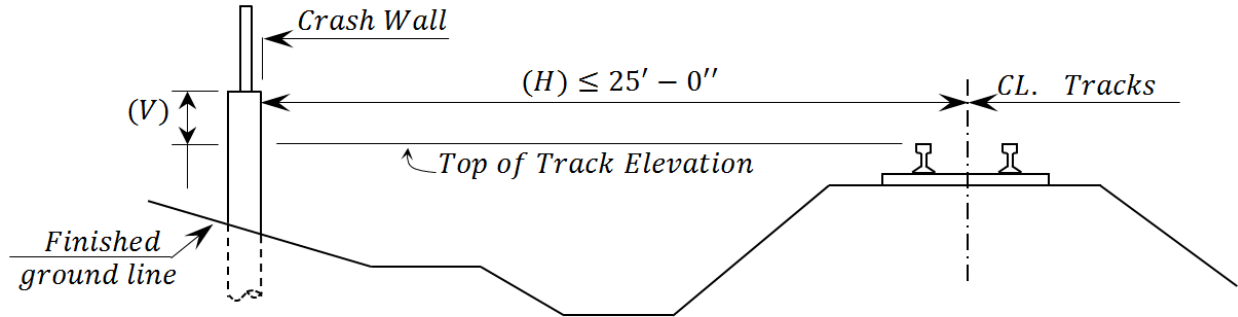


(Source: KDOT-LRFD 2011)

FIGURE 3.12
Distance of Pier from Tracks Is More than 25' and Less than 50'

3. If the force of pier is located less than or equal to 25' from the centerline of the tracks, the design of the pier must include a crash wall in addition to the 400 kip

collision force. See Figure 3.3.4.7-1 for design and geometry requirements of the crash wall.



(Source: KDOT-LRFD 2011)

FIGURE 3.13
Distance of Pier from Tracks in Less than 25'

3.2.3 Earthquake Effects (EQ)

In section 3.3.4.8 of the KDOT-LRFD (2011) Design Manual it simplifies design requirements in terms of seismic effects on bridge structures. Kansas is located mostly in Seismic Zone 1. Article 4.7.4.1 in AASHTO-LRFD (2010) states that bridges in Seismic Zone 1 need not to be analyzed for seismic loads. However, minimum superstructure to substructure connections and minimum bearing support lengths according AASHTO-LRFD (2010) specifications are required (Articles 4.7.4.4 and 3.10.9.2).

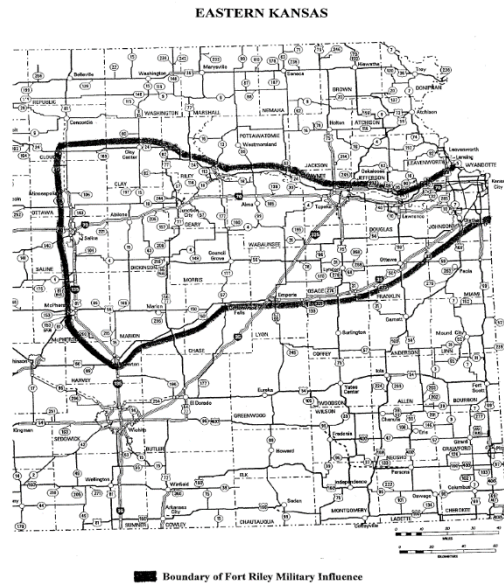
For this design, the tributary horizontal design connection forces shall be determined as follows:

$$A_s = PGA \times F_{pga} \quad \text{Equation 3.9}$$

“Where, PGA and F_{pga} are Peak Ground Acceleration as shown in Figure 3.6, and site class definition as shown in Table 5.2.

- A_s is less than 0.05 then use 0.15 times the vertical reaction due to dead load with $\gamma_{EQ} = 0$
- A_s is greater than 0.05 then use 0.25 times the dead load plus $\gamma_{EQ} = 0.25$

- In Ft. Riley military influence area shown in Figure 3.14, if A_s is greater than 0.05 then use 0.25 times the dead load plus $\gamma_{EQ} = 0.50$ (AASHTO-LRFD 2010).

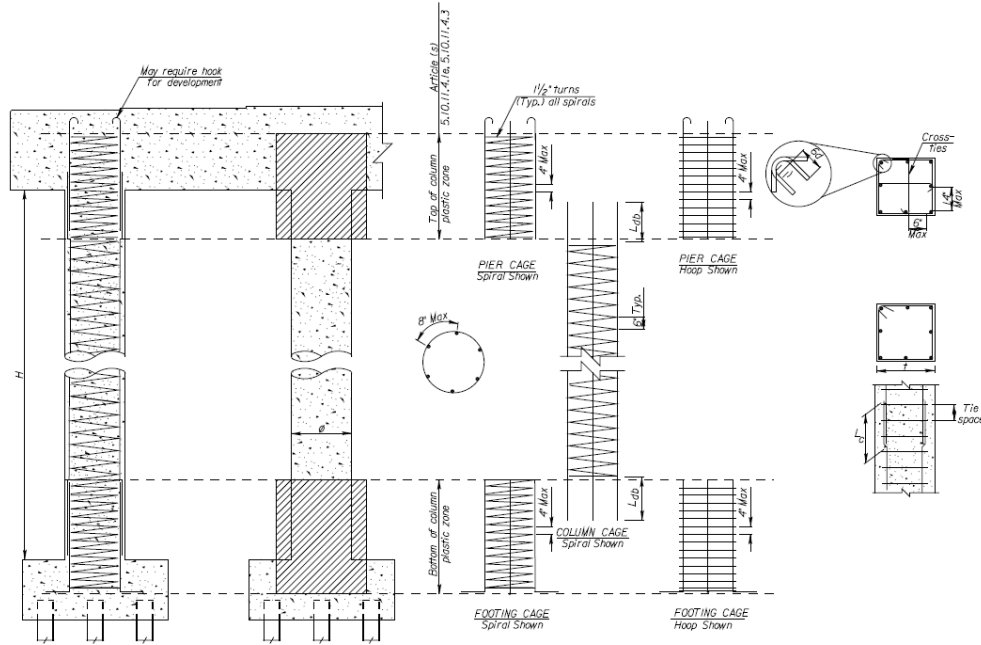


(Source: KDOT-LRFD 2011)

FIGURE 3.14
Fort Riley Military Influence for
Seismic Detailing

3.2.4 Concrete Bridge Reinforcement

KDOT-LRFD strictly follows the requirements of AASHTO-LRFD in terms of minimal and maximal limits of reinforcement, and possible plastic hinge zones. Sometimes, it goes deeper and provides other requirements. For instance, KDOT-LRFD dictates that all columns should be reinforced with between 1% and 2% reinforcement, columns outside this range are candidates for resizing. Although Kansas is located in Seismic Zone 1, some basic requirements for seismic design are necessary in terms concrete detailing as can be seen in Figure 3.15.



(Source: KDOT Figure 3.5.1.6.3-5)

FIGURE 3.15
Seismic Column Detailing

3.3 Evaluation of Two Representative Existing Reinforced Concrete Bridge Piers under New Code Requirement

The main goal of this research is to investigate the efficiency of the existing bridge columns against the new requirements, mentioned in the new version of AASHTO-LRFD (2010) and KDOT-LRFD (2011).

To achieve this goal, two representative columns in two different bridges, designed based on previous edition of these codes were analyzed. The shear capacity, flexural capacity, the plastic hinge length and also the displacement capacity are investigated for these bridge piers.

The first change is related to changing the return period of the design earthquake. The incensement in the return period of the design earthquake from 500 to 1000 years, has affected seismic design provisions even in Zone 1.

The second change implemented in KDOT-LRFD (2011) based on AASHTO-LRFD (2010) provisions, is designing bridge piers for vehicular collision force (a static force of 400 kip 4 ft above the ground). It should be noted that in the current version of AASHTO-LRFD

(2012) this equivalent static force is changed to 600 kip acting in the distance of 5 ft above the ground.

And the third change is estimating the plastic hinge length and considering special transverse reinforcement in it.

3.4 Assessment of Concrete Bridge Piers under Earthquake Loads

3.4.1 Response Spectrum

Section 3.10.2.1 of AASHTO-LRFD (2010) states

“Values of the coefficient PGA , S_s and S_1 are based on a uniform risk model off seismic hazard. The probability that a coefficient will not be exceeded at a given location during a 75-year period is estimated to be about 93 percent, i.e., a seven percent probability of exceedance. It can be shown that an event with the above probability of exceedance has a return period of about 1,000 yr. and is called the design earthquake.”

For investigating the effect of the first change in new version of AASHTO-LRFD (2010), the effective seismic forces on the columns of these bridges were evaluated. For this purpose, the spectrum should be calculated in advance. Based on AASHTO-LRFD (2010), “The General Procedure shall use the peak ground acceleration coefficient (PGA) and the short- and long-period spectral acceleration coefficients (S_s and S_1 , respectively) to calculate the spectrum”. As mentioned, values of PGA , S_s and S_1 shall be determined from either Figure 3.10.2.1-1 to 3.10.2.1-21 of AASHTO-LRFD (2010) as appropriate, or from state ground motion as approved by the owner. These coefficients are determined for three cities in Kansas and shown in Table 3.3.

TABLE 3.3
Seismic Coefficient of Three Cities in Kansas

City	PGA	S_s	S_1
Manhattan	0.05	0.0318	0.1
Topeka	0.04	0.0342	0.084
Kansas City	0.032	0.0371	0.076

Considering the USB 1997 which states “where soil profile properties are not known in sufficient detail, soil profile ‘D’ can be used”, soil profile “D” is used in this study. Considering site class “D” and having PGA , S_s and S_1 the site factors F_{pga} , F_a , and F_{py} , are specified by using Tables 3.10.3.2.1 to 3.10.3.2-3 in AASHTO-LRFD (2010) which are expressed in Table 3.4.

TABLE 3.4
Site Factors for Three Cities in Kansas

City	F_{pga}	F_a	F_v
Manhattan	1.6	1.6	2.4
Topeka	1.6	1.6	2.4
Kansas City	1.6	1.6	2.4

Using the mapped peak ground acceleration coefficient and the spectral acceleration coefficients, scaled by the zero-, short-, and long-period site factors, the five-percent-damped-design response spectrums for these three cities are specified and shown in Figure 3.16 through Figure 3.18.

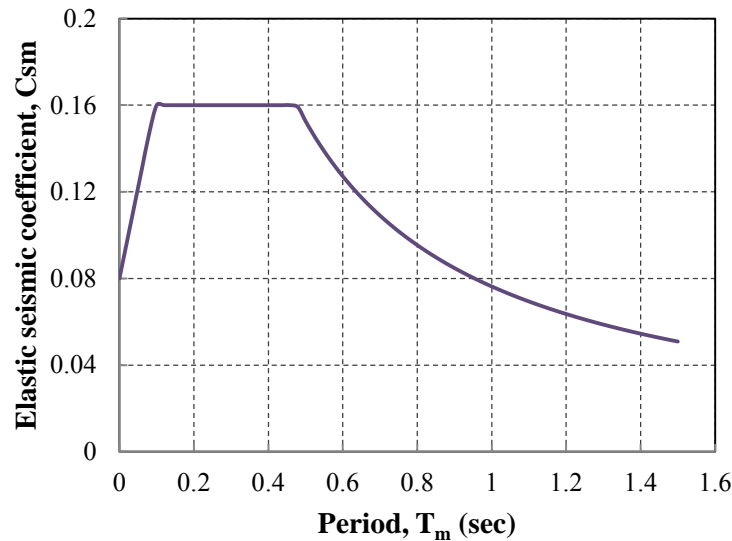


FIGURE 3.16
The Five-Percent-Damped-Design Response Spectrum for Manhattan, Kansas

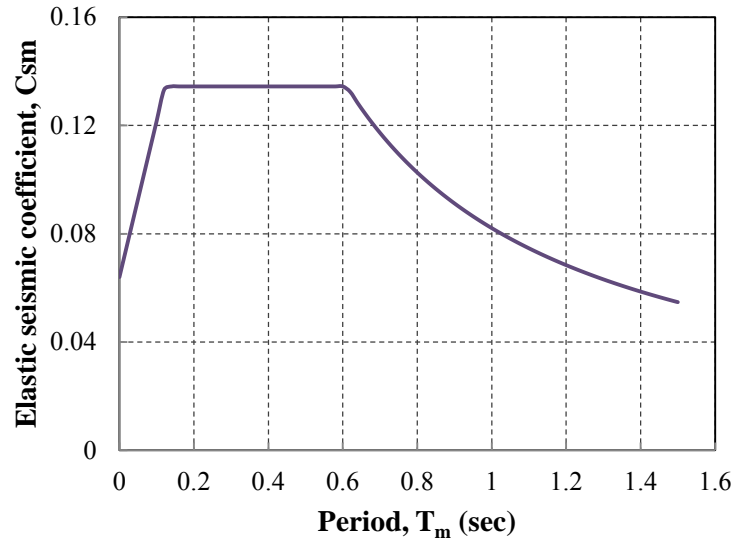


FIGURE 3.17
The Five-Percent-Damped-Design Response Spectrum for Topeka, Kansas

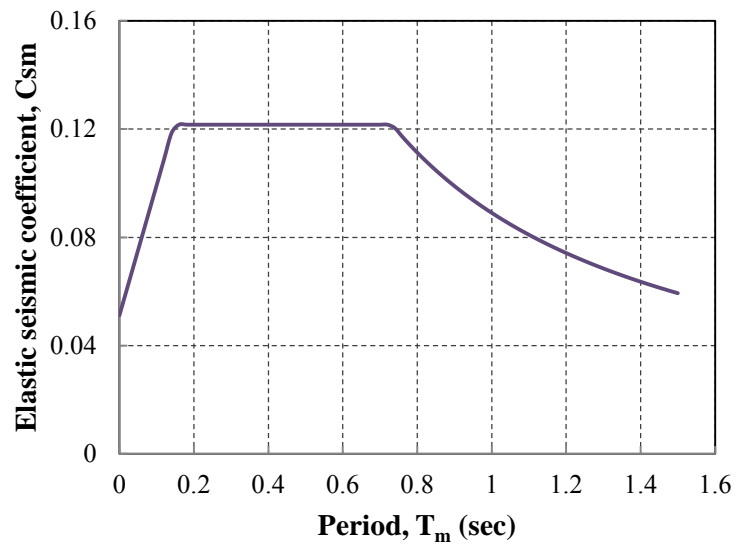


FIGURE 3.18
The Five-Percent-Damped-Design Response Spectrum for Kansas City, Kansas

The values of acceleration coefficient, for these three cities are shown in Table 3.5. Based on values of acceleration coefficient and four seismic zone, specified in Table 3.10.6-1 of AASHTO-LRFD (2010) it's calculated that all these cities are in Seismic Zone 1 ($S_{D1} \leq 0.15$).

TABLE 3.5
Acceleration Coefficient for Three Cities in Kansas

City	S_{D1}	A_s
Manhattan	0.07632	0.08
Topeka	0.08208	0.064
Kansas City	0.08904	0.0512

3.4.2 Equivalent Static Seismic Loading

KDOT-LRFD (2011) expresses that “In general Kansas is in Seismic Zone 1, LRFD Specification Article 4.7.4.1 states that bridge in Seismic Zone 1 need not to be analyzed for seismic loads, regardless of their importance and geometry. However, minimum superstructure to substructure connections indicated in Article 3.10.9.2 and minimum bearing support length Article 4.7.4.4 are required.” Although, we don’t need to design bridge’s columns for earthquake load, based on new seismic requirement, the earthquake effective loads are calculated herein to show that the Extreme I load combination, including earthquake loads, is not the dominant load combination. For achieving this goal, the intensity of the equivalent static seismic loading should be calculated which is expressed as follow.

For calculating the equivalent static seismic loading, the natural period of these two bridges should be calculated. AASHTO-LRFD (2010) uses two methods for determining the natural period of bridges in order to calculating the earthquake force effects, (a). Single-Mode Spectral method and (b). Uniform Load method (*Article 4.7.3.2*). The single-mode spectral method, used in this report, is based on fundamental mode of vibration in either the longitudinal or transverse direction. *Article 4.7.4.3.2b* in AASHTO-LRFD (2010) states that “For regular bridges, the fundamental modes of vibration in the horizontal plane coincide with the longitudinal and transverse axes of the bridge structure. This mode shape may be found by applying a uniform horizontal load to the structures and calculating the corresponding deformed shape. The natural period may be calculated by equating the maximum potential and kinetic energies associated with the fundamental mode shape.” The single-mode spectral analysis method, described in section C4.7.4.3.2b of AASHTO-LRFD (2010), can be done by going through the following steps:

- As shown in Figure 3.19 and Figure 3.20, the static displacements $v_s(x)$ due to an assumed uniform loading p_0 , is calculated.

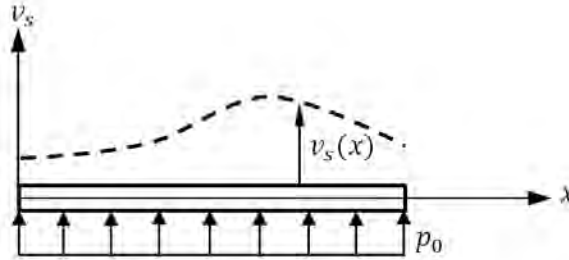


FIGURE 3.19
Bridge Deck Subjected to Assumed
Transverse Loading

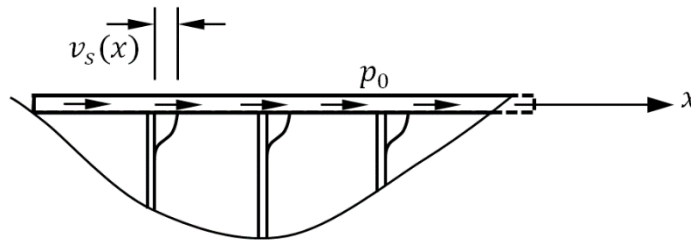


FIGURE 3.20
Bridge Deck Subjected to Assumed Longitudinal
Loading

- Factors α , β and γ are calculated based on following equations:

$$\alpha = \int v_s(x) dx \quad \text{Equation 3.10}$$

$$\beta = \int w(x) \cdot v_s(x) dx \quad \text{Equation 3.11}$$

$$\gamma = \int w(x) \cdot v_s^2(x) dx \quad \text{Equation 3.12}$$

Where, p_0 , $v_s(x)$, $w(x)$ are a uniform load arbitrarily set equal to 1 (kip/ft), deformation corresponding to p_0 (ft) and nominal, unfactored dead load of the bridge superstructure and tributary substructure (kip/ft), respectively.

- The natural period of the bridges is calculated as follows:

$$T_m = 2\pi \sqrt{\frac{\gamma}{p_0 g \alpha}} \quad \text{Equation 3.13}$$

Where, g is the acceleration of gravity (ft/sec²).

- Using T_m and Eqs. 3.10.4.2-1, 3.10.4.2-4, or 3.10.4.2-5 in AASHTO-LRFD (2010), C_{sm} is calculated.
- The equivalent earthquake loading is calculated as follows:

$$p_e(x) = \frac{\beta C_{sm}}{\gamma} w(x) \cdot v_s(x) \quad \text{Equation 3.14}$$

Where, C_{sm} and $p_e(x)$ are the dimensionless elastic seismic response coefficient given by Eqs. 3.10.4.2-1, 3.10.4.2-4, or 3.10.4.2-5 in AASHTO-LRFD (2010) and the intensity of the equivalent static seismic loading applied to represent the primary mode of vibration (kip/ft), respectively.

- At the end the equivalent static load is applied to the structure and the resulting member force effect are determined.

3.4.2.1 Equivalent Static Seismic Loading for Bridge No. 1

The properties of column section and also material properties for the first and second bridge are specified in Appendix B. The moment of inertia for column section of the first bridge is calculated as follows:

$$E_c = 57\sqrt{f'_c} = 57\sqrt{4000} = 3605 \text{ ksi} = 519120 \text{ kip/ft}^2 \quad \text{Equation 3.15}$$

$$n = \frac{E_s}{E_c} = \frac{29000}{3605} = 8.044 \quad \text{Equation 3.16}$$

$$I_c = \frac{\pi R^4}{4} = \frac{\pi \times (1.5 \times 12)^4}{4} = 82448 \text{ in}^4 \quad \text{Equation 3.17}$$

$$\begin{aligned} I_g &= I_c + \sum (n-1)A_i d_i^2 = 82448 + 1267.1 \times 7.04 = 91374.3 \text{ in}^4 \\ &= 4.41 \text{ ft}^4 \end{aligned} \quad \text{Equation 3.18}$$

Where, f'_c , R , E_c , E_s , I_c , and I_g are the concrete compressive strength in 28 days, the circular column radius, the modulus of elasticity of concrete, the modulus of elasticity of steel, the moment of inertia of the column cross-section without considering steel bars, and the moment of inertia of circular column cross-section with considering steel bars, respectively.

As shown in Figure 3.21, the lateral stiffness of column with two clamped supports is $12EI/l^3$, where l is the column's height. Followings are the lateral stiffness for three types of columns in Bridge No. 1. It should be noted that based on section 10.10.4.1 in ACI-318 (2011), for the beam it is permitted to use $I = 0.35I_g$ and for the column we can use $I = 0.70I_g$.

$$k_{c1} = \frac{12EI}{l^3} = \frac{12 \times 519120 \times 0.7 \times 4.41}{34^3} = 489.27 \text{ kips/ft} \quad \text{Equation 3.19}$$

$$k_{c2} = \frac{12EI}{l^3} = \frac{12 \times 519120 \times 0.7 \times 4.41}{36^3} = 412.172 \text{ kips/ft} \quad \text{Equation 3.20}$$

$$k_{c3} = \frac{12EI}{l^3} = \frac{12 \times 519120 \times 0.7 \times 4.41}{31^3} = 645.506 \text{ kips/ft} \quad \text{Equation 3.21}$$

Calculating lateral stiffness for each column, the lateral stiffness of each bent with three columns, is calculated as follows:

$$k_1 = 3k_{c1} = 1467.81 \text{ kips/ft} \quad \text{Equation 3.22}$$

$$k_2 = 3k_{c2} = 1236.52 \text{ kips/ft} \quad \text{Equation 3.23}$$

$$k_3 = 3k_{c3} = 1936.52 \text{ kips/ft} \quad \text{Equation 3.24}$$

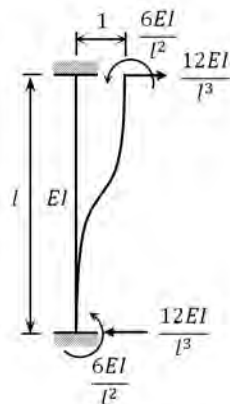


FIGURE 3.21
The Stiffness of Column
Subjected to a Horizontal Unit
Displacement

The next step in calculating natural period of the bridge is to calculate the moment of inertia of the slab. Since, we didn't have enough detailed information about the slab, regarding the bridge's width and span's length, the section shown in Figure 3.22 is used for calculating the moment of inertia of the slab, with a reasonable accuracy.

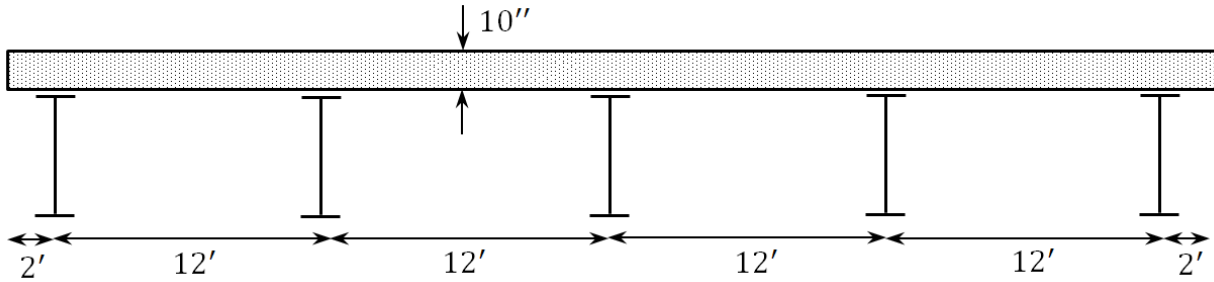


FIGURE 3.22
The Slab Section for Bridge No. 1

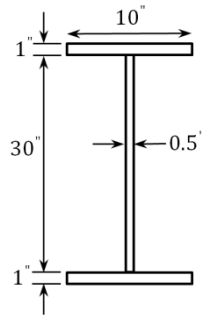


FIGURE 3.23
The Section of Girder

$$\bar{x} = \frac{\sum A_i x_i}{\sum A_i} = 26 \text{ ft} \quad \text{Equation 3.25}$$

$$I_{shape} = \frac{1}{12} \times 30 \times 0.5^3 + 2 \times \left(\frac{1}{12} \times 1 \times 10^3 \right) = 166.979 \text{ in}^4 \quad \text{Equation 3.26}$$

$$I_{slab} = \frac{1}{12} \times 10 \times 624^3 + 5 \times 8.044 \times 166.979 + 8.044 \times (2 \times 35 \times ((26 - 2) \times 12)^2 + 2 \times 35 \times ((26 - 14) \times 12)^2) = 2.608 \times 10^8 \text{ in}^4 = 12580.2 \text{ ft}^4$$

Equation 3.27

$$EI = 519120 \times 0.35 \times 9784.32 = 2.286 \times 10^9 \text{ kip.ft}^2$$

Equation 3.28

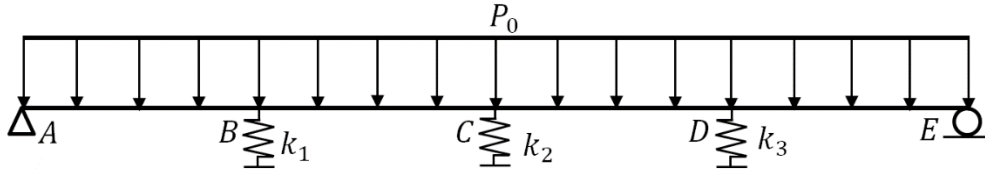


FIGURE 3.24
Bridge Deck Subjected to Assumed Transverse Loading

Using slope-deflection method, the flexural moment and spring's forces are obtained as follows:

$$M_{AB} = \frac{2EI}{l_1} \left(2\theta_A + \theta_B - \frac{3\Delta_1}{l_1} \right) - M_{FAB} = \frac{2EI}{90} \left(2\theta_A + \theta_B - \frac{3\Delta_1}{l_1} \right) - \frac{1 \times 90^2}{12}$$

$$M_{BA} = \frac{2EI}{l_1} \left(2\theta_B + \theta_A - \frac{3\Delta_1}{l_1} \right) + M_{FAB} = \frac{2EI}{90} \left(2\theta_B + \theta_A - \frac{3\Delta_1}{l_1} \right) + \frac{1 \times 90^2}{12}$$

$$\begin{aligned} M_{BC} &= \frac{2EI}{l_2} \left(2\theta_B + \theta_C - \frac{3(\Delta_2 - \Delta_1)}{l_2} \right) - M_{FBC} \\ &= \frac{2EI}{91} \left(2\theta_B + \theta_C - \frac{3(\Delta_2 - \Delta_1)}{l_2} \right) - \frac{1 \times 91^2}{12} \end{aligned}$$

Equation 3.29

$$\begin{aligned} M_{CB} &= \frac{2EI}{l_2} \left(2\theta_C + \theta_B - \frac{3(\Delta_2 - \Delta_1)}{l_2} \right) + M_{FBC} \\ &= \frac{2EI}{91} \left(2\theta_B + \theta_C - \frac{3(\Delta_2 - \Delta_1)}{l_2} \right) + \frac{1 \times 91^2}{12} \end{aligned}$$

$$\begin{aligned} M_{CD} &= \frac{2EI}{l_2} \left(2\theta_C + \theta_D - \frac{3(\Delta_3 - \Delta_2)}{l_2} \right) - M_{FCD} \\ &= \frac{2EI}{91} \left(2\theta_C + \theta_D - \frac{3(\Delta_3 - \Delta_2)}{l_2} \right) - \frac{1 \times 91^2}{12} \end{aligned}$$

$$\begin{aligned}
M_{DC} &= \frac{2EI}{l_2} \left(2\theta_D + \theta_C - \frac{3(\Delta_3 - \Delta_2)}{l_2} \right) - M_{FCD} \\
&= \frac{2EI}{91} \left(2\theta_D + \theta_C - \frac{3(\Delta_3 - \Delta_2)}{l_2} \right) + \frac{1 \times 91^2}{12} \\
M_{DE} &= \frac{2EI}{l_1} \left(2\theta_D + \theta_E + \frac{3\Delta_3}{l_1} \right) - M_{FDE} = \frac{2EI}{90} \left(2\theta_D + \theta_C + \frac{3\Delta_3}{l_1} \right) - \frac{1 \times 90^2}{12} \\
M_{ED} &= \frac{2EI}{l_1} \left(2\theta_E + \theta_D + \frac{3\Delta_3}{l_1} \right) + M_{FCD} = \frac{2EI}{90} \left(2\theta_E + \theta_D + \frac{3\Delta_3}{l_1} \right) + \frac{1 \times 90^2}{12}
\end{aligned}$$

The boundary condition for continuous beam shown in Figure 3.24 are as follows:

$$\begin{aligned}
M_{AB} &= 0; \\
M_{BA} + M_{BC} &= 0; \\
M_{CB} + M_{CD} &= 0; \\
M_{DC} + M_{DE} &= 0; \\
M_{ED} &= 0; \\
k_1\Delta_1 &= \frac{1}{l_1} \times \left(M_{AB} + M_{BA} + \frac{P_0 l_1^2}{2} \right) - \frac{1}{l_2} \times \left(M_{BC} + M_{CB} - \frac{P_0 l_2^2}{2} \right); \\
k_2\Delta_2 &= \frac{1}{l_2} \times \left(M_{BC} + M_{CB} + \frac{P_0 l_2^2}{2} \right) - \frac{1}{l_2} \times \left(M_{CD} + M_{DC} - \frac{P_0 l_2^2}{2} \right); \\
k_3\Delta_3 &= \frac{1}{l_2} \times \left(M_{CD} + M_{DC} + \frac{P_0 l_2^2}{2} \right) - \frac{1}{l_1} \times \left(M_{DE} + M_{ED} - \frac{P_0 l_1^2}{2} \right).
\end{aligned}$$

Equation 3.30

Solving above equations, the unknown variables are specified as follows:

$$\begin{aligned}
 \theta_A &= 0.0003964 \\
 \theta_B &= 0.0002638 \\
 \theta_C &= -5.937 \times 10^{-6} \\
 \theta_D &= -0.0002638 \\
 \theta_E &= -0.0003845 \\
 \Delta_1 &= 0.03130 \\
 \Delta_2 &= 0.04346 \\
 \Delta_3 &= 0.03036
 \end{aligned}
 \tag{Equation 3.31}$$

Substituting variables in Equations 3.29, the flexural moment are calculated as follows:

$$\begin{aligned}
 M_{BA} &= -5389.08 \text{ k.ft} \\
 M_{BC} &= 5389.08 \text{ k.ft} \\
 M_{CB} &= -6783.94 \text{ k.ft} \\
 M_{CD} &= 6783.94 \text{ k.ft} \\
 M_{DE} &= -4788.04 \text{ k.ft} \\
 M_{ED} &= 4788.04 \text{ k.ft}
 \end{aligned}
 \tag{Equation 3.32}$$

In the next step, the deflection of continuous beam should be specified. Using flexural moments in Equation 3.32 and following equations, the beam deflection in each span is specified.

$$EI \cdot y = -P_0 \frac{x^4}{24} + c_1 \frac{x^3}{6} + c_2 \frac{x^2}{2} + c_3 x + c_4
 \tag{Equation 3.33}$$

$$M = EI \frac{d^2 y}{dx^2} = -P_0 \frac{x^2}{2} + c_1 x + c_2
 \tag{Equation 3.34}$$

where, y is the deflection function, x is the distance from initial point of each span, and c_i ($i = 1:4$) is the unknown coefficient depending on boundary conditions. For example for the first span the procedure is like below:

$$\begin{aligned}
 @x = 0 &\rightarrow y = 0 \\
 @x = l_1 &\rightarrow y = \Delta_1 = -0.0313 \\
 @x = 0 &\rightarrow M = 0 \\
 @x = l_1 &\rightarrow M = 5389.08 \text{ kip.ft} \\
 EIy &= -\frac{x^4}{24} + 73.0353x^3 - 1.35623 \times 10^6 x
 \end{aligned}
 \tag{Equation 3.35}$$

The following are the deflection functions for other spans, calculated as done for the first one:

- Second span:

$$EIy = -\frac{x^4}{24} + 10.138 x^3 + 2694.54 x^2 - 601720x - 7.15518 \times 10^7
 \tag{Equation 3.36}$$

- Third span:

$$EIy = -\frac{x^4}{24} + 3.9278 x^3 + 3391.97 x^2 + 11746 x - 9.9212 \times 10^7
 \tag{Equation 3.37}$$

- Fourth span:

$$EIy = -\frac{x^4}{24} - 1.3667 x^3 + 2394.02 x^2 + 603206x - 6.995 \times 10^7
 \tag{Equation 3.38}$$

Substituting above equations in Equations 3.9 to 3.11, the factors α , β and γ are calculated as follows. For this bridge $w = 9.9895 \text{ kips/ft}$.

$$\alpha = \frac{1}{EI} (4.344 \times 10^9 + 8.2039 \times 10^9 + 8.112 \times 10^9 + 3.342 \times 10^9) = 10.4995
 \tag{Equation 3.39}$$

$$\gamma = \frac{w}{(EI)^2} (2.5626 \times 10^{17} + 7.459 \times 10^{17} + 7.301 \times 10^{17} + 1.6159 \times 10^{17}) = 3.62$$

Equation 3.40

$$\beta = w \times 10.4995 = 104.885$$

Equation 3.41

Having factors α , β and γ , the natural period and equivalent static load are calculated:

$$T_m = 2\pi \sqrt{\frac{3.62}{1 \times 32.2 \times 10.4995}} = 0.65 \text{ sec} \rightarrow \begin{aligned} C_{sm}(\text{Manhattan}) &= 0.1139 \\ C_{sm}(\text{Topeka}) &= 0.1262 \\ C_{sm}(\text{Kansas City}) &= 0.1216 \end{aligned}$$

Equation 3.42

Among the mentioned three cities in Kansas, the equivalent static force is calculated only for Kansas City or Topeka which have the largest C_{sm} .

$$P_e(x) = \frac{104.885 \times 0.1262}{3.62} \times 9.9895 \times v_s(x) = 36.52656 v_s(x)$$

Equation 3.43

As mentioned, the final step is applying the equivalent static load on bridge and determining the resulting member force effects. In this study, as shown in Figure 3.25, in each span a uniform load with a magnitude equal to the area under the actual load divided by the span length is used to determine the members' force effects.

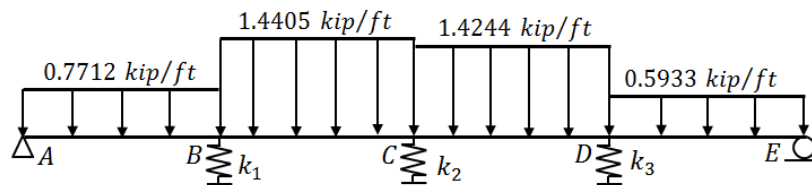


FIGURE 3.25
The Bridge Subjected to the Transverse Uniform Loads

Using slope-deflection method, the spring forces are obtained:

$$F_1 = k_1 \cdot \Delta_1 = 55.8684 \text{ kips}$$

$$F_2 = k_2 \cdot \Delta_2 = 65.8358 \text{ kips}$$

$$F_3 = k_3 \cdot \Delta_3 = 70.9858 \text{ kips}$$

Equation 3.44

For each column in each bent, the shear force and flexural moment due to equivalent static load are specified as follows:

$$F_{x1} = \frac{F_1}{3} = 18.6228 \text{ kips}, \quad M_{z1} = \frac{18.6228 \times 34}{2} = 316.588 \text{ kip.ft}$$

$$F_{x2} = \frac{F_2}{3} = 21.9453 \text{ kips}, \quad M_{z2} = \frac{21.9453 \times 36}{2} = 395.015 \text{ kip.ft}$$

$$F_{x3} = \frac{F_3}{3} = 23.6619 \text{ kips}, \quad M_{z3} = \frac{23.6619 \times 31}{2} = 366.759 \text{ kip.ft}$$

Equation 3.45

Using load combinations, expressed in Table 3.1, demand flexural moment and axial force are obtained. These forces are shown in Table 3.6 through Table 3.8.

TABLE 3.6
Demand Forces for Column No. 1 in Bridge No. 1

Load Combination	M (kip.ft)	P(kips)
Extreme event I Min DL Case I LL	356.1885	451.6015
Extreme event I Min DL Case II LL	355.7859	449.659
Extreme event I Max DL Case I LL	354.7538	610.7715
Extreme event I Max DL Case II LL	354.3512	608.829

TABLE 3.7
Demand Forces for Column No. 2 in Bridge No. 1

Load Combination	M (kip.ft)	P(kips)
Extreme event I Min DL Case I LL	435.6677	504.467
Extreme event I Min DL Case II LL	435.9530	512.169
Extreme event I Max DL Case I LL	435.6676	686.667
Extreme event I Max DL Case II LL	435.9528	694.369

TABLE 3.8
Demand Forces for Column No. 3 in Bridge No. 1

Load Combination	M (kip.ft)	P(kips)
Extreme event I Min DL Case I LL	411.5166	436.107
Extreme event I Min DL Case II LL	411.7610	438.144
Extreme event I Max DL Case I LL	412.9506	595.272
Extreme event I Max DL Case II LL	413.1950	597.309

3.4.2.2 Equivalent Static Seismic Loading for Bridge No. 2

The moment of inertia for the column section of the second bridge is calculated as follows:

$$E_c = 57\sqrt{f'_c} = 57\sqrt{4000} = 3605 \text{ ksi} = 519120 \text{ kip/ft}^2 \quad \text{Equation 3.46}$$

$$n = \frac{E_s}{E_c} = \frac{29000}{3605} = 8.044 \quad \text{Equation 3.47}$$

$$I_c = \frac{\pi R^4}{4} = \frac{\pi \times (1.5 \times 12)^4}{4} = 82448 \text{ in}^4 \quad \text{Equation 3.48}$$

$$I_g = I_c + \sum (n - 1)A_i d_i^2 = 82448 + 11974 = 94422 \text{ in}^4 = 4.55 \text{ ft}^4 \quad \text{Equation 3.49}$$

Following is the lateral stiffness for columns in Bridge No. 2:

$$k_c = \frac{12EI}{l^3} = \frac{12 \times 519120 \times 4.55 \times 0.7}{13.615^3} = 7861.5 \text{ kips/ft} \quad \text{Equation 3.50}$$

Calculating lateral stiffness for each column, the lateral stiffness of the bent with four columns, is calculated as follows:

$$k = 4k_c = 31446 \text{ kips/ft} \quad \text{Equation 3.51}$$

As done for Bridge No. 1, the next step for calculating the natural period of the bridge is calculating moment of inertia of the slab. Regarding the bridge width and span length, the section shown in Figure 3.26 is used for calculating the moment of inertia of the slab.

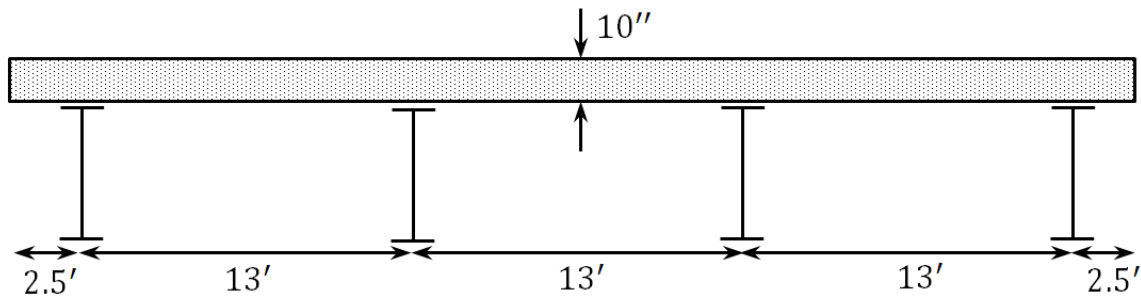


FIGURE 3.26
The Slab Section for Bridge No. 2

$$\bar{x} = \frac{\sum A_i x_i}{\sum A_i} = 22 \text{ ft} \quad \text{Equation 3.52}$$

$$I_{shape} = \frac{1}{12} \times 30 \times 0.5^3 + 2 \times \left(\frac{1}{12} \times 1 \times 10^3 \right) = 166.979 \text{ in}^4 \quad \text{Equation 3.53}$$

$$\begin{aligned} I_{slab} &= \frac{1}{12} \times 10 \times 528^3 + 4 \times 8.044 \times 166.979 + 8.044 \\ &\quad \times (2 \times 35 \times (6.5 \times 12)^2) + 2 \times 35 \times (19.5 \times 12)^2 = 1.57 \times 10^8 \text{ in}^4 \\ &= 7567.91 \text{ ft}^4 \end{aligned}$$

Equation 3.54

$$EI = 519120 \times 7567.91 \times 0.35 = 1.375 \times 10^9 \text{ kip.ft}^2$$

Equation 3.55

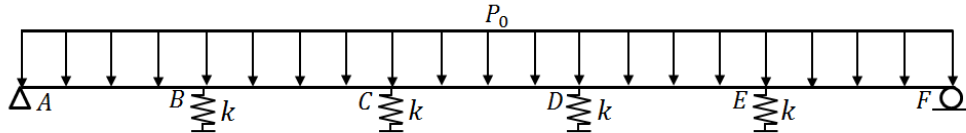


FIGURE 3.27
Bridge Deck Subjected to Assumed Transverse Loading

Using slope-deflection method, the flexural moment and spring's forces are obtained as follows:

$$\begin{aligned} M_{AB} &= \frac{2EI}{l_1} \left(2\theta_A + \theta_B - \frac{3\Delta_1}{l_1} \right) - M_{FAB} \\ &= \frac{2EI}{150.92} \left(2\theta_A + \theta_B - \frac{3\Delta_1}{l_1} \right) - \frac{1 \times 150.92^2}{12} \end{aligned}$$

$$\begin{aligned} M_{BA} &= \frac{2EI}{l_1} \left(2\theta_B + \theta_A - \frac{3\Delta_1}{l_1} \right) + M_{FAB} \\ &= \frac{2EI}{150.92} \left(2\theta_B + \theta_A - \frac{3\Delta_1}{l_1} \right) + \frac{1 \times 150.92^2}{12} \end{aligned}$$

Equation 3.56

$$\begin{aligned} M_{BC} &= \frac{2EI}{l_2} \left(2\theta_B + \theta_C - \frac{3(\Delta_2 - \Delta_1)}{l_2} \right) - M_{FBC} \\ &= \frac{2EI}{190.3} \left(2\theta_B + \theta_C - \frac{3(\Delta_2 - \Delta_1)}{l_2} \right) - \frac{1 \times 190.3^2}{12} \end{aligned}$$

$$\begin{aligned} M_{CB} &= \frac{2EI}{l_2} \left(2\theta_C + \theta_B - \frac{3(\Delta_2 - \Delta_1)}{l_2} \right) + M_{FBC} \\ &= \frac{2EI}{190.3} \left(2\theta_C + \theta_B - \frac{3(\Delta_2 - \Delta_1)}{l_2} \right) + \frac{1 \times 190.3^2}{12} \end{aligned}$$

$$M_{CD} = \frac{2EI}{l_2} \left(2\theta_C + \theta_D - \frac{3(\Delta_3 - \Delta_2)}{l_2} \right) - M_{FCD}$$

$$= \frac{2EI}{190.3} \left(2\theta_C + \theta_D - \frac{3(\Delta_3 - \Delta_2)}{l_2} \right) - \frac{1 \times 190.3^2}{12}$$

$$M_{DC} = \frac{2EI}{l_2} \left(2\theta_D + \theta_C - \frac{3(\Delta_3 - \Delta_2)}{l_2} \right) - M_{FCD}$$

$$= \frac{2EI}{190.3} \left(2\theta_D + \theta_C - \frac{3(\Delta_3 - \Delta_2)}{l_2} \right) + \frac{1 \times 190.3^2}{12}$$

$$M_{DE} = \frac{2EI}{l_2} \left(2\theta_D + \theta_E + \frac{3(\Delta_4 - \Delta_3)}{l_2} \right) - M_{FDE}$$

$$= \frac{2EI}{190.3} \left(2\theta_D + \theta_C + \frac{3(\Delta_4 - \Delta_3)}{l_2} \right) - \frac{1 \times 190.3^2}{12}$$

$$M_{ED} = \frac{2EI}{l_2} \left(2\theta_E + \theta_D - \frac{3(\Delta_4 - \Delta_3)}{l_2} \right) + M_{FCD}$$

$$= \frac{2EI}{190.3} \left(2\theta_E + \theta_D - \frac{3(\Delta_4 - \Delta_3)}{l_2} \right) + \frac{1 \times 190.3^2}{12}$$

$$M_{EF} = \frac{2EI}{l_1} \left(2\theta_E + \theta_F + \frac{3\Delta_4}{l_1} \right) - M_{FCD}$$

$$= \frac{2EI}{150.92} \left(2\theta_E + \theta_F + \frac{3\Delta_4}{l_1} \right) - \frac{1 \times 150.92^2}{12}$$

$$M_{FE} = \frac{2EI}{l_1} \left(2\theta_F + \theta_E + \frac{3\Delta_4}{l_1} \right) + M_{FCD}$$

$$= \frac{2EI}{150.92} \left(2\theta_F + \theta_E + \frac{3\Delta_4}{l_1} \right) + \frac{1 \times 150.92^2}{12}$$

The boundary conditions for continuous beam shown in Figure 3.27 are:

$$M_{AB} = 0;$$

$$M_{BA} + M_{BC} = 0;$$

$$M_{CB} + M_{CD} = 0;$$

$$M_{DC} + M_{DE} = 0;$$

$$M_{ED} + M_{Ef} = 0;$$

$$M_{FE} = 0;$$

Equation 3.57

$$\begin{aligned}
k\Delta_1 &= \frac{1}{l_1} \times \left(M_{AB} + M_{BA} + \frac{P_0 l_1^2}{2} \right) - \frac{1}{l_2} \times \left(M_{BC} + M_{CB} - \frac{P_0 l_2^2}{2} \right); \\
k\Delta_2 &= \frac{1}{l_2} \times \left(M_{BC} + M_{CB} + \frac{P_0 l_2^2}{2} \right) - \frac{1}{l_2} \times \left(M_{CD} + M_{DC} - \frac{P_0 l_2^2}{2} \right); \\
k\Delta_3 &= \frac{1}{l_2} \times \left(M_{CD} + M_{DC} + \frac{P_0 l_2^2}{2} \right) - \frac{1}{l_2} \times \left(M_{DE} + M_{ED} - \frac{P_0 l_2^2}{2} \right) \\
k\Delta_4 &= \frac{1}{l_2} \times \left(M_{DE} + M_{ED} - \frac{P_0 l_2^2}{2} \right) - \frac{1}{l_1} \times \left(M_{EF} + M_{FE} - \frac{P_0 l_1^2}{2} \right)
\end{aligned}$$

Solving Equation 3.57, the unknown variables are specified as follows:

$$\begin{aligned}
\theta_A &= 0.0000977 \\
\theta_B &= 0.0000248 \\
\theta_C &= -6.588 \times 10^{-6} \\
\theta_D &= 6.588 \times 10^{-6} \\
\theta_E &= -0.0000248 \\
\theta_F &= -0.0000977 \\
\Delta_1 &= 0.005838 \\
\Delta_2 &= 0.006159 \\
\Delta_3 &= 0.006159 \\
\Delta_4 &= 0.005838
\end{aligned}$$

Equation 3.58

Substituting variables in Equation 3.58 in Equation 3.56, the flexural moments are calculated as follows:

$$\begin{aligned}
M_{BA} &= 2468.56 \text{ kip.ft} \\
M_{BC} &= -2468.56 \text{ kip.ft} \\
M_{CB} &= 3113.05 \text{ kip.ft} \\
M_{CD} &= -3113.05 \text{ kip.ft} \\
M_{DC} &= 3113.05 \text{ kip.ft} \\
M_{DE} &= -3113.05 \text{ kip.ft} \\
M_{ED} &= 2468.56 \text{ kip.ft}
\end{aligned}$$

Equation 3.59

$$M_{EF} = -2468.56 \text{ kip.ft}$$

The beam deflection function is specified as done for Bridge No. 1. The following are the deflection functions for five spans of Bridge No. 2:

- First span:

$$EIy = -\frac{x^4}{24} + 9.85055x^3 - 134325x \quad \text{Equation 3.60}$$

- Second span:

$$EIy = -\frac{x^4}{24} + 15.2939x^3 - 1234.28x^2 - 34143.7x - 8.027 \times 10^6 \quad \text{Equation 3.61}$$

- Third span:

$$EIy = -\frac{x^4}{24} + 15.8583x^3 - 1556.53x^2 + 9059.15x - 8.468 \times 10^6 \quad \text{Equation 3.62}$$

- Fourth span:

$$EIy = -\frac{x^4}{24} + 16.4228x^3 - 1556.53x^2 - 9068.81x - 8.468 \times 10^6 \quad \text{Equation 3.63}$$

- Fifth span:

$$EIy = -\frac{x^4}{24} + 15.3028x^3 - 1234.28x^2 + 34143.9x - 8.027 \times 10^6 \quad \text{Equation 3.64}$$

Substituting above equations in Equations 3.9 to 3.11, the factors α , β and γ are calculated. For Bridge No. 2 $w = 6.023 \text{ kips/ft}$.

$$\alpha = \frac{1}{EI} (9.04629 \times 10^8 + 2.04657 \times 10^9 + 1.903 \times 10^9 + 2.04657 \times 10^9 + 9.04629 \times 10^8) = 5.6766$$

Equation 3.65

$$\gamma = \frac{w}{(EI)^2} (6.21919 \times 10^{15} + 2.243 \times 10^{16} + 1.9255 \times 10^{16} + 2.243 \times 10^{16} + 6.21919 \times 10^{15}) = 0.2438$$

Equation 3.66

$$\beta = w \times 5.6766 = 34.1902$$

Equation 3.67

Having factors α , β and γ , the natural period and equivalent static load are calculated as follows:

$$T_m = 2\pi \sqrt{\frac{0.2438}{1 \times 32.2 \times 5.6766}} = 0.23 \text{ sec} \rightarrow \begin{array}{l} C_{sm}(\text{Manhattan}) = 0.16 \\ C_{sm}(\text{Topeka}) = 0.1344 \\ C_{sm}(\text{Kansas City}) = 0.1216 \end{array}$$

Equation 3.68

Among the aforementioned three cities in Kansas, the equivalent static force is calculated only for Kansas City, which has the largest C_{sm} among these three cities:

$$P_e(x) = \frac{34.1902 \times 0.16}{0.2438} \times 6.023 \times v_s(x) = 135.423 v_s(x)$$

Equation 3.69

The final step is applying the equivalent static load on the bridge and determining the resulting member force effects. In each span a uniform load with a magnitude equal to the area under the actual load divided by the span length is used to determine the member force effects.

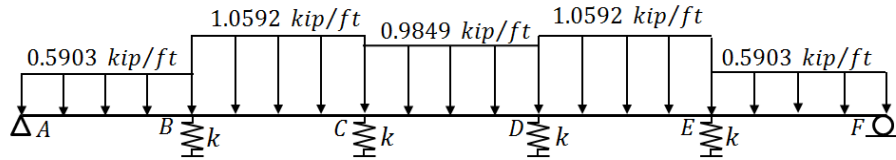


FIGURE 3.28
The Bridge Subjected to the Transverse Uniform Loads

Using slope-deflection method, the spring forces are obtained:

$$F_1 = k \cdot \Delta_1 = 154.961$$

$$F_2 = k \cdot \Delta_2 = 199.59$$

$$F_3 = k \cdot \Delta_3 = 199.59$$

$$F_4 = k \cdot \Delta_4 = 154.961$$

Equation 3.70

For each column in each bent, the shear force and flexural moment due to equivalent static load are specified as follows:

$$F_{x1} = \frac{F_1}{4} = 38.74 \text{ kips}, \quad M_{z1} = \frac{38.74 \times 13.615}{2} = 263.723 \text{ kip.ft}$$

$$F_{x2} = \frac{F_2}{4} = 49.89 \text{ kips}, \quad M_{z2} = \frac{49.89 \times 13.615}{2} = 339.626 \text{ kip.ft}$$

$$F_{x3} = \frac{F_3}{4} = 49.89 \text{ kips}, \quad M_{z3} = \frac{49.89 \times 13.615}{2} = 339.626 \text{ kip.ft}$$

$$F_{x4} = \frac{F_4}{4} = 38.74 \text{ kips}, \quad M_{z3} = \frac{38.74 \times 13.615}{2} = 263.723 \text{ kip.ft}$$

Equation 3.71

Using load combinations, expressed in Table 3.1, demand flexural moment and axial force are obtained. These forces are shown in Table 3.9 and Table 3.10.

TABLE 3.9
Demand Forces for Column No. 1 in Bridge No. 2

Load Combination	M (kip.ft)	P(kips)
Extreme event I Min DL Case I LL	289.1136	456.7860
Extreme event I Min DL Case II LL	288.8500	418.6015
Extreme event I Max DL Case I LL	289.2090	615.966
Extreme event I Max DL Case II LL	288.9454	577.7815

TABLE 3.10
Demand Forces for Column No. 2 in Bridge No. 2

Load Combination	M (kip.ft)	P(kips)
Extreme event I Min DL Case I LL	363.3483	331.934
Extreme event I Min DL Case II LL	363.2473	340.022
Extreme event I Max DL Case I LL	363.3215	453.044
Extreme event I Max DL Case II LL	363.2205	461.132

3.4.3 Vehicle Collision Force for Columns of the Two Existing Bridges

As mentioned before, when the face of pier is located inside the Clear Zone, the design of the pier must include the 400 kips collision force based on AASHTO-LRFD (2010) and KDOT-LRFD (2011) (In AASHTO-LRFD 2012 this force is increased to 600 kips, acting at a distance of 5 ft above ground). For these two bridges which cross the river, there is not any road under the bridge. Although, 400 kips (600 kips according to AASHTO-LRFD (2012)) impact load isn't required to be consider for these two special cases, we consider it to investigate the efficiency of the column sections against the collision force. For river-crossing bridges, according to *Article 2.3.2.2.5* in AASHTO-LRFD (2010), the ship collision should be considered. As mentioned in Section C3.14.8 in AASHTO-LRFD (2010) "The determination of the impact load on a bridge structure during a ship collision is complex and depends on many factors". Furthermore, we don't think that there is any navigation under these two cases; therefore, the ship collision force is not considered.

To consider the vehicular collision force, the load combination "Extreme Event II" should be applied. The following data are the demand flexural moment and axial force, by considering the load combination "Extreme Event II" for all columns:

TABLE 3.11
Demand Forces in Extreme Event II for Column No. 1 in Bridge No. 1

Load Combination	VC. Force	M(kip.ft)	P(kips)
Extreme event II Min DL Case I LL	400 kip	1285.276	451.6015
Extreme event II Min DL Case II LL		1284.873	449.659
Extreme event II Max DL Case I LL		1283.841	610.7715
Extreme event II Max DL Case II LL		1283.438	608.829
Extreme event II Min DL Case I LL	600 kip ($\theta = 0^\circ$)	2182.885	456.786
Extreme event II Min DL Case II LL		2182.877	449.659
Extreme event II Max DL Case I LL		2182.859	610.7715
Extreme event II Max DL Case II LL		2182.852	608.829
Extreme event II Min DL Case I LL	600 kip ($\theta = 15^\circ$)	2193.109	451.6015
Extreme event II Min DL Case II LL		2192.998	449.659
Extreme event II Max DL Case I LL		2192.713	610.7715
Extreme event II Max DL Case II LL		2192.602	608.829

TABLE 3.12
Demand Forces in Extreme Event II for Column No. 2 in Bridge No. 1

Load Combination	VC. Force	M(kip.ft)	P(kips)
Extreme event II Min DL Case I LL	400 kip	1304.85	504.467
Extreme event II Min DL Case II LL		1305.135	512.169
Extreme event II Max DL Case I LL		1304.85	686.667
Extreme event II Max DL Case II LL		1305.135	694.369
Extreme event II Min DL Case I LL	600 kip ($\theta = 0^\circ$)	2494.274	504.467
Extreme event II Min DL Case II LL		2494.279	512.169
Extreme event II Max DL Case I LL		2494.272	686.667
Extreme event II Max DL Case II LL		2494.276	694.369
Extreme event II Min DL Case I LL	600 kip ($\theta = 15^\circ$)	2235.402	504.467
Extreme event II Min DL Case II LL		2235.48	512.169
Extreme event II Max DL Case I LL		2235.399	686.667
Extreme event II Max DL Case II LL		2235.478	694.369

TABLE 3.13
Demand Forces in Extreme Event II for Column No. 3 in Bridge No. 1

Load Combination	VC. Force	M(kip.ft)	P(kips)
Extreme event II Min DL Case I LL	400 kip	1258.493	436.107
Extreme event II Min DL Case II LL		1258.737	438.144
Extreme event II Max DL Case I LL		1259.927	595.272
Extreme event II Max DL Case II LL		1260.171	597.309
Extreme event II Min DL Case I LL	600 kip ($\theta = 0^\circ$)	2110.776	436.107
Extreme event II Min DL Case II LL		2110.781	438.144
Extreme event II Max DL Case I LL		2110.806	595.272
Extreme event II Max DL Case II LL		2110.811	597.309
Extreme event II Min DL Case I LL	600 kip ($\theta = 15^\circ$)	2122.326	436.107
Extreme event II Min DL Case II LL		2122.394	438.144
Extreme event II Max DL Case I LL		2122.725	595.272
Extreme event II Max DL Case II LL		2122.793	597.309

TABLE 3.14
Demand Forces in Extreme Event II for Column No. 1 in Bridge No. 2

Load Combination	VC. Force	M(kip.ft)	P(kips)
Extreme event II Min DL Case I LL	400 kip	819.0343	456.786
Extreme event II Min DL Case II LL		818.7654	418.6015
Extreme event II Max DL Case I LL		819.1317	615.966
Extreme event II Max DL Case II LL		818.8628	577.7815
Extreme event II Min DL Case I LL	600 kip ($\theta = 0^\circ$)	1262.899	456.786
Extreme event II Min DL Case II LL		1262.895	418.6015
Extreme event II Max DL Case I LL		1262.901	615.966
Extreme event II Max DL Case II LL		1262.897	577.7815
Extreme event II Min DL Case I LL	600 kip ($\theta = 15^\circ$)	1265.516	456.786
Extreme event II Min DL Case II LL		1265.445	418.6015
Extreme event II Max DL Case I LL		1265.541	615.966
Extreme event II Max DL Case II LL		1265.471	577.7815

The demand forces in above tables are obtained by considering a single column subjected to the vehicular collision force. The following are the calculations related to the internal forces due to vehicular collision force applied on a column in the related bent. These calculations have been done to see how much the demand forces obtained by a single column assumption are reliable. For each bent, the vehicular collision force were applied on both the first and the second column. In this section, the angle of equivalent static force with respect to the edge of pavement is assumed to be equal to zero ($\theta = 0$).

TABLE 3.15
Demand Forces in Extreme Event II for Column No. 2 in Bridge No. 2

Load Combination	VC. Force	M(kip.ft)	P(kips)
Extreme event II Min DL Case I LL		818.7455	331.934
Extreme event II Min DL Case II LL		818.6432	340.022
Extreme event II Max DL Case I LL	400 kip	818.7184	453.044
Extreme event II Max DL Case II LL		818.6162	461.132
Extreme event II Min DL Case I LL		1262.898	331.934
Extreme event II Min DL Case II LL	600 kip	1262.897	340.022
Extreme event II Max DL Case I LL	($\theta = 0^\circ$)	1262.898	453.044
Extreme event II Max DL Case II LL		1262.897	461.132
Extreme event II Min DL Case I LL		1265.443	331.934
Extreme event II Min DL Case II LL	600 kip	1265.416	340.022
Extreme event II Max DL Case I LL	($\theta = 15^\circ$)	1265.436	453.044
Extreme event II Max DL Case II LL		1265.409	461.132

3.4.3.1 Demand Forces Due to Vehicular Collision Force in Bridge No. 1

At first, the moment of inertia for the column and the column cap are calculated. As mentioned, based on section 10.10.4.1 in ACI-318 (2011), for the beam it's permitted to use $I = 0.35I_g$ and for the column $I = 0.70I_g$. The moment of inertia for the column is already calculated. The moment of inertia for the column cap is calculated as follows:

$$\begin{aligned}
 I_g &= \frac{1}{12} \times 4 \times 4.2^3 + (8.04 - 1) \\
 &\quad \times \left[16 \times \frac{1.266}{12^2} \times 1.8804^2 + 4 \times \frac{0.196}{12^2} \times 1.077^2 + 4 \times \frac{0.196}{12^2} \times 0.41^2 \right] \\
 &= 28.2485 \text{ ft}^4
 \end{aligned}$$

Equation 3.72

The cracked moment of inertia for columns and the column caps are as follows:

$$I_1 = 0.7I_g = 0.7 \times 4.41 = 3.087 \text{ ft}^4$$

Equation 3.73

$$I_2 = 0.35I_g = 0.35 \times 28.2485 = 9.8869 \text{ ft}^4$$

Equation 3.74

Considering a frame as shown in Table 3.29, and Table 3.30, and using slope-deflection method the internal forces in columns are obtained.

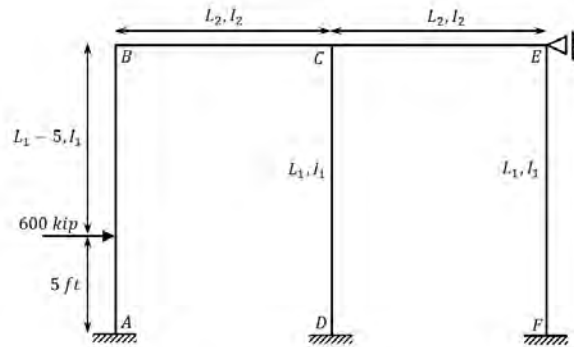


FIGURE 3.29
A Bent in Bridge No. 1 with Vehicular Collision Force Acting on the First Column

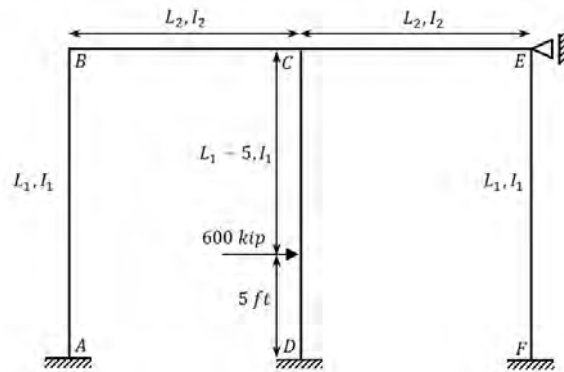


FIGURE 3.30
A Bent in Bridge No. 1 with Vehicular Collision Force Acting on the Second Column

TABLE 3.16
The Internal Forces in Bent No. 1 in Bridge No. 1

Column No.	M_u (kip.in)	M'_u (kip.in)	V_u (kip)	V'_u (kip)
1	2182.52	2258.66	564.889	568.248
2	2182.52	2203.56	564.889	566.745

TABLE 3.17
The Internal Forces in Bent No. 2 in Bridge No. 1

Column No.	M_u (kip.in)	M'_u (kip.in)	V_u (kip)	V'_u (kip)
1	2493.945	2293.54	568.493	571.368
2	2493.945	2243.63	568.493	570.084

TABLE 3.18
The Internal Forces in Bent No. 3 in Bridge No. 1

Column No.	M_u (kip.in)	M'_u (kip.in)	V_u (kip)	V'_u (kip)
1	2110.302	2199.36	558.209	562.518
2	2110.302	2199.03	558.209	560.584

In Table 3.16 through Table 5.18, M_u and V_u are the internal force in column subjected to vehicular collision force with a single column assumption, and M'_u and V'_u are the internal forces in column subjected to the vehicular collision force with considering column in related bent.

3.4.3.2 Demand Forces Due to Vehicular Collision Force in Bridge No. 2

The moment of inertia for the column cap in Bridge No. 2 is calculated as follows:

$$\begin{aligned}
 I_g &= \frac{1}{12} \times 4 \times 5.108^3 + 7.04 \\
 &\times \left[12 \times \frac{0.785}{12^2} \times 2.2915^2 + 6 \times \frac{0.785}{12^2} \times 2.2915^2 + 6 \right. \\
 &\times \frac{0.785}{12^2} \times 1.9635^2 + 2 \times \frac{0.4908}{12^2} \times 1.1125^2 + 2 \times \frac{0.4908}{12^2} \\
 &\times 1.4405^2 + 2 \times \frac{0.4908}{12^2} \times 0.5895^2 + 2 \times \frac{0.4908}{12^2} \times 0.2615^2 \left. \right] \\
 &= 49.1195 \text{ ft}^4
 \end{aligned}
 \tag{Equation 3.75}$$

The cracked moment of inertia for columns and the column caps are:

$$I_1 = 0.7I_g = 0.7 \times 4.55 = 3.185 \text{ ft}^4$$

Equation 3.76

$$I_2 = 0.35I_g = 0.35 \times 49.1195 = 17.2 \text{ ft}^4$$

Equation 3.77

Considering a frame as shown in Figure 3.31 and Figure 3.32 and using slope-deflection method the internal forces are calculated.

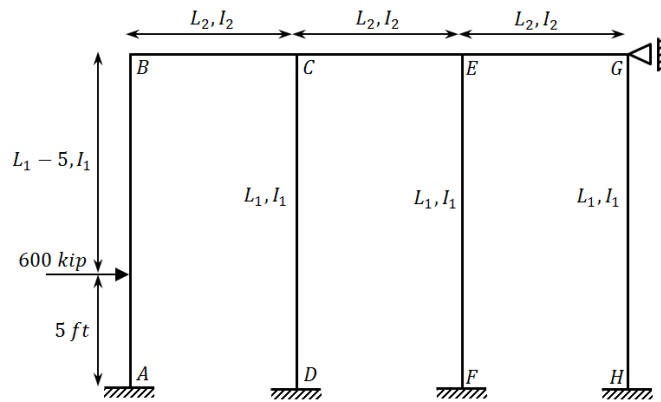


FIGURE 3.31
A Bent in Bridge No. 2 with Vehicular Collision Force Acting in the First Column

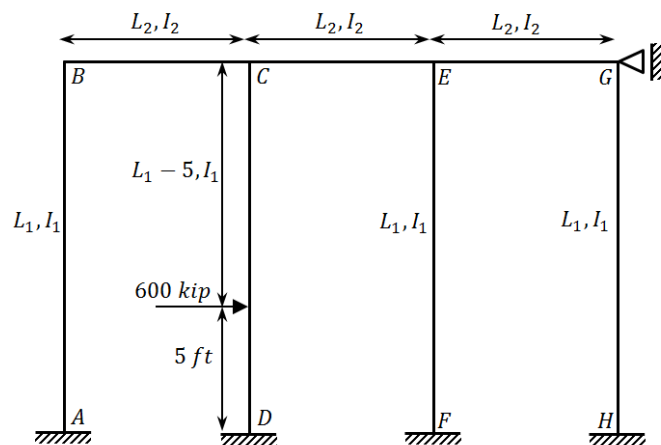


FIGURE 3.32
A Bent in Bridge No. 2 with Vehicular Collision Force Acting in the Second Column

TABLE 3.19
The Internal Forces in Bent No. 1 in Bridge No. 2

Column No.	M_u (kip. in)	M'_u (kip. in)	V_u (kip)	V'_u (kip)
1	1201.148	1264.96	416.674	430.734
2	1201.148	1264.96	416.674	424.8

In Table 3.19, M_u and V_u are the internal force in column subjected to vehicular collision force with a single column assumption, and M'_u and V'_u are the internal forces in column subjected to the vehicular collision force considering column in related bent. As seen in tables; although, the demand flexural moment and shear forces obtained by considering a column in the related bent is more than demand forces obtained by assumption of a single column, the difference between these two values are relatively small.

3.4.4 Investigation of the Flexural Capacity of the Existing Columns

In this section, the flexural capacity of columns in two existing bridges is determined. For this purpose, two methods are used. In the first method, the ultimate capacity of each section is determined by considering confinement effect. This is accomplished by using KSU-RC software which can capture the real performance considering the confinement and load pattern (Esmaeily 2013). Columns three and four in Table 3.20 through Table 3.24 show the capacity of columns considering confinement effect. In the second method, the capacity of columns are calculated based on the ACI-318 (2011) code as shown in columns five and six in Table 3.20 through Table 3.24.

TABLE 3.20
The Flexural Capacity of Column No. 1 in Bridge No. 1 Subjected to Different Axial Forces

Load Combination	Demand forces		KSU-RC		AASHTO (2010)	
	P_u	M_u	M_n	ϕM_n	M_n	ϕM_n
Strength I						
Min DL Case I LL	651.859	386.5345	1432.964	1289.668	1327.7	1165.986
Min DL Case II LL	645.045	386.4609	1428.778	1285.9	1322.8	1164.461
Max DL Case I LL	810.921	405.7024	1541.171	1345.991	1413.4	1184.571
Max DL Case II LL	804.104	405.635	1535.021	1343.231	1410.1	1183.92
Strength V						
Min DL Case I LL	709.949	475.7818	1469.727	1322.754	1362.2	1174.761
Min DL Case II LL	546.098	454.623	1366.637	1229.973	1254.6	1129.14
Max DL Case I LL	709.949	475.7818	1469.727	1322.754	1362.2	1174.761
Max DL Case II LL	704.67	475.6097	1466.881	1320.193	1359.5	1174.2
Strength III Min DL	265.59	473.4048	1186.298	1067.669	1069.3	962.37
Extreme event I						
Min DL Case I LL	451.6015	557.5569	1309.105	1178.195	1194.3	1074.87
Min DL Case II LL	449.659	557.1543	1306.47	1175.823	1192.9	1073.61
Max DL Case I LL	610.7715	556.1222	1406.038	1265.434	1297.7	1156.51
Max DL Case II LL	608.829	555.7196	1405.003	1264.502	1296.2	1155.951
Extreme event II						
Min DL Case I LL	451.6015	557.5569	1309.109	1178.198	1194.3	1074.87
Min DL Case II LL	449.659	557.1543	1308.193	1177.374	1192.9	1073.61
Max DL Case I LL	610.7715	556.1222	1406.038	1265.434	1297.7	1156.51
Max DL Case II LL	608.829	555.7196	1405.003	1264.502	1296.2	1155.951

TABLE 3.21
The Flexural Capacity of Column No. 2 in Bridge No. 1 Subjected to Different Axial Forces

Load Combination	Demand forces		KSU-RC		AASHTO (2010)	
	P_u	M_u	M_n	ϕM_n	M_n	ϕM_n
Strength I						
Min DL Case I LL	703.585	308.4053	1466.298	1319.669	1358.9	1174.09
Min DL Case II LL	730.546	309.4241	1483.17	1329.556	1372.8	1176.49
Max DL Case I LL	885.787	323.7628	1589.396	1361.544	1449.5	1189.895
Max DL Case II LL	912.751	324.8261	1609.972	1361.491	1461.9	1191.449
Strength V						
Min DL Case I LL	808.535	409.8232	1539.705	1345.145	1412.2	1184.271
Min DL Case II LL	647.143	392.1338	1430.065	1287.059	1324.3	1164.987
Max DL Case I LL	808.535	409.8232	1539.705	1345.145	1412.2	1184.271
Max DL Case II LL	829.333	411.0261	1554.851	1351.43	1422.5	1186.081
Strength III Min DL	375.776	479.4845	1260.173	1134.156	1144.1	1029.69
Extreme event I						
Min DL Case I LL	504.467	510.1661	1341.128	1207.016	1228.4	1105.56
Min DL Case II LL	512.169	510.4514	1346.131	1211.518	1233.3	1109.97
Max DL Case I LL	686.667	510.1660	1456.769	1311.092	1350.1	1172.157
Max DL Case II LL	694.369	510.4512	1461.433	1315.289	1354.1	1173.057
Extreme event II						
Min DL Case I LL	504.467	510.1661	1341.128	1207.016	1228.4	1105.56
Min DL Case II LL	512.169	510.4514	1346.131	1211.518	1233.3	1109.97
Max DL Case I LL	686.667	510.1660	1456.769	1311.092	1350.1	1172.157
Max DL Case II LL	694.369	510.4512	1461.433	1315.289	1354.1	1173.057

TABLE 3.22
The Capacity Flexural of Column No. 3 in Bridge No. 1 Subjected to Different Axial Forces

Load Combination	Demand forces		KSU-RC		AASHTO (2010)	
	P_u	M_u	M_n	ϕM_n	M_n	ϕM_n
Strength I						
Min DL Case I LL	595.141	228.4587	1395.235	1255.712	1286.2	1152.435
Min DL Case II LL	602.282	229.9055	1399.565	1259.609	1291.5	1154.472
Max DL Case I LL	754.394	239.6395	1497.588	1333.101	1385	1179.328
Max DL Case II LL	761.537	241.1768	1502.723	1333.991	1388.6	1178.783
Strength V						
Min DL Case I LL	716.24	343.907	1375.626	1237.562	1365.4	1175.336
Min DL Case II LL	562.027	329.1504	1474.622	1327.16	1264.5	1138.05
Max DL Case I LL	716.24	343.907	1477.984	1329.648	1365.4	1175.336
Max DL Case II LL	721.772	345.486	1272.672	1143.71	1368.3	1176.054
Strength III Min DL	395.66	487.5753	1272.672	1145.405	1157.5	1041.75
Extreme event I						
Min DL Case I LL	436.107	455.2622	1298.708	1168.837	1184.2	1065.78
Min DL Case II LL	438.144	455.5066	1299.269	1169.342	1185.6	1067.04
Max DL Case I LL	595.272	456.6962	1395.317	1255.785	1286.3	1152.782
Max DL Case II LL	597.309	456.9406	1396.551	1256.896	1287.8	1153.225
Extreme event II						
Min DL Case I LL	436.107	455.2622	1298.708	1168.837	1184.2	1065.78
Min DL Case II LL	438.144	455.5066	1299.269	1169.342	1185.6	1067.04
Max DL Case I LL	595.272	456.6962	1395.317	1255.785	1286.3	1152.782
Max DL Case II LL	597.309	456.9406	1396.551	1256.896	1287.8	1153.225

TABLE 3.23
The Flexural Capacity of Column No. 1 in Bridge No. 2 Subjected to Different Axial Forces

Load Combination	Demand forces		KSU-RC		AASHTO (2010)	
	P_u	M_u	M_n	ϕM_n	M_n	ϕM_n
Strength I						
Min DL Case I LL	803.1	627.3885	1684.722	1450.086	1607.3	1327.791
Min DL Case II LL	669.529	626.8575	1591.353	1415.735	1525.7	1313.933
Max DL Case I LL	962.24	674.9158	1779.57	1471.076	1662.3	1320.032
Max DL Case II LL	828.632	674.5145	1698.134	1452.322	1617.6	1327.564
Strength V						
Min DL Case I LL	837.864	803.5966	1703.068	1297.813	1620.9	1327.031
Min DL Case II LL	575.925	748.9155	1521.563	1532.761	1470.4	1304.098
Max DL Case I LL	837.864	803.5966	1703.068	1452.624	1620.9	1327.031
Max DL Case II LL	734.839	802.7868	1703.064	1434.791	1566.66	1321.634
Strength III Min DL	209.556	743.0459	1640.19	1476.171	1248	1123.2
Extreme event I						
Min DL Case I LL	456.786	289.1136	1434.123	1290.71	1408.3	1267.47
Min DL Case II LL	418.6015	288.8500	1406.162	1265.546	1386.8	1248.12
Max DL Case I LL	615.966	289.2090	1551.284	1396.156	1493.1	1307.508
Max DL Case II LL	577.7815	288.9454	1522.803	1370.523	1471.4	1304.249
Extreme event II						
Min DL Case I LL	456.786	819.0343	1434.123	1290.71	1408.3	1267.47
Min DL Case II LL	418.6015	818.7654	1406.162	1265.546	1386.8	1248.12
Max DL Case I LL	615.966	819.1317	1551.284	1396.156	1493.1	1307.508
Max DL Case II LL	577.7815	818.8628	1522.803	1370.523	1471.4	1304.249

TABLE 3.24
The Flexural Capacity of Column No. 2 in Bridge No. 2 Subjected to Different Axial Forces

Load Combination	Demand forces		KSU-RC		AASHTO (2010)	
	P_u	M_u	M_n	ϕM_n	M_n	ϕM_n
Strength I						
Min DL Case I LL	544.198	625.6375	1498.434	1348.591	1452.4	1301.205
Min DL Case II LL	572.5	628.9199	1519.272	1367.345	1468.5	1303.881
Max DL Case I LL	665.303	673.23	1585.707	1421.692	1523	1313.283
Max DL Case II LL	693.603	676.9195	1610.68	1423.607	1541	1317.093
Strength V						
Min DL Case I LL	595.504	796.8046	1463.636	1317.272	1481.5	1305.794
Min DL Case II LL	496.253	745.7537	1536.234	1382.611	1427.8	1285.02
Max DL Case I LL	595.504	796.8046	1552.173	1396.955	1481.5	1305.794
Max DL Case II LL	617.336	799.8025	1227.702	1104.932	1493.9	1307.611
Strength III Min DL	164.133	726.0116	1227.702	1104.932	1216.5	1094.85
Extreme event I						
Min DL Case I LL	331.934	363.3483	1342.129	1207.916	1330.5	1197.45
Min DL Case II LL	340.022	363.2473	1450.509	1305.458	1335.9	1202.31
Max DL Case I LL	453.044	363.3215	1431.464	1288.318	1406.5	1265.85
Max DL Case II LL	461.132	363.2205	1437.197	1293.477	1410	1269
Extreme event II						
Min DL Case I LL	331.934	818.745	1342.129	1207.916	1330.5	1197.45
Min DL Case II LL	340.022	818.6432	1450.509	1305.458	1335.9	1202.31
Max DL Case I LL	453.044	818.7184	1431.464	1288.318	1406.5	1265.85
Max DL Case II LL	461.132	818.6162	1437.197	1293.477	1410	1269

3.4.5 Investigation of the Shear Capacity of the Existing Columns

Another important issue for the representative existing bridge piers is the shear strength. Applying 400 kips vehicular collision force at a distance of 4 ft from the bottom of the column induces a large shear force. The shear capacity of columns in these two representative existing bridge piers are calculated by means of two methods. The first is proposed by AASHTO-LRFD (2010) and the second is based on the ACI-318 (2011).

3.4.5.1 Assessment of Shear Capacity Based on AASHTO-LRFD (2010)

In AASHTO (2010) the nominal shear resistance of the section is determined as the lesser of:

$$\begin{aligned} V_n &= V_c + V_s + V_p \\ V_n &= 0.25f'_c b_v d_v + V_p \end{aligned} \quad \text{Equation 3.78}$$

where, V_c is the nominal shear strength, provided by concrete, and is calculated by the following equation:

$$V_c = 0.0316\beta\sqrt{f'_c}b_v d_v \quad \text{Equation 3.79}$$

In Equation 3.79, b_v is the effective web width taken as the minimum web width within the depth d_v , as determined in the Article 5.8.2.9 (in), d_v is effective shear depth as determined in Article 5.8.2.9 (in) and it should be more than $\max(0.9d, 0.72h)$, β is the factor indicating the ability of diagonally cracked concrete to transmit tension and shear. According Article 5.8.3.4.1 $\beta = 2.0$ is used. (The simplified AASHTO-LRFD (2010) procedure is used in this study.)

V_s is the nominal shear strength provided by shear reinforcement and is calculated using the following equation:

$$V_s = \frac{A_v f_y d_v \cot \theta}{s} \quad \text{Equation 3.80}$$

where, A_v is the area of shear reinforcement within a distance s (in^2), θ is the angle of inclination of diagonal compressive stress and, as per the Article 5.8.3.4.1, $\theta = 45^\circ$ is considered in this report. V_p is the component in the direction of the applied shear of the effective prestressing force which is equal to zero here. Parameters β and θ may be determined by the procedure presented in Article 5.8.3.3.

According to Article 5.5.4.2, the resistance factor ϕ shall be taken .09 for normal weight concrete in shear and torsion.

The representative bridge piers have a circular section with longitudinal reinforcement distributed uniformly around the perimeter of the section. According to Article 5.8.2.9 in AASHTO-LRFD (2010) when this kind of section cracks, the highest shear stresses typically

takes place near the mid-depth of the section. This is also true when the section is not cracked. Accordingly, the effective web width can be taken as the diameter of the section. The parameters b_v and d_v are illustrated in Figure 3.33.

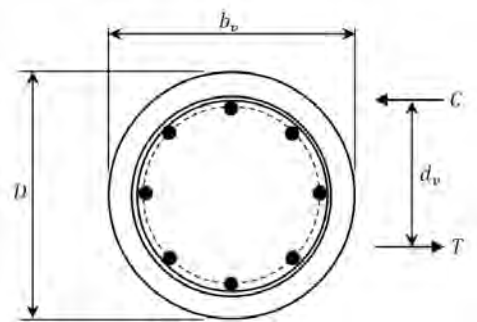


FIGURE 3.33
Illustration of Terms b_v and d_v

3.4.5.2 Assessment of the Shear Capacity Based on the ACI-318

As mentioned earlier, the nominal shear strength of a non-pre-stressed concrete section, is summation of nominal shear strength provided by plain concrete, V_c , and the nominal shear strength provided by transverse reinforcement, V_s . The shear strength provided by concrete in ACI-318 (2011) is estimated by the following equation:

$$V_c = 2\lambda\sqrt{f'_c}b_wd$$

Equation 3.81

where, λ is the modification factor reflecting the reduced mechanical properties of lightweight concrete. Article 8.6.1 in ACI-318 (2011) says that

“ $\lambda = 0.85$ for sand-lightweight concrete and 0.75 for all-lightweight concrete. Linear interpolation between 0.75 and 0.85 shall be permitted, on the basis of volumetric fractions, when a portion of the lightweight fine aggregate is replaced with normal-weight fine aggregate. Linear interpolation between 0.85 and 1.0 shall be permitted, on the basis of volumetric fraction, for concrete containing normalweight fine aggregate and a blend of lightweight and normalweight coarse aggregate. For normalweight concrete, $\lambda = 1.0$.”

b_w is the web width, f'_c is the specified compressive strength of concrete, and d is the distance from the extreme compression fiber to the centroid of longitudinal tension reinforcement. This value is permitted to be taken as $d = 0.8D$ for circular sections with longitudinal reinforcement distributed uniformly on the perimeter of section.

In addition to above equation, some detailed equations are proposed in ACI-318 (2011). The effect of flexural moment and axial force are considered in determining the nominal shear strength provided by concrete in these equations. The following equation is used in this study to determine the shear strength provided by concrete:

$$V_c = 2\left(1 + \frac{N_u}{2000A_g}\right)\lambda\sqrt{f'_c}b_wd \quad \text{Equation 3.82}$$

where, N_u is factored axial force normal to cross section occurring simultaneously with V_u , to be taken as positive for compression and negative for tension (lb).

The shear strength provided by transverse reinforcement is determined by the following equation:

$$V_s = \frac{A_v f_y d}{s} \quad \text{Equation 3.83}$$

Using simplified AASHTO-LRFD (2010) procedure and ACI-318 (2011) method, the shear strength of sections under different axial force are calculated and expressed in Table 3.25 through Table 3.29. It should be noted that resistance factor ϕ in ACI-318 (2011) for shear is equal to 0.75, while as mentioned earlier, $\phi = 0.9$ in AASHTO-LRFD (2010). Therefore, to avoid misunderstanding, the resistance factor is shown with ϕ for ACI-318 and ϕ' for AASHTO-LRFD (2010) in the following tables. Bold fonts highlights cases where the demand values are more than the available strength as evaluated by the related code procedure. It is obvious that for a considerable number of cases, the calculated shear strength of the columns do not meet the shear strength requirement dictated by the code.

TABLE 3.25
The Shear Capacity of Column No. 1 in Bridge No. 1*

Load Combination	demand shear	ACI-318 (2011)	AASHTO (2010)
	V_u	ϕV_n	$\phi' V_n$
Strength I			
Min DL Case I LL	22.97	132.97	
Min DL Case II LL	22.92	132.54	115.31
Max DL Case I LL	23.94	143.27	
Max DL Case II LL	23.90	142.81	
Strength V			
Min DL Case I LL	29.90	136.68	
Min DL Case II LL	28.76	124.61	115.31
Max DL Case I LL	29.90	136.68	
Max DL Case II LL	29.85	136.34	
Strength III Min DL	33.29	106279.69	115.31
Extreme event I			
Min DL Case I LL	40.29	113.42	
Min DL Case II LL	40.27	113.31	115.31
Max DL Case I LL	40.30	123.01	
Max DL Case II LL	40.28	122.89	
Extreme event II (400 kip)			
Min DL Case I LL	376.34	113.42	
Min DL Case II LL	376.38	113.31	115.31
Max DL Case I LL	376.49	123.01	
Max DL Case II LL	376.54	122.89	
Extreme event II (600 kip, $\theta = 0^\circ$)			
Min DL Case I LL	556.54	113.42	
Min DL Case II LL	556.58	113.31	115.31
Max DL Case I LL	556.69	123.01	
Max DL Case II LL	556.73	122.89	
Extreme event II (600 kip, $\theta = 15^\circ$)			
Min DL Case I LL	562.78	113.42	
Min DL Case II LL	562.79	113.31	115.31
Max DL Case I LL	562.82	123.01	
Max DL Case II LL	562.83	122.89	

* Resistance factor is named ϕ for ACI-318 (2011) and ϕ' for AASHTO-LRFD (2010)

TABLE 3.26
The Shear Capacity of Column No. 2 in Bridge No. 1*

Load Combination	demand shear	ACI-318 (2011)	AASHTO (2010)
	V_u	ϕV_n	$\phi' V_n$
Strength I			
Min DL Case I LL	17.93	136.27	
Min DL Case II LL	18.01	138.73	115.31
Max DL Case I LL	18.76	148.57	
Max DL Case II LL	18.84	150.53	
Strength V			
Min DL Case I LL	31.5566	143.10	
Min DL Case II LL	31.5316	132.68	115.31
Max DL Case I LL	31.5566	143.10	
Max DL Case II LL	31.5316	144.55	
Strength III Min DL	31.32	113026.65	115.31
Extreme event I			
Min DL Case I LL	51.39	116.55	
Min DL Case II LL	51.38	117.01	115.31
Max DL Case I LL	51.39	128.03	
Max DL Case II LL	51.38	128.60	
Extreme event II (400 kip)			
Min DL Case I LL	380.81	116.55	
Min DL Case II LL	380.84	117.01	115.31
Max DL Case I LL	380.81	128.03	
Max DL Case II LL	380.84	128.60	
Extreme event II (600 kip, $\theta = 0^\circ$)			
Min DL Case I LL	563.02	116.55	
Min DL Case II LL	563.04	117.01	115.31
Max DL Case I LL	563.02	128.03	
Max DL Case II LL	563.04	128.60	
Extreme event II (600 kip, $\theta = 15^\circ$)			
Min DL Case I LL	563.73	116.55	
Min DL Case II LL	563.74	117.01	115.31
Max DL Case I LL	563.73	128.03	
Max DL Case II LL	563.74	128.60	

* Resistance factor is named ϕ for ACI-318 (2011) and ϕ' for AASHTO-LRFD (2010)

TABLE 3.27
The Shear Capacity of Column No. 3 in Bridge No. 1*

Load Combination	demand shear	ACI-318 (2011)	AASHTO (2010)
	V_u	ϕV_n	$\phi' V_n$
Strength I			
Min DL Case I LL	13.89	128.48	
Min DL Case II LL	13.99	129.05	115.31
Max DL Case I LL	14.53	139.56	
Max DL Case II LL	14.63	140.02	
Strength V			
Min DL Case I LL	21.94	137.09	
Min DL Case II LL	21.09	125.85	115.31
Max DL Case I LL	21.94	137.09	
Max DL Case II LL	22.04	137.44	
Strength III Min DL	31.89	114246.56	115.31
Extreme event I			
Min DL Case I LL	32.3992	112.51	
Min DL Case II LL	32.4187	112.63	115.31
Max DL Case I LL	32.5502	122.02	
Max DL Case II LL	32.5697	122.15	
Extreme event II (400 kip)			
Min DL Case I LL	375.82	112.51	
Min DL Case II LL	375.80	112.63	115.31
Max DL Case I LL	375.67	122.02	
Max DL Case II LL	375.65	122.15	
Extreme event II (600 kip, $\theta = 0^\circ$)			
Min DL Case I LL	552.29	112.51	
Min DL Case II LL	552.27	112.63	115.31
Max DL Case I LL	552.14	122.02	
Max DL Case II LL	552.12	122.15	
Extreme event II (600 kip, $\theta = 15^\circ$)			
Min DL Case I LL	556.71	112.51	
Min DL Case II LL	556.70	112.63	115.31
Max DL Case I LL	556.67	122.02	
Max DL Case II LL	556.66	122.15	

* Resistance factor is named ϕ for ACI-318 (2011) and ϕ' for AASHTO-LRFD (2010)

TABLE 3.28
The Shear Capacity of Column No. 1 in Bridge No. 2*

Load Combination	demand shear	ACI-318 (2011)	AASHTO (2010)
	V_u	ϕV_n	$\phi' V_n$
Strength I			
Min DL Case I LL	23.47	137.55	
Min DL Case II LL	23.01	128.98	109.59
Max DL Case I LL	25.19	148.88	
Max DL Case II LL	24.70	139.31	
Strength V			
Min DL Case I LL	35.10	139.93	
Min DL Case II LL	32.74	121.82	115.31
Max DL Case I LL	35.10	139.93	
Max DL Case II LL	34.65	133.14	
Strength III Min DL	41.39	98.20	109.59
Extreme event I			
Min DL Case I LL	41.3404	114.90	
Min DL Case II LL	41.3200	110.83	109.59
Max DL Case I LL	41.3485	125.10	
Max DL Case II LL	41.3281	122.09	
Extreme event II (400 kip)			
Min DL Case I LL	315.30	114.90	
Min DL Case II LL	315.32	110.83	109.59
Max DL Case I LL	315.29	125.10	
Max DL Case II LL	315.31	122.09	
Extreme event II (600 kip, $\theta = 0^\circ$)			
Min DL Case I LL	415.26	114.90	
Min DL Case II LL	415.28	110.83	109.59
Max DL Case I LL	415.25	125.10	
Max DL Case II LL	415.27	122.09	
Extreme event II (600 kip, $\theta = 15^\circ$)			
Min DL Case I LL	546.52	114.90	
Min DL Case II LL	546.52	110.83	109.59
Max DL Case I LL	546.52	125.10	
Max DL Case II LL	546.52	122.09	

* Resistance factor is named ϕ for ACI-318 (2011) and ϕ' for AASHTO-LRFD (2010)

TABLE 3.29
The Shear Capacity of Column No. 2 in Bridge No. 2*

Load Combination	demand shear	ACI-318 (2011)	AASHTO (2010)
	V_u	ϕV_n	$\phi' V_n$
Strength I			
Min DL Case I LL	23.21	119.51	
Min DL Case II LL	23.37	121.68	109.59
Max DL Case I LL	24.93	128.72	
Max DL Case II LL	25.11	130.51	
Strength V			
Min DL Case I LL	33.65	123.48	
Min DL Case II LL	31.86	116.05	115.31
Max DL Case I LL	33.65	123.48	
Max DL Case II LL	33.78	125.22	
Strength III Min DL	39.49	95.50	109.59
Extreme event I			
Min DL Case I LL	12.3781	105.58	
Min DL Case II LL	12.3708	106.07	109.59
Max DL Case I LL	12.3751	113.05	
Max DL Case II LL	12.3679	113.60	
Extreme event II (400 kip)			
Min DL Case I LL	315.32	105.58	
Min DL Case II LL	315.33	106.07	109.59
Max DL Case I LL	315.32	113.05	
Max DL Case II LL	315.33	113.60	
Extreme event II (600 kip, $\theta = 0^\circ$)			
Min DL Case I LL	415.28	105.58	
Min DL Case II LL	415.29	106.07	109.59
Max DL Case I LL	415.28	113.05	
Max DL Case II LL	415.29	113.60	
Extreme event II (600 kip, $\theta = 15^\circ$)			
Min DL Case I LL	546.52	105.58	
Min DL Case II LL	546.52	106.07	109.59
Max DL Case I LL	546.52	113.05	
Max DL Case II LL	546.52	113.60	

* Resistance factor is named ϕ for ACI-318 (2011) and ϕ' for AASHTO-LRFD (2010)

3.4.6 Investigation of the Plastic Hinge Length for the Existing Columns

There are a large number of models that can be used to evaluate the plastic hinge length. In this section, the plastic hinge length of columns in the existing bridges is calculated based on different models proposed so far. These models are selected among a larger number of the models after a comprehensive assessment of the models and the analytical procedures implemented in the pertinent method. For each column, the load combination that has the largest amount of axial load is chosen. In the following figures and tables, the plastic hinge length of each column is compared to the plastic hinge length required by AASHTO-LRFD (2010) and KDOT-LRFD (2011).

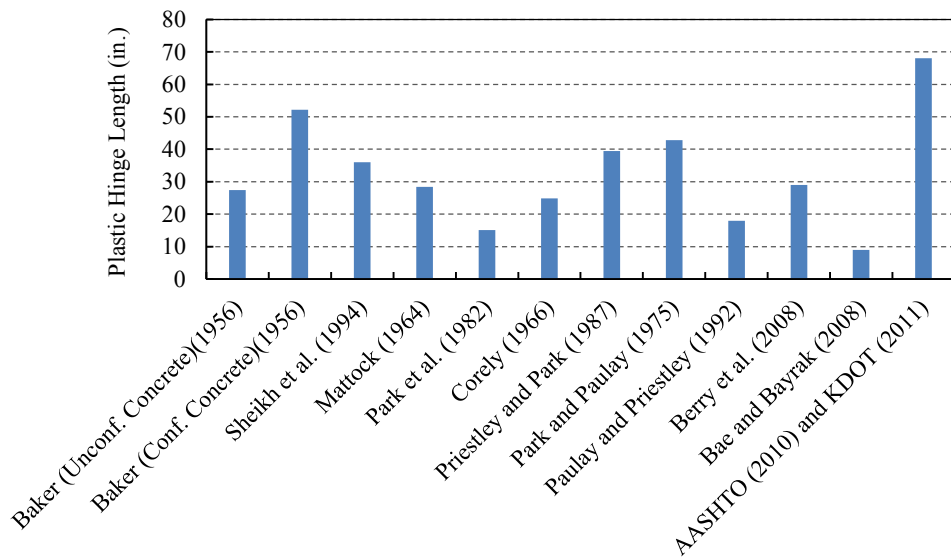


FIGURE 3.34
The Plastic Hinge Lengths for Column No. 1 in Bridge No. 1

TABLE 3.30
The Plastic Hinge Lengths for Column No. 1 in Bridge No. 1

Model	Plastic Hinge Length (in)	Model	Plastic Hinge Length (in)
Baker (Unconf. Concrete) (1956)	27.46	Priestley and Park (1987)	39.41
Baker (Conf. Concerte) (1956)	52.19	Park and Paulay (1975)	42.79
Sheikh et al. (1994)	36	Paulay and Priestley (1992)	18
Mattock (1964)	28.41	Berry et al. (2008)	28.96
Park et al. (1982)	15.12	Bae and Bayrak (2008)	9
Corley (1966)	24.87	AASHTO (2010) and KDOT (2011)	68

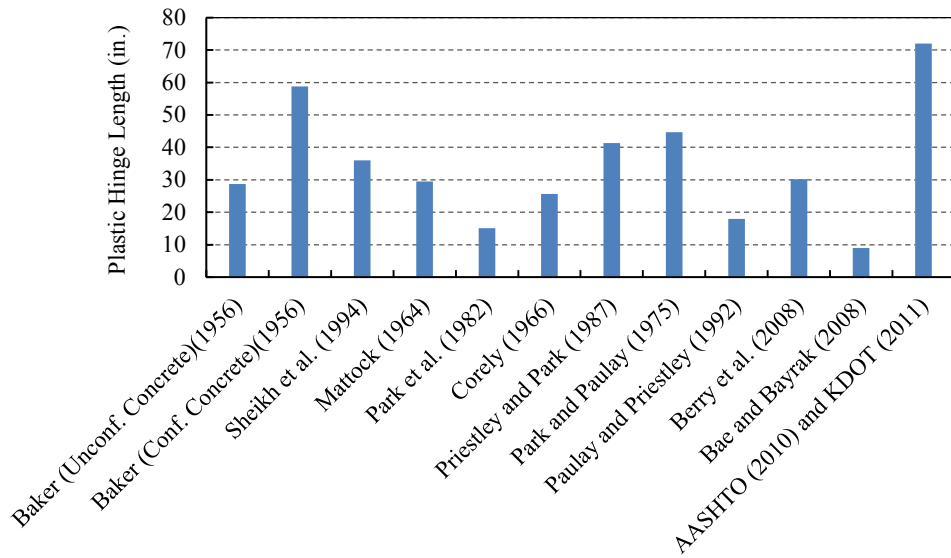


FIGURE 3.35
The Plastic Hinge Lengths for Column No. 2 in Bridge No. 1

TABLE 3.31
The Plastic Hinge Lengths for Column No. 2 in Bridge No. 1

Model	Plastic Hinge Length (in)	Model	Plastic Hinge Length (in)
Baker (Unconf. Concrete) (1956)	28.66	Priestley and Park (1987)	41.33
Baker (Conf. Concrete) (1956)	58.73	Park and Paulay (1975)	44.71
Sheikh et al. (1994)	36	Paulay and Priestley (1992)	18
Mattock (1964)	29.48	Berry et al. (2008)	30.16
Park et al. (1982)	15.12	Bae and Bayrak (2008)	9
Corley (1966)	25.65	AASHTO (2010) and KDOT (2011)	72

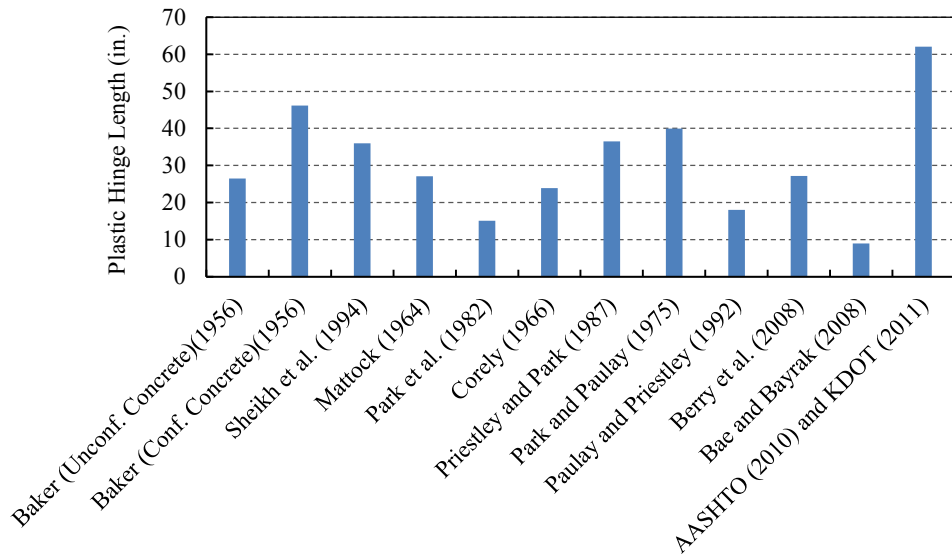


FIGURE 3.36
The Plastic Hinge Lengths for Column No. 3 in Bridge No. 1

TABLE 3.32
The Plastic Hinge Lengths for Column No. 3 in Bridge No. 1

Model	Plastic Hinge Length (in)	Model	Plastic Hinge Length (in)
Baker (Unconf. Concrete) (1956)	26.49	Priestley and Park (1987)	36.53
Baker (Conf. Concrete) (1956)	46.13	Park and Paulay (1975)	39.91
Sheikh et al. (1994)	36	Paulay and Priestley (1992)	18
Mattock (1964)	27.06	Berry et al. (2008)	27.16
Park et al. (1982)	15.12	Bae and Bayrak (2008)	9
Corley (1966)	23.87	AASHTO (2010) and KDOT (2011)	62

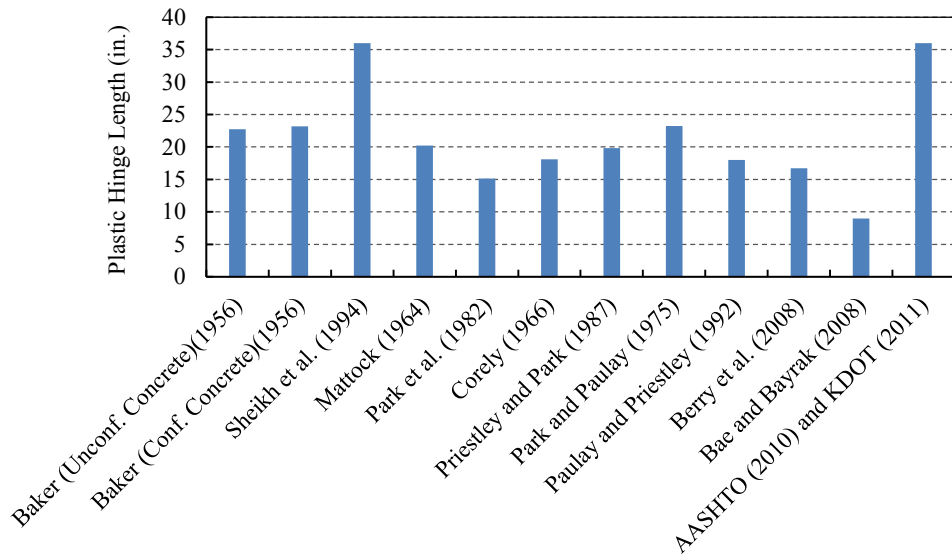


FIGURE 3.37
The Plastic Hinge Lengths for Column No. 1 in Bridge No. 2

TABLE 3.33
The Plastic Hinge Lengths for Column No. 1 in Bridge No. 2

Model	Plastic Hinge Length (in)	Model	Plastic Hinge Length (in)
Baker (Unconf. Concrete) (1956)	22.72	Priestley and Park (1987)	19.84
Baker (Conf. Concrete) (1956)	23.17	Park and Paulay (1975)	23.22
Sheikh et al. (1994)	36	Paulay and Priestley (1992)	18
Mattock (1964)	20.20	Berry et al. (2008)	16.73
Park et al. (1982)	15.12	Bae and Bayrak (2008)	9
Corley (1966)	18.73	AASHTO (2010) and KDOT (2011)	36

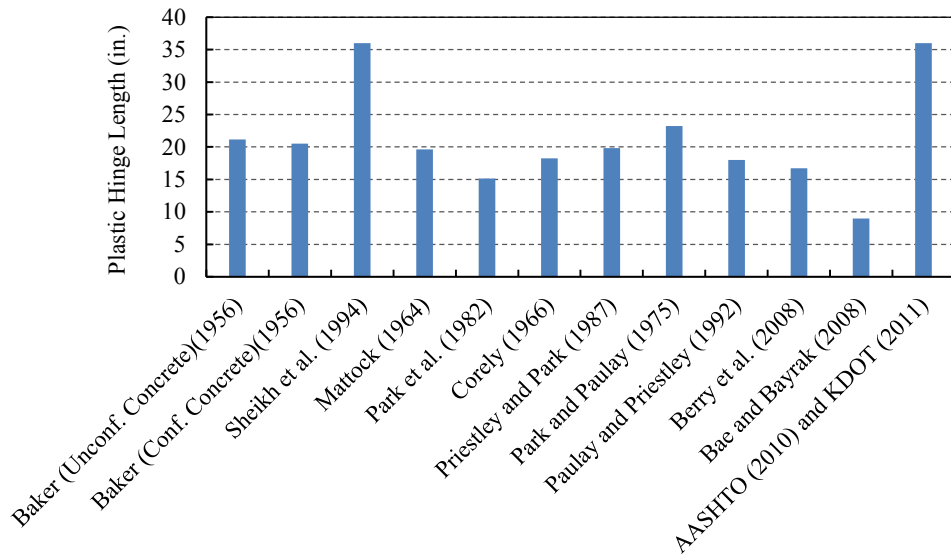


FIGURE 3.38
The Plastic Hinge Lengths for Column No. 2 in Bridge No. 2

TABLE 3.34
The Plastic Hinge Lengths for Column No. 2 in Bridge No. 2

Model	Plastic Hinge Length (in)	Model	Plastic Hinge Length (in)
Baker (Unconf. Concrete) (1956)	21.15	Priestley and Park (1987)	19.84
Baker (Conf. Concrete) (1956)	20.52	Park and Paulay (1975)	23.22
Sheikh et al. (1994)	36	Paulay and Priestley (1992)	18
Mattock (1964)	19.63	Berry et al. (2008)	16.73
Park et al. (1982)	15.12	Bae and Bayrak (2008)	9
Corley (1966)	18.25	AASHTO (2010) and KDOT (2011)	36

As seen in above figures, the plastic hinge length, required by AASHTO-LRFD (2010) and KDOT-LRFD (2011) are very conservative compared to the lengths required by different authors. In bridge No. 2 which was designed in 2004, the plastic hinge length was not considered; however, for the bridge No. 1, designed in 2009, the plastic hinge length is equal to 74 in., which is conservative according to AASHTO-LRFD (2010) and KDOT-LRFD (2010).

3.4.7 Investigation of the Displacement Capacity of the Existing Columns

The goal of this section is to obtain the displacement capacity of columns in the representative existing bridges. KSU-RC, the windows-based analytical software that can analyze the performance of a reinforced concrete column with different geometry, confinement and loading pattern for a realistic assessment of the performance and available strength and displacement capacity, was utilized for assessment of the displacement capacity of columns (Esmaily 2013).

TABLE 3.35
The Displacement Capacity of Column No. 1 in Bridge No. 1

Load Combination	P_u	Displacement Capacity (in)	Reason of Failure
Strength I			
Min DL Case I LL	651.859	40.7944	
Min DL Case II LL	645.045	40.796	
Max DL Case I LL	810.921	36.8159	
Max DL Case II LL	804.104	42.33	
Strength V			
Min DL Case I LL	709.949	40.98	
Min DL Case II LL	546.098	38.56	
Max DL Case I LL	709.949	40.98	
Max DL Case II LL	704.67	40.97	
Strength III Min DL	265.59	33.61	
Extreme event I			
Min DL Case I LL	451.6015	36.94	Confined concrete strain exceeded allowable maximum strain of 0.01622
Min DL Case II LL	449.659	36.91	
Max DL Case I LL	610.7715	39.63	
Max DL Case II LL	608.829	39.6	
Extreme event II			
Min DL Case I LL	451.6015	36.94	
Min DL Case II LL	449.659	36.91	
Max DL Case I LL	610.7715	39.63	
Max DL Case II LL	608.829	39.6	

TABLE 3.36
The Displacement Capacity of Column No. 2 in Bridge No. 1

Load Combination	P_u	Displacement Capacity (in)	Reason of Failure
Strength I			
Min DL Case I LL	703.585	44.9727	
Min DL Case II LL	730.546	44.0698	
Max DL Case I LL	885.787	39.5731	
Max DL Case II LL	912.751	38.6936	
Strength V			
Min DL Case I LL	808.535	41.3142	
Min DL Case II LL	647.143	45.7013	
Max DL Case I LL	808.535	41.3142	
Max DL Case II LL	829.333	41.3358	
Strength III Min DL	375.776	49.3837	
Extreme event I			
Min DL Case I LL	504.467	47.7845	Confined concrete strain exceeded allowable maximum strain of 0.01622
Min DL Case II LL	512.169	47.797	
Max DL Case I LL	686.667	44.9073	
Max DL Case II LL	694.369	44.9296	
Extreme event II			
Min DL Case I LL	504.467	47.7845	
Min DL Case II LL	512.169	47.797	
Max DL Case I LL	686.667	44.9073	
Max DL Case II LL	694.369	44.9296	

TABLE 3.37
The Displacement Capacity of Column No. 3 in Bridge No. 1

Load Combination	P_u	Displacement Capacity (in)	Reason of Failure	
Strength I				
Min DL Case I LL	595.141	34.3914		
Min DL Case II LL	602.282	34.4113		
Max DL Case I LL	754.394	31.9659		
Max DL Case II LL	761.537	31.9715		
Strength V				
Min DL Case I LL	716.24	32.6251		
Min DL Case II LL	562.027	34.9654		
Max DL Case I LL	716.24	32.6251		
Max DL Case II LL	721.772	32.6486		
Strength III Min DL	395.66	36.792	Confined concrete strain exceeded allowable maximum strain of 0.01622	
Extreme event I				
Min DL Case I LL	436.107	36.4336		
Min DL Case II LL	438.144	36.4425		
Max DL Case I LL	595.272	34.3924		
Max DL Case II LL	597.309	34.4075		
Extreme event II				
Min DL Case I LL	436.107	36.4336		
Min DL Case II LL	438.144	36.4425		
Max DL Case I LL	595.272	34.3924		
Max DL Case II LL	597.309	34.4075		

TABLE 3.38
The Displacement Capacity of Column No. 1 in Bridge No. 2

Load Combination	P_u	Displacement Capacity (in)	Reason of Failure
Strength I			
Min DL Case I LL	803.1	4.0072	
Min DL Case II LL	669.529	4.2673	
Max DL Case I LL	962.24	3.6451	
Max DL Case II LL	828.632	3.8801	
Strength V			
Min DL Case I LL	837.864	3.8831	
Min DL Case II LL	575.925	4.3958	
Max DL Case I LL	837.864	3.8831	
Max DL Case II LL	734.839	4.14	Confined concrete strain exceeded allowable maximum strain of 0.01072
Strength III Min DL	209.556	5.4731	
Extreme event I			
Min DL Case I LL	456.786	4.6395	
Min DL Case II LL	418.6015	4.6263	
Max DL Case I LL	615.966	4.2643	
Max DL Case II LL	577.7815	4.3933	
Extreme event II			
Min DL Case I LL	456.786	4.6395	
Min DL Case II LL	418.6015	4.6263	
Max DL Case I LL	615.966	4.2643	
Max DL Case II LL	577.7815	4.3933	

TABLE 3.39
The Displacement Capacity of Column No. 2 in Bridge No. 2

Load Combination	P_u	Displacement Capacity (in)	Reason of Failure	
Strength I				
Min DL Case I LL	544.198	4.3978		
Min DL Case II LL	572.5	4.3947		
Max DL Case I LL	665.303	4.2687		
Max DL Case II LL	693.603	4.1364		
Strength V				
Min DL Case I LL	595.504	4.3967		
Min DL Case II LL	496.253	4.5183		
Max DL Case I LL	595.504	4.3967		
Max DL Case II LL	617.336	4.2646		
Strength III Min DL	164.133	5.7811	Confined concrete strain exceeded allowable maximum strain of 0.01072	
Extreme event I				
Min DL Case I LL	331.934	4.837		
Min DL Case II LL	340.022	4.8492		
Max DL Case I LL	453.044	4.6377		
Max DL Case II LL	461.132	4.6439		
Extreme event II				
Min DL Case I LL	331.934	4.837		
Min DL Case II LL	340.022	4.8492		
Max DL Case I LL	453.044	4.6377		
Max DL Case II LL	461.132	4.6439		

Chapter 4: Retrofitting

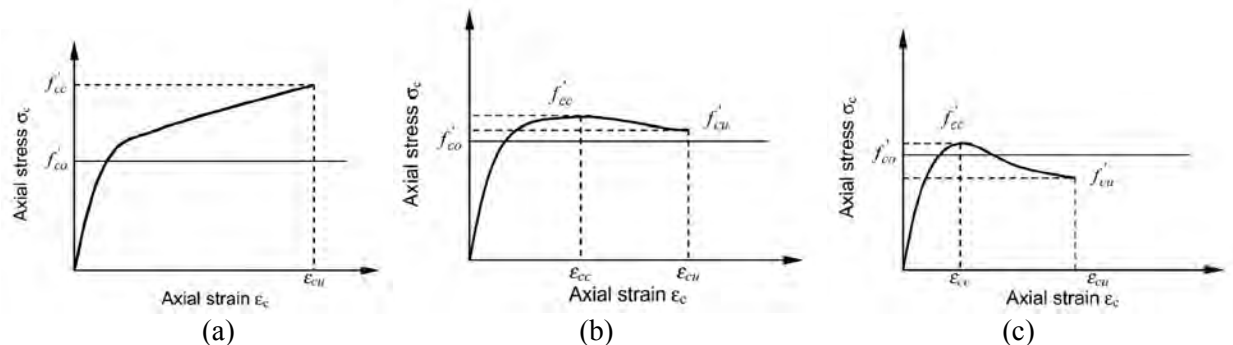
4.1 Retrofitting

In recent years, a significant amount of research has been devoted to the study of various techniques to enhance the seismic performance of reinforced concrete structures. This is due to the fact that according to the current seismic design codes; there are many reinforced concrete structures that don't have adequate strength against seismic loads. Furthermore, there are many deteriorated reinforced concrete structures and infrastructures in United States that need to be replaced or repaired to handle increased loads. In many structures, steel reinforcement has corroded from years of weathering, causing cracking or spalling of the cover concrete. This is a major concern in the repair and strengthening of columns. Typically in columns with severe corrosion of the reinforcing bars, the entire column must be replaced or all of the reinforcement must be replaced in order to restore strength and protect the bars. There are various retrofit techniques that should be considered before selecting the retrofit scheme. These schemes should be thoroughly investigated by assessment of the performance of a deficient column before and after retrofit. This needs a suitable and relevant analytical tool. KSU-RC has been developed having this in mind. In addition to the updates implemented in the software during the course of this study to be able to have realistic assessment of the strength, ductility and general performance of the columns, the next generation of the program with a revised and more intuitive interface, more analytical procedures and models and enhanced functionality will be released in a near future. It should be noted that this is not under this study, and the authors are looking for a proper resource to have the important task done. The result, as a stand-alone software, then, can be used by various private and public engineering agencies, including departments of transportation for assessment of columns with any geometry, confinement and load-displacement pattern. Note that a simple monotonic moment-curvature or force deflection analysis under no or a constant axial load cannot provide the real performance when a column experiences a different load pattern. This user-friendly software will replace the need for high-end finite element method (FEM) programs and provides the same functionality with much less learning time and computational effort.

4.2 Retrofitting by Fiber Reinforced Polymer (FRP)

One method of strengthening structures while increasing durability against steel corrosion is using Fiber Reinforced Polymer (FRP) wrap or lamina. FRP fabric can be wrapped around structural members, acting as a confining jacket. Early application of FRP fabric has been used mainly for strengthening structures against non-seismic loads. Nonetheless, their high strength-to-weight ratio, immunity to corrosion and easy handling and installation make FRP jackets and stirrups the best material in an increasingly large number of seismic retrofitting projects, despite the relatively high material costs. Antonopoulos and Triantafillou mention the main uses of FRPs in seismic retrofitting of existing reinforced concrete elements as follows (2003):

- The shear capacity of sub-standard elements (columns, shear walls, etc.) can be enhanced by providing externally bonded FRPs with the fibers in the hoop direction.
- A ductile behavior of flexural plastic hinges at beam or column ends can be achieved through added confinement in the form of FRP jackets, with the fibers placed along the beam or column perimeter.
- The flexural strength of reinforced concrete columns can only be developed when debonding of the reinforcement in lap splices is prevented. Such debonding occurs once vertical cracks develop in the cover concrete and progresses with increased dilation and cover spalling. The associated rapid flexural strength degradation can be prevented or limited with increased lap confinement, again with fibers along the column perimeter.



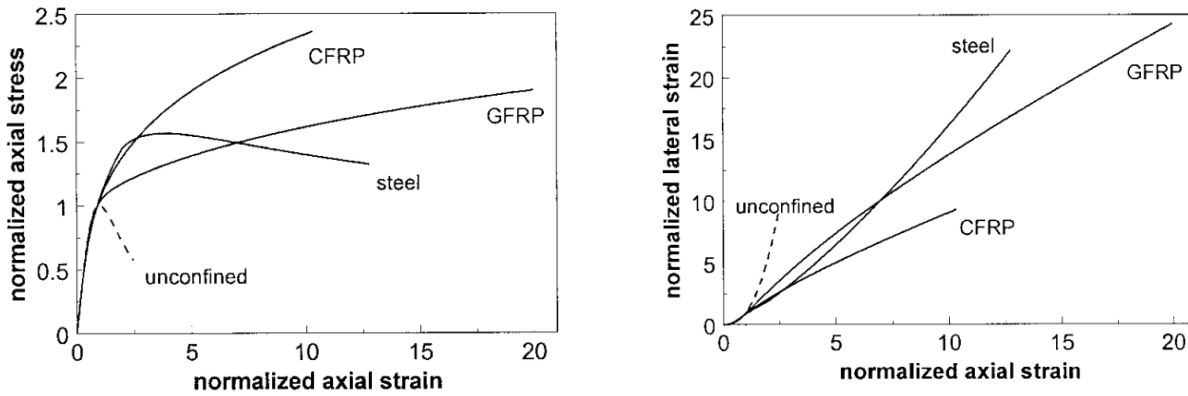
(Source: Lam and Teng 2003)

FIGURE 4.1
Classification of Stress-Strain Curve of FRP-Confined Concrete. (a) Increasing Type; (b) Decreasing Type with $f'_{cu} > f'_{co}$; (c) Decreasing Type with $f'_{cu} < f'_{co}$

4.2.1 FRP-Confined versus Steel-Confined Concrete Behavior

As previously mentioned, confined concrete with steel follows a parabola branch until reaching the peak stress, after that, it follows a descending branch. However, the stress-strain diagram for confined concrete with FRP has an ascending bi-linear shape (the increasing type) if the concrete section is confined sufficiently. The increasing type of stress-strain curve has been observed in the most tests, done so far. In some cases, the stress-strain curve features a post-peak descending branch. In this type, which is called the descending type, the compressive strength is reached before FRP ruptures. In the descending type, two different types of strain-strain behavior have been observed. In the first one, the stress-strain curve terminates at a stress $f'_{cu} < f'_{co}$, where f'_{co} is the compressive strength of unconfined concrete. It would happen when the specimen is said to be insufficiently confined where little strength enhancement can be expected. In the second one, which is illustrated in Figure 4.1, the stress-strain curve terminate at a concrete stress f'_{cu} above the compressive strength of unconfined concrete, f'_{co} . In this case the confinement is sufficient (Lam and Teng 2003).

The differences in behavior of concrete confined with steel, carbon fiber reinforced polymer (CFRP) and glass fiber reinforced polymer (GFRP) shown in Figure 4.2. As seen in this figure, the ultimate strength of FRP-confined concrete is at the same time that ultimate strain occurs; therefore, there is not any stiffness degradation. The FRP-confined strength is determined by the maximum confining pressure applied by FRP, while the slope of the second branch, and the maximum strain, are related to the confinement stiffness (De Lorenzis and Tepfers 2003).



(Source: Soppelstra 1999)

FIGURE 4.2
Modeling of Behavior of Concrete Confined with Steel, CFRP, and GFRP: (a) Axial Stress versus Axial Strain, (b) Lateral Strain versus Axial Strain

4.2.2 Carbon Fiber Jacketing

Carbon strands which are impregnated with resin in the form of sheet is called carbon fiber sheet. Carbon strands are set in one direction in the sheet, therefore, the sheet only has strength in that direction. There are some carbon fiber sheets that have carbon fibers in two directions, but they are not widely used. Carbon fiber was first introduced to repair damaged concrete structures and has been used for seismic retrofit of columns since 1980.



(a)

(b)

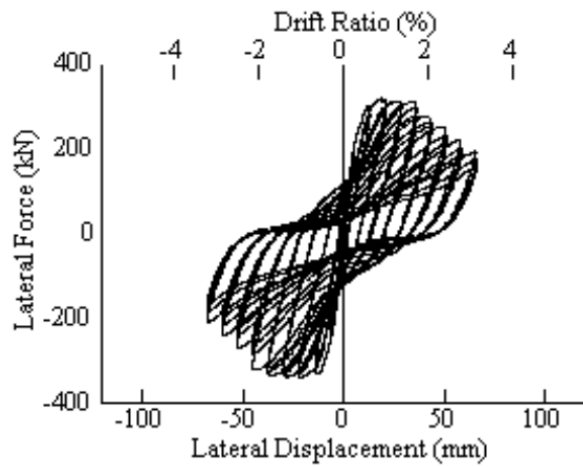
(c)

(Source: Calvi et al. 2007)

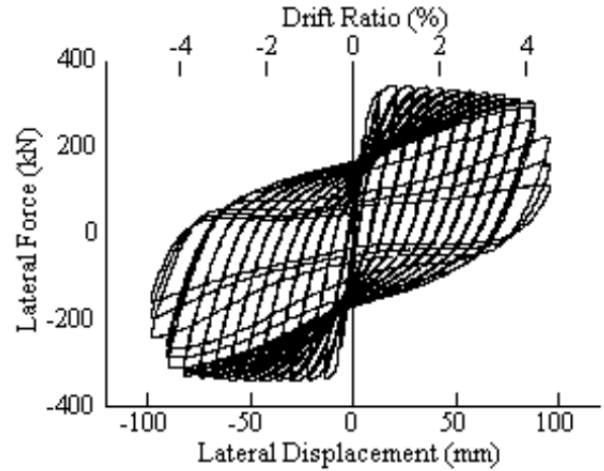
FIGURE 4.3
Wrapping of Carbon Fiber Sheet: (a) Pasting Glue, (b) Wrapping the First Layer and (c) Bonding on the First Layer

The elastic modulus and strength of standard carbon fiber are the same with and ten times larger, respectively, than those of reinforcing steel. Carbon fibers have the linear stress-strain relationship up to failure. Rupture strain is about 2%. Because residual plastic strains do not remain in the carbon fibers jacket, as long as carbon fiber is used to laterally confine the concrete in elastic range, it is more effective than reinforcing steel in flexural retrofit and to resist shear in the shear retrofit.

Results of a cyclic loading test on carbon fiber sheet jacketing for circular column with 2.1 m high and 700 mm diameter are shown in Figure 4.4. The carbon fiber sheet was wrapped in two ways; lateral direction, and both lateral and vertical directions. The carbon fiber sheet, wrapped in the lateral direction and both lateral and vertical direction enhanced the displacement ductility capacity by a factor of 200% and 300%, respectively (Hoshikuma et al. 1996, Unjoh et al. 1997).



(a) As-built



(b) Retrofitted (horizontal wrapping)

(Source: Hoshikuma et al. 1996; Unjoh et al. 1997)

FIGURE 4.4
Effect of Carbon Fiber Sheet Jacketing for Circular Column



(Source: Ogata and Osada 1999)

FIGURE 4.5
Carbon Fiber Sheet Jacketing of Hollow Reinforced Concrete Column, Sakawa-Gawa Bridge, Tomei Expressway

4.2.3 Aramid and Glass Fiber Jacketing

“Benefits of aramid fiber jacketing are same as carbon fiber jacketing. It is light and easy to wrap without heavy machines. Aramid fibers are available in three different forms:

- Braided tape
- Unidirectional tape
- Sheet



(Source: Okamoto et al. 1994)

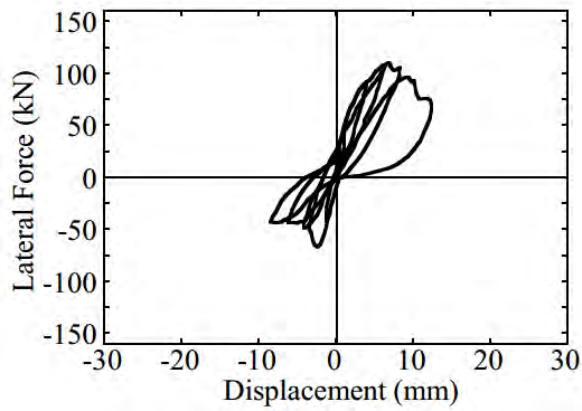
FIGURE 4.6
Retrofitting by Aramid Fiber; (a) Braided Tape and Unidirectional Tape, (b) Sheet

Braided tape typically has 20 mm width, and it consists of aramid fibers, woven in a braided form. Unidirectional tape consists of fabrics woven in a tape form with typically 75 mm width. Unidirectional tape and sheet have aramid fibers in axial direction and Glass fibers in the transverse direction. Strength of aramid fibers depends on quantity of fibers per cross section. For example, tensile strength of braided and unidirectional tape with 307,200 deniers (1 *denier* = 1 g/9,000 m) and 34.5 mm² which are impregnated with epoxy resin is 54.7 kN and 36.0 kN, respectively” (Calvi et al. 2007).

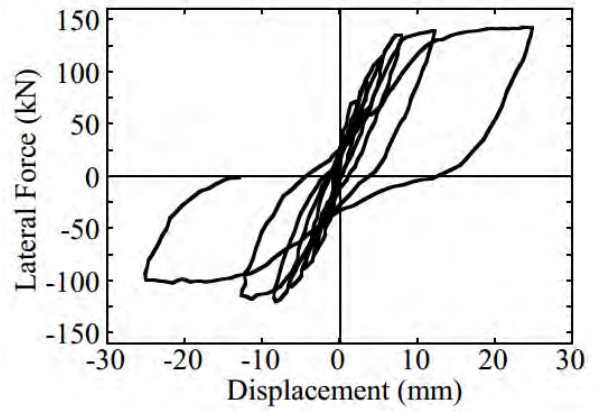


(Source: Japan Railway Research Institute)

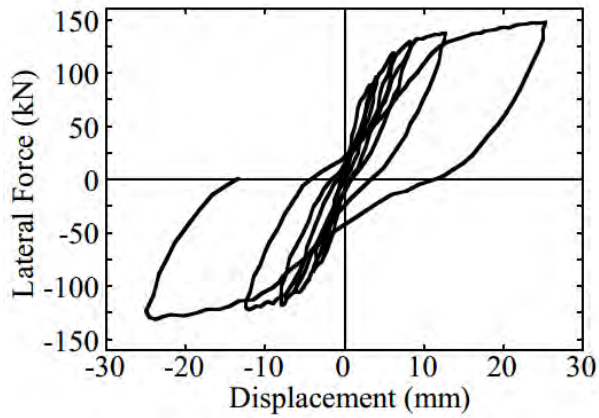
FIGURE 4.7
Aramid Fibers Reinforced Plastic Jacketing



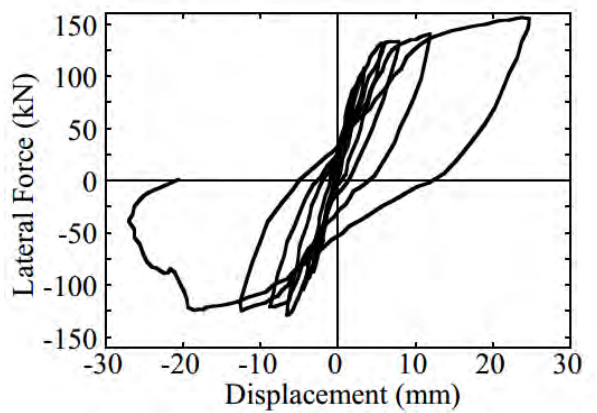
(a)



(b)



(c)

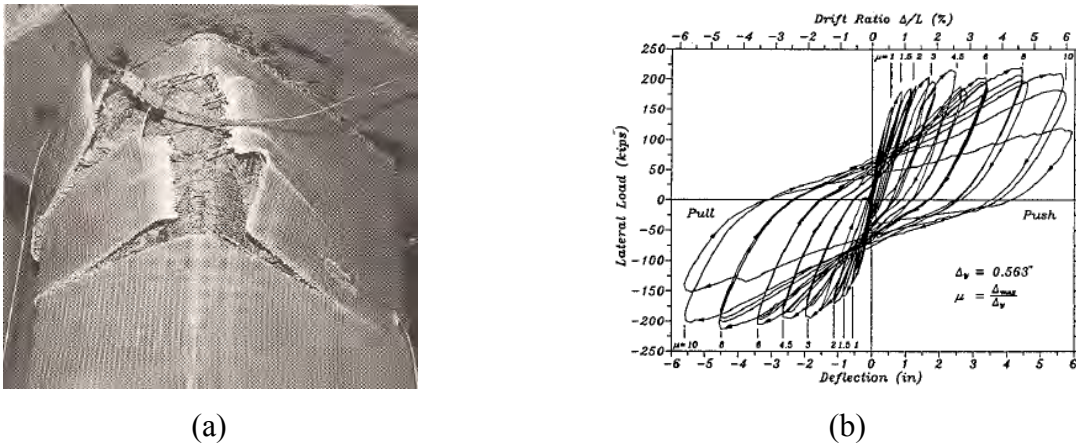


(d)

(Source: Priestley 1996)

FIGURE 4.8
Effect of Retrofitting by Different Types of Aramid Fiber

Okamoto et al. (1994) conducted some cyclic loading tests to investigate the effect of Aramid fiber jacketing on the columns. Columns in their tests had 250 mm width, 625 mm height and they designed to fail in shear. These columns were retrofitted by aramid braided tape, unidirectional tape and sheet. Smoothing of square section at corners was not done. The cyclic response of as-built column and columns retrofitted by aramid fibers are shown in Figure 4.8. As seen in figures, none of columns retrofitted with different types of aramid fibers rupture until final loading except column with retrofitted by aramid fiber where sheet ruptured at a corner, at a drift of 20/625.



(Source: Priestley 1996)

FIGURE 4.9
Rectangular Column with Glass Fiber-Epoxy Rectangular Jacket. (a) Failure by Jacket Fracture; (b) Lateral Force-Displacement Response

Glass fiber is also utilized for seismic retrofitting of columns. Figure 4.9 shows a rectangular column, retrofitted by glass fiber-epoxy jacket. As seen in this figure, the retrofitted column sustained displacement ductility up to 8, corresponding to drift angle of 4% before jacket failure (Priestley 1996).

Figure 4.10 shows another technique to implementation of glass fiber. In this technique, glass fiber with resin mixture was blasted by a spray gun. For enhancing the strength and ductility of the columns, steel cross-mesh was used with glass fiber. The cyclic loading tests show that the ductility of the steel cross-mesh with glass fiber is significantly more than ductility of steel jacketing.



(Source: Japan Railway Research Institute)

FIGURE 4.10
Glass Fiber Jacketing

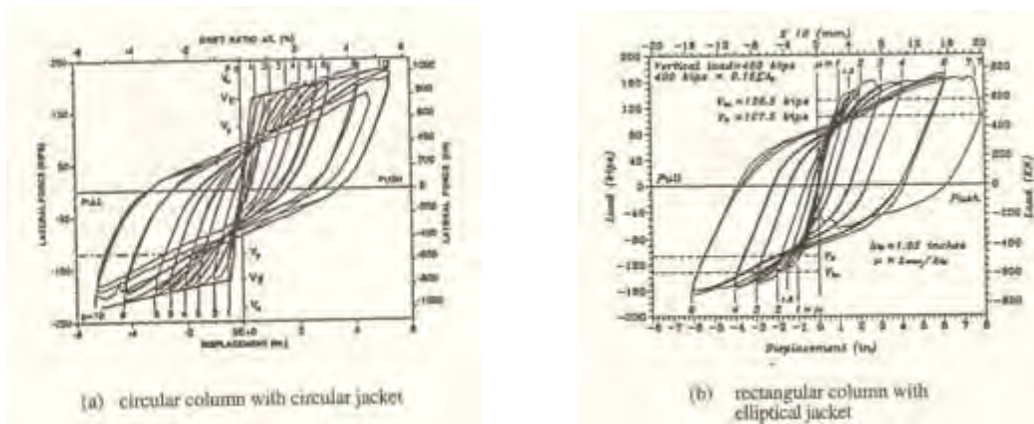
4.3 Retrofitting Using Steel Jackets

Another strategy to reinforce concrete columns to withstand lateral loads is to retrofit them with steel jackets. There are different types of jackets being used such as concrete, and composite, but steel jackets are most commonly used, mainly in California and Japan (Daudey and Filiatrault 2000). Steel jacket improve the seismic behavior of bridge piers by offering passive confinement of the original concrete cross section. The confinement pressure is carried by hoop stress in the jacket.

4.3.1 Steel Jacket Configuration

Steel jackets can be made to any desired shape such as circular or elliptical, but the most common shape is a circular shape. If the column that is being retrofitted is a rectangular column the jacket can be an oval jacket (circular or elliptical), since these kind of jackets provide uniform confining pressure to the original section. The empty space between the rectangular or circular column and the steel jacket is filled with a cement-based material such as concrete or grout. The steel jackets are usually 12.5-25 mm larger than the radius of the cross section (Calvi et al. 2007). The length of the jacket is built to the required length calculated to resist plastic hinge formation.

Although rectangular steel jacket can be expected to be effective for shear strength enhancement, they are not generally recommended. As shown in Figure 4.12, circular and elliptical steel jacket are recommended for rectangular columns. In contrast, because elliptical jacket enlarge the column width after retrofitting, effective measures of using rectangular steel jacket on rectangular columns have been studied in Japan.



(a) Circular column with circular jacket

(b) Rectangular column with elliptical jacket

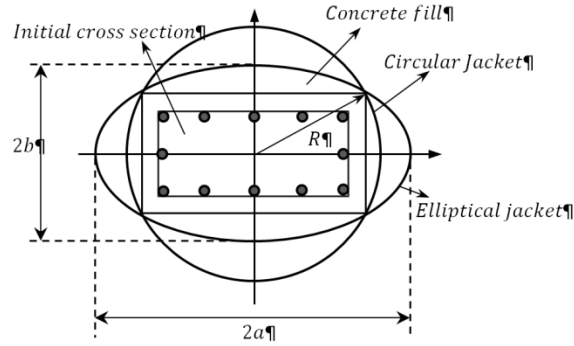
(Source: Priestley 1996)

FIGURE 4.11
Lateral Force-Displacement Response of Columns Retrofitted with Steel Jackets for Enhanced Ductility

The lateral force-displacement hysteretic for retrofitted columns of both circular and rectangular shape are shown in Figure 4.11. For circular column, flexural response of column is limited by the effective ultimate tension strain of the longitudinal reinforcement that is equal to $0.75\varepsilon_{su}$, where ε_{su} is the strain at maximum stress. The longitudinal steel ratio in steel column is about 5% and this column is confined with elliptical steel jacket extending beyond the expected plastic end region. As a result of inadequate shear strength in the unconfined region beyond the jacket, failure occurred at a displacement ductility factor 8.

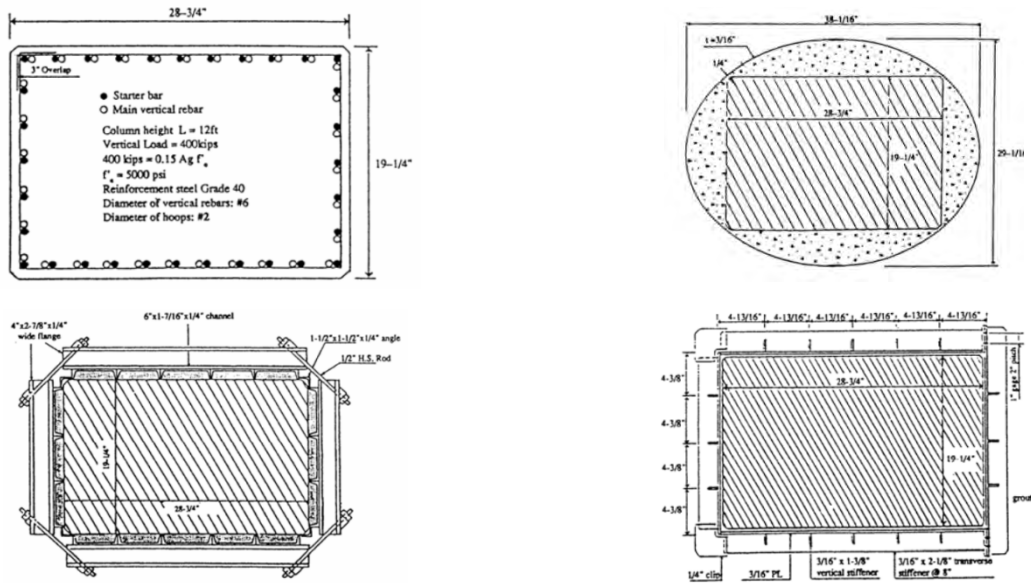
Figure 4.15 shows the effect of elliptical jacket, built-up steel channels, and stiffened rectangular jacket on lap splices in critical region. As seen in these figures, stiffened rectangular jacket indicated as earlier and more rapid deterioration of strength. The bolted system of retrofitting, using built-up steel jacket shows stable response up to six times yield displacement

after which bond failure at the lap-splice was the cause for strength deterioration. With the elliptical jacket, column showed improved behavior compare to the as-built column.



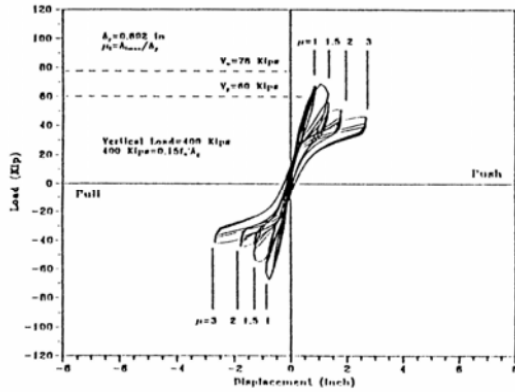
(Source: Priestley 1996)

FIGURE 4.12
Elliptical and Circular Steel Jacket over Rectangular Column

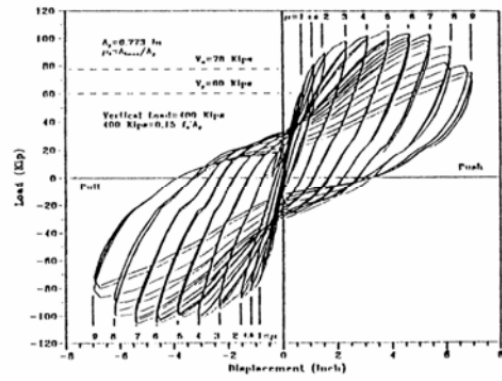


(Source: Priestley 1996)

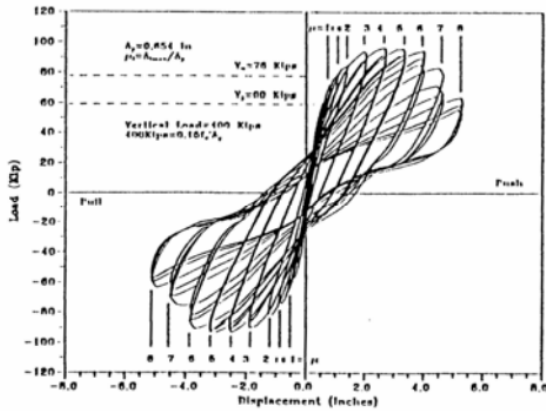
FIGURE 4.13
Retrofit for Rectangular Column



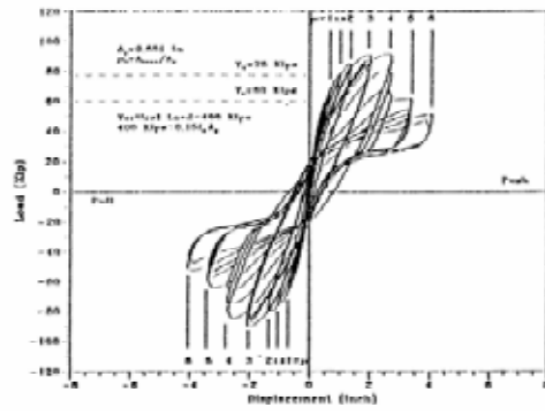
(a) As Built



(b) Elliptical Retrofit



(c) Built-up Steel Channel

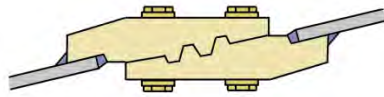


(d) Stiffened Rectangular Jacket

(Source: Priestley 1996)

FIGURE 4.14
Hysteretic Response of Rectangular Flexural Columns

Steel jacket is generally assembled by welding at site. However the quality of welding depends on workmanship and weather condition, and the welding takes time. Therefore, as a replacement of welding, an engagement joint can be applied. The engagement joints can be implemented to retrofit columns at high location as shown in Figure 4.15.



(a)



(b)

(Source: Japan Railway Research Institute)

FIGURE 4.15
(a) Engagement Joint, (b) Effective Use of Engagement Joint for Retrofit at High Location

4.3.2 Advantages of Steel Jackets

Steel jackets improve the flexural capacity of the columns that are retrofitted. The columns without retrofit had poor confinement in their concrete core which made it the weakest area, leading to development of the plastic hinges in the lower parts of the columns close to the footings. Furthermore, steel jackets add confinement which increases the compressive strength of the core concrete and improves the flexural ductility capacity of the already existing regions (Priestley et al. 1996). Steel jackets are also one of the simplest forms of retrofitting.

Another advantage of installing a steel jacket is increasing the shear strength. It is commonly known by researchers that the shear strength of concrete under an axial load can be represented by:

$$V_u = V_c + V_s + V_N$$

Equation 4.1

Where, V_u is the ultimate shear strength of concrete corresponding to large flexural ductility, V_c is the minimum shear strength of the concrete, V_s is shear strength provided by the transverse reinforcement, and V_N is the shear strength contributed by presence of a compressive axial load (Priestley 1996).

Based on the research done by Priestley et al. (1996), the required shear strength to be contributed by the steel jacket, V_{sj} , can be expressed as follows:

$$\beta V_{sj} \geq V_0 - \beta(V_c + V_s + V_N)$$

Equation 4.2

Where, V_0 is the shear force induced by the maximum probable flexural capacity of the plastic hinge and $\beta = 0.7$. For estimating V_{sj} , the jacket is taken as a continuous transverse reinforcement of cross section equal to its thickness and of spacing equal to unity.

4.4 Retrofitting by Precast Concrete Segment Jacket and Cable-Strand Jacket

For the columns in the river, lake and seas, because steel jacket is vulnerable to corrosion and impact with floating material, another technique should be used. One of these techniques is using reinforced concrete jacket. Because construction is faster, precast segment jacket is also used. Depending on capacity of column, new longitudinal reinforcement is set around the existing column, and precast concrete segment are set around the new reinforcement. The segments are tied together by strands. After injecting non-shrinking mortar between the existing concrete and precast concrete segment, pre-stressed force was introduced in the strands to assure the contact of the segments. The laboratory tests are shown that the precast concrete segment jacket is effective to enhance the strength and ductility capacity.

Moreover, for providing protection for columns against corrosion and impact with floating materials, another unique technique can be used. In this technique, reinforced concrete columns are wrapped by high strength strands. A special device is used for wrapping strands around the column.

Chapter 5: Conclusion and Recommendations

5.1 Conclusion

Kansas Department of Transportation (KDOT) has implemented the new AASHTO-LRFD provisions in the state specific LRFD design procedure (KDOT-LRFD). There have been some significant updates in new version of AASHTO-LRFD (2010), compared to previous versions of the code. Most of the existing bridges constructed before the new provisions, have been designed and constructed based on the old provisions. In this study, these changes have been assessed against the latest pertinent research. Also, adequacy of the bridges designed and constructed based on the old code has been studied by analyzing several representative bridge columns from two main different categories. The main changes in the AASHTO-LRFD (2010) and KDOT-LRFD (2011) compared to previous versions, here called old code, studied in this report are as follows:

- The return period of the design earthquake has been changed from 500-years to 1000-years (AASHTO-LRFD (2010))
- The vehicular collision impact force has been changed to the 400 *kips* applied at a height of 4 ft above the ground surface (this change was updated later as follows)
- A length of plastic hinge region has been specified and required when designing reinforced concrete bridge columns to enhance the strength and ductility of the bridge structure. Accordingly, a minimum amount of lateral reinforcement is required within the plastic hinge region, as specified by the revised code.
- Subsequently, in AASHTO-LRFD (2012), the vehicular collision force was updated to 600 kips applied in a direction of 0 to 15 degrees with the edge of the pavement in a horizontal plane at a distance of 5.0 ft above the ground level (this change is not reflected in the KDOT-LRFD as of the time of this study).

Since the existing bridges (as of the time of this study) are designed based on the old codes, they need to be evaluated to know if they meet the new requirements. This assessment is necessary to decide if a column needs to be retrofitted or not.

Assessment of the strength and ductility of bridge columns can be done by using the code procedure in which the real strength of the column may be underestimated, or by analyzing the column performance using the most realistic material models and analytical tools in which the real strength and ductility can be evaluated.

In this study, both procedures were used, and the models and analytical methods were scaled to the latest models and methods backed by the latest research findings. A windows-based computer program was used for assessment of the real performance of bridge columns. The program KSU-RC uses the latest analytical models and methods and can be used to analyze the performance of reinforced concrete bridge columns with various geometry, confining material, and load pattern.

5.1.1 Flexural Capacity

To explore the efficiency of the existing reinforced concrete bridge piers based on the new provisions, two representative existing bridges were selected by KDOT (project monitor). The flexural capacity of the reinforced concrete sections has been assessed based on AASHTO-LRFD (2010) stress-block method with and without considering confinement effect. For a realistic assessment of the flexural capacity of these bridge piers considering the confinement effect, the KSU-RC software was utilized. Based on the results of this study, the flexural strength of all bridge piers were enough and the bridge piers address the new code requirements in terms of the demanded flexural capacities under all of the load combinations.

5.1.2 Shear Capacity

Considering the axial force level evaluated based on specific load combinations and structural properties, the shear strength of each bridge pier was evaluated based on the ACI-318 (2011). In addition, the simplified AASHTO-LRFD (2010) procedure was used to evaluate the shear strength. The calculated shear strength of piers of the two representative existing bridges were enough under all load combinations dictated by the latest code requirements, except for the load combinations including the extreme vehicular impact load. Therefore, to address the new code requirements for this extremely rare event, some piers need to be retrofitted for

enhancement of their shear capacity. However, considering the real shear capacity of pier sections, redundancy of bridge structures and the inheriting load redistribution process, it is reasonable to say that these piers can withstand the aforesaid extreme load under their existing conditions without a major damage that can affect the serviceability of the bridge, let alone its collapse.

5.1.3 Plastic Hinge Region

A large number of models have been proposed by different researchers, including the author, for estimation of the plastic hinge length. Some of these models are introduced here in this report and used for evaluation of the plastic hinge length. The plastic hinge lengths, obtained by means of these models, were compared with the plastic hinge length, required by AASHTO-LRFD (2010) and KDOT-LRFD (2011). The plastic hinge length, required by AASHTO-LRFD (2010) was conservative compared to all of the models proposed by different researchers. It should be noted that a plastic hinge length has been considered for bridges design in 2009 and after; however, bridges same as the representative Bridge No. 2 in this study, no plastic hinge length has been considered. As mentioned for the shear capacity of old bridges when it comes to the extreme event of vehicular impact, these bridge piers, can safely address the flexural strength and ductility required by the latest code provisions; hence, there is no concern in terms of serviceability and safety of these bridges. However, to address the new code requirements for the minimum lateral reinforcement in the plastic hinge region, one of the methods, explained in Chapter 2, can be used after assessment of each case.

In general, the two representative bridges provided by KDOT for this study, represented state bridges designed and constructed based on two different versions of the code that can safely address the demanded loads considering their actual strength and bridge structural-redundancy and load redistribution process. So, there is no immediate concern in terms of serviceability or collapse of these bridges under demanded loads, including the extreme vehicular impact load. However, the calculated shear strength of most of the columns designed and constructed based on the old codes may not be enough considering the new vehicular impact load required by the new code revisions as shown in this study.

While no immediate action seems to be necessary in terms of serviceability and safety of these bridges, engineering judgment and a realistic case-based performance assessment is needed to decide if enhancement of the shear strength and the amount of lateral reinforcement within the plastic hinge length is necessary. Proper method to retrofit these types of columns as detailed in Chapter 2 can be used, once a decision is made for a case to implement the aforesaid enhancement. Choosing the appropriate method for retrofitting is case specific and can be done for each case considering the column geometry, service load, reinforcement details and material properties.

5.2 Recommendations

Based on the result of this study, bridges in the state of Kansas, represented by the two bridges analyzed in this study, can safely address the demanded loads considering their actual strength, bridge structural-redundancy and load redistribution process; and no immediate action is required considering the serviceability and safety of these bridges.

The following recommendations are made to update the conditions of reinforced concrete bridge piers that their calculated strength and lateral reinforcement in the plastic-hinge region may be found to be deficient based on the revised code provisions:

- Assessment of the efficiency of stream (river) crossing bridges in the state of Kansas under vessel collision forces as dictated by the new code revisions.
- Assessment of the real performance of all important bridges designed and constructed based on the old code provisions considering involved factors such as the bridge geometry, service load, material properties, reinforcement details, etc. This performance may well address the new demanded load combinations, including extreme events such as vehicular impact load.

References

- American Association of State Highway and Transportation Officials. 2007. *AASHTO LRFD Bridge Design Specifications*. Washington, D.C.
- American Association of State Highway and Transportation Officials. 2010. *AASHTO LRFD Bridge Design Specifications*. Washington, D.C.
- American Association of State Highway and Transportation Officials. 2012. *AASHTO LRFD Bridge Design Specifications*. Washington, D.C.
- American Concrete Institute 318. 2011. *Building Code Requirements for Reinforced Concrete (ACI318-11) and Commentary*. American Concrete Institute. Farmington Hills, Michigan.
- Antonopoulos, C.P., and T.C. Triantafillou. 2003. “Experimental Investigation of FRP-Strengthened RC Beam-Column Joints.” *ASCE Journal of Composite for Construction* 7 (1): 39–49.
- ASTM Standard D1586. 2011. “Standard Test Method for Standard Penetration Test (SPT) and Split-Barrel Sampling of Soils.” ASTM International, West Conshohocken, PA.
- ASTM Standard D2166. 2006. “Standard Test Method for Unconfined Compressive Strength of Cohesive Soil,” ASTM International, West Conshohocken, PA.
- ASTM Standard D2216. 2010. “Standard Test Methods for Laboratory Determination of Water (Moisture) Content of Soil and Rock by Mass.” ASTM International, West Conshohocken, PA.
- ASTM Standard D2850. 2007. “Standard Test Method for Unconsolidated-Undrained Triaxial Compression Test on Cohesive Soils.” ASTM International, West Conshohocken, PA.
- ASTM Standard D4318. 2010. “Standard Test Methods for Liquid Limit, Plastic Limit, and Plasticity Index of Soils.” ASTM International, West Conshohocken, PA.
- Bae, S.B., and O. Bayrak. 2008. “Plastic Hinge Length of Reinforced Concrete Columns.” *ACI Structural Journal* 105 (3): 290–300.
- Baker, A.L.L. 1956. *The Ultimate Load Theory Applied to the Design of Reinforced and Prestressed Concrete Frames*. London, UK: Concrete Publication Ltd.

- Baker, A.L.L., and A.M.N. Amarakone. 1964. "Inelastic Hyperstatic Frame Analysis." *ACI Special Publication 12*: 85–142.
- Balan, T.A., F.C. Filippou, and E.P. Popov. 1998. "Hysteretic Model of Ordinary and High-Strength Reinforcing Steel." *Journal of Structural Engineering* 124 (3): 288–298.
- Balmer, G.G. 1949. "Shearing Strength of Concrete Under High Triaxial Stress- Computation of Mohr's Envelope as a Curve." *Structural Research Laboratory Report sp-23*. United States Department of the Interior, Bureau of Reclamation. Denver, Colorado.
- Bayrak, O.S., and S.A. Sheikh. 1998. "Confinement Reinforcement Design Consideration for Ductile HSC Columns." *ASCE Journal of Structural Engineering* 124 (9): 999–1010.
- Berry, M.P., D.E. Lehman, and L.N. Lowes. 2008. "Lumped-Plasticity Models for Performance Simulation of Bridge Columns." *ACI Structural Journal* 105 (3): 270–279.
- Calvi, G.M., K. Kawashima, I. Billings, A. Elnashai, C. Nuti, and A. Pecker. 2007. "FIB Bulletin 39: Seismic Bridge Design and Retrofit—Structural Solutions—Chapter 6: Design for Enhanced Control of Damage." *Fédération Internationale du Béton*.
- Chen, W.F., and A.F. Saleeb. 1982. *Constitutive Equation for Engineering Materials*. Volume 1: Elasticity and Modeling. New York: Wiley Interscience.
- Correal, J.F., M.S. Saiidi, D. Sanders, and S. El-Azazy. 2007. "Shake Table Studies of Bridge Columns with Double Interlocking Spiral." *ACI Structural Journal* 104 (4): 393–401.
- Corley, W.G. 1966. "Rotational Capacity of Reinforced Concrete Beams." *Journal of the Structural Division, ASCE* 92 (ST5): 121–146.
- Daudey, X., and A. Filiatrault. 2000. "Seismic Evaluation and Retrofit with Steel Jackets of Reinforced Concrete Bridge Piers Detailed with Lap-Slices." *Canadian Journal of Civil Engineering* 27 (1): 1–16.
- De Lonzis, L.T., and R. Tepfers. 2003. "Comparative Study of Models on Confinement of Concrete Cylinders with Fiber-Reinforced Polymer Composites." *Journal of Composites for Construction, ASCE*: 219–237.
- Dodd, L.L., and J.I. Restrepo-Posada. 1995. "Model for Predicting Cyclic Behavior of Reinforcing Steel." *ASCE Journal of Structural Engineering* 121 (3): 433–445.

- El-Tawill, S.S., E. Severino, and P. Fonseca. 2005. "Vehicular Collision with Bridge Piers." *ASCE Journal of Bridge Engineering* 10 (3): 345–353.
- Esmaeily, A. 2010. *Effects of Load Pattern on the Performance of RC Columns; Seismic Performance of Bridge Columns Subjected to Various Load Patterns*. doi:978-3-639-29168-1
- Esmaeily, A. 2013. KSU-RC. Retrieved December 2013, from Esmaeily: http://www.ce.ksu.edu/faculty/esmaeily/KSU_RC.htm
- Esmaeily, A., and R. Peterman. 2007. "Performance Analysis Tool for Reinforced Concrete Members." *Computers and Concrete* 4 (5): 331–346.
- Esmaeily, A., and Y. Xiao. 2002. *Seismic Behavior of Bridge Columns Subjected to Various Loading Patterns*. Pacific Earthquake Engineering Research Center (PEER), College of Engineering, University of California.
- Esmaeily, A., and Y. Xiao. 2004. "Behavior of Reinforced Concrete Columns under Variable Axial Loads." *American Concrete Institute, ACI Structural Journal* 101 (1): 124–132.
- Esmaeily, A., and Y. Xiao. 2005. "Behavior of Reinforced Concrete Columns under Variable Axial Loads: Analysis." *American Concrete Institute, ACI Structural Journal* 102 (5): 736–744.
- Fafitis, A., and S.P. Shah. 1985. "Lateral Reinforcement for High Strength Concrete Column." *ACI Special Publication, SP 87*: 213–232.
- Giuffre, A.P., and P.E. Pinto 1970. "Il Comportamento del Cemento Armato per Sollecitazioni Cicliche di Forte Intensita [Behavior of Reinforced Concrete under Strong Cyclic Loads.]" *Giornale del Genio Civile* 5 (1): 391–408.
- Gomes, A., and J. Appleton. 1997. "Nonlinear Cyclic Stress-Strain Relationship of Reinforcing Bars Including Buckling." *Engineering Structures* 19 (10): 822–826.
- Hoshikuma, J., H. Otsuka, and K. Nagaya. 1996. "Seismic Retrofit of Square RC Columns by Steel Jacketing." *Proceedings of the Third U.S.-Japan Workshop on Seismic Retrofit of Bridges*: 125–140.
- Japan Railway Research Institute. <http://www.rtri.or.jp/eng>

- Kansas Department of Transportation. 2011. *Design Manual Volume III - Bridge Section, U.S. Customary Units*. Topeka, KS.
- KDOT LRFD. 2010. *The LRFD Bridge Design Manual*. The Kansas Department of Transportation. Topeka, Kansas
- Kent, D.C., and R. Park. 1971. "Flexural Members with Confined Concrete." *ASCE Journal of Structural Engineering* 97 (ST7): 1969–1990.
- Kuramoto, H.K., T. Kabeyasawa, and F.-H. Shen. 1995. "Influence of Axial Deformation on Ductility of High Strength Reinforced Concrete Columns Under Varying Triaxial Forces." *ACI Structural Journal* 92 (5): 610–618.
- Lam, L., and J.G. Teng. 2003. "Design-Oriented Stress-Strain Model for FRP-Confined Concrete in Rectangular Columns." *Journal of Reinforced Plastic and Composites* 22 (13): 1149–1186.
- Mander John B., Michael J.N. Priestley, and R. Park. 1988. "Theoretical Stress-Strain Model for Confined Concrete." *ASCE Journal of Structural Engineering* 114 (8): 1804–1826.
- Mander, J.B., M.J.N Priestley, and R. Park. 1984. "Seismic Design of Bridge Piers." Research Report No. 84-2, University of Canterbury Department of Civil Engineering. Christchurch, New Zealand. <http://nisee.berkeley.edu/elibrary/Text/S20292>
- Mattock, A.H. 1964. "Rotational Capacity of Hinging Regions in Reinforced Concrete Beams." *American Concrete Institute Special Publication* 12: 143–181. Miami, Florida.
- Mattock, A.H. 1967. "Discussion of Rotational Capacity of Hinging Region in Reinforced Concrete Beams by W.D.G. Corley." *Journal of the Structural Division of the ASCE* 93 (2): 519–522.
- Mendis, P. 2001. "Plastic Hinge Lengths of Normal and High-Strength Concrete in Flexure." *Advances in Structural Engineering* 4 (4): 189–195.
- Menegotto M., and P. Pinto. 1973. "Method of Analysis for Cyclically Loaded Reinforced Concrete Plane Frames Including Changes in Geometry and Non-Elastic Behavior of Elements under Combined Normal Force and Bending." *Proceedings of IABSE Symposium of Resistance and Ultimate Deformability of Structures Acted on by Well Defined Repeated Loads*. International Association for Bridge and Structural Engineering, Zurich, Switzerland: 15–22.

- Michio, S. 1982. "Analysis of Elastic-Plastic Behavior of Steel Brace Subjected to Repeated Axial Force." *International Journal of Solids and Structures* 18 (3): 217–228.
- Mortezaei, A.R., and H.R. Ronagh. 2011. "Plastic Hinge Length of Reinforced Concrete Columns Subjected to Both Far-Fault and Near-Fault Ground Motions Having Forward Directivity." *The Structural Design of Tall and Special Buildings*.
- Ogata, T.O., and K. Osada. 1999. "Seismic Retrofitting of Expressway Bridges." *Cement and Composites* 19: 185–192.
- Okamoto, T.T., M. Tanigaki, M. Oda, and A. Asakura. 1994. "Shear Strengthening of Existing Reinforced Concrete Column by Winding with Aramid Fiber." *Proceedings of the 2nd US-Japan Workshop on Sesmic Retrofit of Bridge*. Berkeley, USA: Earthquake Enginnering Research Center, University of California.
- Park R., and T. Paulay. 1975. *Reinforced Concrete Structures*. USA: John Wiley and Sons.
- Park, R.K., D.C. Kent, and R.A. Sampson. 1972. "Reinforced Concrete Members with Cyclic Loading." *ASCE Journal of the Structural Division* 98 (ST7): 1341–1360.
- Park, R.P., M.J. Priestley, and W.D. Gill. 1982. "Ductility of Square-Confined Concrete Columns." *ASCE Journal of the Structural Division* 108 (ST4): 929–950.
- Paulay, T.P., and M.J.N. Priestley. 1992. *Seismic Design of Reinforced Concrete and Masonry Structures*. New York: John Wiley and Sons.
- Priestley, M.J. Nigel. 1996. *Seismic Design and Retrofit of Bridges*. New York: John Wiley and Sons.
- Priestley, M.J.N., and R. Park. 1987. "Strength and Ductility of Concrete Bridge Columns Under Seismic Loading." *ACI Structural Journal* 84 (1): 61–76.
- Ramberg W., and W.R. Osgood. 1943. *Description of Stress-Strain Curves by Three Parameters*. Technical Note No. 902, National Advisory Committee for Aeronautics. Washington, D.C.
- Richart, F.E., A. Brandtzaeg, and R.L. Brown. 1928. "A Study of the Failure of Concrete under Combined Compressive Stresses." *University of Illinois Engineering Experiment Station* 26 (12): 1–105.

- Riva, P.C., and M.Z. Cohn. 1990. "Engineering Approach to Nonlinear Analysis of Concrete Structures." *ASCE Journal of the the Structural Division* 116 (8): 2162–2186.
- Saatcioglu M., and S. Razvi. 1992. "Strength and Ductility of Confined Concrete." *ASCE Journal of Structural Engineering* 118 (6): 590–1607.
- Sakai, K.S., and S.A. Sheikh. 1989. "What Do We Know About Confinement in Reinforced Concrete Columns? A Critical Review of Previous Work and Code Provisions." *ACI Structural Journal* 86 (2): 192–207.
- Sakino, K., and Y.P. Sun. 1993. "Axial Behavior of Confined High Strength Concrete," *Proceedings of the Japan Concrete Institute* 15 (2): 713–718.
- Sawyer, Jr., H.A. 1965. "Design of Concrete Frames for two Failure Stages." *American Concrete Institute Special Publication* 12: 405–431.
- Sheikh, S.A., and S.M. Uzumeri. 1982. "Analytical Model for Concrete Confinement in Tied Columns." *ASCE Journal of Structural Engineering Division* 108 (ST12): 2703–2722.
- Sheikh, S.A., and S.S. Khoury. 1993. "Confined Concrete Columns with Stubs." *ACI Structural Journal* 90 (4): 414–431.
- Sheikh, S.A., D.V. Shah, and S.S. Khoury. 1994. "Confinement of High-Strength Concrete Columns." *ACI Structural Journal* 91 (1): 100–111.
- Spoelstra, M.R., and G. Monti. 1999. "FRP-Confined Concrete Model." *Journal of Composites for Construction* 3 (3): 143–150.
- Takiguchi, K.O., K. Okada, and M. Sakai. 1976. "Ductility Capacity of Bonded and Unbonded Reinforced Concrete Members." *Proceedings of the Architectural Institute of Japan* 249: 1–11.
- Unjoh, S., T. Terayama, Y. Adachi, and J. Hoshikuma. 1997. "Seismic Retrofit of Existing Highway Bridges in Japan." *Proceedings 29th Joint Meeting, U.S-Japan Panel on Wind and Seismic Effects, UJNR*: 61–178.
- Woisin, G. 1976. "The Collision Tests of the GKSS." In *Jahrbuch der Schiffbautechnischen Gesellschaft*, Vol. 70, Berlin, Germany, 465–487.
- Xiao Y., M.J.N. Priestley, and F. Seible. 1996. "Seismic Assessment and Retrofit of Bridge Column Footings." *ACI Structural Journal* 93 (1): 199–207.

Appendix A: KSU-RC Program

A.1 KSU-RC General Description

KSU-RC was initially developed as a tool to address the analytical needs of a research on the seismic behavior of bridge piers under various loading patterns (a PEER-NSF funded research program). It was initially called USC_RC and after some revisions and adding some features it was renamed KSU-RC. It is a Windows-based program that can handle two different systems, several major cross sections, any arrangement of longitudinal and lateral reinforcement, and any kind of steel behavior, as well as various models for unconfined and confined concrete monotonic or cyclic stress-strain relationship.

The application can analyze the moment-curvature response of a section as well as force-deflection response of a column under any load and displacement pattern, namely a variable axial load and a monotonic or cyclic curvature or lateral deflection/force.

The application can be downloaded at:

http://www.ce.ksu.edu/faculty/esmaeily/KSU_RC.htm. However, compatibility of the application with the latest Windows operating system, and additional features such as bi-axial analysis, more analytical models and methods and graphical interface for input/output data, will be available in the next version of the software.

A.2 Example

The ultimate flexural capacity of a section can be assessed using various methods. Code-based methods are too conservative compared to realistic assessment of the capacity using the latest material models, cyclic rules and analytical procedures.

For a given axial load, the closest value of a section flexural strength to its real value, is the maximum moment achieved during a complete moment-curvature analysis under that axial load.

Demanded loads dictated by any load combination are tied to the axial load necessary to calculate the section flexural capacity. Therefore, for the columns of the representative bridges, a thorough analysis has been performed to find the axial load level, in addition to other demanded forces, as detailed in Chapter 3; and the section capacity is then evaluated using KSU-RC.

Detailed process and values can be found in Chapter 3.

Columns of the representative Bridges No. 1 and No. 2 were analyzed for their actual flexural moment and displacement capacity using KSU-RC.

Following are the steps to calculate the ultimate flexural capacity of each column:

1. Entering the geometrical and material properties of the column. Figure A.1 shows the geometrical properties as well as material properties of bridge piers in Bridge No. 1 and Bridge No. 2.

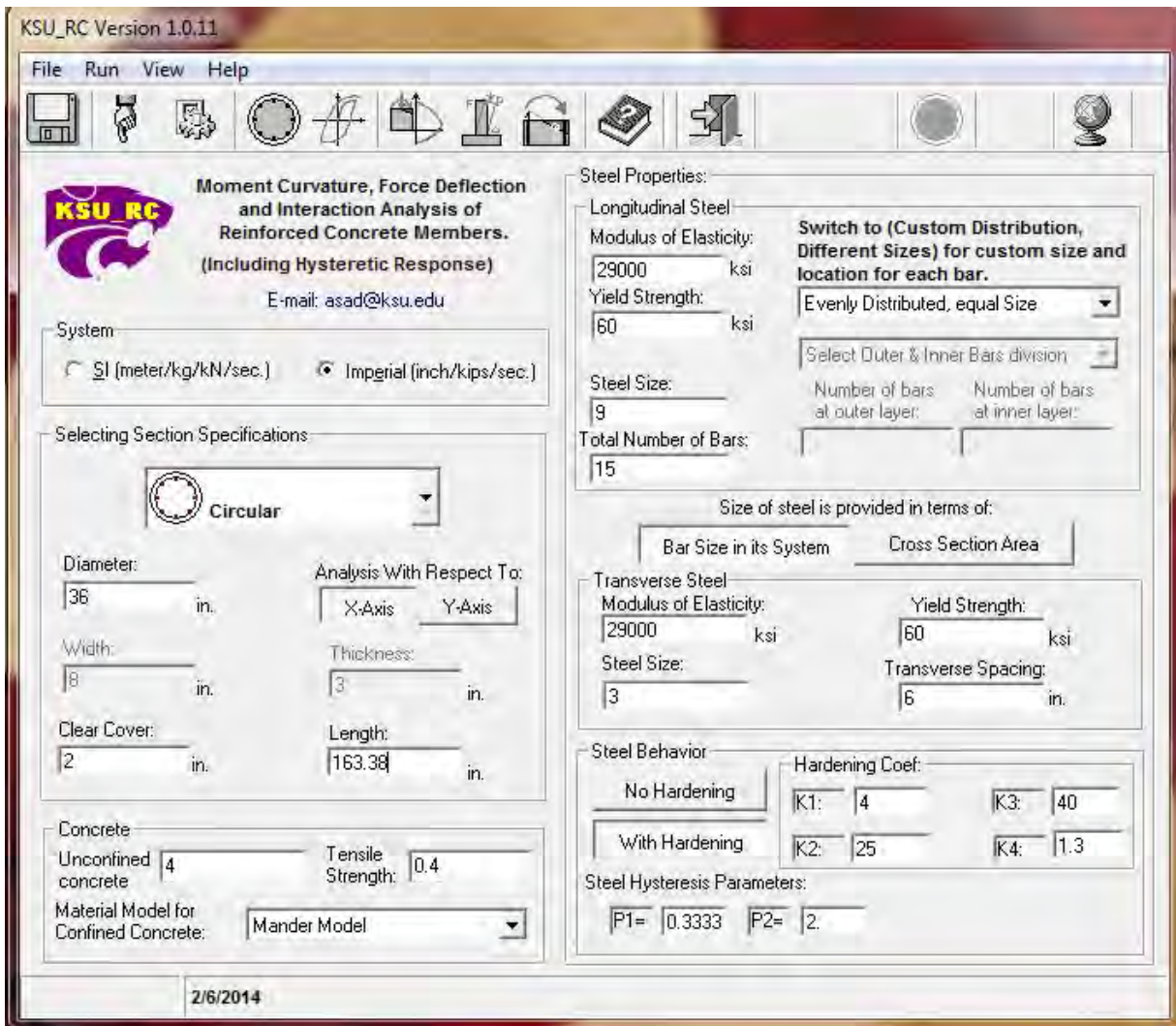


FIGURE A.1
Window Interface for Entering the Main Input Data

As a demonstrative example, the geometrical and material properties of Column No.1 in Bridge No. 2 have been used. The longitudinal steel bars can be distributed evenly or customized by choosing the desired option on the right top corner of the main window. The steel bars for Column No. 1 of Bridge No.2 are evenly distributed as shown in Figure A.2.

The input data file for this example saved by KSU-RC is as follows:

```
Date: Thursday, February-6 Year:2014 (2/6/2014 )
Time:2:50:21 PM
The Input Data for the Moment Curvature/Force Deflection Analysis
-----
Unit system was selected to be English. (pound, in.)
So, the data is in ksi, kips, and in.

GEOMETRY OF THE CASE:
Circular
-----
Diameter=36
Clear Cover Thickness=2
Length (In case of a Force-Deflection Analysis)=163.38

CONCRETE:
-----
Unconfined Concrete Strength=4
Unconfined Concrete Tensile Strength=0.4

LONGITUDINAL STEEL:
-----
Yield Strength=60
Modulus of Elasticity=29000
KSU-RC Steel Coefficients:
-----
With strain hardening
K1=4
K2=25
K3=40
K4=1.3
KSU-RC Steel Hysteresis Parameters:
-----
P1=0.333333
P2=2.
Bar Size will be in terms of number in the system.

Number of Rebars=15
Evenly distributed on the section
```

Location of the Rebars (With respect to the centroid of the section):

Bar	X Coordinate	Y Coordinate	Size
1	6.1265	13.7603	9.
2	11.1936	10.0788	9.
3	14.3253	4.6546	9.
4	14.98	-1.5745	9.
5	13.0445	-7.5313	9.
6	8.8535	-12.1858	9.
7	3.1317	-14.7333	9.
8	-3.1317	-14.7333	9.
9	-8.8535	-12.1858	9.
10	-13.0445	-7.5312	9.
11	-14.98	-1.5745	9.
12	-14.3253	4.6546	9.
13	-11.1936	10.0788	9.
14	-6.1265	13.7603	9.
15	0.	15.0625	9.

TRANSVERSE REINFORCEMENT:

Transverse steel Yield Strength=60
Transverse steel Modulus of Elasticity=29000
Steel Size (Number in the system)=3
Transverse steel spacing=6

2. The moment-curvature analysis is the required analysis to calculate the maximum flexural capacity of the concrete column under a specific axial force. The axial force is the nominal a required axial force which is calculated based on each load combination.

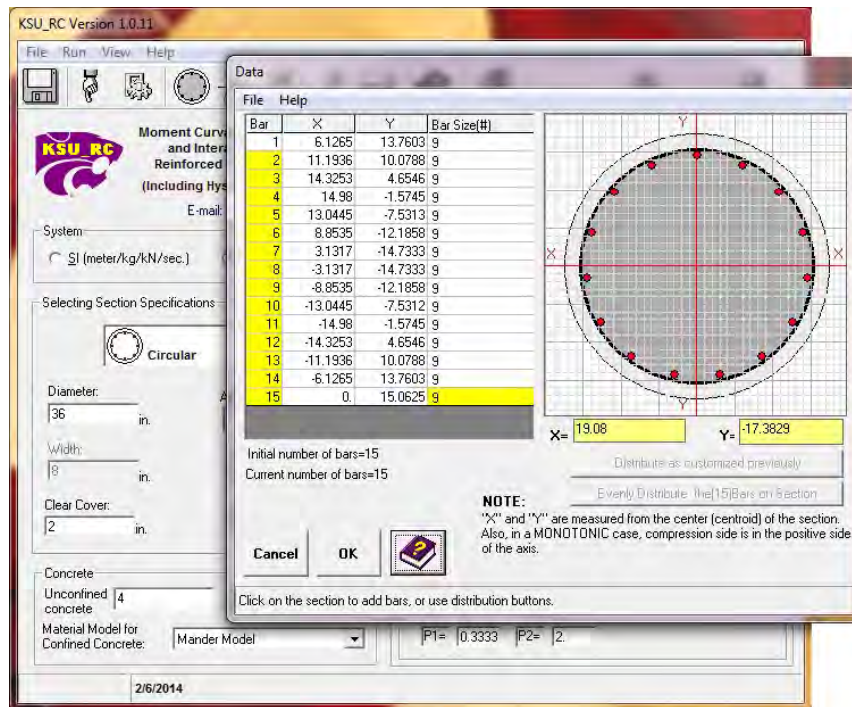


FIGURE A.2
Longitudinal Steel Bars Distribution in KSU-RC

The moment-curvature analysis used different cyclic and monotonic material models. The monotonic model for confined concrete can be selected as shown in Figure A.3. The flexural capacity of all columns has been calculated using Mander et al.'s model (1988). The cyclic behavior of longitudinal steel bars, as an example of steel, confined concrete and unconfined concrete hysteresis response is shown in Figure A.4.

TABLE A.1
Geometrical and Material Properties of Bridge Piers at Bridge No. 1 and Bridge No. 2

Properties	Bridge 1 (2009)	Bridge 2 (2004)
Compressive Strength of Concrete (ksi)	4.0	4.0
Steel Yield Strength (ksi)	60.0	60.0
Longitudinal Reinforcement	12 No. 9	15 No. 9
Lateral Reinforcement	No. 4 @ 6 in.	No. 3 @ 6 in.
Section Diameter	36.0 in.	36.0 in.
Clear Cover	2.0 in.	2.0 in.
Column Height (ft)	34, 36, 31	13.615

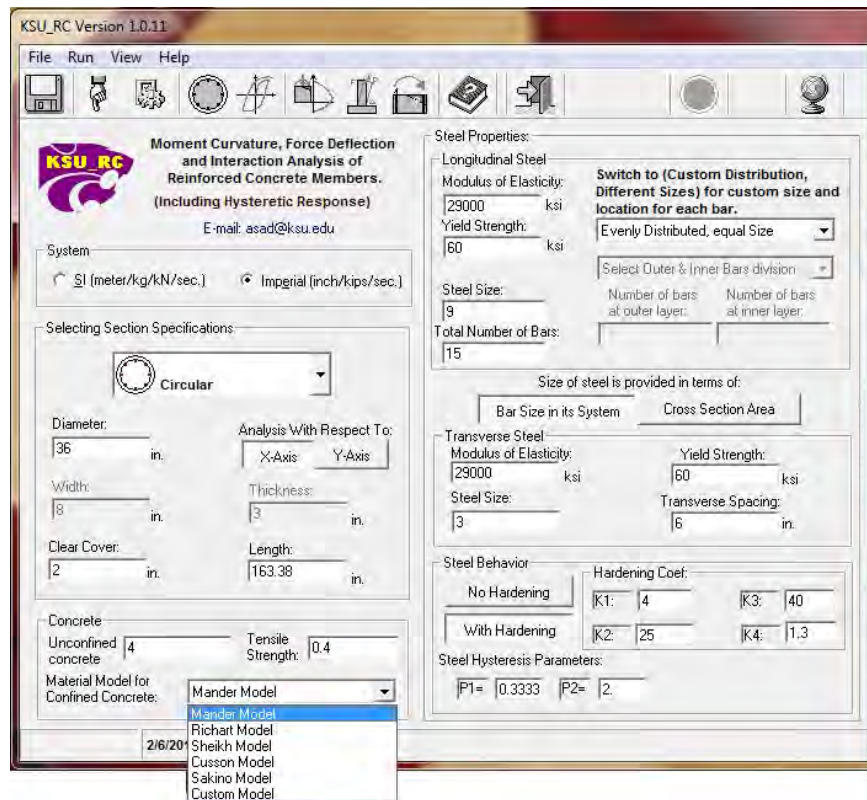


FIGURE A.3
Different Monotonic Model for Confined Concrete at KSU-RC

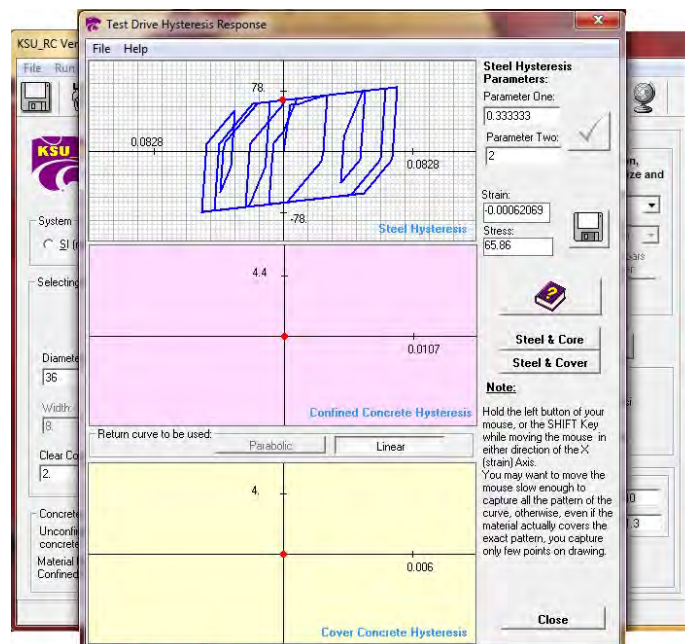


FIGURE A.4
A Sample of Cyclic Behavior of Longitudinal Steel Bars in KSU-RC

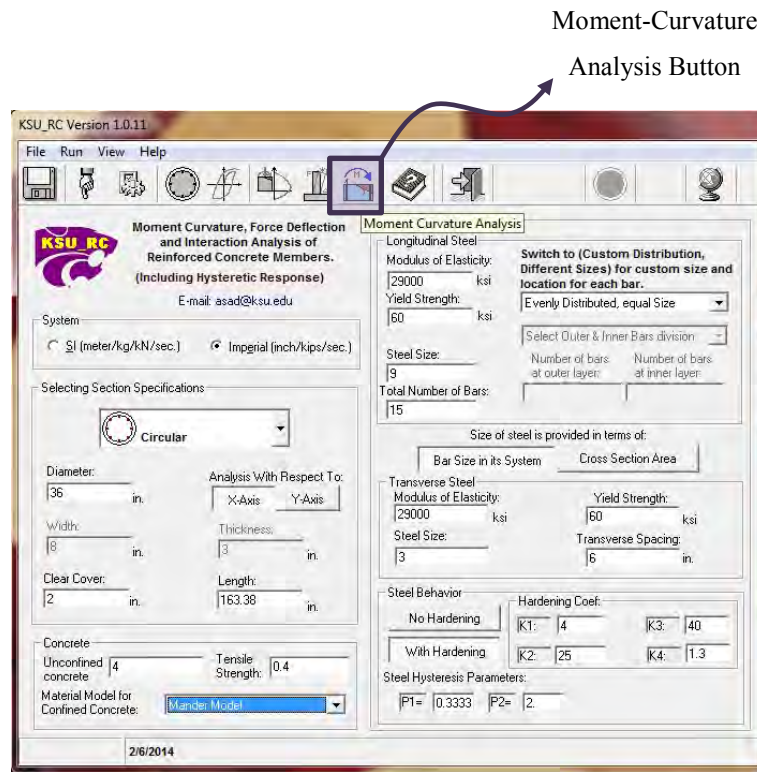


FIGURE A.5
Moment-Curvature Analysis Button at KSU-RC

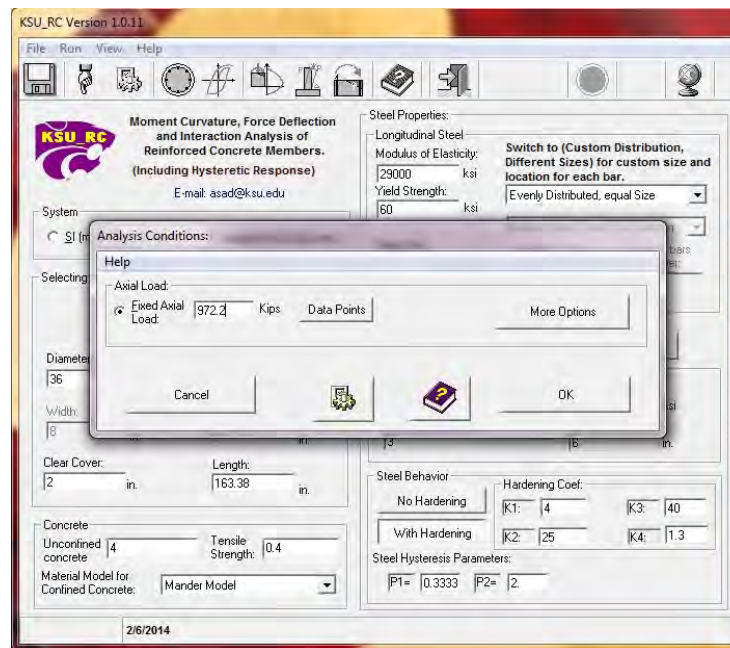


FIGURE A.6
Moment-Curvature Analysis Condition Window

In order to calculate the capacity of the section under static loads, the “Fixed Axial Load” radio-button should be chosen. The value of the axial load from each load combination should be entered in the textbox of “Analytical Condition” window. As shown in Figure A.7, the number of data points can be set using “Data Points” button at the “Analytical Condition” window. The axial force which is shown in Figure A.6 is related to Column No. 1 in Bridge No. 2 under “Min DL case I LL” load combination. As explained in Chapter 3, the demanded axial forces (P_u) and flexural moments for all columns have been calculated using various load combinations. The demanded axial force for Column No.1 in Bridge No.2 under load combination “Min DL case I LL” is 803.1 kips. Considering $P_u = \phi P_n$ and $M_u = \phi M_n$ the depth of neutral axis and reduction factor are calculated for each column under each load combination. For Column No. 1 in Bridge No. 2, $P_n = 972.2$ kips.

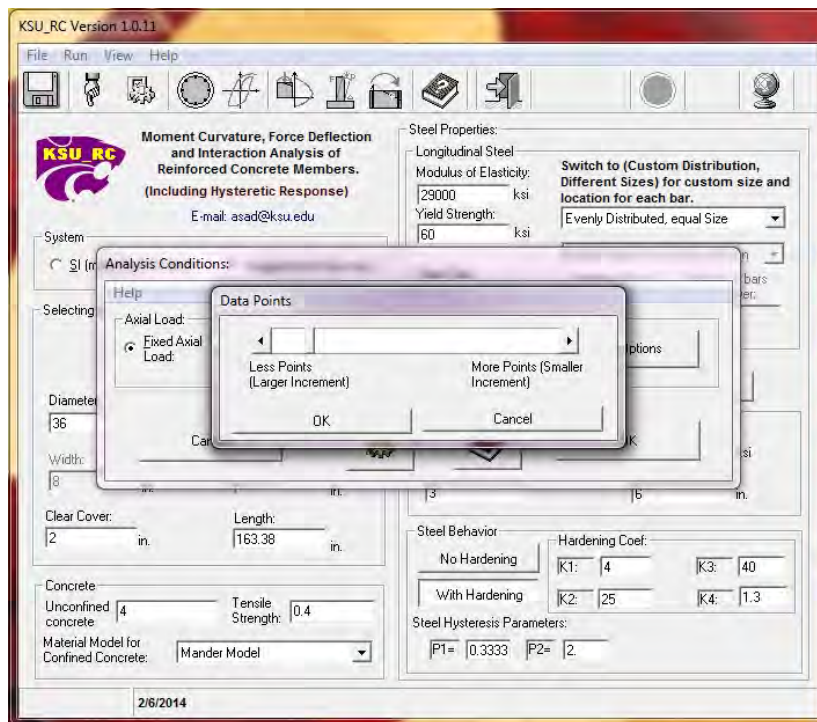


FIGURE A.7
Setting the Density of Ddata Points at Moment-Curvature
Analysis Graph



FIGURE A.8
Axial Force Setting

If the axial load is not constant, the moment-curvature analysis can be done using the variable axial load. The variable axial load can be non-proportional or proportional to flexural moment. All these options and settings can be reached using “More Option” button.

For non-proportional axial force, the axial force versus curvature should be provided in a text file; and for proportional axial force the ratio should be entered in the related textbox.

1. By pressing the “OK” button the moment-curvature analysis graph as shown in Figure A.9.

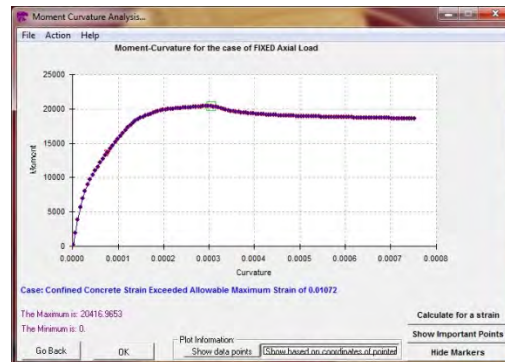


FIGURE A.9
Moment-Curvature Graph in KSU-RC

- The details of each point in this graph can be gotten by pressing the “Show data points” button at the bottom of this page. The point with maximum moment is the interested point in this graph. The information about this point is listed at the bottom of “Moment Curvature Analysis” window. The calculated flexural moment is the maximum nominal capacity of the concrete column.

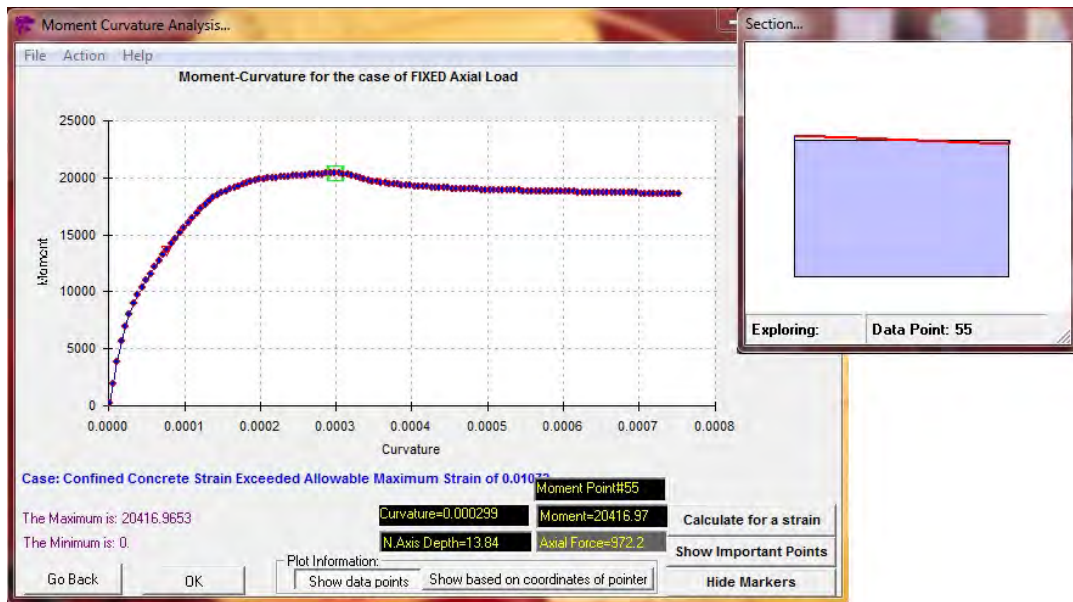


FIGURE A.10
Moment-Curvature Maximum Point Information

- To save the information about all points including the maximum point of moment-curvature graph, at the tool bar of “File”, one of the two “Save” options can be selected as shown in Figure A.11.

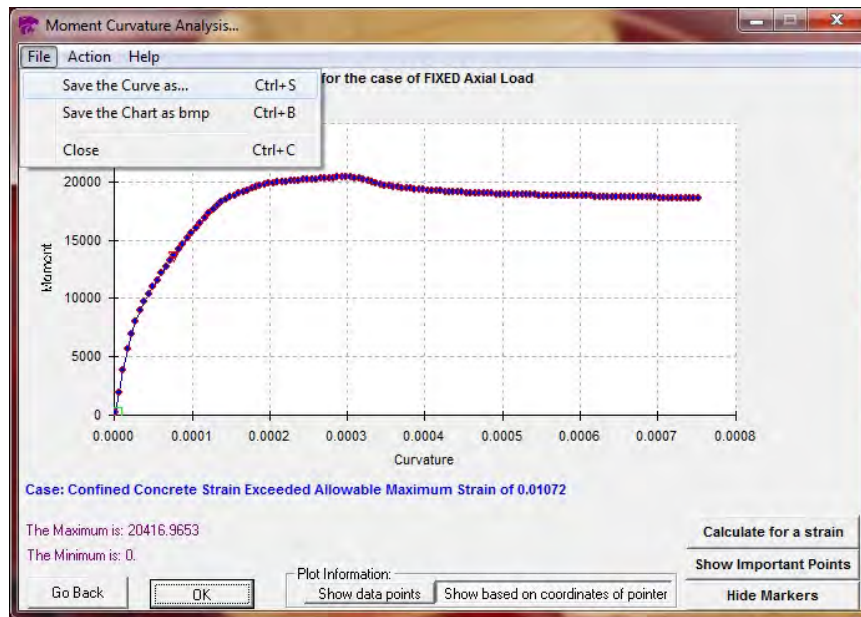


FIGURE A.11
Creating the Text File of Moment-Curvature Analysis Result

The output data for moment-curvature analysis for aforesaid column is as follows:

Date: Thursday, February-6 Year:2014 (2/6/2014)
Time: 3:25:34 PM
The Resulted Moment-Curvature Data
For the case when:
The Axial Load is Constant and equal to: 972.2
and curvature is applied MONOTONICALLY.
Steel Yield Strain: 0.00206897
Cover Concrete Strain at Pick Strength: 4.
Confined Concrete Strength: 4.396
Confined Concrete Strain at Pick Strength: 0.00314094
Confined Concrete Ultimate Strain: 0.01061
Number of data points: 160

CURVATURE	MOMENT	N.AXIS	C. STRAIN	S. STRAIN	AXIAL LOAD	Allowable Input
0.00000047	161.740	510.594	0.000239	0.000223	972. 972.2	
0.00000468	1616.33	67.3300	0.000315	0.000156	972. 972.2	
.....						
.....						
0.00029990	20416.97	13.844	0.004085	-0.005941	972. 972.2	
.....						
.....						
0.00073022	18584.02	14.301	0.010443	-0.014385	972. 972.2	
0.00073490	18579.48	14.303	0.010511	-0.014476	972. 972.2	
0.00073958	18575.59	14.305	0.010580	-0.014566	972. 972.2	
0.00074427	18570.48	14.309	0.010650	-0.014655	972. 972.2	

Appendix B: Representative Bridges

The following tables show the information of the two representative bridges. The first table belongs to Bridge No. 1 for which some of the data is shown as follows:

TABLE B.1

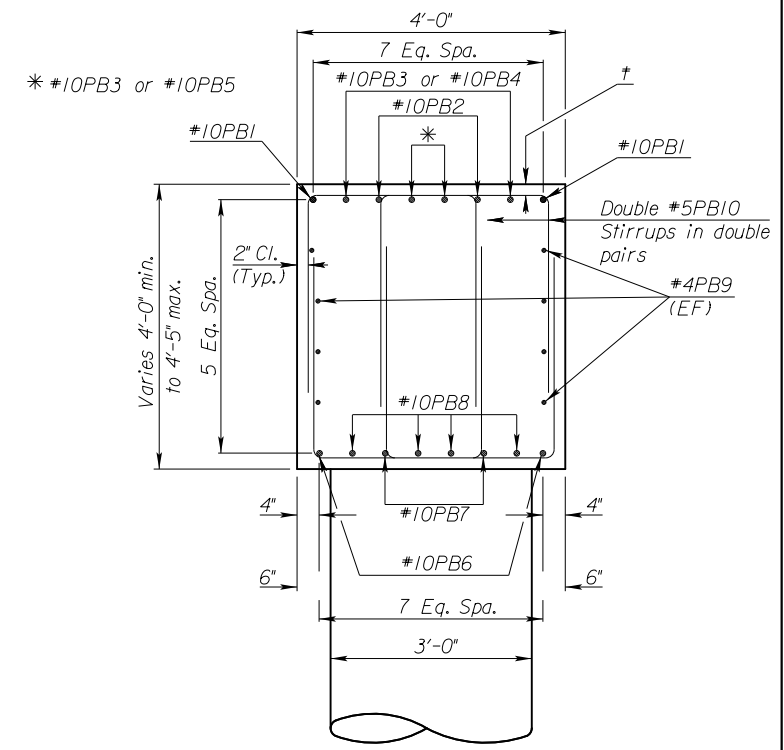
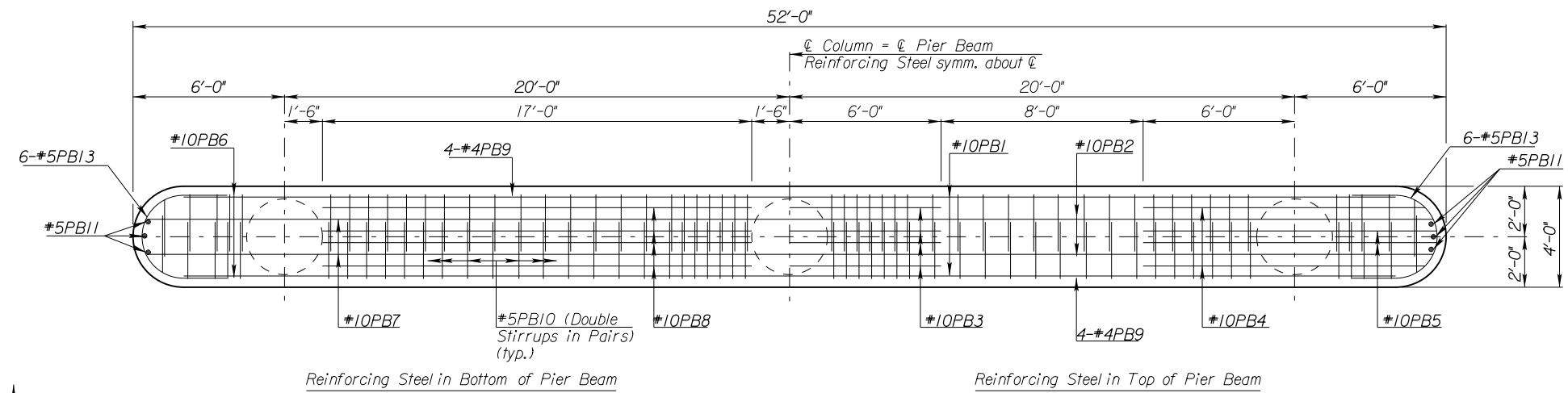
Properties	Bridge 1 (2009)
Compressive Strength of Concrete (ksi)	4.0
Steel Yield Strength (ksi)	60.0
Longitudinal Reinforcement	12 No. 9
Lateral Reinforcement	No. 4 @ 6 in.
Section Diameter	36.0 in.
Clear Cover	2.0 in.
Column Height (ft)	34, 36,31

The remaining table belongs to Bridge No. 2 for which some of the data is shown as follows:

TABLE B.2

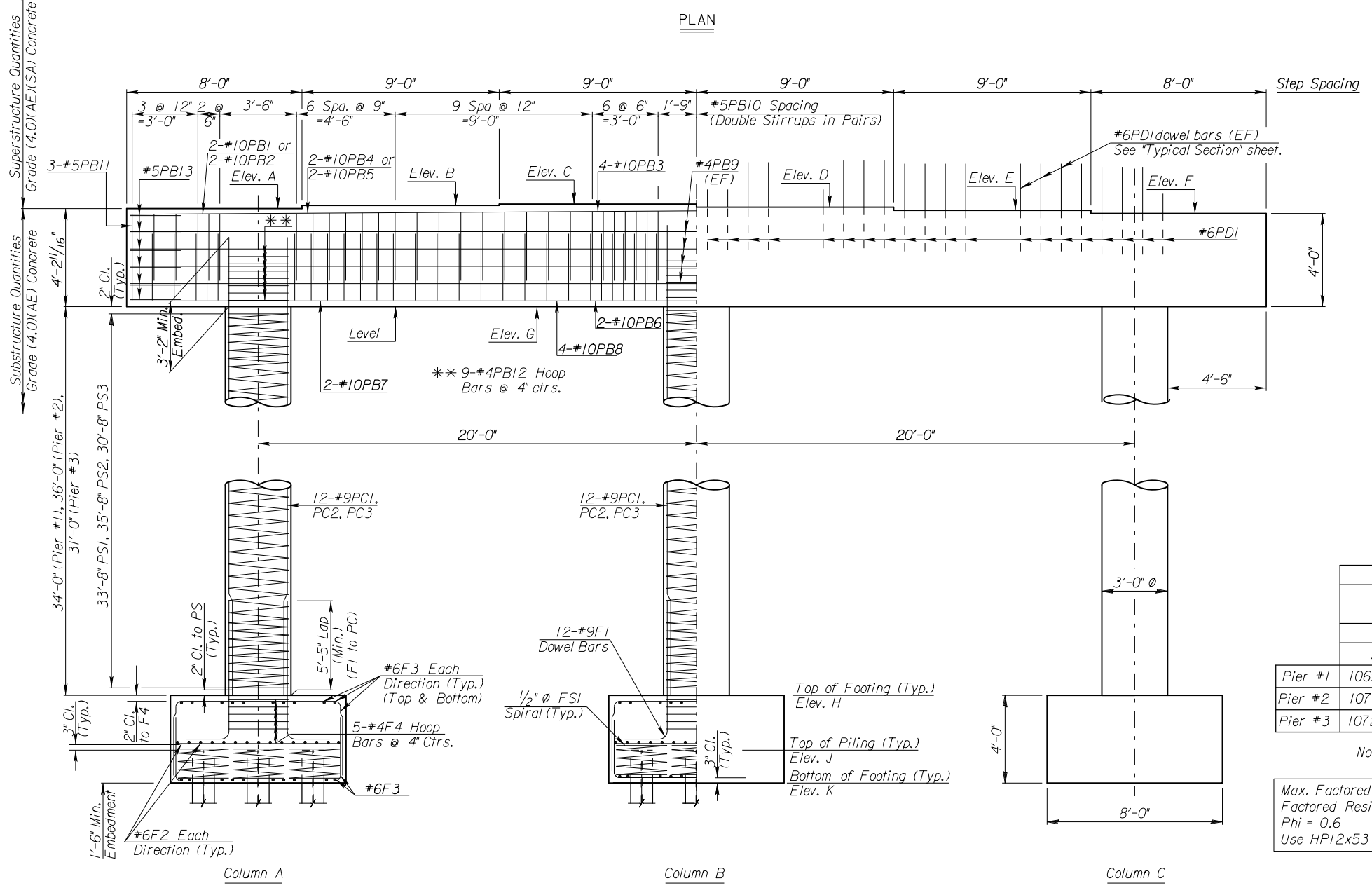
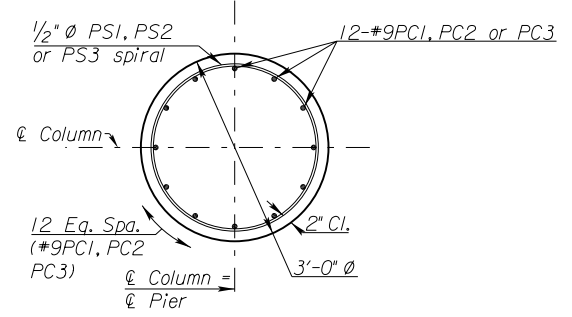
Properties	Bridge 2 (2004)
Compressive Strength of Concrete (ksi)	4.0
Steel Yield Strength (ksi)	60.0
Longitudinal Reinforcement	15 No. 9
Lateral Reinforcement	No. 3 @ 6 in.
Section Diameter	36.0 in.
Clear Cover	2.0 in.
Column Height (ft)	13.615

STATE	PROJECT NO.	YEAR	SHEET NO.	TOTAL SHEETS
KANSAS	18-81KA-0410-03	2009	540	1707



SECTION THROUGH PIER BEAM

† Clearance to top stirrup varies from a minimum of 2"



PIER ELEVATION

	Top of Pier Beam Steps						Bottom of Pier Beam	Top of Footing	Top of Piling	Bottom of Footing
	A	B	C	D	E	F				
Pier #1	1069.69	1069.83	1069.89	1069.75	1069.61	1069.46	1065.46	1031.46	1028.96	1027.46
Pier #2	1071.35	1071.49	1071.55	1071.41	1071.27	1071.12	1067.12	1031.12	1028.62	1027.12
Pier #3	1072.88	1073.03	1073.09	1072.95	1072.80	1072.66	1068.66	1037.66	1035.16	1033.66

Note: "I" intentionally skipped in labeling sequence.

Max. Factored Design Pile Load (Strength I) = 111 tons
 Factored Resistance of Pile = 125 tons
 Phi = 0.6
 Use HPI2x53 GR. 50 Steel Piles

NO.	DATE	REVISIONS	BY	APP'D
3				
2				
1				

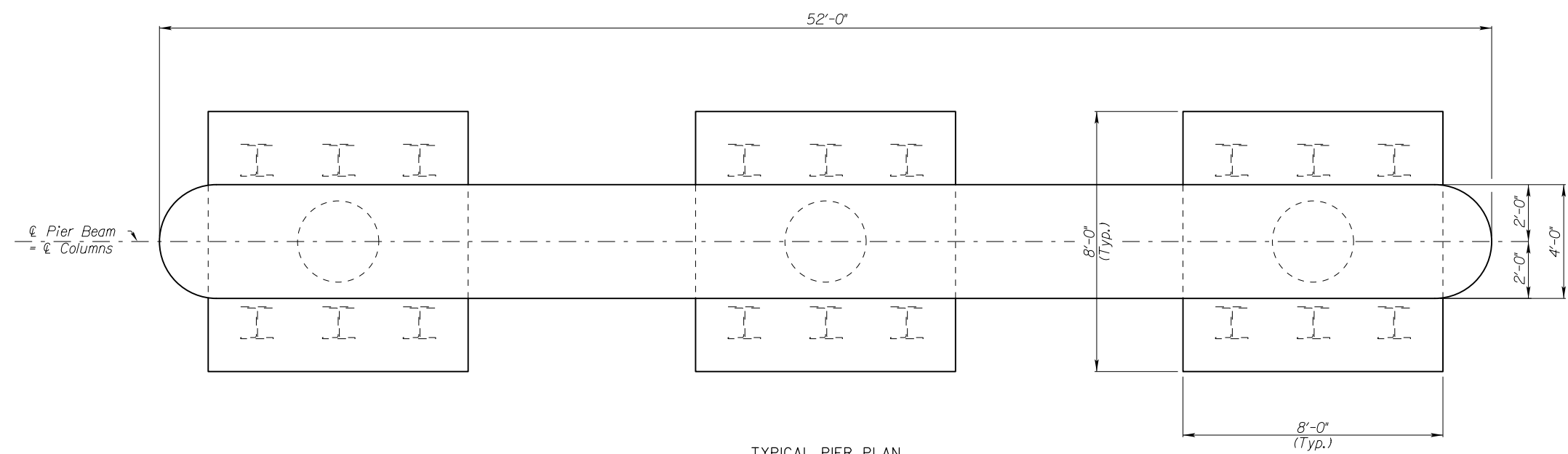
KANSAS DEPARTMENT OF TRANSPORTATION
 Br. No. 18-81-02.35 (070) EB Sta. 124+21.00
 PIER DETAILS

DESIGNED	CEM DETAILED	BLB QUANTITIES	CEM/CADD	BLB
DESIGN CK.	JSR DETAIL CK.	JSR QUAN. CK.	CADD CK.	

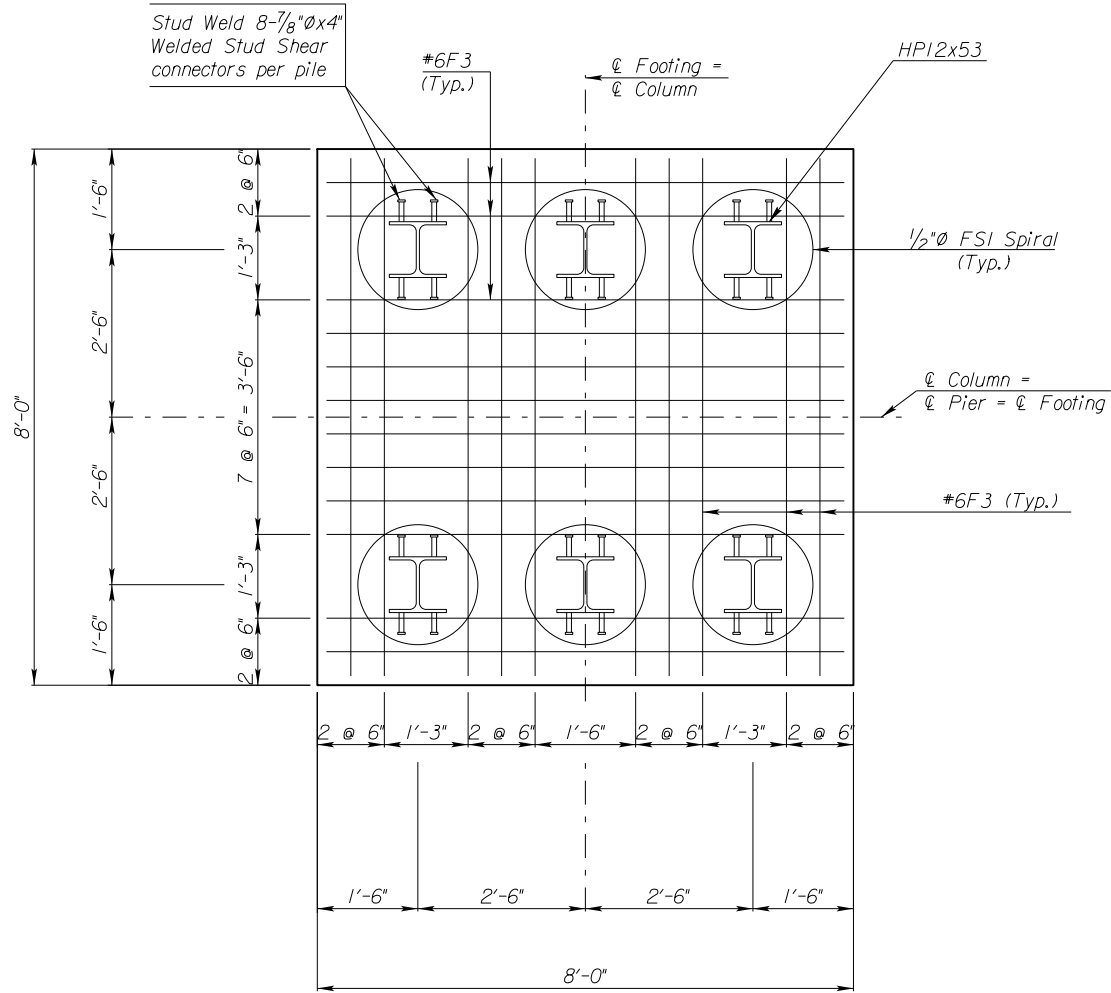
LEGEND
 EF = Each Face

Plotted By: Iruby
 Plot Location: Bridge Design
 File: 041003-070-09.dgn (041003-070-09)
 Plot Date: 14-FEB-2012 08:53

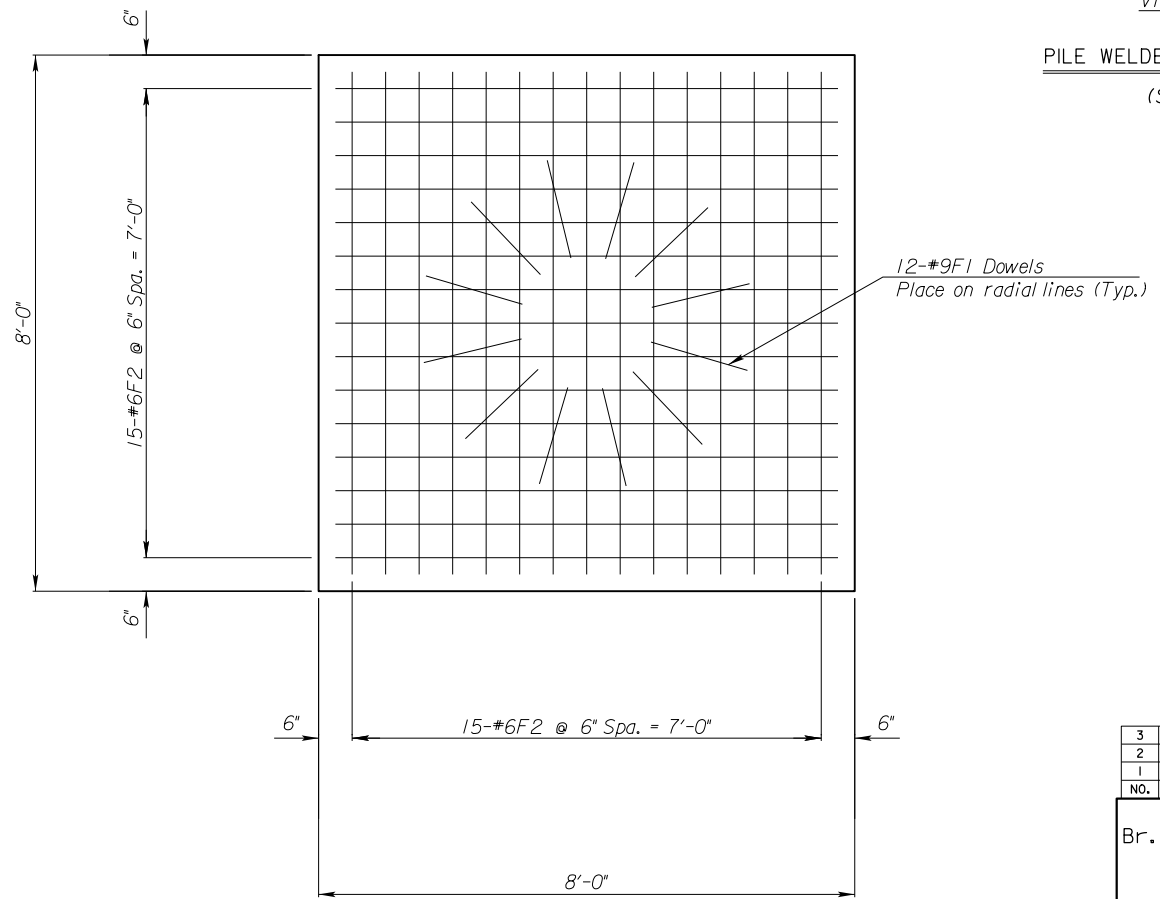
STATE	PROJECT NO.	YEAR	SHEET NO.	TOTAL SHEETS
KANSAS	18-81KA-0410-03	2009	541	1707



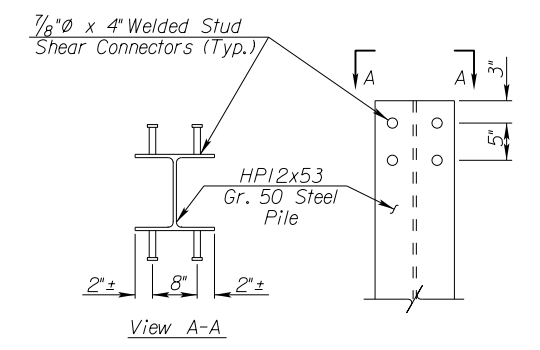
TYPICAL PIER PLAN



FOOTING PLAN
(Top & Bottom layer of reinforcing)



FOOTING REINFORCING PLAN
(Middle layer)



PILE WELDED STUD SHEAR CONNECTOR DETAIL
(Subsidiary to "Piles (Steel)")

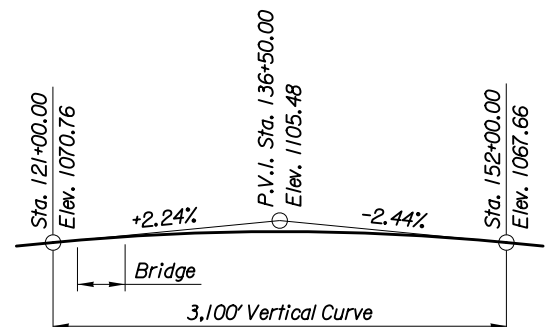
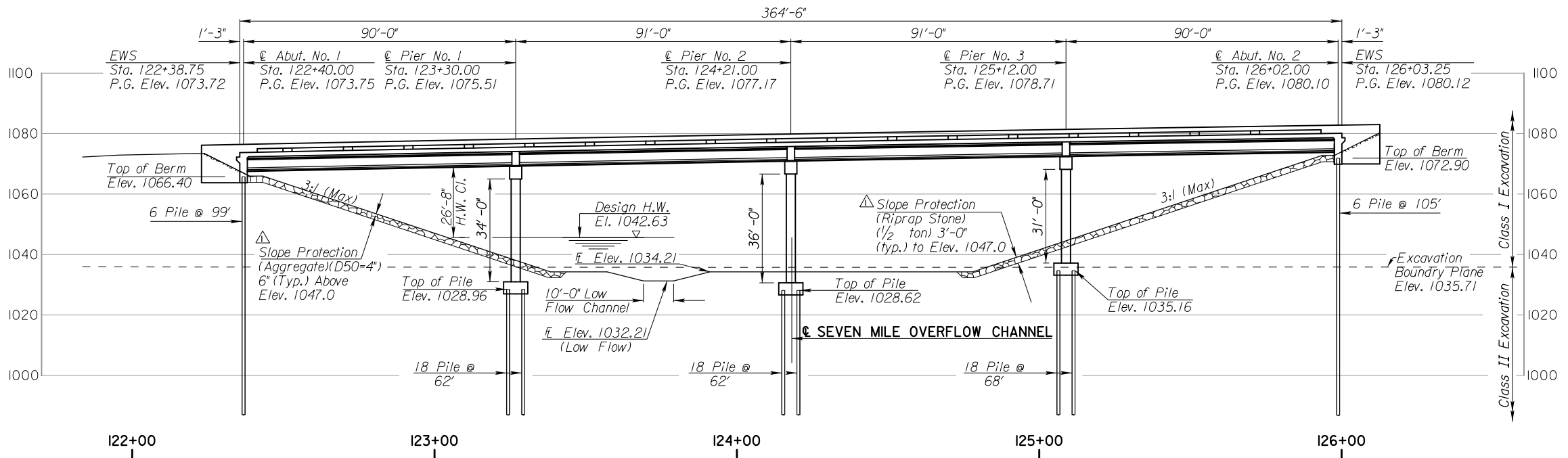
Plotted By: /rudy
 Plot Location: Bridge Design
 File: 041003-070-10.dgn 1041003-070-10
 Plot Date: 14-FEB-2012 08:53

3				
2				
1				
NO.	DATE	REVISIONS	BY	APP'D
KANSAS DEPARTMENT OF TRANSPORTATION Br. No. 18-81-2.35 (070) EB Sta. 124+21.00 AUXILIARY PIER DETAILS Proj. No. 18-81KA-0410-03 Riley Co.				
SHEET NO.	OF	SCALE	APP'D	
DESIGNED	CEM	DETAILED	BLB	QUANTITIES
DESIGN CK.	JSR	DETAIL CK.	JSR	QUAN. CK.
			CEM	CADD
				CADD CK.



STATE	PROJECT NO.	YEAR	SHEET NO.	TOTAL SHEETS
KANSAS	18-81 KA-0410-03	2009	535	1707

Revised Plans



**PROFILE GRADE
PROPOSED IMPROVEMENT**

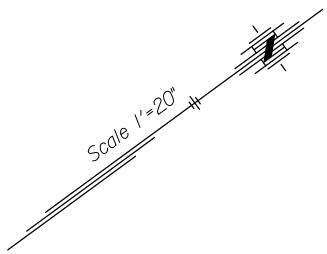
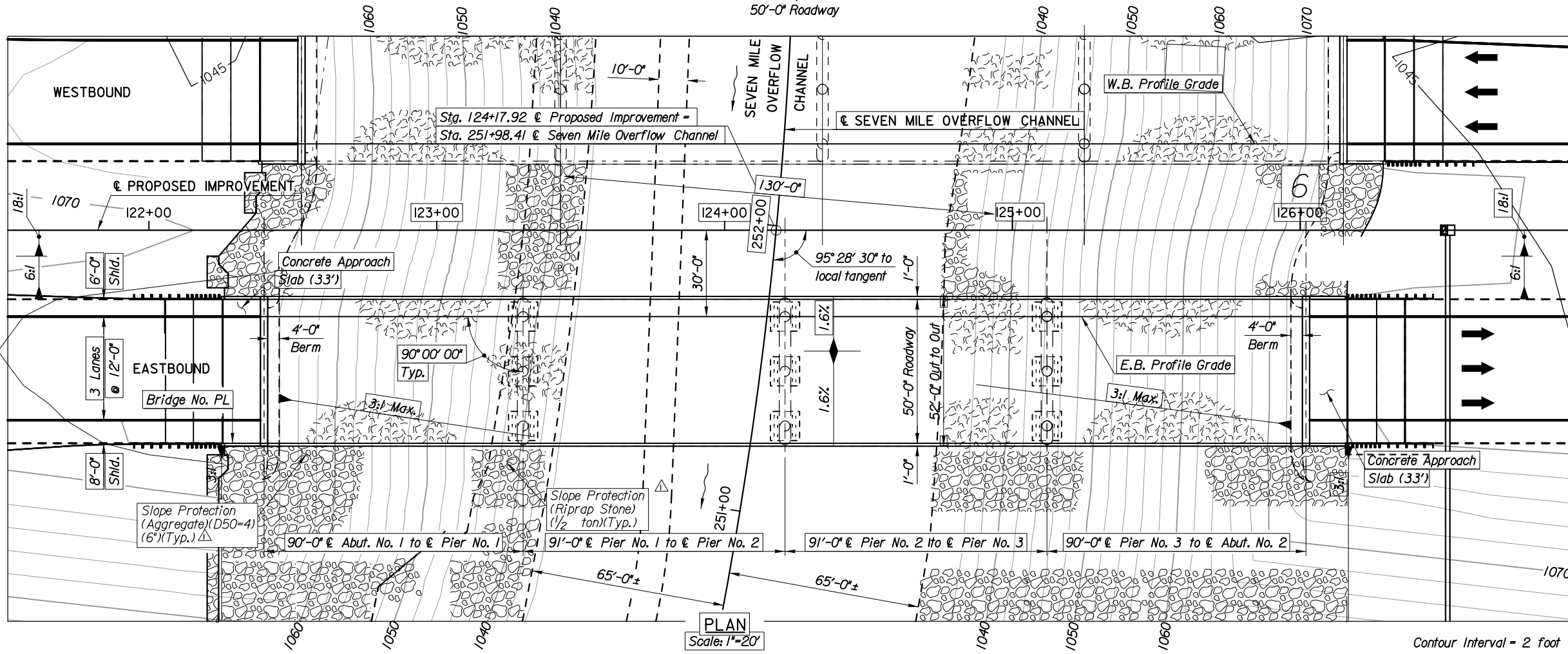
Profile Grade is located 30' left and right of \mathcal{C} Proposed Improvement.

B.M. #15: \square cut top N. end RCP under E. Bd. lanes K-18 Hwy, 1,266.61' Lt. \mathcal{C} Sta. 135+95.34 Elev. 1129.53

ELEVATION

Scale: 1"=20'
90'-91'-91'-90' Prestressed Concrete Beam Spans (PBMC)
Pile Bent Abutments, Column Bent Piers
50'-0" Roadway

B.M. #16: \square cut top E. end 24" RCP at asphalt turnaround 819.04' Lt. \mathcal{C} Sta. 142+89.03 Elev. 1109.15



Plotted By: Iruby
 Plot Location: Bridge Design
 File: 041003-070-04.dgn (041003-070-04)
 Plot Date: 06-MAR-2012 13:37

NO.	DATE	REVISIONS	BY	APP'D
3				
2				
1	7/30/10	Defined Limits of Slope Protection	CEM	TLF

KANSAS DEPARTMENT OF TRANSPORTATION
 Br. No. 18-81-2.35 (070) EB Sta. 124+21.00
CONSTRUCTION LAYOUT
 K-18 over Seven Mile of Channel
 Proj. No. 18-81 KA-0410-03 Riley Co.

SHEET NO.	OF	SCALE	APP'D
DESIGNED	CEM	DETAILED	BLB
DESIGN CK.	JSR	DETAIL CK.	JSR
QUANTITIES	CEM	CADD	BLB
QUAN. CK.	JSR	CADD CK.	JSR

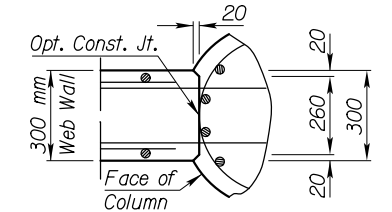
STATE	PROJECT NO.	YEAR	SHEET NO.	TOTAL SHEETS
KANSAS	75-16 K-7389-01	2004	56	237

Dimension	Pier #1	Pier #2	Pier #3	Pier #4
K	15 100	16 000	16 600	17 700
L	14 950	15 850	16 450	17 550
M	2 747	3 099	3 182	3 201
N	7 837	8 129	9 002	10 311
P	1 500	1 500	1 502	1 521
Q	1 536	1 517	1 500	1 500

Location	Pier #1	Pier #2	Pier #3	Pier #4
A	313.709	313.668	313.738	313.919
B	313.748	313.712	313.787	313.972
C	313.787	313.756	313.835	314.025
D	313.730	313.704	313.788	313.982
E	313.673	313.651	313.740	313.939
F	312.173	312.151	312.238	312.419
G	308.023	308.001	308.088	308.269
H	300.760	300.130	300.490	300.880
J	292.923	292.001	291.488	290.569

Dim. "0" not used.

Elev. "I" not used

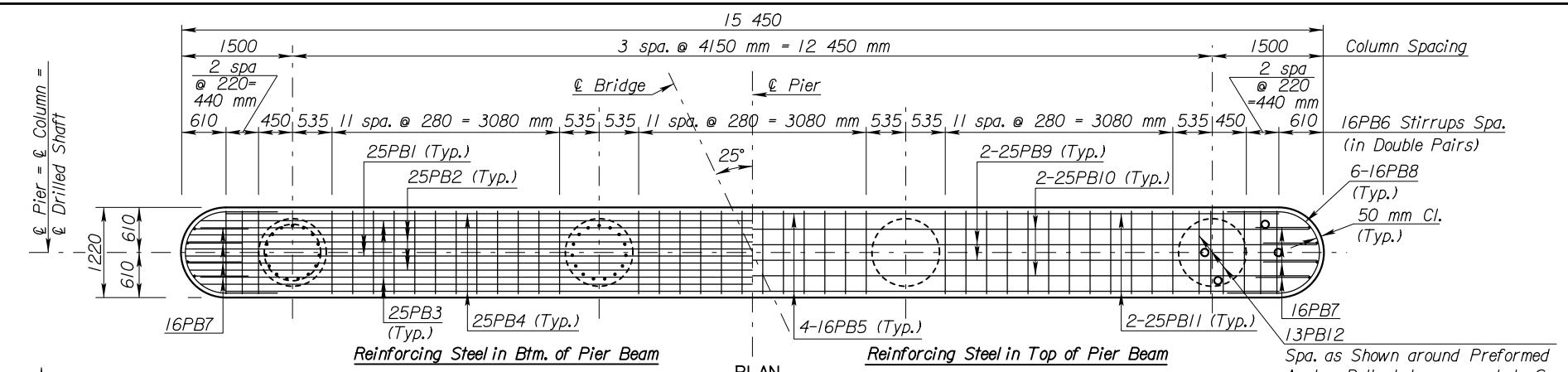


WEB WALL CONSTRUCTION JOINT DETAIL

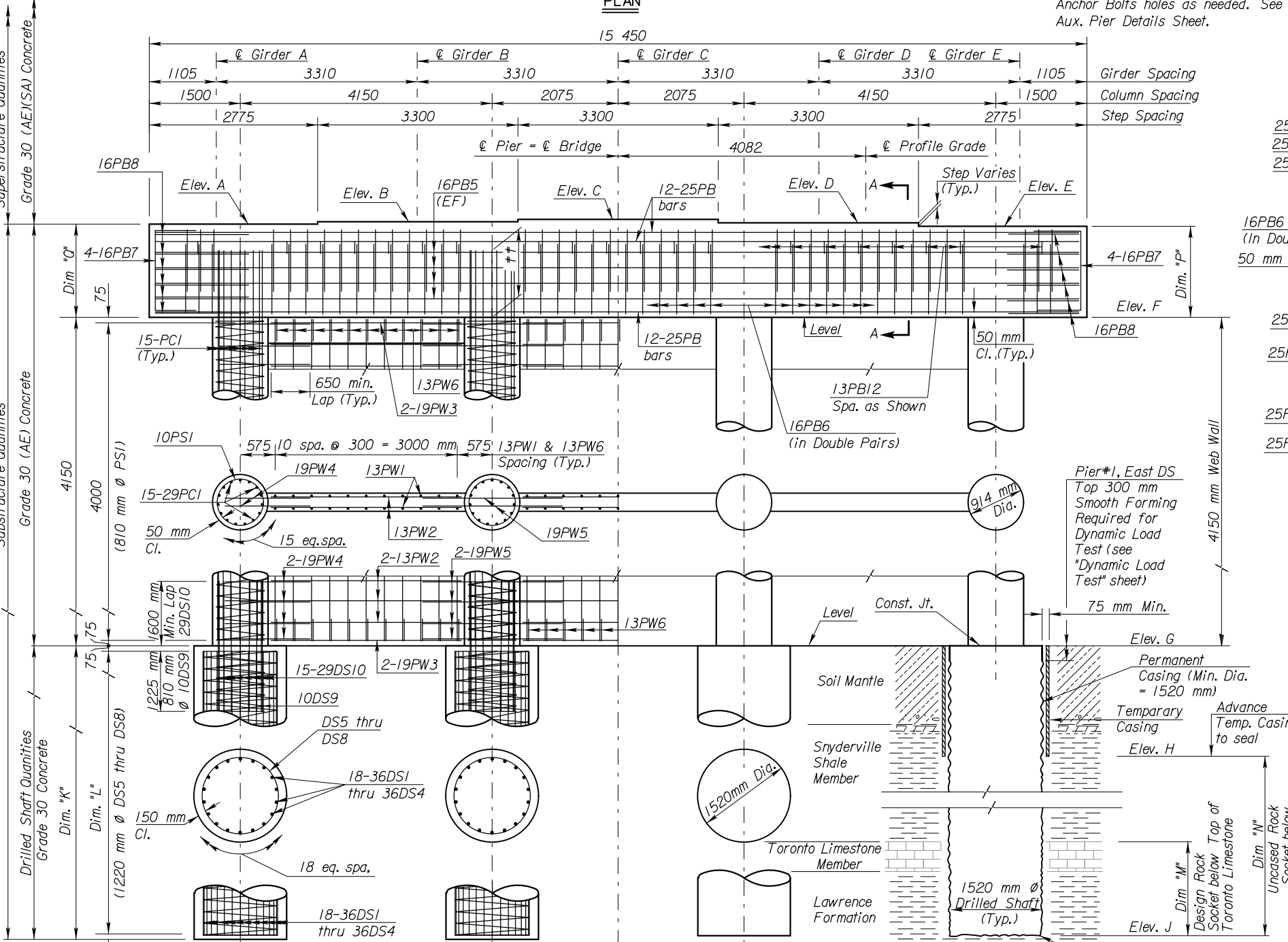
LEGEND

1100 mm Min. Embed. Length.

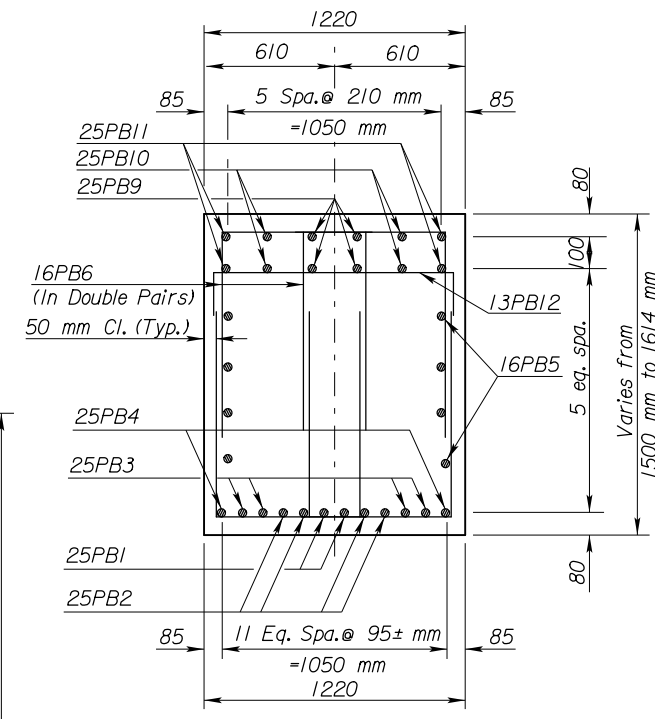
Note: Either cast the columns and pier web monolithically or cast the columns separately using a keyed joint as shown in Detail A. If the columns are cast separately, use threaded deformed bars in lieu of the PW4 and PW5 dowel bars. Bar diameter and embedment length into the web wall shall be as designated. The inserts shall develop the full yield strength of the bars. No change in compensation is allowed with the use of inserts. Coil inserts are not allowed.



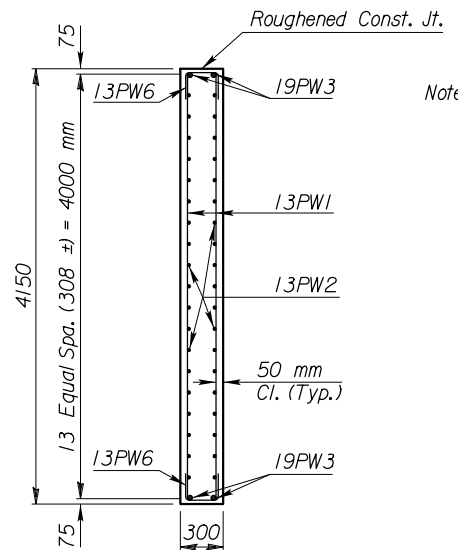
PLAN



ELEVATION



SECTION A-A



SECTION THRU WEB WALL

TYPICAL DRILLED SHAFT

Bottom of the rock socket shall be clean and relatively flat.

Plotted By: Jruby
 File: 738901-059-16.dgn (738901-059-16)
 Plot Date: 14-FEB-2012 09:17

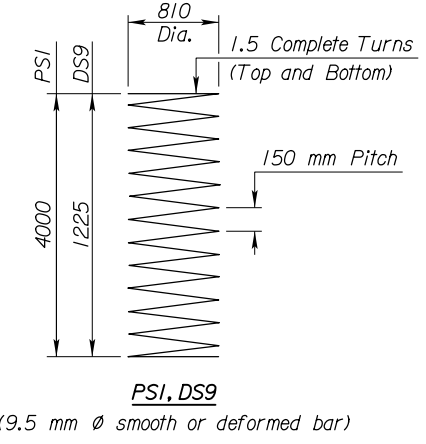
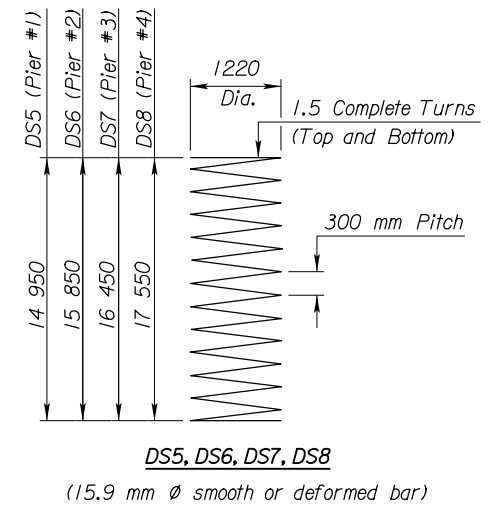
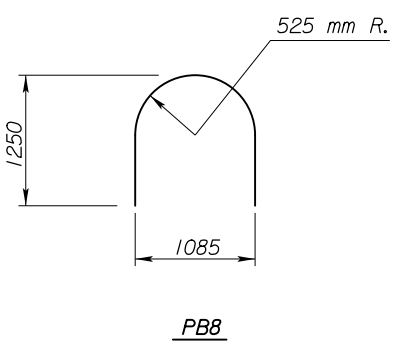
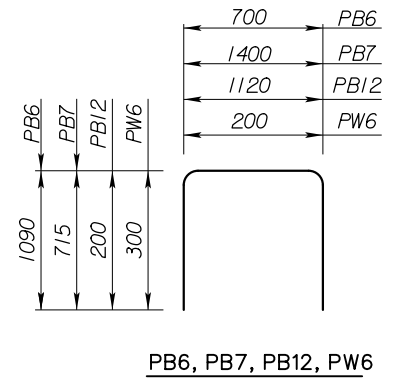
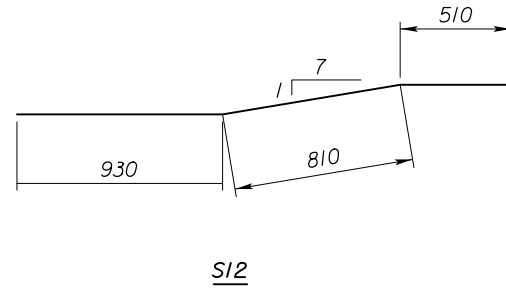
NO.	DATE	REVISIONS	BY	APP'D
3				
2				
1				

KANSAS DEPARTMENT OF TRANSPORTATION
 Br. No. 75-16-12.66(059) Sta. 10+471.000

PIER DETAILS
 US-75 over Neosho River

Proj. No. 75-16 K-7389-01 Coffey Co.

SHEET NO. 16 OF 40 SCALE: AS SHOWN
 DESIGNED: JSR DETAILED: JSR QUANTITIES: JSR CADD: JSR
 DESIGN CK: SGB DETAIL CK: JDK QUAN. CK: AAA CADD CK: JDK



BILL OF REINFORCING STEEL Epoxy Coated Grade 420							
Straight Bars				Bent Bars			
Mark	Size	Number	Length	Mark	Size	Number	Length
A26	19	192	2 300	R1	22	68	4 930
A29	19	48	2 000	R2	22	4	2 750
A47	19	56	4 350	R3	22	1440	2 310
R11	19	24	3 610				
R12	19	1044	2 890	A33	19	4	3 510
R13	19	24	2 750				
SI	19	1330	15 330	A34	16	86	1 010
S4	19	165	6080	A41	16	8	4 400
S5	19	66	14 620	A45	16	48	960
S6	19	516	18 280	R5	16	8	1 990
S7	19	240	16 730	R6	16	8	3 250
S8	19	240	12 590	SP1	16	900	1 330
S9	19	120	10 000				
				C1	13	144	1 040
A39	16	36	15 350	A31	13	16	1 630
S2	16	1441	15 330	A35	13	86	1 650
				A36	13	92	1 040
A32	13	8	1 600	A37	13	92	2 100
A40	13	4	14 750	A38	13	92	2 385
A43	13	24	2 090	A42	13	16	3 350
C2	13	16	9 810	A44	13	24	2 150
S3	13	1638	13 130	A46	13	48	1 870
				R4	13	1440	1 030
				R7	13	4	3 240
				S10	13	156	2 250
				R8	10	2422	1 340
				R9	10	1472	1 340
				R10	10	368	1 360

BILL OF REINFORCING STEEL Non-Epoxy Coated Grade 420							
Straight Bars				Bent Bars			
Mark	Size	Number	Length	Mark	Size	Number	Length
DS1	36	72	15 000	DS5	15.9	4	*
DS2	36	72	15 900	DS6	15.9	4	*
DS3	36	72	16 500	DS7	15.9	4	*
DS4	36	72	17 600	DS8	15.9	4	*
DS10	29	240	2 900	DS9	9.5	16	*

* Subsidiary to the bid item
* Drilled Shaft (1520mm)(Cased)*

BILL OF REINFORCING STEEL Non-Epoxy Coated Grade 420							
Straight Bars				Bent Bars			
Mark	Size	Number	Length	Mark	Size	Number	Length
PCI	29	240	5 300	A22	19	160	3 080
				A23	19	32	3 220
A24	25	26	15 300				
A27	25	48	2 600	PB6	16	672	2 880
PB1	25	8	15 350	PB7	16	32	2 830
PB2	25	16	15 240	PB8	16	48	3 090
PB3	25	16	14 930				
PB4	25	8	14 250				
PB9	25	16	15 330	A1	13	2	3 320
PB10	25	16	15 150	A2	13	2	3 360
PB11	25	16	14 250	A3	13	2	3 400
				A4	13	2	3 500
PW3	19	48	3 140	A5	13	2	3 540
PW4	19	224	1 510	A6	13	2	3 580
PW5	19	224	2 310	A7	13	2	3 640
				A8	13	2	3 700
A25	16	12	15 300	A9	13	2	3 420
PB5	16	32	14 250	A10	13	2	3 480
				A11	13	2	3 540
A28	13	48	2 360	A12	13	2	3 700
PW1	13	264	4 050	A13	13	2	3 800
PW2	13	288	3 140	A14	13	2	3 900
				A15	13	2	3 600
				A16	13	2	3 700
				A17	13	2	3 800
				A18	13	2	4 040
				A19	13	2	4 180
				A20	13	2	4 320
				A21	13	2	4 440
				A30	13	10	2 750
				PB12	13	200	1 520
				PW6	13	264	800
				PSI	9.5	16	*

* See Bending Diagram

Spiral reinforcing shall meet the requirements of ASTM A615M-96 Grade (420 or 300) or ASTM A82M.
Spiral Spacer Bars:
1) Are included in the mass of reinforcing steel.
2) Minimum section modulus = 490 mm³
3) 4 required per spiral.

Spiral reinforcing shall meet the requirements of ASTM A615M-96 Grade (420 or 300) or ASTM A82M.
Spiral Spacer Bars:
1) Are included in the mass of reinforcing steel.
2) Minimum section modulus = 130 mm³
3) 4 required per spiral.

BENDING DIAGRAMS
(All dimensions are out to out of bars.)

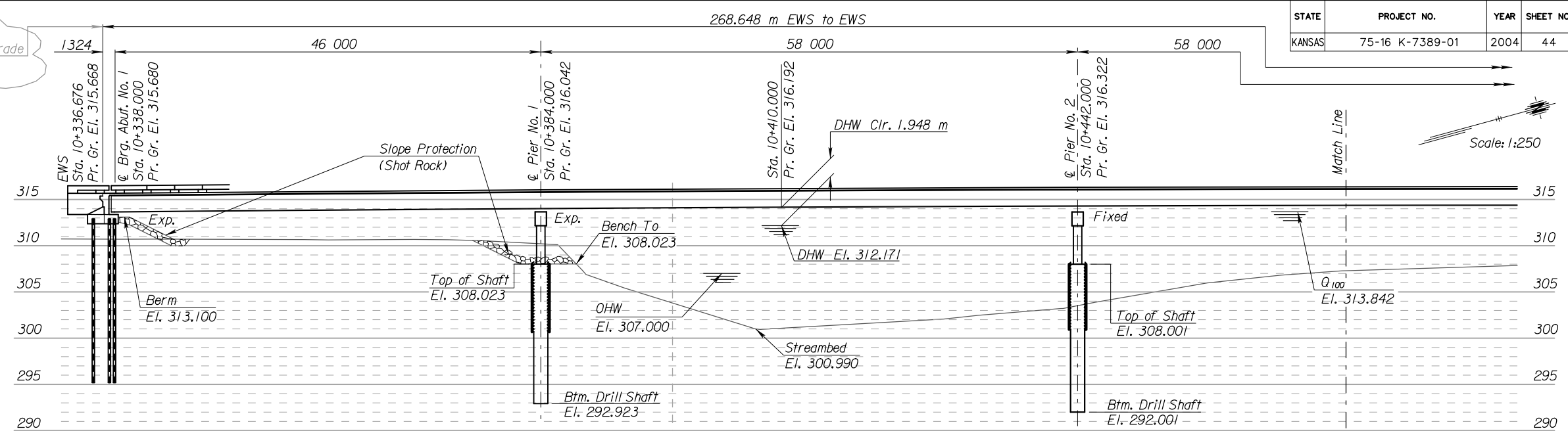
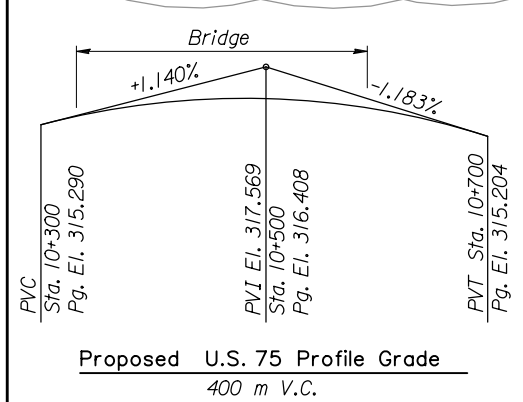
Plotted By: Jruby
File: 738901-059-39.dgn (738901-059-39)
Plot Date: 14-FEB-2012 09:13

3				
2				
1				
NO.	DATE	REVISIONS	BY	APP'D

KANSAS DEPARTMENT OF TRANSPORTATION
Br. No. 75-16-12.66(059) Sta. 10+471.000
BILL OF REINFORCING STEEL
& BENDING DIAGRAMS
US-75 over Neosho River
Proj. No. 75-16 K-7389-01 Coffey Co.
SHEET NO. 39 OF 40 SCALE APP'D
DESIGNED JSR DETAILED JSR QUANTITIES JSR CADD JSR
DESIGN CK.JDK/MJO DETAIL CK.JDK/MJO QUAN. CK. MLI CADD CK.JDK/MJO

STATE	PROJECT NO.	YEAR	SHEET NO.	TOTAL SHEETS
KANSAS	75-16 K-7389-01	2004	44	237

Reference Line = Sta. and Elev. Along the Profile Grade
(3.7 m Right of Δ Bridge = Crown Grade)
(9.1 m Left of Project)

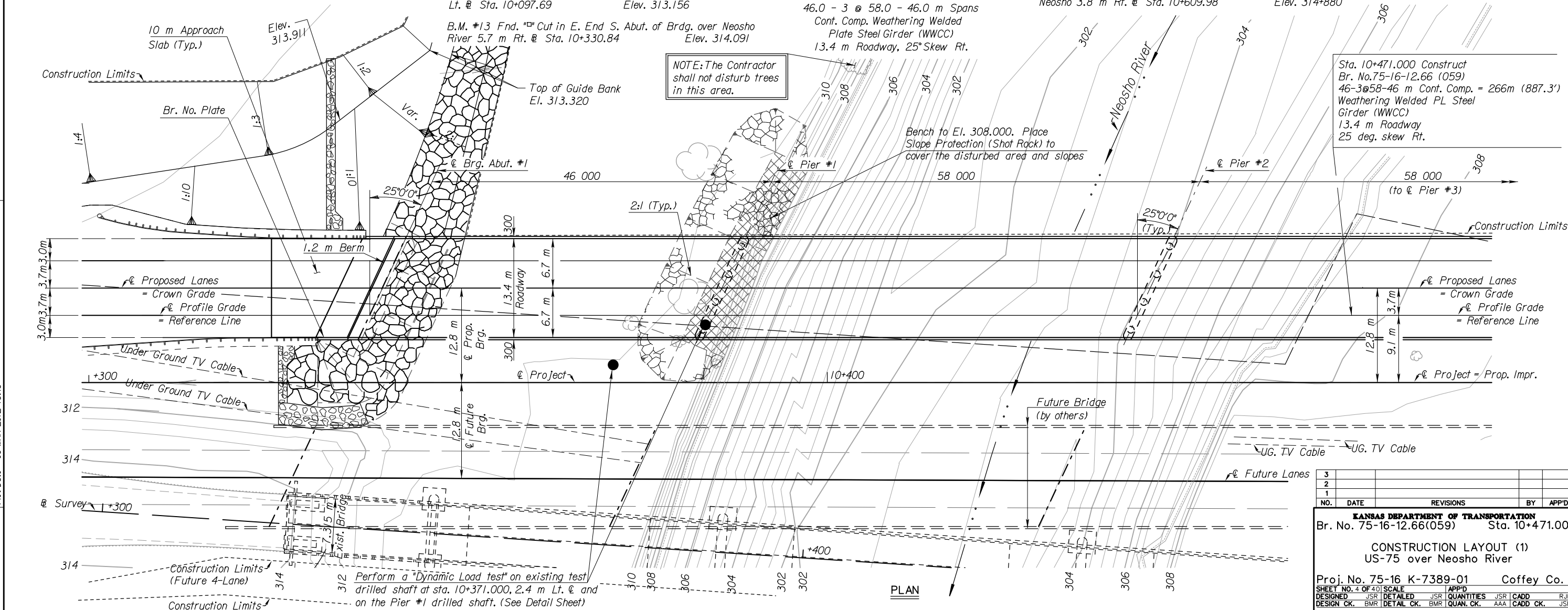


B.M. #12 Fnd. "Cut in W. Hdwl. of RCB 2.0 m Lt. @ Sta. 10+097.69 Elev. 313.156
 B.M. #13 Fnd. "Cut in E. End S. Abut. of Brdg. over Neosho River 5.7 m Rt. @ Sta. 10+330.84 Elev. 314.091
 B.M. #14 Fnd. "Cut in top N. End E. Handrail of Brdg. over Neosho 3.8 m Rt. @ Sta. 10+609.98 Elev. 314+880

10+400 ELEVATION
 46.0 - 3 @ 58.0 - 46.0 m Spans
 Cont. Comp. Weathering Welded Plate Steel Girder (WWCC)
 13.4 m Roadway, 25° Skew Rt.

NOTE: The Contractor shall not disturb trees in this area.

Sta. 10+471.000 Construct Br. No. 75-16-12.66 (059) 46-3@58-46 m Cont. Comp. = 266m (887.3') Weathering Welded PL Steel Girder (WWCC) 13.4 m Roadway 25 deg. skew Rt.



Perform a "Dynamic Load test" on existing test drilled shaft at sta. 10+371.000, 2.4 m Lt. Δ and on the Pier #1 drilled shaft. (See Detail Sheet)

NO.	DATE	REVISIONS	BY	APP'D
3				
2				
1				

KANSAS DEPARTMENT OF TRANSPORTATION
 Br. No. 75-16-12.66(059) Sta. 10+471.000
 CONSTRUCTION LAYOUT (1)
 US-75 over Neosho River
 Proj. No. 75-16 K-7389-01 Coffey Co.
 SHEET NO. 4 OF 40 SCALE APP'D
 DESIGNED JSR DETAILED JSR QUANTITIES JSR CADD RJH
 DESIGN CK. BMR DETAIL CK. BMR QUAN. CK. AAA CADD CK. JSR

Plotted By: Iruby
 File: 738901-059-04asubuilt.dgn (738901-059-04asubuilt)
 Plot Date: 06-MAR-2012 13:43

K-TRAN

KANSAS TRANSPORTATION RESEARCH AND NEW-DEVELOPMENT PROGRAM

